Overcoming the limitations of direct transmission of continuous-variable quantum information

Bjerrum, Anders Jannik Ehlers

Publication date:
2023

Document Version
Publisher's PDF, also known as Version of record

Overcoming the limitations of direct transmission of continuous-variable quantum information

Ph.D. Thesis

Anders Jannik Ehlers Bjerrum

Supervised by
Ulrik Lund Andersen, DTU Physics
Jonatan Bohr Brask, DTU Physics
Jonas Schou Neergaard-Nielsen, DTU Physics

Department of Physics
Technical University of Denmark
Denmark
30th of September 2023

Overcoming the limitations of direct transmission of continuous-variable quantum information

Ph.D. Thesis
By Anders Jannik Ehlers Bjerrum

Supervisor	Ulrik Lund Andersen
Co-supervisors	Jonatan Bohr Brask Jonas Schou Neergaard-Nielsen
Period	August 2020 to September 2023
University	Technical University of Denmark
Department	DTU Physics, Department of Physics Section of Quantum Physics and Information Technology, QPIT, Center for Macroscopic Quantum States, bigQ

Abstract

We investigate the difficulties associated with the transmission of quantum information and correlation through lossy channels, and we propose solutions to compensate the losses in different contexts. The distribution of quantum information and quantum correlation over distances relevant for telecommunication, enables the distribution of secure encryption keys and experimental tests of non-locality. In this work we use optical photons as information carriers, and we employ the theory of quantum optics to perform theoretical investigations into the distribution of quantum information and correlation.

We propose a Bell test employing an all-optical setup with multiple parties, and using a probabilistic entanglement swap. The Bell test is designed to be within reach of current experimental capabilities, and the design of the setup is restricted to standard quantum optical elements. The parties have dichotomic inputs and outputs and we test the W^3ZB inequality, and the associated linear inequalities. The experiment uses displacement-based measurements. The Bell inequality violation is robust against transmission losses, with violations being possible for transmissions as low as 10% for the channels connecting the parties. We furthermore investigate the robustness of the violation toward phase-, amplitude, and dark-count noise.

We then propose a repeater based on light-matter entangled states. We investigate how a two-mode squeezed state that has undergone transmission loss, can be purified and amplified using an array of noiseless amplifiers. The noiseless amplifiers consist of a light-matter entangled state, and the purified state is transferred directly from an optical mode to an atomic quantum memory. We present two applications, one is the creation of entangled qubit registers, and the second is the formation of a quantum repeater. We calculate secret key rates for the repeater, and find conditions under which the repeater can violate the PLOB bound. We then perform a thorough analysis of the sensitivity of the scheme toward relevant experimental errors.

We then present unpublished calculations on the generation of Gottesman-Kitaev-Preskill (GKP) states using an interaction between a collection of qubits and an oscillator. We present a probabilistic scheme based on an interaction between a

single qubit and an oscillator. We show that GKP states are fixed points of the oscillator for this interaction, and therefore result naturally. We then present two deterministic schemes employing certain quadrature operators defined for a set of qubits. The first of these schemes uses a measurement to collapse the oscillator into a GKP state. The second scheme enables the formation of a GKP state without using a projective measurement. All of the schemes require that the oscillator is initially in a squeezed state. Both of the deterministic schemes produce GKP states, with the width of the gaussian peaks of the GKP state, decreasing exponentially in the number of used qubits.

Resumé

I denne afhandling undersøger vi problemerne associeret med transmissionen af kvanteinformation og korrelation igennem transmissionskanaler med tab, og vi foreslår løsninger til at modvirke tabet i forskellige eksperimentelle kontekst. Distribueringen af kvante- information og korrelation over distancer relevante for telekommunikation, tillader distribuering af krypteringsnøgler og eksperimentelle tests af ikke-lokalitet. I dette arbejde bruger vi optiske fotoner som informations-bærer, og vi anvender kvanteoptikken til at gennemføre en teoretisk undersøgelse af hvordan kvante- information og korrelation kan distribueres.

Vi foreslår en Bell test som kun anvender optiske komponenter, og med en variabel mængde af deltagere. Vi anvender kvantemekanisk forvitring og projektive målinger til at lave et såkaldt entanglement swap. Bell testen er designet til at kunne gennemføres med nuværende eksperimentelle begrænsninger, og opstillingen anvender standard kvanteoptiske komponenter. Deltagerne bruger dikotomiske inputs og outputs, og vi tester W^3ZB uligheden, og associerede linære uligheder. Eksperimentet bruger forskydnings-baserede målinger. Brydningen af Bell uligheden er robust imod transmissionstab, med brydningen værende mulig for en transmission helt ned til 10% for de optiske fibre der forbinder deltagerne. Vi undersøger derudover robustheden af brydningen imod fase støj, amplitude støj og detektor fejl (dark-counts).

Vi foreslår dernæst et design på en såkaldt repeater, baseret på lys-stof forvitrede tilstande. Vi undersøger hvordan en tilstand bestående af forvitret klemt lys, som har undergået transmissionstab, kan blive purified med et array af støjfrie forstærkere. De støjfrie forstærkere består af lys-stof forvitrede tilstande, og den resulterende purified tilstand bliver overført fra en optisk bærer til en atomar kvantehukommelse. Vi præsenterer to anvendelser, den ene er dannelsen af forvitrede qubit registrer, den anden er en kvante-repeater. Vi beregner rater for distribuering af krypteringsnøgler med repeateren, og vi finder betingelser under hvilket repeateren kan bryde PLOB bounded. Vi gennemfører så en grundig analyse af eksperimentets følsomhed overfor relevante eksperimentelle fejlkilder.

Endelig præsenterer vi ikke-publicerede beregninger vedrørende præparationen

af Gottesman-Kitaev-Preskill (GKP) tilstande. Præparationen forløber ved en interaktion imellem en samling qubits og en oscillator. Vi præsenterer en probabilistisk protokol baseret på en interaktion imellem en enkelt qubit og en oscillator. Vi viser at GKP tilstande er fikspunkter for oscillatoren i denne interaktion, og derfor opstår naturligt. Vi præsenterer derefter to deterministiske protokoller, som anvender visse kvadratur operatorer, defineret for et sæt qubits. Den første protokol bruger en måling til at kollapse oscillatoren ned i en GKP tilstand. Den anden protokol tillader dannelsen af en GKP tilstand uden anvendelsen af en projektiv måling. Alle protokollerne kræver at oscillatoren til at starte med er i en klemt tilstand. Begge deterministiske protokoller producerer GKP tilstande, hvor bredden af GKP tilstandens gaussiske kurver, falder eksponentielt i mængden af anvendte qubits.

Acknowledgments

The work contained in this thesis was made possible by the help and guidance from my supervisors Ulrik L. Andersen, Jonatan B. Brask, and Jonas S. Neergaard-Nielsen. I am grateful for their support. I would like to thank my girlfriend Karen D. Pedersen for always being supportive and patient with me. I am also indebted to the whole QPIT group for the good discussions we have had, and in particular to my office mates, Olga Solodovnikova, Carles Roch i Carceller, Kristian Toccacelo, Niklas Budinger, Mathias Jørgensen, and Jacob Hastrup. Finally, I would like to thank my brother Lars Bo Bjerrum and his wife Victoria Laureau for being good company.

List of publications

We list the publications included in this thesis.

- *Proposal for a long-distance nonlocality test with entanglement swapping and displacement-based measurements.* Authored by Anders J. E. Bjerrum, Jonatan B. Brask, Jonas S. Neergaard-Nielsen, and Ulrik L. Andersen. The paper was published in Physical Review A with the reference Phys. Rev. A 107, 052611 (2023).

- *Quantum repeater using two-mode squeezed states and atomic noiseless amplifiers.* Authored by Anders J. E. Bjerrum, Jonatan B. Brask, Jonas S. Neergaard-Nielsen, and Ulrik L. Andersen. The paper was published in Physical Review A with the reference Phys. Rev. A 107, 042606 (2023).

Contents

1 Introduction **1**

2 The theory of quantum optics **6**
2.1 Correspondence between quantum electrodynamics and classical electrodynamics . . . 6
2.1.1 Quantization . . . 12
2.2 Fock states . . . 13
2.2.1 Energy density of the free field . . . 15
2.3 Coherent states, the displacement operator and the Wigner characteristic function . . . 15
2.4 Gaussian states . . . 19
2.5 Modes . . . 21
2.6 Gaussian operations . . . 25
2.7 Simplified model of a polychromatic squeezer . . . 28

3 Bell inequalities and non-locality **35**
3.1 The counter-factual decomposition . . . 38
3.2 The Clauser-Horne inequalities . . . 42
3.3 The no-signalling polytope . . . 48
3.4 More than two participants . . . 50

4 Proposal for a long-distance nonlocality test with entanglement swapping and displacement-based measurements **55**
4.1 Abstract . . . 55
4.2 Introduction . . . 55
4.3 Model . . . 60
4.4 Results and Discussion . . . 64
4.5 Conclusion . . . 71
4.6 Acknowledgment . . . 72
4.7 Appendix . . . 73
4.7.1 A1 . . . 73
4.7.2 A2 . . . 81
4.8 Converting the nonlinear W^3ZB inequality into linear inequalities . . . 82

5 Quantum repeater using two-mode squeezed states and atomic noiseless amplifiers **85**
5.1 Abstract . . . 85
5.2 Introduction . . . 85
5.3 Analysis of a single repeater segment . . . 87
5.4 Entanglement of the Registers . . . 92
5.5 Connecting the Segments via Deterministic Entanglement Swapping . 96
5.6 Performance of the Quantum Repeater . . . 98
5.6.1 Bell Inequality Violation and Device-Independent QKD . . . 99
5.6.2 Robustness of the Scheme . . . 101
5.7 Conclusion . . . 103
5.8 Acknowledgment . . . 105
5.9 Appendix . . . 106
5.9.1 Generating Entangled Registers . . . 106
5.9.2 Secret Key Rate . . . 114
5.9.3 Trials Needed Before M Repeater Segments Succeed . . . 115
5.9.4 Optimal Parameters - 1 Qubit per Register . . . 117
5.9.5 Phase and Thermal Noise . . . 117

6 Modular interactions and Gottesman-Kitaev-Preskill states **122**
6.1 Peaked periodic states as fixed points . . . 123
6.2 Encoding quadratures into qubits . . . 130
6.2.1 Measurement-based protocol . . . 133
6.2.2 Measurement-free protocol . . . 139
6.3 Summary . . . 140

7 Conclusion **143**

Chapter 1

Introduction

In this thesis we seek solutions to overcoming the difficulties associated with the transmission of quantum information over distance. We focus on optical communication, where quantum information is encoded in a quantum optical state, and then sent through a transmission fiber. The difficulties referred to, are then primarily transmission losses. Our approach in this thesis is analytical, but where we have been able, we have with scrutiny included experimental sources of error in our analysis. The question of how to tackle transmission loss is rather open ended, and different answers can be found within different contexts. We will in this thesis explore a few.

To introduce the effects associated with transmission loss, we give the corresponding transformation of a single-mode Wigner function. We let $W_0(X)$ be the Wigner function of the mode entering a channel of transmission η, then the Wigner function of the mode exiting the channel $W_\eta(X)$ is given by [1],

$$W_\eta(X) = \frac{1}{\eta}\int_{\mathbb{R}^2} d^2Z W_0(Z/\sqrt{\eta})\mathcal{N}[X, V_\eta](Z). \tag{1.1}$$

where $\mathcal{N}[X, V](Z)$ is the symmetric two dimensional normal distribution of mean X and variance V,

$$\mathcal{N}[X, V](Z) = \frac{1}{2\pi V}\exp\left[-\frac{1}{2V}\left(Z - X\right)^T\left(Z - X\right)\right] \tag{1.2}$$

and the variance is given by the transmission,

$$V_\eta = 1 - \eta. \tag{1.3}$$

We see that the effect of the lossy channel is to scale the Wigner function $W_0(X)$ in its argument by a factor $\sqrt{\eta}$, followed by gaussian blurring. The effect of this map on a displaced two-photon state is sketched in Fig. 1.1 for various η. We note that the effect of the lossy channel on a coherent state of amplitude α, is simply to

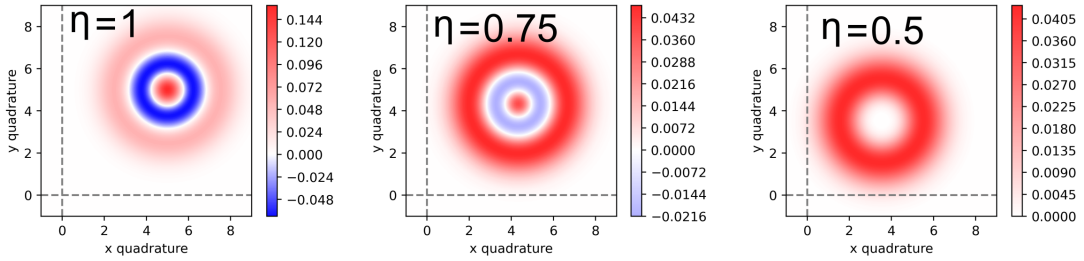

Figure 1.1: *We sketch the effect of loss on the Wigner function of a displaced two-photon state. η is the transmission of the lossy channel.*

generate a coherent state of amplitude $\sqrt{\eta}\alpha$.

In classical telecommunication information can be encoded in the central phase and central amplitude of an optical state, idealized as a strong coherent state. Under these circumstances, transmission losses can be compensated by the use of a gain medium, which through stimulated emission increases the amplitude of the incoming field. To show how this works, we let $W_g(X)$ be the Wigner function of a single mode quantum state that has passed through a gain medium with gain g. We let $W_0(X)$ be the Wigner function of the mode prior to the gain medium. The transformation relating the two Wigner functions is [2],

$$W_g(X) = \frac{1}{g^2}\int_{\mathbb{R}^2} d^2Z W_0(Z/g)\mathcal{N}[X, V_g](Z). \tag{1.4}$$

V_g is related to the gain as,

$$V_g = \frac{1/2}{n_1 - n_2}\left(g^2 - 1\right) \tag{1.5}$$

where n_1 is the fraction of the gain medium atoms that are in the excited state, and n_2 is the fraction of the gain medium atoms that are in the ground state. We see that the effect of the gain medium Eq. 1.4 is very similar to the effect of the lossy channel Eq. 1.1. The gain medium can compensate for the rescaling by $\sqrt{\eta}$ applied in Eq. 1.1, provided $g = 1/\sqrt{\eta}$, however both the lossy channel *and* the gain medium applies gaussian blurring on the Wigner function. In Fig. 1.2 we show the effect of the map in Eq. 1.4 on a displaced 2 photon state (a), and a coherent state of large amplitude (b). From (b) we find that any classical information encoded in the central phase and central amplitude of the field is well preserved under transmission through the gain medium, given that the gain factor is known. The effect on the displaced 2 photon state (a) is more detrimental, and negative regions of the Wigner function are entirely washed out for a gain of 2.

While classical information can be encoded in the central phase and amplitude of

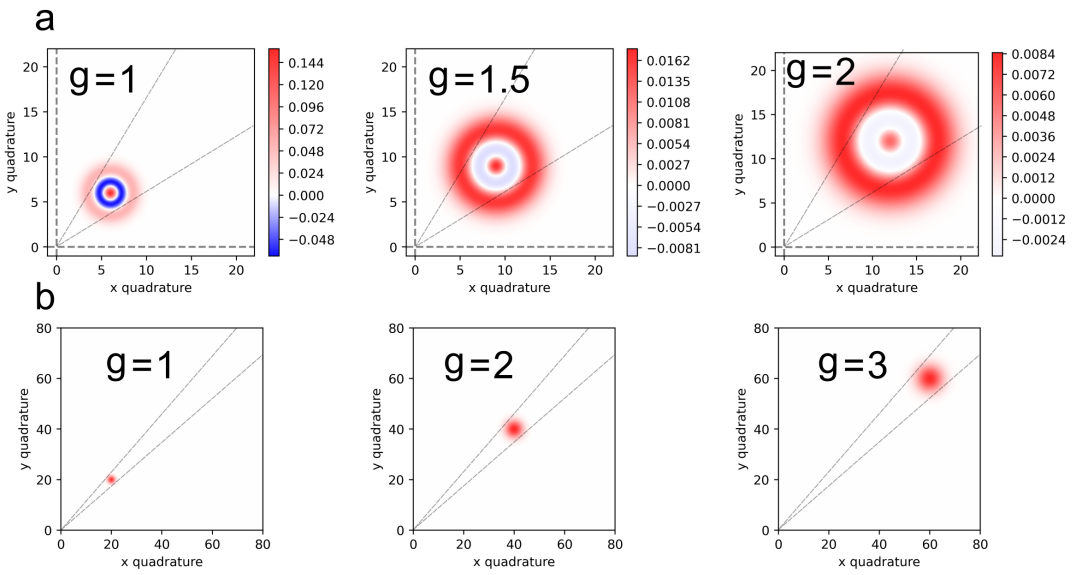

Figure 1.2: *g is the amplification factor and the fraction of excited atoms n_1 is set to 1.* ***a.*** *The effect of a gain medium on the Wigner function of a displaced two photon state. The Wigner function is scaled by g in the argument, and gaussian smoothing with radius $\sqrt{V_g}$ is applied.* ***b.*** *The effect of a gain medium on the Wigner function of a strong coherent state. We observe no significant increase in phase angle noise, and the signal-to-noise ratio of the amplitude is nearly unchanged.*

a signal, quantum information can be understood as the information encoded in the details of the Wigner function. It is now clear that passage through a lossy channel distorts quantum information, and subsequent passage through a gain medium further distorts the information, rather than recovering it.
Evidently gain media cannot be used to recover quantum information that has passed through a lossy fiber, and new techniques must be developed if we are to distribute quantum information through lossy channels.

But *why* should we distribute quantum information over distance ? The technological answer to this question seems to be, for the purpose of distributing encryption keys. Quantum information differs substantially from classical information, and while we can freely copy classical information, one finds that quantum information cannot in general be copied [3]. This fact forms the basis for many key distribution protocols based on quantum information [4], [5].

It is in the correlations between subsystems, that we find the starkest difference between classical information and quantum information. Correlations between classical subsystems describe logical relations between unknown parameters, e.g. A and B. Mathematically, two parameters are mutually dependent if the joint distribution $p(A, B)$ does not factorize as $p(A)p(B)$. In a classical system A and B would be unknown because of some random classical process. Correlations in quantum systems however, can describe logical relations between quantum mechanically uncertain parameters. This distinction in the underlying reason for the uncertainty in A and B, embodies quantum correlations with structure that we do not find in classical correlations. For a pure quantum system, we assume that the quantum state $|\psi\rangle$ encodes all information that can be known about the statistics of the observables A and B [6]. Supposing that A and B are properties of different subsystems, then we may often assume $[A, B] = 0$, and we can express $|\psi\rangle$ in a common eigenvector basis of the observables [3],

$$|\psi\rangle = \sum_{a,b} c_{a,b} \, |a\rangle_1 \, |b\rangle_2 \tag{1.6}$$

where $|a\rangle_1 \, |b\rangle_2$ is an eigenstate of A and B with eigenvalues a and b respectively. The subscript 1 indicates that a measurement of A acts on this part of the vector (subsystem 1), and likewise the subscript 2 indicates that a measurement of B acts on this part of the vector. The joint distribution $p(a, b) = |c_{a,b}|^2$ might not factorize, and then we would say that A and B are mutually dependent. However, even if $|c_{a,b}|^2$ factorizes, the two subsystems might still be correlated with respect to other observables. All these potential dependencies between observables, are encoded in the quantum state $|\psi\rangle$, and *only* if the state factorizes with respect to subsystem 1 and 2,

$$|\psi\rangle = |\psi_1\rangle_1 \otimes |\psi_2\rangle_2 \, , \tag{1.7}$$

do we know that the subsystems 1 and 2 are independent in all observables. This correlation structure, encoded in quantum states that do not factorize with respect to subsystems, is called *entanglement*. Certain entangled states can violate correlation inequalities called Bell inequalities, and these inequalities can be violated under conditions where classically correlated systems do not yield a violation [7]. This fact, which we explore further in chapter 3, implies that correlations between quantum observables are somehow different than classical correlations. It is therefore of some scientific interest, to see over how long distances entangled states can be prepared. It is also of practical interest, for the violation of a Bell inequality can be used to prove the security of an encryption key, by using a device-independent quantum key distribution protocol [8].

We now outline the structure of this thesis. In chapter 2 we give an account of the theory of quantum electrodynamics, as it applies to the regime where this thesis operates. We introduce important concepts, such as phase space representations, Fock states, coherent states, gaussian operations, and the fundamental commutation relation. In this chapter we also give a simplified analysis of a polychromatic squeezer.

In chapter 3 we introduce the concept of the Bell polytope, and we derive the important W^3ZB inequality. Following this, we present the paper *Proposal for a long-distance nonlocality test with entanglement swapping and displacement-based measurements* [9] and the paper *Quantum repeater using two-mode squeezed states and atomic noiseless amplifiers* [10]. We also present some unpublished calculations for the first paper, where we replace the non-linear W^3ZB inequality with associated linear inequalities.

In chapter 6 we present an unpublished paper on how to prepare Gottesman-Kitaev-Preskill (GKP) states by employing a modular measurement. GKP states have recently been given some interest as a flying error correctable qudit for distributing quantum information [11]. In this connection it is interesting to examine how they can be prepared. To this end we present three preparation schemes.

Chapter 2

The theory of quantum optics

In this chapter we outline the theory of quantum electrodynamics as it relates to the study of quantum optics. We start from Maxwell's equations and separate the fields into transverse and longitudinal components, with the transverse components being the main subject of quantum optics. We introduce the normal modes of the transverse electromagnetic field and we state the equation of motion for the normal modes. We enforce the fundamental commutation relation on the normal mode operator $a_{np}(t)$ and thereby obtain the annihilation operator of quantum optics.

We introduce the quadratures, Fock states, coherent states and the displacement operator. The Wigner characteristic function is introduced as the expansion coefficient associated with a particular displacement operator, when one expands the density matrix in terms of displacement operators. We briefly discuss the theory of quadratic Hamiltonians and gaussian transformations, and introduce Bogoliubov transformations and symplectic matrices. In this context we also define the concept of a mode. We then apply the developed theory to give a simple analysis of a polychromatic squeezer.

2.1 Correspondence between quantum electrodynamics and classical electrodynamics

In this section we quantize the electromagnetic (EM) field and we introduce the most important operators and observables, along with their commutation relations. The purpose of this section is to give a physical foundation for the algebra of quantum optics, and this is accomplished in part by establishing the correspondence between the classical description of the EM field and the quantized description. In particular we will quantize the EM field in the presence of charges and currents. After all, beamsplitters, squeezers, photodetectors, photoactive two-level systems, these are all matter systems, and so if we wish to understand the nature of the quantized EM

field in the presence of such systems, we should not seek to quantize the EM field in vacuum, rather we ought to quantize the EM field in the presence of currents and charges.

It is not possible to derive the quantum mechanical description of the EM field by starting from the classical description, for the same reason that classical electrodynamics cannot be derived from classical electrostatics. The quantized description of the electromagnetic field is more fundamental, and can at best be guessed from the classical description. Nevertheless it is illuminating to coax classical electrodynamics into a form so that it strongly resembles the correct quantized description. The reason is twofold, firstly it makes it possible to establish the correspondence between the classical field variables and the quantum operators, for instance we will show that the annihilation operator of quantum mechanics finds a correspondence in the classical normal modes of the EM field,

$$\mathbf{a}(\mathbf{k_n}, t) = \sqrt{\frac{\varepsilon_0}{2\hbar\omega}} \left[-i\mathbf{E}_\perp(\mathbf{k}_n, t) + \omega \mathbf{A}_\perp(\mathbf{k}_n, t)\right] \tag{2.1}$$

with $\mathbf{k}_n$ being the wavevector of the field, and where $\mathbf{E}_\perp(\mathbf{k}_n, t)$ and $\mathbf{A}_\perp(\mathbf{k}_n, t)$ are Fourier coefficients of the divergence free parts of the electric field and vector potential respectively, i.e. $\nabla \mathbf{E}_\perp(\mathbf{r}, t) = 0$ and $\nabla \mathbf{A}_\perp(\mathbf{r}, t) = 0$. We note that both of these fields are gauge invariant. Secondly, once the classical description has been coaxed into the right shape, quantization can be achieved simply by postulating the correct commutation relations. The following derivations and arguments follow [12] with some minor modifications.

We will assume that the entirety of the fields and particles are well contained inside a cube of edge L. Inside the cube we will describe the fields by their Fourier series over the discrete set of wavevectors $\mathbf{k}_n$, satisfying the condition $\mathbf{k}_n = (2\pi/L)\mathbf{n}$, with $\mathbf{n}$ being a vector of integers $\mathbf{n} = \begin{pmatrix} n_x & n_y & n_z \end{pmatrix}$. We also introduce the temporal frequency $\omega_n = c|\mathbf{k}_n|$. Note that the subscript n refers to the array $\mathbf{n}$, and it will do so throughout this section.

Given a vector field in real space,

$$\mathbf{V}(\mathbf{r}, t) = \begin{pmatrix} V_x(\mathbf{r}, t) & V_y(\mathbf{r}, t) & V_z\ (\mathbf{r}, t) \end{pmatrix}^T \tag{2.2}$$

the field in reciprocal space is given by,

$$\mathbf{V}(\mathbf{k}_n, t) = \frac{1}{L^{3/2}} \int_{-L/2}^{L/2} d^3 r \mathbf{V}(\mathbf{r}, t) e^{-i\mathbf{k}_n \mathbf{r}}, \tag{2.3}$$

and the field in real space is obtained as the Fourier series,

$$\mathbf{V}(\mathbf{r}, t) = \sum_{n \in \mathbb{Z}^3} \frac{1}{L^{3/2}} \mathbf{V}(\mathbf{k}_n, t) e^{i\mathbf{k}_n \mathbf{r}}. \tag{2.4}$$

Maxwell's equations in reciprocal space can be written as,

$$\text{(I)} \quad i\mathbf{k}_n \cdot \mathbf{E}(\mathbf{k}_n, t) = \frac{1}{\varepsilon_0}\rho(\mathbf{k}_n, t) \tag{2.5}$$

$$\text{(II)} \quad i\mathbf{k}_n \cdot \mathbf{B}(\mathbf{k}_n, t) = 0 \tag{2.6}$$

$$\text{(III)} \quad i\mathbf{k}_n \times \mathbf{E}(\mathbf{k}_n, t) = -\partial_t \mathbf{B}(\mathbf{k}_n, t) \tag{2.7}$$

$$\text{(IV)} \quad i\mathbf{k}_n \times \mathbf{B}(\mathbf{k}_n, t) = \frac{1}{c^2}\partial_t \mathbf{E}(\mathbf{k}_n, t) + \frac{1}{\varepsilon_0 c^2}\mathbf{j}(\mathbf{k}_n, t) \tag{2.8}$$

$\rho(\mathbf{k}_n, t)$ is the distribution of charged matter and $j(\mathbf{k}_n, t)$ is the associated currents,

$$\rho(\mathbf{r}, t) = \sum_\alpha q_\alpha \delta(\mathbf{r} - \mathbf{r}_\alpha(t)) \tag{2.9}$$

$$\mathbf{j}(\mathbf{r}, t) = \sum_\alpha q_\alpha \mathbf{v}_\alpha(t) \delta(\mathbf{r} - \mathbf{r}_\alpha(t)) \tag{2.10}$$

with α labelling a particle of charge q_α and velocity $\mathbf{v}_\alpha$. We decompose each vector field into a longitudinal and transverse part with respect to the wavevector $\mathbf{k}_n$,

$$\mathbf{V}(\mathbf{k}_n, t) = \mathbf{V}_{||}(\mathbf{k}_n, t) + \mathbf{V}_{\perp}(\mathbf{k}_n, t) \tag{2.11}$$

introducing $\boldsymbol{\kappa}_n = \mathbf{k}_n / |\mathbf{k}_n|$ we can define the components as,

$$\mathbf{V}_{||}(\mathbf{k}_n, t) = \boldsymbol{\kappa}_n \left[\boldsymbol{\kappa}_n \cdot \mathbf{V}(\mathbf{k}_n, t)\right] \tag{2.12}$$

$$\mathbf{V}_{\perp}(\mathbf{k}_n, t) = \mathbf{V}(\mathbf{k}_n, t) - \mathbf{V}_{||}(\mathbf{k}_n, t) = (\mathbf{I} - \boldsymbol{\kappa}_n \boldsymbol{\kappa}_n^T)\mathbf{V}(\mathbf{k}_n, t) \tag{2.13}$$

Converting to real space we have,

$$\mathbf{V}(\mathbf{r}, t) = \mathbf{V}_{||}(\mathbf{r}, t) + \mathbf{V}_{\perp}(\mathbf{r}, t) \tag{2.14}$$

Taking the divergence and converting between real and reciprocal space,

$$\begin{aligned} &\nabla \cdot \mathbf{V}(\mathbf{r}, t) = \nabla \cdot \mathbf{V}_{||}(\mathbf{r}, t) + \nabla \cdot \mathbf{V}_{\perp}(\mathbf{r}, t) \\ &\Updownarrow\ i\mathbf{k}_n \cdot \mathbf{V}(\mathbf{k}_n, t) = i\mathbf{k}_n \cdot \mathbf{V}_{||}(\mathbf{k}_n, t) + i\mathbf{k}_n \cdot \mathbf{V}_{\perp}(\mathbf{k}_n, t) = i\mathbf{k}_n \cdot \mathbf{V}_{||}(\mathbf{k}_n, t) \\ &\Updownarrow\ \nabla \cdot \mathbf{V}(\mathbf{r}, t) = \nabla \cdot \mathbf{V}_{||}(\mathbf{r}, t) \end{aligned} \tag{2.15}$$

hence $\mathbf{V}_{\perp}(\mathbf{r}, t)$ is the divergence free part of the field. Likewise we can take the curl and convert between real and reciprocal space,

$$\begin{aligned} &\nabla \times \mathbf{V}(\mathbf{r}, t) = \nabla \times \mathbf{V}_{||}(\mathbf{r}, t) + \nabla \times \mathbf{V}_{\perp}(\mathbf{r}, t) \\ &\Updownarrow\ i\mathbf{k}_n \times \mathbf{V}(\mathbf{k}_n, t) = i\mathbf{k}_n \times \mathbf{V}_{||}(\mathbf{k}_n, t) + i\mathbf{k}_n \times \mathbf{V}_{\perp}(\mathbf{k}_n, t) = i\mathbf{k}_n \times \mathbf{V}_{\perp}(\mathbf{k}_n, t) \\ &\Updownarrow\ \nabla \times \mathbf{V}(\mathbf{r}, t) = \nabla \times \mathbf{V}_{\perp}(\mathbf{k}_n, t) \end{aligned} \tag{2.16}$$

and $\mathbf{V}_{||}(\mathbf{r},t)$ is the curl free part of the field. Applying this decomposition to Maxwell's equations I and II we arrive at the defining equations for the longitudinal fields,

$$\mathbf{E}_{||}(\mathbf{k}_n,t) = \frac{-i}{\varepsilon_0}\rho(\mathbf{k}_n,t)\frac{\mathbf{k}_n}{|\mathbf{k}_n|^2} \tag{2.17}$$

$$\mathbf{B}_{||}(\mathbf{k}_n,t) = 0 \tag{2.18}$$

and $\mathbf{E}_{||}(\mathbf{k}_n,t)$ is seen to be known once the charge distribution $\rho(\mathbf{k}_n,t)$ has been specified. In fact, going to real space one finds that the longitudinal component of the electric field is simply the instantaneous Coulomb field of the charges. Examining the longitudinal components of IV, we arrive at the continuity equation after an application of Gauss law I,

$$\partial_t\rho(\mathbf{k}_n,t) + i\mathbf{k}_n\mathbf{j}(\mathbf{k}_n,t) = 0 \tag{2.19}$$

expressing the conservation of charge. Turning to the transverse components, we obtain from III and IV,

$$\partial_t \begin{pmatrix} \mathbf{E}_\perp(\mathbf{k}_n,t) \\ c\boldsymbol{\kappa}_n \times \mathbf{B}_\perp(\mathbf{k}_n,t) \end{pmatrix} = i\omega_n \begin{pmatrix} 0 & 1 \\ 1 & 0 \end{pmatrix} \begin{pmatrix} \mathbf{E}_\perp(\mathbf{k}_n,t) \\ c\boldsymbol{\kappa}_n \times \mathbf{B}_\perp(k_n,t) \end{pmatrix} - \frac{1}{\varepsilon_0}\mathbf{j}_\perp(\mathbf{k}_n,t) \begin{pmatrix} 1 \\ 0 \end{pmatrix} \tag{2.20}$$

We introduce the rescaled normal modes,

$$\mathbf{a}(\mathbf{k}_n,t) = -i\sqrt{\frac{\varepsilon_0}{2\hbar\omega_n}}\left[\mathbf{E}_\perp(\mathbf{k}_n,t) - c\boldsymbol{\kappa}_n \times \mathbf{B}_\perp(\mathbf{k}_n,t)\right] \tag{2.21}$$

$$\mathbf{b}(\mathbf{k}_n,t) = -i\sqrt{\frac{\varepsilon_0}{2\hbar\omega_n}}\left[\mathbf{E}_\perp(\mathbf{k}_n,t) + c\boldsymbol{\kappa}_n \times \mathbf{B}_\perp(\mathbf{k}_n,t)\right] \tag{2.22}$$

where the prefactor $\sqrt{\frac{\varepsilon_0}{2\hbar\omega_n}}$ has been chosen to bring the classical theory into correspondence with the quantized theory, i.e. this choice will yield simple commutator relations once we quantize the normal modes. In terms of these normal modes, Eq. 2.20 becomes,

$$\partial_t \begin{pmatrix} \mathbf{b}(\mathbf{k}_n,t) \\ \mathbf{a}(\mathbf{k}_n,t) \end{pmatrix} = i\omega_n \begin{pmatrix} 1 & 0 \\ 0 & -1 \end{pmatrix} \begin{pmatrix} \mathbf{b}(\mathbf{k}_n,t) \\ \mathbf{a}(\mathbf{k}_n,t) \end{pmatrix} + i\sqrt{\frac{1}{2\hbar\omega_n\varepsilon_0}}\mathbf{j}_\perp(\mathbf{k}_n,t) \begin{pmatrix} 1 \\ 1 \end{pmatrix}. \tag{2.23}$$

It is seen that we can then express $\mathbf{B}_\perp(\mathbf{k}_n,t)$ and $\mathbf{E}_\perp(\mathbf{k}_n,t)$ as,

$$\mathbf{E}_\perp(\mathbf{k}_n,t) = \sqrt{\frac{\hbar\omega_n}{2\varepsilon_0}}i\left[\mathbf{a}(\mathbf{k}_n,t) + \mathbf{b}(\mathbf{k}_n,t)\right] \tag{2.24}$$

$$\mathbf{B}_\perp(\mathbf{k}_n,t) = \sqrt{\frac{\hbar\omega_n}{2\varepsilon_0}}\frac{i}{c}\left[\boldsymbol{\kappa}_n \times \mathbf{a}(\mathbf{k}_n,t) - \boldsymbol{\kappa}_n \times \mathbf{b}(\mathbf{k}_n,t)\right] \tag{2.25}$$

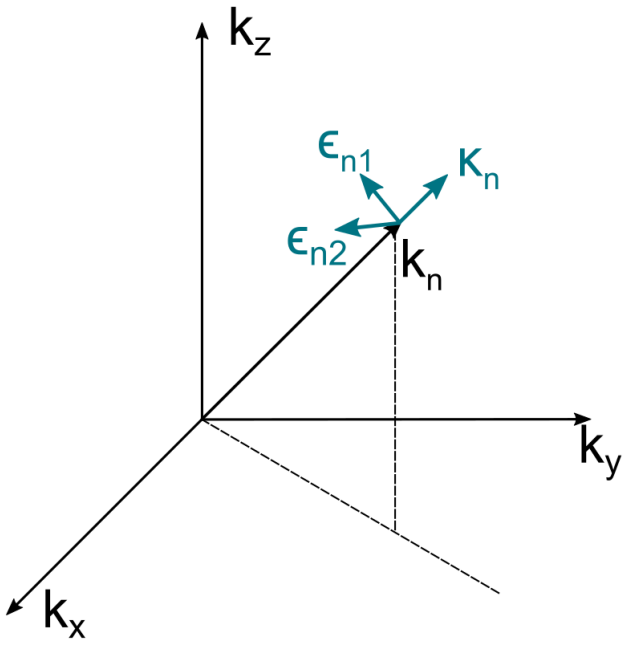

Figure 2.1: *The two polarization vectors $\boldsymbol{\epsilon}_{np}$ associated with a wavevector $\mathbf{k}_n$ are orthogonal to the wavevector.*

Since $\mathbf{E}_\perp(\mathbf{r},t)$ and $\mathbf{B}_\perp(\mathbf{r},t)$ are real, it follows that $\mathbf{E}_\perp(-\mathbf{k}_n,t) = \mathbf{E}^*_\perp(\mathbf{k}_n,t)$ and $\mathbf{B}_\perp(-\mathbf{k}_n,t) = \mathbf{B}^*_\perp(\mathbf{k}_n,t)$ and one can show that this implies,

$$\mathbf{b}(\mathbf{k}_n,t) = -\mathbf{a}^*(-\mathbf{k}_n,t) \tag{2.26}$$

and our equation for the normal modes Eq. 2.23 becomes just the same equation twice,

$$\partial_t \mathbf{a}(\mathbf{k}_n,t) = -i\omega_n \mathbf{a}(\mathbf{k}_n,t) + i\sqrt{\frac{1}{2\hbar\omega_n\varepsilon_0}}\mathbf{j}_\perp(\mathbf{k}_n,t). \tag{2.27}$$

We note that since $\mathbf{a}(\mathbf{k}_n,t)$ is entirely transversal, we can decompose it into two orthogonal components (polarizations) with respect to the $\mathbf{k}_n$ dependent coordinate system drawn in Fig. 2.1.

$$\begin{aligned}\mathbf{a}(\mathbf{k}_n,t) &= \boldsymbol{\epsilon}_{n1}\langle\boldsymbol{\epsilon}_{n1},\mathbf{a}(\mathbf{k}_n,t)\rangle + \boldsymbol{\epsilon}_{n2}\langle\boldsymbol{\epsilon}_{n2},\mathbf{a}(\mathbf{k}_n,t)\rangle \\ &= \boldsymbol{\epsilon}_{n1}a_1(\mathbf{k}_n,t) + \boldsymbol{\epsilon}_{n2}a_2(\mathbf{k}_n,t)\end{aligned} \tag{2.28}$$

where $\boldsymbol{\epsilon}_{np}$ with $p \in \{1,2\}$ are the two polarization vectors associated with wavevector $\mathbf{k}_n$. We have defined the scalar fields $a_p(\mathbf{k}_n,t)$ as the overlap, $a_p(\mathbf{k}_n,t) = \langle\boldsymbol{\epsilon}_{np},\mathbf{a}(\mathbf{k}_n,t)\rangle$. From Eq. 2.27 we see that the normal modes can be non-zero even in the absence of currents and charges. They form the degrees of freedom of the

electromagnetic field, present even when currents and charges are absent. The configuration of the field plus matter system is entirely specified by the variables,

$$\{\mathbf{a}(\mathbf{k}_n, t_0), \mathbf{r}_\alpha(t_0), \frac{d}{dt}\mathbf{r}_\alpha(t_0)\} \tag{2.29}$$

at a single time t_0 and for all wavevectors $\mathbf{k}_n$ and particles α [12]. Since $a_p(\mathbf{k}_n, t)$ has both a real and an imaginary component, it corresponds to two degrees of freedom. These are called quadratures $x_p(\mathbf{k}_n, t)$ and $y_p(\mathbf{k}_n, t)$, and in this thesis we define them by the relations,

$$\begin{aligned} x_p(\mathbf{k}_n, t) &= a_p(\mathbf{k}_n, t) + a_p^*(\mathbf{k}_n, t) \\ y_p(\mathbf{k}_n, t) &= i\left(a_p^*(\mathbf{k}_n, t) - a_p(\mathbf{k}_n, t)\right). \end{aligned} \tag{2.30}$$

We note that the normal modes are complex and therefore not observable, however the quadratures are real and routinely measured in quantum optics experiments. We will from now on be working in the Coloumb gauge where the vector potential satisfies,

$$\begin{aligned} \nabla \cdot \mathbf{A}(\mathbf{r}, t) &= 0 \\ \Updownarrow\, i\mathbf{k}_n \cdot \mathbf{A}(\mathbf{k}_n, t) &= 0 \end{aligned} \tag{2.31}$$

hence $\mathbf{A}(\mathbf{k}_n, t)$ is entirely transversal, $\mathbf{A}(\mathbf{k}_n, t) = \mathbf{A}_\perp(\mathbf{k}_n, t)$. We express $\mathbf{A}_\perp(\mathbf{k}_n, t)$ in terms of $\mathbf{a}(\mathbf{k}_n, t)$,

$$\mathbf{B}_\perp(\mathbf{k}_n, t) = i\mathbf{k}_n \times \mathbf{A}_\perp(\mathbf{k}_n, t) \tag{2.32}$$

So for non-zero $\mathbf{k}_n$ we obtain

$$\mathbf{A}_\perp(\mathbf{k}_n, t) = i\frac{\mathbf{k}_n}{|\mathbf{k}_n|^2} \times \mathbf{B}_\perp(\mathbf{k}_n, t) = \sqrt{\frac{\hbar\omega_n}{2\varepsilon_0}}\frac{1}{\omega_n}\left[\mathbf{a}(\mathbf{k}_n, t) + \mathbf{a}^*(-\mathbf{k}_n, t)\right] \tag{2.33}$$

$$\mathbf{E}_\perp(\mathbf{k}_n, t) = \sqrt{\frac{\hbar\omega_n}{2\varepsilon_0}} i\left[\mathbf{a}(\mathbf{k}_n, t) - \mathbf{a}^*(-\mathbf{k}_n, t)\right] \tag{2.34}$$

$$\mathbf{B}_\perp(\mathbf{k}_n, t) = \sqrt{\frac{\hbar\omega_n}{2\varepsilon_0}}\frac{i}{c}\boldsymbol{\kappa}_n \times \left[\mathbf{a}(\mathbf{k}_n, t) + \mathbf{a}^*(-\mathbf{k}_n, t)\right]. \tag{2.35}$$

Correspondingly we have that,

$$\mathbf{a}(\mathbf{k}_n, t) = \sqrt{\frac{\varepsilon_0}{2\hbar\omega_n}}\left[-i\mathbf{E}_\perp(\mathbf{k}_n, t) + \omega_n \mathbf{A}_\perp(\mathbf{k}_n, t)\right] \tag{2.36}$$

as stated in the beginning of this section. The total (non-relativistic) energy of the field plus matter system can computed as,

$$\begin{aligned} H(t) = \sum_\alpha \frac{1}{2m_\alpha}\left[\mathbf{p}_\alpha(t) - q_\alpha \mathbf{A}_\perp(\mathbf{r}_\alpha, t)\right]^2 + V_{\text{Coul}} \\ + \sum_n \frac{\hbar\omega_n}{2} \sum_p \left[a_p^*(\mathbf{k}_n, t) a_p(\mathbf{k}_n, t) + a_p(\mathbf{k}_n, t) a_p^*(\mathbf{k}_n, t)\right] \end{aligned} \tag{2.37}$$

with m_α being the mass of particle α and,

$$\mathbf{p}_\alpha(t) = m_\alpha \mathbf{v}_\alpha(t) + q_\alpha \mathbf{A}_\perp(\mathbf{r}_\alpha, t) \tag{2.38}$$

being the conjugate momentum of $\mathbf{r}_\alpha$. V_{Coul} is the Coulomb energy associated with the longitudinal electric field $\mathbf{E}_{||}(\mathbf{k}_n, t)$. To ease notation we introduce the following symbols,

$$\begin{aligned} a_{np}(t) &= a_p(\mathbf{k}_n, t) \\ \mathbf{a}_n(t) &= \mathbf{a}(\mathbf{k}_n, t) \\ x_{np}(t) &= x_p(\mathbf{k}_n, t) \\ \mathcal{E}_n &= \sqrt{\frac{\hbar\omega_n}{2\varepsilon_0 L^3}} \end{aligned} \tag{2.39}$$

Then the fields in real space are given by their Fourier series,

$$\begin{aligned} \mathbf{a}(\mathbf{r}, t) &= \sum_n \sum_p \left(\frac{1}{L}\right)^{3/2} \boldsymbol{\epsilon}_{np} a_{np}(t) e^{i\mathbf{k}_n \mathbf{r}} \\ \mathbf{E}_\perp(\mathbf{r}, t) &= i \sum_n \sum_p \mathcal{E}_n \boldsymbol{\epsilon}_{np} \left[a_{np}(t) e^{i\mathbf{k}_n \mathbf{r}} - a^*_{np}(t) e^{-i\mathbf{k}_n \mathbf{r}} \right] \\ \mathbf{B}_\perp(\mathbf{r}, t) &= i \sum_n \sum_p \frac{\mathcal{E}_n}{c} \left(\boldsymbol{\kappa}_n \times \boldsymbol{\epsilon}_{np}\right) \left[a_{np}(t) e^{i\mathbf{k}_n \mathbf{r}} - a^*_{np}(t) e^{-i\mathbf{k}_n \mathbf{r}} \right] \\ \mathbf{A}_\perp(\mathbf{r}, t) &= \sum_n \sum_p \frac{\mathcal{E}_n}{\omega_n} \boldsymbol{\epsilon}_{np} \left[a_{np}(t) e^{i\mathbf{k}_n \mathbf{r}} + a^*_{np}(t) e^{-i\mathbf{k}_n \mathbf{r}} \right]. \end{aligned} \tag{2.40}$$

2.1.1 Quantization

So far everything has been entirely classical, but we are now in a position to quantize the theory. We proceed by introducing commutators for the charged particles,

$$[r_{\alpha i}(t), r_{\beta j}(t)] = [p_{\alpha i}(t), p_{\beta j}(t)] = 0 \tag{2.41}$$

$$[r_{\alpha i}(t), p_{\beta j}(t)] = i\hbar \delta_{\alpha,\beta} \delta_{i,j} \tag{2.42}$$

where $i, j \in \{x, y, z\}$, and for the normal modes,

$$[a_{np}(t), a_{n'p'}(t)] = [a^*_{np}(t), a^*_{n'p'}(t)] = 0 \tag{2.43}$$

$$[a_{np}(t), a^*_{n'p'}(t)] = \delta_{p,p'} \delta_{n,n'}, \tag{2.44}$$

note that $a^*_{np}(t)$ is the adjoint of $a_{np}(t)$, i.e. $a^\dagger_{np}(t) = a^*_{np}(t)$. This follows from the fact that $x_{np}(t)$ and $y_{np}(t)$ are observable and therefore self-adjoint. $a_{np}(t)$ is called an annihilation operator and $a^\dagger_{np}(t)$ is called a creation operator. Note that the particle

operators commute with the field operators when the operators are evaluated at equal times. Equivalently, in terms of quadratures we have the commutators,

$$[x_{np}(t), x_{n'p'}(t)] = [y_{np}(t), y_{n'p'}(t)] = 0 \tag{2.45}$$

$$[x_{np}(t), y_{n'p'}(t)] = 2i\delta_{p,p'}\delta_{n,n'}. \tag{2.46}$$

Finally, the equations of motion can then be found from Heisenberg's equation. For the annihilation operator we obtain (see [12] for a proof),

$$\begin{aligned}\frac{d}{dt}a_{np}(t) &= \frac{1}{i\hbar}[a_{np}(t), H(t)] \\ &= -i\omega_n a_{np}(t) + \frac{i}{\sqrt{2\varepsilon_0\hbar\omega_n}}j_{np}(t),\end{aligned} \tag{2.47}$$

where we retrieved $H(t)$ from Eq. 2.37. $j_{np}(t)$ are the Fourier coefficients of the symmetrized current projected onto the polarization vector $\boldsymbol{\epsilon}_{np}$,

$$j_{np}(t) = \frac{1}{L^{3/2}}\int_{-L/2}^{L/2} d^3r e^{-i\mathbf{k}_n\mathbf{r}}\boldsymbol{\epsilon}_{np}\mathbf{j}(\mathbf{r},t) \tag{2.48}$$

$$\mathbf{j}(\mathbf{r},t) = \frac{1}{2}\sum_\alpha q_\alpha\left[\mathbf{v}_\alpha(t)\delta(\mathbf{r}-\mathbf{r}_\alpha(t)) + \delta(\mathbf{r}-\mathbf{r}_\alpha(t))\mathbf{v}_\alpha(t)\right] \tag{2.49}$$

Eq. 2.47 is identical to the result obtained from Maxwell's equations Eq. 2.27, indicating that Maxwell's equations remain valid between operators, although one should be careful to symmetrize operators (such as the current). This remarkable result shows that with respect to the transverse fields at least, Maxwell's equations are equivalent to a Heisenberg equation.

2.2 Fock states

We define the free EM field as the absence of charged particles and currents. Note that in free space the annihilation operators evolve as $a_{np}(t) = \mathrm{e}^{-i\omega_n t}a_{np}(0)$. The Fock states are defined as states of the free EM field with definite energy, hence they are eigenstates of the Hamiltonian of the field,

$$\begin{aligned}H_{EM} &= \sum_n \frac{\hbar\omega_n}{2}\sum_p\left[a^\dagger_{np}(t)a_{np}(t) + a_{np}(t)a^\dagger_{np}(t)\right] \\ &= \sum_n \hbar\omega_n\sum_p\left[a^\dagger_{np}(0)a_{np}(0) + \frac{1}{2}\right] = \sum_{n,p}H_{np}\end{aligned} \tag{2.50}$$

and the Fock state $|m\rangle_{np}$, associated with a particular polarization p and wavevector $\mathbf{k}_n = \mathbf{n}2\pi/L$, is defined to solve the eigenvalue problem,

$$H_{np}|m\rangle_{np} = E_{nm}|m\rangle_{np} \tag{2.51}$$

It follows that the Fock states obey the relation,

$$a^\dagger_{np}(t)a_{np}(t)|m\rangle_{np} = a^\dagger_{np}(0)a_{np}(0)|m\rangle_{np} = m|m\rangle_{np}, \tag{2.52}$$

which defines the eigenvalue m. The Fock states $|m+1\rangle$ and $|m-1\rangle$ can be generated from the Fock state $|m\rangle$ using the creation and annihilation operators,

$$\begin{aligned} |m+1\rangle_{np} &= \frac{a^\dagger_{np}(0)}{\sqrt{m+1}}|m\rangle_{np} \\ |m-1\rangle_{np} &= \frac{a_{np}(0)}{\sqrt{m}}|m\rangle_{np}. \end{aligned} \tag{2.53}$$

The ground state $|m_g\rangle_{np}$ satisfies $a_{np}(0)|m_g\rangle_{np} = 0$. This fact together with Eq. 2.52 implies $m_g = 0$. $|m = 0\rangle_{np}$ is referred to as the (electromagnetic) vacuum state. Using the creation operator on $|0\rangle_{np}$ to generate the Fock states, we find the eigenvalue spectrum $m = 0, 1, 2, 3, ...$ The energy eigenvalues E_{nm} are then,

$$E_{nm} = \hbar\omega_n \left(m + 1/2\right). \tag{2.54}$$

These results follow directly from analogy with the quantum harmonic oscillator [13]. One can compute the total momentum of the free field as,

$$\mathbf{P}_{\text{free}} = \varepsilon_0 \int_{-L/2}^{L/2} d^3r \mathbf{E}_\perp(\mathbf{r}, t) \times \mathbf{B}(\mathbf{r}, t) = \sum_n \hbar\mathbf{k}_n \sum_p a^\dagger_{np}(t)a_{np}(t) = \sum_{n,p} \mathbf{P}_{np} \tag{2.55}$$

and we find that the Fock state $|m\rangle_{np}$ is also an eigenstate of the free field momentum $\mathbf{P}_{np}$ with eigenvalue $m\hbar\mathbf{k}_n$, hence Fock states have definite momentum. For these reasons a Fock state $|m\rangle_{np}$ is interpreted as representing a free field with m photons, each photon having energy $\hbar\omega_n$ and momentum $\hbar\mathbf{k}_n$.

From here on we will suppress the index np whenever it is not needed. We also introduce a reference point in time $t_0 = 0$, and an operator $U(t)$ evaluated in t_0 will be written as $U(t_0) = U$. The Fock states are eigenstates of an Hermitian operator $a^\dagger a$ and they form a complete orthonormal basis,

$$I = \sum_{m=0}^{\infty} |m\rangle\langle m|. \tag{2.56}$$

The expectation values of the annihilation and quadrature operators are zero for the Fock states,

$$\langle m|a|m\rangle = \frac{1}{2}\langle m|x + iy|m\rangle = 0. \tag{2.57}$$

However it is only the expectation value that is zero, the variances of the quadratures are non-zero,

$$\langle m|x^2|m\rangle = 2m + 1. \tag{2.58}$$

We note that the even in the case of $m = 0$ photons do we measure a variance in the quadratures. However, one should not commit the fallacy of assigning a reality to the variance of an operator in the absence of a measurement. The variance is associated with the spread in eigenvalues obtained upon measuring the operator, and it is fallacious to think that a measurement merely reveals a pre-existing value [14].

2.2.1 Energy density of the free field

We now seek an operational interpretation of the real space normal mode field. The total energy in the free EM-field associated with photons is,

$$H_\gamma(t) = \sum_n \hbar\omega_n \mathbf{a}_n^\dagger(t)\mathbf{a}_n(t) \tag{2.59}$$

If the field is only excited over a narrow range of frequencies centred on ω, then we can pull out the frequency,

$$\begin{aligned}
&= \hbar\omega \frac{1}{L^3} \sum_n \left(\int_{-L/2}^{L/2} d^3r \mathbf{a}^\dagger(\mathbf{r},t) e^{i\mathbf{k}_n\mathbf{r}} \right) \left(\int_{-L/2}^{L/2} d^3r' \mathbf{a}(\mathbf{r}',t) e^{-i\mathbf{k}_n\mathbf{r}'} \right) \\
&= \hbar\omega \int_{-L/2}^{L/2} d^3r d^3r' \mathbf{a}^\dagger(\mathbf{r},t)\mathbf{a}(\mathbf{r}',t) \frac{1}{L^3} \sum_n e^{i\mathbf{k}_n(\mathbf{r}-\mathbf{r}')} \\
&= \hbar\omega \int_{-L/2}^{L/2} d^3r \mathbf{a}^\dagger(\mathbf{r},t)\mathbf{a}(\mathbf{r},t)
\end{aligned} \tag{2.60}$$

So we have the energy density,

$$u_\gamma(\mathbf{r},t) = \hbar\omega \mathbf{a}^\dagger(\mathbf{r},t)\mathbf{a}(\mathbf{r},t) \tag{2.61}$$

This last equation is seen to provide us with an operational interpretation of the magnitude of the normal mode field.

2.3 Coherent states, the displacement operator and the Wigner characteristic function

The normal modes, or rather the annihilation operators, are unobservable. Nevertheless there exists eigenstates associated with these operators. These are called coherent states and they satisfy the eigenvector equation,

$$a|\alpha\rangle = \alpha|\alpha\rangle \tag{2.62}$$

and solving the equation in the Fock basis yields the expansion,

$$|\alpha\rangle = e^{-\frac{1}{2}|\alpha|^2} \sum_{n=0}^{\infty} \frac{\alpha^n}{\sqrt{n!}} |n\rangle, \tag{2.63}$$

where the eigenvalue α is any complex number. We note that the vacuum state $|0\rangle$ is an eigenstate of a with eigenvalue 0. The coherent states are produced by classical currents, as can be seen by solving Eq. 2.27 with respect to a classical (c-number) current [12]. The coherent states form an overcomplete (not orthonormal) basis [15],

$$\frac{1}{\pi} \int_{\mathbb{C}} d^2\alpha |\alpha\rangle\langle\alpha| = I \tag{2.64}$$

Defining $\lambda = \Lambda_x + i\Lambda_y$ and $\Lambda = \begin{pmatrix} \Lambda_x & \Lambda_y \end{pmatrix}^T$ where Λ_x and Λ_y are real numbers, then the displacement operator is defined as,

$$D(\Lambda) = D(\lambda) = \exp\left[\lambda a^\dagger - \lambda^* a\right] = \exp\left[i\left(\Lambda_y x - \Lambda_x y\right)\right], \tag{2.65}$$

note that $D(\lambda)$ is unitary and that $D(-\lambda) = D^\dagger(\lambda)$ (equivalently $D(-\Lambda) = D^\dagger(\Lambda)$). We will shift between complex notation λ and vector notation Λ throughout this thesis, choosing whichever is the most convenient, with a tendency to work with complex notation when using a and $a^\dagger$, and vector notation when using the quadratures x and y. The displacement operator transforms the quadratures as,

$$\begin{aligned} D^\dagger(\Lambda) x D(\Lambda) &= x + 2\Lambda_x \\ D^\dagger(\Lambda) y D(\Lambda) &= y + 2\Lambda_y \\ D^\dagger(\lambda) a D(\lambda) &= a + \lambda. \end{aligned} \tag{2.66}$$

We can generate the coherent state $|\lambda\rangle$ from the vacuum using the displacement operator,

$$|\lambda\rangle = |\Lambda\rangle = D(\lambda)|0\rangle = D(\Lambda)|0\rangle \tag{2.67}$$

The displacement operator can be rewritten in normal ordered form using the Baker-Campbell-Hausdorff (BCH) lemma,

$$D(\lambda) = \exp\left[-|\lambda|^2/2\right] \exp\left[\lambda a^\dagger\right] \exp\left[-\lambda^* a\right] \tag{2.68}$$

The set consisting of a wavevector and a polarization, $(\mathbf{k}_n, \boldsymbol{\epsilon}_{np})$, is referred to as a mode of the electromagnetic field. We may generalize the displacement operator to act on n modes by introducing the vectors,

$$\begin{aligned} \boldsymbol{\Lambda} &= \begin{pmatrix} \Lambda_{1x} & \Lambda_{2x} & \cdots & \Lambda_{nx} & \Lambda_{1y} & \Lambda_{2y} & \cdots & \Lambda_{ny} \end{pmatrix}^T = \begin{pmatrix} \boldsymbol{\Lambda}_x^T & \boldsymbol{\Lambda}_y^T \end{pmatrix}^T \\ \mathbf{R} &= \begin{pmatrix} x_1 & x_2 & \cdots & x_n & y_1 & y_2 & \cdots & y_n \end{pmatrix}^T = \begin{pmatrix} \mathbf{x}^T & \mathbf{y}^T \end{pmatrix}^T \\ \boldsymbol{\lambda} &= \begin{pmatrix} \lambda_1 & \lambda_2 & \cdots & \lambda_n \end{pmatrix}^T \end{aligned} \tag{2.69}$$

$$\mathbf{a} = \begin{pmatrix} a_1 & a_2 & \cdots & a_n \end{pmatrix}^T \tag{2.70}$$

with Λ_{kx} and Λ_{ky} (or λ_k) being the displacement associated with mode k. Note that we have enumerated the modes from 1 to n, rather than designating them by their wavevector and polarization. Note that $\mathbf{R}$ and $\mathbf{a}$ are vectors of operators. We introduce the $2n \times 2n$ matrix,

$$\mathbf{\Omega} = \begin{pmatrix} \mathbf{0} & \mathbf{I} \\ -\mathbf{I} & \mathbf{0} \end{pmatrix} \tag{2.71}$$

note that $\mathbf{\Omega}^T\mathbf{\Omega} = \mathbf{\Omega}\mathbf{\Omega}^T = \mathbf{I}$ and $\mathbf{\Omega}\mathbf{\Omega} = \mathbf{\Omega}^T\mathbf{\Omega}^T = -\mathbf{I}$. Then we define the n-mode displacement operator as,

$$D(\mathbf{\Lambda}) = D(\boldsymbol{\lambda}) = \bigotimes_{k=1}^{n} \exp\left[\lambda_k a_k^\dagger - \lambda_k^* a_k\right] = \exp\left[\boldsymbol{\lambda}^T\mathbf{a}^\dagger - \boldsymbol{\lambda}^{*T}\mathbf{a}\right] = \exp\left[i\mathbf{R}^T\mathbf{\Omega}\mathbf{\Lambda}\right] \tag{2.72}$$

Note that a product of displacements yields the new displacement,

$$D(\mathbf{\Lambda}_1)D(\mathbf{\Lambda}_2) = D(\mathbf{\Lambda}_1 + \mathbf{\Lambda}_2)\exp\left[-i\mathbf{\Lambda}_1^T\mathbf{\Omega}\mathbf{\Lambda}_2\right]. \tag{2.73}$$

We also define the n-mode coherent basis matrices,

$$|\boldsymbol{\alpha}\rangle\langle\boldsymbol{\beta}| = \bigotimes_{k}^{n} |\alpha_k\rangle_k\langle\beta_k| \tag{2.74}$$

The n-mode vacuum can be represented in terms of displacement operators [1],

$$|\mathbf{0}\rangle\langle\mathbf{0}| = \int_{\mathbb{C}^n} \frac{d^{2n}\lambda}{\pi^n} \exp\left[-\frac{1}{2}\boldsymbol{\lambda}^T\boldsymbol{\lambda}^*\right] D(\boldsymbol{\lambda}) \tag{2.75}$$

as can be verified by using Eq. 2.68 and expanding the exponentials prior to integration, and then evaluating matrix elements in the Fock basis. From the identity Eq. 2.75 one can establish a duality between the displacement operators and matrix elements $|\boldsymbol{\alpha}\rangle\langle\boldsymbol{\beta}|$,

$$\begin{aligned}
D(\boldsymbol{\lambda}) &= \frac{1}{\pi^{2n}} \int_{\mathbb{C}^n} d^{2n}\alpha \int_{\mathbb{C}^n} d^{2n}\beta h^*_{\alpha\beta}(\boldsymbol{\lambda})|\boldsymbol{\alpha}\rangle\langle\boldsymbol{\beta}| \\
|\boldsymbol{\alpha}\rangle\langle\boldsymbol{\beta}| &= \int_{\mathbb{C}^n} \frac{d^{2n}\lambda}{\pi^n} h_{\alpha\beta}(\boldsymbol{\lambda})D(\boldsymbol{\lambda}) \\
h_{\alpha\beta}(\boldsymbol{\lambda}) &= \exp\left[-\frac{1}{2}\left(\boldsymbol{\lambda}^T\boldsymbol{\lambda}^* + \boldsymbol{\alpha}^T\boldsymbol{\alpha}^* + \boldsymbol{\beta}^T\boldsymbol{\beta}^*\right)\right] \exp\left[\boldsymbol{\alpha}^T\boldsymbol{\beta}^*\right] \exp\left[\boldsymbol{\lambda}^{*T}\boldsymbol{\alpha} - \boldsymbol{\lambda}^T\boldsymbol{\beta}^*\right] \\
h_{\alpha\beta}(\boldsymbol{\lambda}) &= h^*_{\beta\alpha}(-\boldsymbol{\lambda}),
\end{aligned} \tag{2.76}$$

from which one can establish the completeness of the the displacement operators over $\boldsymbol{\lambda} \in \mathbb{C}^n$, in the sense that an arbitrary operator O with support on the n modes

can be written as,

$$\begin{aligned}
O &= \frac{1}{\pi^{2n}} \int_{\mathbb{C}^n} d^{2n}\alpha \int_{\mathbb{C}^n} d^{2n}\beta \langle \boldsymbol{\beta}|O|\boldsymbol{\alpha}\rangle |\boldsymbol{\beta}\rangle\langle\boldsymbol{\alpha}| \\
&= \frac{1}{\pi^{2n}} \int_{\mathbb{C}^n} d^{2n}\alpha \int_{\mathbb{C}^n} d^{2n}\beta \mathrm{Tr}\left\{O|\boldsymbol{\alpha}\rangle\langle\boldsymbol{\beta}|\right\} |\boldsymbol{\beta}\rangle\langle\boldsymbol{\alpha}| \\
&= \frac{1}{\pi^{2n}} \int_{\mathbb{C}^n} d^{2n}\alpha \int_{\mathbb{C}^n} d^{2n}\beta \mathrm{Tr}\left\{O \int_{\mathbb{C}^n} \frac{d^{2n}\lambda}{\pi^n} h_{\alpha\beta}(\boldsymbol{\lambda}) D(\boldsymbol{\lambda})\right\} |\boldsymbol{\beta}\rangle\langle\boldsymbol{\alpha}| \\
&= \int_{\mathbb{C}^n} \frac{d^{2n}\lambda}{\pi^n} \mathrm{Tr}\left\{OD(\boldsymbol{\lambda})\right\} \frac{1}{\pi^{2n}} \int_{\mathbb{C}^n} d^{2n}\alpha \int_{\mathbb{C}^n} d^{2n}\beta h_{\alpha\beta}(\boldsymbol{\lambda}) |\boldsymbol{\beta}\rangle\langle\boldsymbol{\alpha}| \\
&= \int_{\mathbb{C}^n} \frac{d^{2n}\lambda}{\pi^n} \mathrm{Tr}\left\{OD(\boldsymbol{\lambda})\right\} D^\dagger(\boldsymbol{\lambda}) \\
&= \int_{\mathbb{R}^{2n}} \frac{d^{2n}\Lambda}{\pi^n} \mathrm{Tr}\left\{OD(\boldsymbol{\Lambda})\right\} D^\dagger(\boldsymbol{\Lambda})
\end{aligned} \tag{2.77}$$

which will be referred to as Glauber's formula. Glauber's formula implies the useful trace identity, $\mathrm{Tr}\left\{D(\boldsymbol{\Lambda})\right\} = \pi^n \delta^{(2n)}(\boldsymbol{\Lambda})$. The trace in the integrand is the (Wigner) characteristic function,

$$\chi[O](\boldsymbol{\Lambda}) = \mathrm{Tr}\left\{OD(\boldsymbol{\Lambda})\right\}. \tag{2.78}$$

and an operator can be represented by its characteristic function. Traces can then be evaluated as integrals over the characteristic functions [1],

$$\mathrm{Tr}\left\{O_1 O_2\right\} = \int_{\mathbb{R}^{2n}} \frac{d^{2n}\Lambda}{\pi^n} \chi[O_1](\boldsymbol{\Lambda}) \chi[O_2](-\boldsymbol{\Lambda}) \tag{2.79}$$

Given a state ρ composed of two subsystems 1 and 2, composed of n and m modes respectively. We can write ρ in terms of its characteristic function,

$$\rho = \int_{\mathbb{R}^{2n}} \frac{d^{2n}\Lambda_1}{\pi^n} \int_{\mathbb{R}^{2m}} \frac{d^{2m}\Lambda_2}{\pi^m} \mathrm{Tr}\left\{\rho D(\boldsymbol{\Lambda}_1) D(\boldsymbol{\Lambda}_2)\right\} D^\dagger(\boldsymbol{\Lambda}_1) D^\dagger(\boldsymbol{\Lambda}_2), \tag{2.80}$$

and we can then trace out subsystem 2 to obtain the reduced density matrix for subsystem 1, that is $\rho_1 = \mathrm{Tr}_2\left\{\rho\right\}$,

$$\rho_1 = \int_{\mathbb{R}^{2n}} \frac{d^{2n}\Lambda_1}{\pi^n} \mathrm{Tr}\left\{\rho D(\boldsymbol{\Lambda}_1)\right\} D^\dagger(\boldsymbol{\Lambda}_1) \tag{2.81}$$

so we have the reduced characteristic function,

$$\chi[\rho_1](\boldsymbol{\Lambda}_1) = \mathrm{Tr}\left\{\rho D(\boldsymbol{\Lambda}_1)\right\} = \chi[\rho](\boldsymbol{\Lambda}_1, \boldsymbol{\Lambda}_2 = \mathbf{0}). \tag{2.82}$$

The Fourier transform of the Wigner characteristic function is the Wigner function [16],

$$W[\rho](\mathbf{X}) = \int_{\mathbb{R}^{2n}} \frac{d^{2n}\Lambda}{(2\pi)^{2n}} \exp\left[-i\mathbf{X}^T \boldsymbol{\Omega} \boldsymbol{\Lambda}\right] \chi[\rho](\boldsymbol{\Lambda}) \tag{2.83}$$

which is necessarily real, since $\chi[\rho](\mathbf{\Lambda})^* = \chi[\rho](-\mathbf{\Lambda})$ because ρ is hermitian. $\mathbf{X}$ is of dimension $2n$. We decompose $\mathbf{X}$ as $\mathbf{X} = \begin{pmatrix}\mathbf{X}_x^T & \mathbf{X}_y^T\end{pmatrix}^T$. The Wigner functions is in correspondence with classical phase space distributions [17], however it can take on negative values, prohibiting an interpretation of $W[\rho](\mathbf{X})$ as a phase space distribution. Suppose we want the joint distribution of the measurement outcomes obtained when observing the quadratures $\mathbf{x}$. The probability that the quadratures $\mathbf{x}$ takes the values $\mathbf{X}_x$ is given by a marginal of the Wigner function,

$$P(\mathbf{X}_x) = \int_{\mathbb{R}^n} d^n X_y W[\rho](\mathbf{X}) \tag{2.84}$$

2.4 Gaussian states

An important class of quantum states with density matrix ρ_G have characteristic functions which are (complex) multivariate gaussians in the displacements $\mathbf{\Lambda}$. Their characteristic function can be written as,

$$\chi[\rho_G](\mathbf{\Lambda}) = \exp\left[-\frac{1}{2}\mathbf{\Lambda}^T\mathbf{\Omega}\mathbf{V}\mathbf{\Omega}^T\mathbf{\Lambda} + i\langle\mathbf{R}\rangle^T\mathbf{\Omega}\mathbf{\Lambda}\right] \tag{2.85}$$

where $\langle\mathbf{R}\rangle$ is the expectation value of the quadratures,

$$\langle\mathbf{R}\rangle = \mathrm{Tr}\left\{\rho_G\mathbf{R}\right\} \tag{2.86}$$

and $\mathbf{V}$ is the (symmetrized) covariance matrix,

$$\begin{aligned} V_{ij} &= V_{ji} = \frac{1}{2}\left[\mathrm{Cov}\left(R_i, R_j\right) + \mathrm{Cov}\left(R_j, R_i\right)\right] \\ \mathrm{Cov}\left(R_i, R_j\right) &= \left\langle\left(R_i - \langle R_i\rangle\right)\left(R_j - \langle R_j\rangle\right)\right\rangle = \mathrm{Tr}\left\{\rho_G\left(R_i - \langle R_i\rangle\right)\left(R_j - \langle R_j\rangle\right)\right\}. \end{aligned} \tag{2.87}$$

A single-mode coherent state $|X_x + iX_y\rangle$ is a gaussian state with,

$$\begin{aligned} \mathbf{V} &= \mathbf{I} \\ \langle\mathbf{R}\rangle &= 2\begin{pmatrix} X_x & X_y \end{pmatrix}^T. \end{aligned} \tag{2.88}$$

Single-mode squeezed states are characterized by having reduced variance in one quadrature and increased variance in the conjugate quadrature, so that the uncertainty relation derived from Eq. 2.46 is satisfied,

$$\Delta x_k \Delta y_k \geq 1 \tag{2.89}$$

for a mode k. Squeezed states are gaussian, and a single-mode squeezed state has covariance matrix (up to a phase rotation) [16],

$$V_{sq} = \begin{pmatrix} \mathrm{e}^{-r} & 0 \\ 0 & \mathrm{e}^{r} \end{pmatrix} \tag{2.90}$$

where r is called the squeezing parameter. The special case of a squeezed state with $\langle \mathbf{R} \rangle = 0$ is referred to as squeezed vacuum, although this field is by no means empty, in fact the average photon number scales exponentially in r as $\sinh^2(r)$ [15]. Squeezed vacuum consists of Fock states with even photon number,

$$|\text{Squeezed vacuum}\rangle = \frac{1}{\sqrt{\cosh(r)}} \sum_{n=0}^{\infty} \left(-\mathrm{e}^{i\theta}\right)^n \frac{\sqrt{(2n)!}}{2^n n!} \tanh(r)^n |2n\rangle \tag{2.91}$$

If we examine the following linear combinations of quadratures from two modes labelled 1 and 2,

$$\begin{aligned} x_A &= \frac{1}{\sqrt{2}} (x_1 - x_2) \\ y_A &= \frac{1}{\sqrt{2}} (y_1 - y_2) \\ x_B &= \frac{1}{\sqrt{2}} (x_1 + x_2) \\ y_B &= \frac{1}{\sqrt{2}} (y_1 + y_2) \end{aligned} \tag{2.92}$$

then we find the commutators,

$$\begin{aligned} [x_A, x_B] = [y_A, y_B] = [x_A, y_B] = [y_A, x_B] = 0 \\ [x_A, y_A] = [x_B, y_B] = 2i. \end{aligned} \tag{2.93}$$

from which we infer the possibility of states which have reduced variance in x_A and y_B, and a correspondingly increased variance in y_A and x_B. A class of states called two-mode squeezed states have the variances,

$$\text{Var}\,(x_A) = \text{Var}\,(y_B) = \mathrm{e}^{-2r} \tag{2.94}$$

$$\text{Var}\,(x_B) = \text{Var}\,(y_A) = \mathrm{e}^{2r} \tag{2.95}$$

where r is the squeezing parameter. They are characterized by having correlations between the quadratures associated with mode 1 and 2. I.e. for zero variance in x_A we have that x_1 and x_2 are perfectly correlated, and if $\langle x_1 \rangle = \langle x_2 \rangle$ then we have $x_1 = x_2$. Note that these correlations are implied by the quantum state, not by a classical probability distribution, hence mode 1 and 2 are entangled. Two-mode squeezed states are gaussian with covariance matrix (up to a phase rotation),

$$V_{2sq} = \begin{pmatrix} v & \sqrt{v^2-1} & 0 & 0 \\ \sqrt{v^2-1} & v & 0 & 0 \\ 0 & 0 & v & -\sqrt{v^2-1} \\ 0 & 0 & -\sqrt{v^2-1} & v \end{pmatrix}, \text{ and } v = \cosh(2r). \tag{2.96}$$

The special case of two-mode squeezed states with $\langle \mathbf{R} \rangle = 0$ are referred to as two-mode squeezed vacuum states. They are characterized by perfect photon number correlations between mode 1 and 2. In the Fock basis we can write the two-mode squeezed vacuum (TMSV) as,

$$|\text{TMSV}\rangle = \sqrt{1-\lambda^2} \sum_{n=0}^{\infty} \mathrm{e}^{in\theta} (-\lambda)^n |n\rangle_1 |n\rangle_2, \quad \lambda = \tanh(r). \tag{2.97}$$

We note that the photon number correlation is in the product structure of the quantum state, and this implies that mode 1 and 2 are entangled in their photon numbers.

2.5 Modes

In this section we describe the concept of modes and the associated annihilation operators and vector fields. A normal mode consist of an annihilation operator $a_{np}(t)$, a quantum state $|\psi\rangle_{np}$, and a set of vector fields $\mathbf{g}_{np}^{(E)}, \mathbf{g}_{np}^{(B)}, \mathbf{g}_{np}^{(A)}$. To ease notation we will replace the index np by i. We can then write the transverse EM fields as,

$$\begin{aligned}
\mathbf{E}_\perp(\mathbf{r},t) &= \sum_i \left(\mathbf{g}_i^{(E)}(\mathbf{r}) a_i(t) + \mathbf{g}_i^{(E)*}(\mathbf{r}) a_i^\dagger(t) \right) \\
\mathbf{B}_\perp(\mathbf{r},t) &= \sum_i \left(\mathbf{g}_i^{(B)}(\mathbf{r}) a_i(t) + \mathbf{g}_i^{(B)*}(\mathbf{r}) a_i^\dagger(t) \right) \\
\mathbf{A}_\perp(\mathbf{r},t) &= \sum_i \left(\mathbf{g}_i^{(A)}(\mathbf{r}) a_i(t) + \mathbf{g}_i^{(A)*}(\mathbf{r}) a_i^\dagger(t) \right).
\end{aligned} \tag{2.98}$$

By comparison with Eq. 2.40 we identify the vector fields as,

$$\begin{aligned}
\mathbf{g}_i^{(E)}(\mathbf{r}) &= i\mathcal{E}_i \boldsymbol{\epsilon}_i e^{i\mathbf{k}_i\mathbf{r}} \\
\mathbf{g}_i^{(B)}(\mathbf{r}) &= i\frac{\mathcal{E}_i}{c}(\boldsymbol{\kappa}_i \times \boldsymbol{\epsilon}_i) e^{i\mathbf{k}_i\mathbf{r}} \\
\mathbf{g}_i^{(A)}(\mathbf{r}) &= \frac{\mathcal{E}_i}{\omega_i} \boldsymbol{\epsilon}_i e^{i\mathbf{k}_i\mathbf{r}}.
\end{aligned} \tag{2.99}$$

The normal mode annihilation operators a_i and their associated state provide a complete quantum mechanical description of the transverse electromagnetic field. However, it is possible to mix the normal mode annihilation operators together, to obtain a new set of annihilation operators, and these new operators together with their associated state, can then also give a complete quantum mechanical account of the transverse electromagnetic field. We examine the following linear combination of annihilation operators,

$$b_k = \sum_i v_i a_i + \sum_i u_i a_i^\dagger = \mathbf{v}^T \mathbf{a} + \mathbf{u}^T \mathbf{a}^\dagger \tag{2.100}$$

We then examine the commutator,

$$\left[b_k, b_k^\dagger\right] = \sum_i \left(|v_i|^2 - |u_i|^2\right), \tag{2.101}$$

so provided that $\mathbf{v}^H\mathbf{v} - \mathbf{u}^H\mathbf{u} = 1$ then b_k is a ladder operator for the hermitian operator $b_k^\dagger b_k$. We can then form a state $|\psi\rangle_k$ using the basis constructed from the eigenstates of $b_k^\dagger b_k$. The expectation value of an operator $f(b_k, b_k^\dagger)$ with respect to $|\psi\rangle_k$, can then be evaluated using the commutation relation $\left[b_k, b_k^\dagger\right] = 1$. b_k is an annihilation operator of the EM field. We have the special case of annihilation operators b_k for which $u_i = 0$ so that,

$$b_k = \sum_i v_i a_i, \tag{2.102}$$

in this case the ground state $b_k|0\rangle = 0$ will be the electromagnetic vacuum state, and the first excited state will be,

$$b_k^\dagger|0\rangle = \sum_i v_i^* a_i^\dagger|0\rangle, \tag{2.103}$$

corresponding to a single photon spread over a superposition of normal modes. The second excited state will then consist of two photons and so forth. So if $u_i = 0$ then we can associate n photons with the n'th excited state of $b_k^\dagger b_k$. Note that the eigenstates associated with $b_k^\dagger b_k$ do not generally have definite energy. The situation is not as straight forward if $u_i \neq 0$, since in this case the ground state is not the vacuum state. In fact if we examine the single-mode annihilation operator,

$$b_k = \cosh(r)a_1 + \sinh(r)\mathrm{e}^{i\theta}a_1^\dagger \tag{2.104}$$

then one can show that [15] the ground state $b_k|g\rangle_k = 0$ is the single-mode squeezed vacuum state given in Eq. 2.91, when expressed in the Fock basis associated with a_1. Furthermore one can show that,

$$b_k = S^\dagger(\xi)a_1 S(\xi) \tag{2.105}$$

when $\xi = r\mathrm{e}^{i\theta}$ and $S(\xi) = \exp\left[\frac{1}{2}\left(\xi a_1^{\dagger 2} - \xi^* a_1^2\right)\right]$. It then follows that the ground state satisfies,

$$S^\dagger(\xi)a_1 S(\xi)|g\rangle_k = 0 \tag{2.106}$$

from which we can read off the solution,

$$|g\rangle_k = S^\dagger(\xi)|0\rangle_1 \tag{2.107}$$

where $|0\rangle_1$ is the ground state of $a_1^\dagger a_1$. It then follows that the first excited state is,

$$|e_1\rangle_k = b_k^\dagger |g\rangle_k = S^\dagger(\xi)S(\xi)b_k^\dagger S^\dagger(\xi)|0\rangle_1 = S^\dagger(\xi)a_1^\dagger|0\rangle_1 = S^\dagger(\xi)|1\rangle_1 \tag{2.108}$$

and so forth for higher excitations. A similar pattern hold in the case of the annihilation operator,

$$b_k = \cosh(r)a_1 + \sinh(r)\mathrm{e}^{i\theta}a_2^\dagger \tag{2.109}$$

where the ground state is a two-mode squeezed vacuum state Eq. 2.97.

We form a set of new annihilation operators $\mathbf{b} = \begin{pmatrix} b_1 & b_2 & b_3 & \cdots \end{pmatrix}^T$,

$$\begin{pmatrix} \mathbf{b} \\ \mathbf{b}^\dagger \end{pmatrix} = \begin{pmatrix} \mathbf{V} & \mathbf{U} \\ \mathbf{U}^* & \mathbf{V}^* \end{pmatrix} \begin{pmatrix} \mathbf{a} \\ \mathbf{a}^\dagger \end{pmatrix} = \mathbf{K} \begin{pmatrix} \mathbf{a} \\ \mathbf{a}^\dagger \end{pmatrix} \tag{2.110}$$

where $\mathbf{V}$ and $\mathbf{U}$ are $N \times N$ matrices where N is the number of mode operators in $\mathbf{a}$. The commutation relations on $\mathbf{a}$ can be stated as,

$$\begin{pmatrix} \mathbf{a} \\ \mathbf{a}^\dagger \end{pmatrix} \otimes \begin{pmatrix} \mathbf{a}^T & \mathbf{a}^H \end{pmatrix} - \begin{pmatrix} \mathbf{a}^T & \mathbf{a}^H \end{pmatrix} \otimes \begin{pmatrix} \mathbf{a} \\ \mathbf{a}^\dagger \end{pmatrix} = \begin{pmatrix} \mathbf{0} & \mathbf{I} \\ -\mathbf{I} & \mathbf{0} \end{pmatrix} \tag{2.111}$$

where $\mathbf{a}^H$is the conjugate transpose $\mathbf{a}^H = \left(\mathbf{a}^\dagger\right)^T$. In order that the new operators $\mathbf{b}$ can be associated with modes, then the same commutation relations must hold,

$$\begin{pmatrix} \mathbf{b} \\ \mathbf{b}^\dagger \end{pmatrix} \otimes \begin{pmatrix} \mathbf{b}^T & \mathbf{b}^H \end{pmatrix} - \begin{pmatrix} \mathbf{b}^T & \mathbf{b}^H \end{pmatrix} \otimes \begin{pmatrix} \mathbf{b} \\ \mathbf{b}^\dagger \end{pmatrix} = \begin{pmatrix} \mathbf{0} & \mathbf{I} \\ -\mathbf{I} & \mathbf{0} \end{pmatrix} \tag{2.112}$$

Relating $\mathbf{b}$ to $\mathbf{a}$ we find the condition on $\mathbf{K}$,

$$\mathbf{K}\begin{pmatrix} \mathbf{0} & \mathbf{I} \\ -\mathbf{I} & \mathbf{0} \end{pmatrix}\mathbf{K}^T = \begin{pmatrix} \mathbf{V} & \mathbf{U} \\ \mathbf{U}^* & \mathbf{V}^* \end{pmatrix} \begin{pmatrix} \mathbf{0} & \mathbf{I} \\ -\mathbf{I} & \mathbf{0} \end{pmatrix} \begin{pmatrix} \mathbf{V}^T & \mathbf{U}^H \\ \mathbf{U}^T & \mathbf{V}^H \end{pmatrix} = \begin{pmatrix} \mathbf{0} & \mathbf{I} \\ -\mathbf{I} & \mathbf{0} \end{pmatrix} \tag{2.113}$$

giving the conditions

$$\begin{aligned} \mathbf{V}\mathbf{U}^T - \mathbf{U}\mathbf{V}^T &= \mathbf{0} \\ \mathbf{V}\mathbf{V}^H - \mathbf{U}\mathbf{U}^H &= \mathbf{I} \\ \mathbf{V}^H\mathbf{V} - \mathbf{U}^T\mathbf{U}^* &= \mathbf{I} \\ \mathbf{V}^H\mathbf{U} - \mathbf{U}^T\mathbf{V}^* &= \mathbf{0}. \end{aligned} \tag{2.114}$$

A complex matrix $\mathbf{K}$ satisfying the above conditions is called a Bogoliubov transformation. The inverse relation is,

$$\begin{pmatrix} \mathbf{a} \\ \mathbf{a}^\dagger \end{pmatrix} = \mathbf{K}^{-1} \begin{pmatrix} \mathbf{b} \\ \mathbf{b}^\dagger \end{pmatrix} = \begin{pmatrix} \mathbf{V}^H & -\mathbf{U}^T \\ -\mathbf{U}^H & \mathbf{V}^T \end{pmatrix} \begin{pmatrix} \mathbf{b} \\ \mathbf{b}^\dagger \end{pmatrix} \tag{2.115}$$

We now determine the vector fields associated to the new annihilation operators $\mathbf{b}$. To this end we will examine the field operator,

$$\mathbf{F}_{\perp}(\mathbf{r},t) = \sum_i \left(\mathbf{g}_i^{(F)}(\mathbf{r}) a_i(t) + \mathbf{g}_i^{(F)*}(\mathbf{r}) a_i^{\dagger}(t) \right) \tag{2.116}$$

With $\mathbf{F}$ being either $\mathbf{E}, \mathbf{A}$ or $\mathbf{B}$. Shifting to the $\mathbf{b}$ modes,

$$\begin{aligned} \mathbf{F}_{\perp}(\mathbf{r},t) &= \sum_{i,k} \left(\mathbf{g}_i^{(F)}(\mathbf{r}) \left[V_{i,k}^H b_k(t) - U_{i,k}^T b_k^{\dagger}(t) \right] + \mathbf{g}_i^{(F)*}(\mathbf{r}) \left[-U_{i,k}^H b_k(t) + V_{i,k}^T b_k^{\dagger}(t) \right] \right) \\ &= \sum_k \left(\mathbf{h}_k^{(F)}(\mathbf{r}) b_k(t) + \mathbf{h}_k^{(F)*}(\mathbf{r}) b_k^{\dagger}(t) \right). \end{aligned} \tag{2.117}$$

So we can determine the statistics of the field from the state associated with the annihilation operators b_k. We associate the annihilation operator b_k with the vector field $\mathbf{h}_k^{(F)}(\mathbf{r})$,

$$\mathbf{h}_k^{(F)}(\mathbf{r}) = \sum_i \left[\mathbf{g}_i^{(F)}(\mathbf{r}) V_{i,k}^H - \mathbf{g}_i^{(F)*}(\mathbf{r}) U_{i,k}^H \right] \tag{2.118}$$

We now give the corresponding transformation rules for the quadratures. Given the vector of quadratures,

$$\mathbf{R}_a = \begin{pmatrix} \mathbf{x}_a \\ \mathbf{y}_a \end{pmatrix} = \begin{pmatrix} \mathbf{I} & \mathbf{I} \\ -i\mathbf{I} & i\mathbf{I} \end{pmatrix} \begin{pmatrix} \mathbf{a} \\ \mathbf{a}^{\dagger} \end{pmatrix}, \tag{2.119}$$

we make a shift to the new quadratures $\mathbf{R}_b$ given by,

$$\mathbf{R}_b = \begin{pmatrix} \mathbf{x}_b \\ \mathbf{y}_b \end{pmatrix} = \begin{pmatrix} \mathbf{I} & \mathbf{I} \\ -i\mathbf{I} & i\mathbf{I} \end{pmatrix} \begin{pmatrix} \mathbf{b} \\ \mathbf{b}^{\dagger} \end{pmatrix} = \mathbf{S} \begin{pmatrix} \mathbf{x}_a \\ \mathbf{y}_a \end{pmatrix} \tag{2.120}$$

where the transformation $\mathbf{S}$ is related to $\mathbf{K}$ as,

$$\mathbf{S} = \begin{pmatrix} \mathrm{Re}\{\mathbf{U}\} & \mathrm{Im}\{\mathbf{U}\} \\ \mathrm{Im}\{\mathbf{U}\} & -\mathrm{Re}\{\mathbf{U}\} \end{pmatrix} + \begin{pmatrix} \mathrm{Re}\{\mathbf{V}\} & -\mathrm{Im}\{\mathbf{V}\} \\ \mathrm{Im}\{\mathbf{V}\} & \mathrm{Re}\{\mathbf{V}\} \end{pmatrix} \tag{2.121}$$

evidently $\mathbf{S}$ is a real matrix. The transformation $\mathbf{S}$ must preserve the commutation relation,

$$\begin{pmatrix} \mathbf{x}_a \\ \mathbf{y}_a \end{pmatrix} \otimes \begin{pmatrix} \mathbf{x}_a^T & \mathbf{y}_a^T \end{pmatrix} - \begin{pmatrix} \mathbf{x}_a^T & \mathbf{y}_a^T \end{pmatrix} \otimes \begin{pmatrix} \mathbf{x}_a \\ \mathbf{y}_a \end{pmatrix} = 2i \begin{pmatrix} \mathbf{0} & \mathbf{I} \\ -\mathbf{I} & \mathbf{0} \end{pmatrix} \tag{2.122}$$

Implying that $\mathbf{S}$ must satisfy,

$$\mathbf{S} \begin{pmatrix} \mathbf{0} & \mathbf{I} \\ -\mathbf{I} & \mathbf{0} \end{pmatrix} \mathbf{S}^T = \begin{pmatrix} \mathbf{0} & \mathbf{I} \\ -\mathbf{I} & \mathbf{0} \end{pmatrix} \tag{2.123}$$

and the transformation to new quadratures $\mathbf{S}$ is symplectic. We say that a pair of quadratures q and p are conjugate when,

$$[q, p] = 2i. \tag{2.124}$$

Expressing the quadratures as the vector products,

$$q = \mathbf{v}_q^T \mathbf{R} = \mathbf{v}_{qx}^T \mathbf{x} + \mathbf{v}_{qy}^T \mathbf{y} \tag{2.125}$$

$$p = \mathbf{v}_p^T \mathbf{R} = \mathbf{v}_{px}^T \mathbf{x} + \mathbf{v}_{py}^T \mathbf{y}, \tag{2.126}$$

then we may associate the quadratures with the vectors $\mathbf{v}_q = \mathbf{v}_{qx} \oplus \mathbf{v}_{qy}$ and $\mathbf{v}_p = \mathbf{v}_{px} \oplus \mathbf{v}_{py}$, and these vectors are said to be conjugate when,

$$\begin{aligned} \mathbf{v}_{qx}^T \mathbf{v}_{py} - \mathbf{v}_{qy}^T \mathbf{v}_{px} &= \begin{pmatrix} \mathbf{v}_{qx}^T & \mathbf{v}_{qy}^T \end{pmatrix} \begin{pmatrix} \mathbf{0} & \mathbf{I} \\ -\mathbf{I} & \mathbf{0} \end{pmatrix} \begin{pmatrix} \mathbf{v}_{px} \\ \mathbf{v}_{py} \end{pmatrix} \\ &= \mathbf{v}_q^T \mathbf{\Omega} \mathbf{v}_p = 1 \end{aligned} \tag{2.127}$$

for then we have $[q, p] = 2i$.

2.6 Gaussian operations

Gaussian operations are characterized by being of the form,

$$U = e^{iG(\mathbf{a}, \mathbf{a}^\dagger)} \tag{2.128}$$

where $G(\mathbf{a}, \mathbf{a}^\dagger)$ is an hermitian operator that is at most quadratic in the quadrature operators, or equivalently in the annihilation and creation operators. We now seek to evaluate the action of a gaussian operation on the ladder operators, and to this end we attach a dependence on a parameter $t \in [0, 1]$ (which we set to 1 in the end),

$$U(t) = e^{itG(\mathbf{a}, \mathbf{a}^\dagger)} \tag{2.129}$$

we find that under $U(t)$ the ladder operators evolve as,

$$\begin{pmatrix} \mathbf{a}(t) \\ \mathbf{a}^\dagger(t) \end{pmatrix} = e^{-itG(\mathbf{a}, \mathbf{a}^\dagger)} \begin{pmatrix} \mathbf{a} \\ \mathbf{a}^\dagger \end{pmatrix} e^{itG(\mathbf{a}, \mathbf{a}^\dagger)} \tag{2.130}$$

which is the solution to the differential equation,

$$\frac{d}{dt} \begin{pmatrix} \mathbf{a}(t) \\ \mathbf{a}^\dagger(t) \end{pmatrix} = -i \left[G\left(\mathbf{a}(t), \mathbf{a}^\dagger(t)\right), \begin{pmatrix} \mathbf{a}(t) \\ \mathbf{a}^\dagger(t) \end{pmatrix} \right] \tag{2.131}$$

since $G\left(\mathbf{a}(t), \mathbf{a}^\dagger(t)\right)$ is at most quadratic in the ladder operators, then the commutator on the right hand side can at most be linear in the ladder operators. This implies that we can write the differential equation as,

$$\frac{d}{dt} \begin{pmatrix} \mathbf{a}(t) \\ \mathbf{a}^\dagger(t) \end{pmatrix} = \mathbf{g} \begin{pmatrix} \mathbf{a}(t) \\ \mathbf{a}^\dagger(t) \end{pmatrix} + \mathbf{d} \tag{2.132}$$

where $\mathbf{g}$ is a complex matrix and $\mathbf{d}$ is a vector of complex numbers. We can solve this equation via a matrix exponential by noting the pattern,

$$\begin{aligned}
&\frac{d}{dt}\begin{pmatrix}\mathbf{a}(t)\\ \mathbf{a}^\dagger(t)\end{pmatrix} = \mathbf{g}\begin{pmatrix}\mathbf{a}(t)\\ \mathbf{a}^\dagger(t)\end{pmatrix} + \mathbf{d}\\
\Updownarrow&\frac{d}{dt}\left[\begin{pmatrix}\mathbf{a}(t)\\ \mathbf{a}^\dagger(t)\end{pmatrix} - t\mathbf{d}\right] = \mathbf{g}\left[\begin{pmatrix}\mathbf{a}(t)\\ \mathbf{a}^\dagger(t)\end{pmatrix} - t\mathbf{d}\right] + t\mathbf{g}\mathbf{d}\\
\Updownarrow&\frac{d}{dt}\left[\begin{pmatrix}\mathbf{a}(t)\\ \mathbf{a}^\dagger(t)\end{pmatrix} - t\mathbf{d} - \frac{1}{2}t^2\mathbf{g}\mathbf{d}\right] = \mathbf{g}\left[\begin{pmatrix}\mathbf{a}(t)\\ \mathbf{a}^\dagger(t)\end{pmatrix} - t\mathbf{d} - \frac{1}{2}t^2\mathbf{g}\mathbf{d}\right] + \frac{1}{2}t^2\mathbf{g}^2\mathbf{d}\\
\Updownarrow&\frac{d}{dt}\left[\begin{pmatrix}\mathbf{a}(t)\\ \mathbf{a}^\dagger(t)\end{pmatrix} - \frac{1}{1!}t\mathbf{d} - \frac{1}{2!}t^2\mathbf{g}\mathbf{d} - \frac{1}{3!}t^3\mathbf{g}^2\mathbf{d}\right] = \mathbf{g}\left[\begin{pmatrix}\mathbf{a}(t)\\ \mathbf{a}^\dagger(t)\end{pmatrix} - \frac{1}{1!}t\mathbf{d} - \frac{1}{2!}t^2\mathbf{g}\mathbf{d} - \frac{1}{3!}t^3\mathbf{g}^2\mathbf{d}\right]\\
&\qquad\qquad + \frac{1}{3!}t^3\mathbf{g}^3\mathbf{d}
\end{aligned} \tag{2.133}$$

and so forth as

$$\frac{1}{1!}t\mathbf{d} + \frac{1}{2!}t^2\mathbf{g}\mathbf{d} + \frac{1}{3!}t^3\mathbf{g}^2\mathbf{d} + \frac{1}{4!}t^4\mathbf{g}^3\mathbf{d} + \cdots = \left(\sum_{n=1}\frac{1}{n!}t^n\mathbf{g}^{n-1}\right)\mathbf{d}. \tag{2.134}$$

If we assume that the n'th extra term (the term outside parenthesis in Eq. 2.133) $\frac{1}{n!}t^n\mathbf{g}^n\mathbf{d}$ vanishes as n tends to infinity for $t \in [0,1]$, then we have the equation,

$$\begin{aligned}
&\frac{d}{dt}\mathbf{f}(t) = \mathbf{g}\mathbf{f}(t)\\
&\mathbf{f}(t) = \begin{pmatrix}\mathbf{a}(t)\\ \mathbf{a}^\dagger(t)\end{pmatrix} - \left(\sum_{n=1}^{\infty}\frac{1}{n!}t^n\mathbf{g}^{n-1}\right)\mathbf{d}
\end{aligned} \tag{2.135}$$

which has the solution $\mathbf{f}(t) = \mathrm{e}^{\mathbf{g}t}\mathbf{f}(0)$, from which we obtain,

$$\begin{pmatrix}\mathbf{a}(t)\\ \mathbf{a}^\dagger(t)\end{pmatrix} - \left(\sum_{n=1}\frac{1}{n!}t^n\mathbf{g}^{n-1}\right)\mathbf{d} = \mathrm{e}^{\mathbf{g}t}\begin{pmatrix}\mathbf{a}\\ \mathbf{a}^\dagger\end{pmatrix} \tag{2.136}$$

setting $t = 1$ and rearranging we find the sought result,

$$e^{-iG(\mathbf{a},\mathbf{a}^\dagger)}\begin{pmatrix}\mathbf{a}\\ \mathbf{a}^\dagger\end{pmatrix}e^{iG(\mathbf{a},\mathbf{a}^\dagger)} = \mathrm{e}^{\mathbf{g}}\begin{pmatrix}\mathbf{a}\\ \mathbf{a}^\dagger\end{pmatrix} + \left(\sum_{n=1}^{\infty}\frac{1}{n!}\mathbf{g}^{n-1}\right)\mathbf{d} \tag{2.137}$$

and so the action of a gaussian operation on the ladder operators is equivalent to a linear transformation. Note that we need only compute a single commutator to obtain $\mathbf{g}$ and $\mathbf{d}$. Note that unitary evolution preserve the ladder operator commutators, and so it follows that $\mathrm{e}^{\mathbf{g}}$ must be a Bogoliubov transformation. The equivalent

transformation on the quadratures is then necessarily given by a symplectic $\mathbf{S}$ and a vector of real numbers $\boldsymbol{\alpha}$,

$$e^{-iG(\mathbf{R})}\mathbf{R}e^{iG(\mathbf{R})} = \mathbf{S}\mathbf{R} + \boldsymbol{\alpha} \tag{2.138}$$

We now investigate how the characteristic function of a state ρ_i transform as we apply a gaussian operation on ρ_i,

$$\rho_f = \mathrm{e}^{iG}\rho_i\mathrm{e}^{-iG} \tag{2.139}$$

Then

$$\begin{aligned}\chi[\rho_f](\boldsymbol{\Lambda}) = \mathrm{Tr}\left\{\rho_f D(\boldsymbol{\Lambda})\right\} &\to \mathrm{Tr}\left\{\mathrm{e}^{iG}\rho_i\mathrm{e}^{-iG}D(\boldsymbol{\Lambda})\right\} &(2.140)\\ &= \mathrm{Tr}\left\{\rho_i\mathrm{e}^{-iG}D(\boldsymbol{\Lambda})\mathrm{e}^{iG}\right\}, &(2.141)\end{aligned}$$

where we find,

$$\begin{aligned}\mathrm{e}^{-iG}D(\boldsymbol{\Lambda})\mathrm{e}^{iG} &= \exp\left[i\mathrm{e}^{-iG}\mathbf{R}^T\mathrm{e}^{iG}\boldsymbol{\Omega}\boldsymbol{\Lambda}\right] = \exp\left[i\left(\mathbf{S}\mathbf{R}+\boldsymbol{\alpha}\right)^T\boldsymbol{\Omega}\boldsymbol{\Lambda}\right]\\ &= \exp\left[i\mathbf{R}^T\mathbf{S}^T\boldsymbol{\Omega}\boldsymbol{\Lambda}\right]\exp\left[i\boldsymbol{\alpha}^T\boldsymbol{\Omega}\boldsymbol{\Lambda}\right]\\ &= \exp\left[i\mathbf{R}^T\mathbf{S}^T\boldsymbol{\Omega}\mathbf{S}\mathbf{S}^{-1}\boldsymbol{\Lambda}\right]\exp\left[i\boldsymbol{\alpha}^T(\mathbf{S}\mathbf{S}^{-1})^T\boldsymbol{\Omega}\mathbf{S}\mathbf{S}^{-1}\boldsymbol{\Lambda}\right]\\ &= \exp\left[i\mathbf{R}^T\mathbf{S}^T\boldsymbol{\Omega}\mathbf{S}\mathbf{S}^{-1}\boldsymbol{\Lambda}\right]\exp\left[i(\mathbf{S}^{-1}\boldsymbol{\alpha})^T\mathbf{S}^T\boldsymbol{\Omega}\mathbf{S}\mathbf{S}^{-1}\boldsymbol{\Lambda}\right]\\ &= \exp\left[i\mathbf{R}^T\boldsymbol{\Omega}\mathbf{S}^{-1}\boldsymbol{\Lambda}\right]\exp\left[i(\mathbf{S}^{-1}\boldsymbol{\alpha})^T\boldsymbol{\Omega}\mathbf{S}^{-1}\boldsymbol{\Lambda}\right] \qquad (2.142)\end{aligned}$$

So we have the transformation,

$$\chi[\rho_f](\boldsymbol{\Lambda}) = \mathrm{Tr}\left\{\rho_i D(\mathbf{S}^{-1}\boldsymbol{\Lambda})\right\}\exp\left[i(\mathbf{S}^{-1}\boldsymbol{\alpha})^T\boldsymbol{\Omega}\mathbf{S}^{-1}\boldsymbol{\Lambda}\right] \tag{2.143}$$

note that $\mathbf{S}^{-1} = \boldsymbol{\Omega}^T\mathbf{S}^T\boldsymbol{\Omega}$ is also symplectic. So we can deduce the relation,

$$\chi[\rho_f](\boldsymbol{\Lambda}) = \chi[\rho_i](\mathbf{S}^{-1}\boldsymbol{\Lambda})\exp\left[i(\mathbf{S}^{-1}\boldsymbol{\alpha})^T\boldsymbol{\Omega}\mathbf{S}^{-1}\boldsymbol{\Lambda}\right], \tag{2.144}$$

and the characteristic function of ρ_f can be found from the characteristic function of ρ_i by displacing by $\mathbf{S}^{-1}\boldsymbol{\alpha}/2$ and then deforming the conjugate quadratures as $\boldsymbol{\Lambda} \to \mathbf{S}^{-1}\boldsymbol{\Lambda}$. Using this relation, one can show that the effect of a gaussian operation on a gaussian state is simply to transform the covariance matrix and displacement as,

$$\begin{aligned}\mathbf{V}_f &= \mathbf{S}\mathbf{V}_i\mathbf{S}^T &(2.145)\\ \langle\mathbf{R}_f\rangle &= \mathbf{S}\langle\mathbf{R}_i\rangle + \boldsymbol{\alpha} &(2.146)\end{aligned}$$

The beamsplitter transformation is a gaussian transformation which we will use extensively. Its effect on two annihilation operators is to mix them according to an energy preserving (hence unitary) Bogoliubov transformation,

$$\begin{pmatrix} a \\ b \end{pmatrix} \to \begin{pmatrix} \tau & \rho \\ -\rho & \tau \end{pmatrix}\begin{pmatrix} a \\ b \end{pmatrix} \tag{2.147}$$

where $|\tau|^2+|\rho|^2 = 1$ and $\rho\tau^* - \rho^*\tau = 0$. A second important gaussian transformation is the phase rotation, $a \to e^{-i\theta}a$. A phase rotation corresponds to the symplectic map,

$$e^{i\theta a^\dagger a}\begin{pmatrix} x \\ y \end{pmatrix} e^{-i\theta a^\dagger a} = \begin{pmatrix} \cos(\theta) & \sin(\theta) \\ -\sin(\theta) & \cos(\theta) \end{pmatrix}\begin{pmatrix} x \\ y \end{pmatrix} \tag{2.148}$$

2.7 Simplified model of a polychromatic squeezer

We apply some of the concepts and techniques developed in the previous sections to model the generation of squeezed light in a cavity. To this end we will need a model for the intracavity field, and a model for coupling the intracavity field to external input and output fields. We assume that the cavity stretches from 0 to d in z, has cross sectional area A, and we assume that all fields propagate in z. We will assume that the cavity has periodic boundary conditions, and our calculations may then be thought of as a simple model of a ring cavity. We largely follow the work in [18] and [19]. We divide the intracavity electric field into two components,

$$E(z,t) = E_s(z,t) + E_p(z,t) \tag{2.149}$$

with $E_s(z,t)$ being the signal and $E_p(z,t)$ the pump field, with the central frequency of the pump ω_p being twice the central frequency of the signal ω_s. We will assume that the speed of light in the cavity is the same for the pump and signal, and this speed will be labelled by $c = c_0/n_r$. The signal field is initially empty, but will be populated by down-converted photons from the pump field. We assume that the field remains in the vacuum state at other frequencies than the signal and pump. We will assume that the pump field is bright and it will be described as classical, whereas the signal field is weak.

We assume that the signal field is linearly polarized in x and can be approximately described by a single narrow band mode $b(t)$, so we write the signal field as,

$$E_s(z,t) = f(z)b(t) + f^*(z)b^\dagger(t) \tag{2.150}$$

$$b(t) = \sum_n v_n a_n(t) \tag{2.151}$$

$$f(z) = i\sum_n v_n^* \sqrt{\frac{\hbar\omega_n}{2\varepsilon_0 A d}} \mathrm{e}^{ik_n z} \tag{2.152}$$

$$E_s^{(+)}(z,t) = f(z)b(t) \tag{2.153}$$

where $a_n(t)$ is the annihilation operator associated with the wavevector $\mathbf{k}_n = \frac{2\pi}{d}n\hat{\mathbf{z}}$ and polarization in x. Likewise we assume that the pump field amplitude can ap-

proximately be factorized as,

$$E_p(z,t) = g(z)p(t) + g^*(z)p^*(t) \tag{2.154}$$
$$E_p^{(+)}(z,t) = g(z)p(t). \tag{2.155}$$

We will assume that the fields are to a good approximation plane waves, $f(z) \approx i\sqrt{\frac{\hbar\omega_s}{2\varepsilon_0 Ad}}\mathrm{e}^{i\frac{\omega_s}{c}z}$ and $g(z) \approx i\sqrt{\frac{\hbar 2\omega_s}{2\varepsilon_0 Ad}}\mathrm{e}^{i\frac{2\omega_s}{c}z}$.

We model the evolution of an intracavity plane wave mode $a_n(t)$ using the Heisenberg equation and the Hamiltonian [2],

$$\frac{d}{dt}a_n(t) = \frac{1}{i\hbar}\left[a_n(t), H(t)\right] \tag{2.156}$$
$$H(t) = H_0 + H_I(t) \tag{2.157}$$
$$H_0(t) = \sum_{n,p}\hbar\omega_n a_{np}^\dagger(t)a_{np}(t) \tag{2.158}$$
$$H_I(t) = \chi\int_0^d dz\int_A dxdy E_p^{(+)}(r,t)E_s^{(-)}(r,t)^2 + \mathrm{H.c} \tag{2.159}$$

where $\omega_n = |k_n|c$. Since the fields are approximately plane waves, we have,

$$H_I(t) \approx -i\hbar\frac{\kappa}{2}p(t)b^\dagger(t)^2 + \mathrm{H.c} \tag{2.160}$$
$$\kappa = \chi\sqrt{\frac{\hbar}{Ad}}\left[\frac{\omega_s}{\varepsilon_0}\right]^{3/2} \tag{2.161}$$

If the wavevector of the pump is not exactly twice the wavevector of the signal, then the integral over space would have been reduced by the oscillatory integrand, effectively reducing the coupling constant κ.

From the linearity of the Heisenberg equation we obtain the equation of motion,

$$\frac{d}{dt}b(t) = \frac{1}{i\hbar}\left[b(t), H(t)\right] \tag{2.162}$$

we can then evaluate the commutators,

$$\begin{aligned}[b(t), H_0(t)] &= \left[\sum_n v_n a_n(t), H_0(t)\right] \\ &= \sum_n \hbar\omega_n v_n a_n(t) \approx \hbar\omega_s b(t)\end{aligned} \tag{2.163}$$

and

$$\begin{aligned}[b(t), H_I(t)] &= -i\hbar\frac{\kappa}{2}p(t)\left[b(t), b^\dagger(t)^2\right] \\ &= -i\hbar\kappa p(t)b^\dagger(t)\end{aligned} \tag{2.164}$$

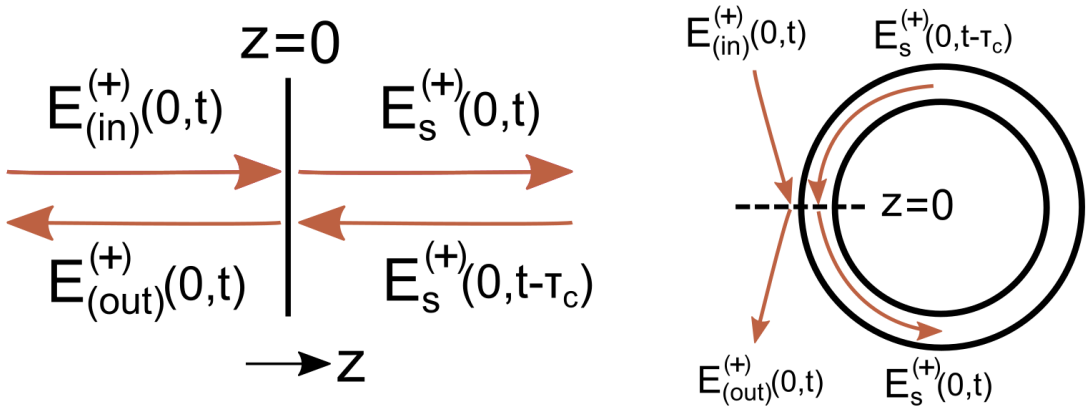

Figure 2.2: *A sketch of the beamsplitter boundary conditions.*

So we have the equation of motion,

$$\frac{d}{dt}b(t) = -i\omega_s b(t) - \kappa p(t) b^\dagger(t) \tag{2.165}$$

We factor out the central frequencies as $b(t) = c(t)\mathrm{e}^{-i\omega_s t}$ and $p(t) = \mathrm{e}^{-i2\omega_s t}e(t)$, then our equation of motion is,

$$\frac{d}{dt}c(t) = -\kappa e(t) c^\dagger(t). \tag{2.166}$$

Before we can solve this equation, we need a model for how the intracavity field couples to an external input field $E^{(+)}_{(\mathrm{in})}(z,t)$ and an external output field $E^{(+)}_{(\mathrm{out})}(z,t)$. This coupling is modelled as a beamsplitter boundary condition on the cavity at $z = 0$,

$$E^{(+)}_{(\mathrm{out})}(0,t) = -\rho E^{(+)}_{(\mathrm{in})}(0,t) + \sqrt{1-\rho^2}E^{(+)}_s(0,t-\tau_c) \tag{2.167}$$

$$E^{(+)}_s(0,t) = \rho E^{(+)}_s(0,t-\tau_c) + \sqrt{1-\rho^2}E^{(+)}_{(\mathrm{in})}(0,t) \tag{2.168}$$

where $\tau_c = d/c$ is the roundtrip time and ρ is the reflection coefficient. These relations are sketched in Fig. 2.2. We multiply through by $-i\sqrt{\frac{2\varepsilon_0 Ad}{\hbar\omega_s}}\mathrm{e}^{i\omega_s t}$, and for brevity we will write,

$$a_{(\mathrm{out})/(\mathrm{in})}(z,t) = -i\sqrt{\frac{2\varepsilon_0 Ad}{\hbar\omega_s}}\mathrm{e}^{i\omega_s t}E^{(+)}_{(\mathrm{out})/(\mathrm{in})}(z,t). \tag{2.169}$$

Let L be the length of the box over which we want to describe the external fields (with cross sectional area A). We will assume that $L \gg d$ and that we can approximately write the central frequency as $\omega_s = \frac{2\pi}{L}sc_0$, where s is the index we associate with

ω_s. We let $r_n(t)$ be a plane wave annihilation operator for the input field, associated with wavevector $\frac{2\pi}{L}(s+n)\hat{\mathbf{z}}$. The incoming field can then be written,

$$a_{(\mathrm{in})}(z,t) \approx \sqrt{\frac{d}{L}} \mathrm{e}^{i\omega_s t} \sum_{n=-\Delta}^{\Delta} r_n(t) \mathrm{e}^{i\frac{2\pi}{L}(n+s)z} \tag{2.170}$$

where 2Δ is the range of relevant wavevectors, centred on $\frac{2\pi}{L}s\hat{\mathbf{z}}$. Note that the external fields are free fields, hence we know the time dependence, $r_n(t) = r_n(0)\mathrm{e}^{-i\frac{2\pi}{L}(n+s)c_0 t}$. We let $l_n(t)$ be an annihilation operator associated with the outgoing field, having wavevector $-\frac{2\pi}{L}(s+n)\hat{\mathbf{z}}$. Then we can write the external fields evaluated in $z=0$ as,

$$\begin{aligned} a_{(\mathrm{in})}(t) &= a_{(\mathrm{in})}(z=0,t) = \sqrt{\frac{d}{L}} \sum_{n=-\Delta}^{\Delta} r_n(0)\mathrm{e}^{-i\frac{2\pi}{L}nc_0 t} \\ a_{(\mathrm{out})}(t) &= a_{(\mathrm{out})}(z=0,t) = \sqrt{\frac{d}{L}} \sum_{n=-\Delta}^{\Delta} l_n(0)\mathrm{e}^{-i\frac{2\pi}{L}nc_0 t} \end{aligned} \tag{2.171}$$

Meanwhile we also have,

$$\left(-i\sqrt{\frac{2\varepsilon_0 A d}{\hbar\omega_s}}\mathrm{e}^{i\omega_s t}\right) E_s^{(+)}(0, t-\tau_c) = \phi c(t-\tau_c)\mathrm{e}^{i\omega_s\tau_c} \tag{2.172}$$

where $\phi = \sum_n v_n^*$. ϕ relates to the amplitude of the intracavity field at the boundary. With this new notation the beamsplitter boundary conditions read,

$$a_{(\mathrm{out})}(t) = -\rho a_{(\mathrm{in})}(t) + \sqrt{1-\rho^2}\mathrm{e}^{i\omega_s\tau_c}c(t-\tau_c) \tag{2.173}$$

$$c(t) = \mathrm{e}^{i\omega_s\tau_c}\rho c(t-\tau_c) + \sqrt{1-\rho^2}a_{(\mathrm{in})}(t). \tag{2.174}$$

Note that $1/\phi$ has been absorbed into $a_{\mathrm{out}}(t)$ and $a_{\mathrm{in}}(t)$, and we will reintroduce ϕ later in the calculations. Also note that the above beamsplitter relations assume that $|\phi|$ is relatively large, so that the external fields mainly couple to the intracavity mode described by $b(t)$. Given that ω_s is the central frequency of a resonance then $\mathrm{e}^{i\omega_s\tau_c} = 1$.

However, we find that we can approximately substitute this boundary condition for a term in our equation of motion when the bandwidth of $c(t)$ is smaller than $1/\tau_c$, and the cavity loss per round trip is small. Under this condition we have to a good approximation,

$$\frac{d}{dt}c(t) \approx \frac{c(t) - c(t-\tau_c)}{\tau_c}. \tag{2.175}$$

We write the change in $c(t)$ generated by the equation of motion, over a round trip, as,

$$\Delta c_H(t) = -\kappa e(t) c^\dagger(t) \tau_c \tag{2.176}$$

Likewise there is a change in $c(t)$ generated by the boundary condition, over a round trip,

$$\Delta c_B(t) = c(t) - c(t-\tau_c) = (\rho - 1)\, c(t-\tau_c) + \sqrt{1-\rho^2}\, a_{(\mathrm{in})}(t). \tag{2.177}$$

We write the reflection coefficient as $\rho = \mathrm{e}^{-\gamma\tau_c} \approx 1 - \gamma\tau_c$ where γ is the coupling rate between the external fields and the intracavity field. We write the transmission coefficient as, $\sqrt{1-\rho^2} \approx \sqrt{2\gamma\tau_c}$. So we find,

$$\Delta c_B(t) = -\gamma\tau_c c(t-\tau_c) + \sqrt{2\gamma\tau_c}\, a_{(\mathrm{in})}(t) \approx -\gamma\tau_c c(t) + \sqrt{2\gamma\tau_c}\, a_{(\mathrm{in})}(t) \tag{2.178}$$

and the total differential is then,

$$\Delta c(t) = \Delta c_H(t) + \Delta c_B(t) \tag{2.179}$$

from which we obtain a differential equation,

$$\frac{\Delta c(t)}{\tau_c} = -\kappa e(t) c^\dagger(t) - \gamma c(t) + \sqrt{\frac{2\gamma}{\tau_c}}\, a_{(\mathrm{in})}(t). \tag{2.180}$$

A more rigorous justification for the coupling terms is given in [19]. Finally then, we state our equation of motion, with a boundary condition, as,

$$\frac{d}{dt} c(t) \approx \frac{\Delta c(t)}{\tau_c} = -\kappa e(t) c^\dagger(t) - \gamma c(t) + \sqrt{\frac{2\gamma}{\tau_c}}\, a_{(\mathrm{in})}(t) \tag{2.181}$$

$$a_{(\mathrm{out})}(t) = -a_{(\mathrm{in})}(t) + \sqrt{2\gamma\tau_c}\, c(t) \tag{2.182}$$

We eliminate the intracavity field using the boundary condtion,

$$\frac{d}{dt}\left[a_{(\mathrm{out})}(t) + a_{(\mathrm{in})}(t)\right] + \kappa e(t)\left[a^\dagger_{(\mathrm{out})}(t) + a^\dagger_{(\mathrm{in})}(t)\right] + \gamma\left[a_{(\mathrm{out})}(t) - a_{(\mathrm{in})}(t)\right] = 0. \tag{2.183}$$

We now reintroduce the coupling factor ϕ, thereby obtaining,

$$\frac{d}{dt}\left[a_{(\mathrm{out})}(t) + a_{(\mathrm{in})}(t)\right] + \frac{\phi}{\phi^*}\kappa e(t)\left[a^\dagger_{(\mathrm{out})}(t) + a^\dagger_{(\mathrm{in})}(t)\right] + \gamma\left[a_{(\mathrm{out})}(t) - a_{(\mathrm{in})}(t)\right] = 0, \tag{2.184}$$

we will absorb the phase factor ϕ/ϕ^* into κ. We can split this equation into frequency components by multiplying with $\mathrm{e}^{i\frac{2\pi}{L}kc_0t}$ for $k \in [-\Delta, \Delta]$, and integrating from $-L/(2c_0)$ to $L/(2c_0)$ over t. We introduce the symbols,

$$\alpha_v = \frac{2\pi}{L/c_0}v \tag{2.185}$$

$$e(\alpha_v) = \frac{1}{L/c_0}\int_{-L/(2c_0)}^{L/(2c_0)} dt e(t)\mathrm{e}^{-i\frac{2\pi}{L/c_0}tv} \tag{2.186}$$

from which we obtain,

$$-i\alpha_k\left(l_k(0)+r_k(0)\right)+\kappa\sum_{n=-\Delta}^{\Delta}e\left(\alpha_{-n-k}\right)\left(l_n^\dagger(0)+r_n^\dagger(0)\right)+\gamma\left(l_k(0)-r_k(0)\right)=0. \tag{2.187}$$

We rewrite the above system of equations as a matrix equation, and to this end we introduce the vectors and matrices,

$$\mathbf{a}_{(\mathrm{in})} = \begin{pmatrix} r_{-\Delta}(0) & r_{-\Delta+1}(0) & \cdots & r_{\Delta}(0) \end{pmatrix}^T \tag{2.188}$$

$$\mathbf{a}_{(\mathrm{out})} = \begin{pmatrix} l_{-\Delta}(0) & l_{-\Delta+1}(0) & \cdots & l_{\Delta}(0) \end{pmatrix}^T \tag{2.189}$$

$$D_{ij} = \delta_{ij}\alpha_i \tag{2.190}$$

$$E_{ij} = e\left(\alpha_{-i-j}\right) \tag{2.191}$$

with the indices being in the interval $i, j \in [-\Delta, \Delta]$ and $\left(\mathbf{a}_{(\mathrm{in})}\right)_i = r_i(0)$ and $\left(\mathbf{a}_{(\mathrm{out})}\right)_i = l_i(0)$. So we obtain the matrix equation,

$$-i\mathbf{D}\left(\mathbf{a}_{(\mathrm{out})}+\mathbf{a}_{(\mathrm{in})}\right)+\kappa\mathbf{E}\left(\mathbf{a}_{(\mathrm{out})}^\dagger+\mathbf{a}_{(\mathrm{in})}^\dagger\right)+\gamma\left(\mathbf{a}_{(\mathrm{out})}-\mathbf{a}_{(\mathrm{in})}\right)=0. \tag{2.192}$$

Upon rearranging and combining with the conjugate equation we obtain,

$$\begin{pmatrix} \mathbf{a}_{(\mathrm{out})} \\ \mathbf{a}_{(\mathrm{out})}^\dagger \end{pmatrix} = \left(2\gamma\mathbf{M}^{-1}-\mathbf{I}\right)\begin{pmatrix} \mathbf{a}_{(\mathrm{in})} \\ \mathbf{a}_{(\mathrm{in})}^\dagger \end{pmatrix} \tag{2.193}$$

where we've defined the matrix,

$$\mathbf{M} = \begin{pmatrix} \gamma\mathbf{I}-i\mathbf{D} & \kappa\mathbf{E} \\ \kappa^*\mathbf{E}^* & \gamma\mathbf{I}+i\mathbf{D} \end{pmatrix}. \tag{2.194}$$

This is a transformation connecting two sets of ladder operators. Since both sets of ladder operators satisfy the fundamental commutation relations, it follows that the transformation relating them is a Bogoliubov transform (at least to within the used approximations). We make a change to quadratures as,

$$\begin{pmatrix} \mathbf{x} \\ \mathbf{y} \end{pmatrix} = \begin{pmatrix} \mathbf{I} & \mathbf{I} \\ -i\mathbf{I} & i\mathbf{I} \end{pmatrix}\begin{pmatrix} \mathbf{a} \\ \mathbf{a}^\dagger \end{pmatrix} = \mathbf{T}\begin{pmatrix} \mathbf{a} \\ \mathbf{a}^\dagger \end{pmatrix} \tag{2.195}$$

so Eq. 2.193 becomes,

$$\begin{pmatrix} \mathbf{x}^{(\text{out})} \\ \mathbf{y}^{(\text{out})} \end{pmatrix} = \left(2\gamma \mathbf{L}^{-1} - \mathbf{I}\right) \begin{pmatrix} \mathbf{x}^{(\text{in})} \\ \mathbf{y}^{(\text{in})} \end{pmatrix}, \tag{2.196}$$

where we've defined the matrix,

$$\mathbf{L} = \mathbf{T}\mathbf{M}\mathbf{T}^{-1} = \begin{pmatrix} \gamma\mathbf{I} & \mathbf{D} \\ -\mathbf{D} & \gamma\mathbf{I} \end{pmatrix} + \begin{pmatrix} \text{Re}\left\{\kappa\mathbf{E}\right\} & \text{Im}\left\{\kappa\mathbf{E}\right\} \\ \text{Im}\left\{\kappa\mathbf{E}\right\} & -\text{Re}\left\{\kappa\mathbf{E}\right\} \end{pmatrix}. \tag{2.197}$$

Since the matrix transform in Eq. 2.196 connects two sets of quadrature operators, it must be symplectic and we label it as $\mathbf{S}$,

$$\mathbf{S} = 2\gamma\mathbf{L}^{-1} - \mathbf{I}. \tag{2.198}$$

We can obtain the reduced characteristic function for the output modes as,

$$\chi[\rho_{(\text{out})}](\mathbf{\Lambda}) = \text{Tr}\left\{\rho D_{(\text{out})}(\mathbf{\Lambda})\right\}, \tag{2.199}$$

where ρ is the total density matrix, including the input and output modes, and $\rho_{(\text{out})}$ is the reduced density matrix for the output modes, and $D_{(\text{out})}(\mathbf{\Lambda})$ is the displacement operator for the output modes. If we let $\mathbf{R}_{(\text{out})} = \begin{pmatrix} \mathbf{x}^{(\text{out})} & \mathbf{y}^{(\text{out})} \end{pmatrix}^T$ then we have the displacement operator,

$$\begin{aligned} D_{(\text{out})}(\mathbf{\Lambda}) &= \exp\left[i\mathbf{R}_{(\text{out})}^T \mathbf{\Omega}\mathbf{\Lambda}\right] \\ &= \exp\left[i\mathbf{R}_{(\text{in})}^T \mathbf{\Omega}\mathbf{S}^{-1}\mathbf{\Lambda}\right]. \end{aligned} \tag{2.200}$$

So we can evaluate the output characteristic function as,

$$\begin{aligned} &\chi[\rho_{(\text{out})}](\mathbf{\Lambda}) = \text{Tr}\left\{\rho \exp\left[i\mathbf{R}_{(\text{in})}^T \mathbf{\Omega}\mathbf{S}^{-1}\mathbf{\Lambda}\right]\right\} = \chi[\rho_{(\text{in})}](\mathbf{S}^{-1}\mathbf{\Lambda}) \\ &= \exp\left[-\frac{1}{2}\mathbf{\Lambda}^T\mathbf{S}^{-T}\mathbf{S}^{-1}\mathbf{\Lambda}\right] = \exp\left[-\frac{1}{2}\mathbf{\Lambda}^T\mathbf{\Omega}\mathbf{S}\mathbf{S}^T\mathbf{\Omega}^T\mathbf{\Lambda}\right] \end{aligned} \tag{2.201}$$

since the input state was the vacuum state. The density matrix of the output modes can then be computed as,

$$\rho_{(\text{out})} = \int_{\mathbb{R}^{2d}} \frac{d^{2d}\mathbf{\Lambda}}{\pi^d} \chi[\rho_{(\text{out})}](\mathbf{\Lambda}) D^\dagger(\mathbf{\Lambda}) \tag{2.202}$$

where $d = 2\Delta + 1$.

Chapter 3

Bell inequalities and non-locality

In this chapter we describe the concept of Bell inequalities and what the implications are of the experimentally observed violation of said inequalities. We start by introducing the mathematical structure and philosophy connected with Bell inequalities. We will mainly use the expositions given in [7], [20], [21], however we will in this work arrive at the concept of the Bell polytope via a slightly different route than the cited references. We do this to try and get another perspective on the arguments leading to the Bell polytope.

We then derive an important Bell inequality, the W^3ZB inequality. Following this we present an analysis of an all optical setup, designed with the intent of demonstrating a violation of the W^3ZB inequality in a multi-party scenario, with the participants separated by up to 60 km (assuming a fiber loss of 0.3 dB/km).

The predictions made by quantum mechanics are statistical, in the sense that the theory predicts probability distributions for observing particular outcomes, with respect to a particular measurement, rather than giving an exact account of what will actually occur. These various distributions associated with different measurements are however not independent, as they are all derivable once the quantum state is known. It seems a reasonable question to ask, whether it is possible to formulate a theory of the microscopic which gives more definite predictions, rather than just probability distributions. In particular it seems natural that such a theory should contain particle-like objects, since such objects are observed in experiment. The question then becomes how quantum mechanics, a theory of probability, would arise from such an underlying model. As pointed out by Pitowsky [20], it has been realized repeatedly that the probabilities predicted by quantum mechanics differs somehow from what we encounter in a probabilistic description of classical physics. That is, a description of classical physics were certain things, such as detailed trajectories of the involved particles, are unknown (e.g. the kinetic theory of gases). This difference was noticed for example when it was attempted to reformulate quantum mechanics as a phase space theory. That is, for a single particle we want to introduce a function

in the position and momentum $W(x,p)$, such that if an observable $\hat{O}$ is expressed as a function of the position and momentum operators,

$$\hat{O} = f(\hat{q},\hat{p}) \tag{3.1}$$

then we can compute the expectation value $\langle\hat{O}\rangle$ as,

$$\langle\hat{O}\rangle = \int_{\infty}^{\infty} dq \int_{\infty}^{\infty} dp f(q,p) W(q,p) \tag{3.2}$$

and the operators have been replaced by scalars in $f(q,p)$. Such a function cannot exist, since the idea is spoiled by the non-commutativity of the position and momentum operators [22]. Following Ballentine, consider the expectation values of the Hermitian operators $\frac{1}{2}\left(\hat{q}^2\hat{p}^2 + \hat{p}^2\hat{q}^2\right)$ and $\frac{1}{4}(\hat{q}\hat{p}+\hat{p}\hat{q})^2$, the existence of a phase space distribution would imply,

$$\begin{aligned}\left\langle \frac{1}{2}\left(\hat{q}^2\hat{p}^2 + \hat{p}^2\hat{q}^2\right)\right\rangle &= \int_{\infty}^{\infty} dq \int_{\infty}^{\infty} dp \frac{1}{2}\left(q^2p^2 + p^2q^2\right) W(q,p) \\ &= \int_{\infty}^{\infty} dq \int_{\infty}^{\infty} dp \frac{1}{4}\left(qp+pq\right)^2 W(q,p) = \left\langle \frac{1}{4}(\hat{q}\hat{p}+\hat{p}\hat{q})^2 \right\rangle \end{aligned} \tag{3.3}$$

Which is incorrect since,

$$\frac{1}{4}(\hat{q}\hat{p}+\hat{p}\hat{q})^2 = \frac{1}{2}\left(\hat{q}^2\hat{p}^2 + \hat{p}^2\hat{q}^2\right) + \frac{3}{4}\hbar^2. \tag{3.4}$$

In general one finds that a phase space distribution $W(\alpha)$ can be defined with respect to a particular mapping from an observable $\hat{G}$ to a scalar function $g(\alpha)$ [2], [15]. An example is the Wigner quasi-probability distribution $W(q,p)$, which is obtained from the Wigner-Weyl transform of the density matrix, and the function $g(q,p)$ is then obtained as the Wigner-Weyl transform of the operator $\hat{G}$ [1], [17]. However, the Wigner quasi-probability distribution can take on negative values in general, prohibiting a probabilistic interpretation of the distribution.

Following the pioneering thought experiment due to Einstein, Podolsky and Rosen [6], [23], it was realized that if the predictions of quantum theory are correct, then the workings of nature cannot be explained by a local causal hidden variable model. That is, an event A is not constrained to only depend on other events contained within the past light-cone of A. To arrive at this conclusion, we follow Pitowsky [20] and start with the work of the mathematician George Bool. Bool noted that the probabilities of the occurrence of logically related events, must satisfy *linear* inequalities as well as equalities.
As an example, let $P(E)$ be the relative frequency of the event E occurring, and $P(E_1 \cap E_2)$ be the relative frequency of the events E_1 and E_2 co-occurring, then naturally,

$$P(E_1) - P(E_1 \cap E_2) \geq 0 \tag{3.5}$$

Let $P(E_1 \cup E_2)$ be the relative frequency of either E_1 or E_2 (or both) occurring, then

$$P(E_1) + P(E_2) = P(E_1 \cap E_2) + P(E_1 \cup E_2) \tag{3.6}$$

From the fact that $P(E_1 \cup E_2) \leq 1$, we have,

$$P(E_1) + P(E_2) - P(E_1 \cap E_2) \leq 1. \tag{3.7}$$

Finally, we have conditions of positivity and normalization,

$$1 \geq P(E_1 \cap E_2) \geq 0 \quad , \quad 1 \geq P(E_1) \geq 0 \quad , \quad 1 \geq P(E_2) \geq 0 \tag{3.8}$$

Boole dubbed such inequalities as *'conditions of possible experience'*, and their violation would indicate that the data from which the relative frequencies were extracted, could not have been obtained from actual observation, *"When satisfied they indicate that the data may have, when not satisfied they indicate that the data cannot have, resulted from actual observation"*.
Considering the, in principal independent, set of relative frequencies $P(E_1)$, $P(E_2)$ and $P(E_1 \cap E_2)$ as coordinates in $\mathcal{R}^3$, we realize that the above inequalities must restrict the points $(P(E_1), P(E_2), P(E_1 \cap E_2))$ to a region P of the full space. Since this region is bounded by linear inequalities it will be a convex polytope. A convex polytope is describable via a set of linear inequalities, or as a convex sum of the vertices of the polytope. The validity of this duality in arbitrary dimension is known as the Weyl-Minkowski theorem [20], [24]. One might then wonder, what procedure would yield the vertices of this polytope. A method proposed by Pitowsky is to write up the truth table for the logically related events E_1, E_2, and $E_1 \cap E_2$,

E_1	E_2	$E_1 \cap E_2$
0	0	0
1	0	0
0	1	0
1	1	1

(3.9)

with 0 corresponding to the event not occurring, and 1 corresponding to the event occurring. Each row corresponds to a scenario where certain events are true. Supposing that the system under study has a probability of realizing each of these four possible scenarios, from the top row we might denote these probabilities by p_1, p_2, p_3, p_4. Given that the truth table lists all possibilities, then we have $p_1 + p_2 + p_3 + p_4 = 1$. The observed relative frequencies $(p(E_1), p(E_2), p(E_1 \cap E_2))$ will then be given by the vector sum,

$$\begin{pmatrix} p(E_1) \\ p(E_2) \\ p(E_1 \cap E_2) \end{pmatrix} = p_1 \begin{pmatrix} 0 \\ 0 \\ 0 \end{pmatrix} + p_2 \begin{pmatrix} 1 \\ 0 \\ 0 \end{pmatrix} + p_3 \begin{pmatrix} 0 \\ 1 \\ 0 \end{pmatrix} + p_4 \begin{pmatrix} 1 \\ 1 \\ 1 \end{pmatrix}, \tag{3.10}$$

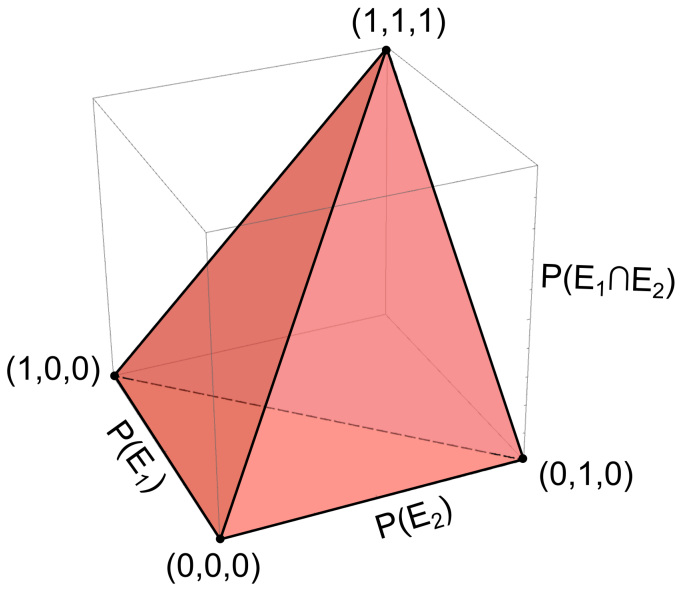

Figure 3.1: *We sketch the polytope with its vertices given by the rows of table 3.9.*

i.e. the probability of a particular event occurring is the sum of all p_n that would result in that event. Hence we see that the region P can be described as a convex sum of the rows of the truth table. It is well known from geometry that such a convex sum over vectors will span a polytope, with the vertices of the polytope corresponding to the vectors [24]. This convex polytope is sketched in Fig 3.1 and can equally well be described by the above convex sum, or the above inequalities.

3.1 The counter-factual decomposition

We will now analyse a hypothetical experimental record, obtained from measurements on some system. We will write up the experimental outcomes in a truth table as above. We will attempt to describe the probabilities of particular observations, via convex sums over scenarios, as in Eq. 3.10.
For our purposes we can think of a measurement on a microscopic system, as being composed of the stages,

- An input is chosen by the scientists, this input is typically a measurement setting, i.e. the configuration of the measurement apparatus. We symbolize a particular input by an integer x. A particular value of x could for example correspond to some number of degrees by which we turn a knob.

- Some, usually uncontrolled, physical events unfold.

- We obtain an output, which could for example be a detector clicking, or a meter showing a particular value, etc. We symbolize a particular output by an integer a. That is, a particular value of a implies that some particular physical condition was met, for example a meter gave a reading lying within some range.

As an example, we suppose that we have two possible inputs corresponding to $x = 1$ and $x = 2$. For brevity we will denote $x = 1$ as 1_x, and $x = 2$ as 2_x. For 1_x we have two possible outputs, 1_a ($a = 1$) and 2_a ($a = 2$). For 2_x we have three possible outputs $1_a, 2_a$ and 3_a. For experiments where we use input 1_x we measure the probabilities $p_s^{(1)}$ for the following scenarios,

1_a	2_a	1_x
1	0	$p_1^{(1)}$
0	1	$p_2^{(1)}$

(3.11)

where a scenario is a particular row of the above table. The measurement of $p_s^{(1)}$ proceeds simply by noting how often the two scenarios each occur. That is, the probabilities are defined by counting,

$$p_s^{(1)} = \frac{\text{Number of observations of scenario s with input } 1_x}{\text{Total number of observations where the input was } 1_x} \tag{3.12}$$

Note that since all possible scenarios are covered, we have $\sum_s p_s^{(1)} = 1$.
Likewise for experiments where we use input 2_x, we measure the probabilities $p_s^{(2)}$,

1_a	2_a	2_x
1	0	$p_1^{(2)}$
0	1	$p_2^{(2)}$
0	0	$p_3^{(2)}$

(3.13)

and we likewise have $\sum_s p_s^{(2)} = 1$. We define a behaviour $B^{(n)}$ as the set of probabilities, that the outputs specified in the columns occur,

$$B^{(1)} = \begin{pmatrix} p(1_a|1_x) \\ p(2_a|1_x) \end{pmatrix} \quad , \quad B^{(2)} = \begin{pmatrix} p(1_a|2_x) \\ p(2_a|2_x) \end{pmatrix} \tag{3.14}$$

From the tables we can extract the two matrices,

$$\begin{aligned} M^{(1)} &= \begin{pmatrix} 1 & 0 \\ 0 & 1 \end{pmatrix} \\ M^{(2)} &= \begin{pmatrix} 1 & 0 \\ 0 & 1 \\ 0 & 0 \end{pmatrix}^T = \begin{pmatrix} 1 & 0 & 0 \\ 0 & 1 & 0 \end{pmatrix}. \end{aligned} \tag{3.15}$$

Letting $M_s^{(n)}$ be the s'th column of $M^{(n)}$, we can compute the behaviours as,

$$B^{(n)} = \sum_s M_s^{(n)} p_s^{(n)}. \tag{3.16}$$

We will now make an important assumption. We assume that the observed frequencies $p_s^{(n)}$ can be decomposed as,

$$\begin{aligned} p_1^{(1)} &= \pi_{11} + \pi_{12} + \pi_{13} \\ p_2^{(1)} &= \pi_{21} + \pi_{22} + \pi_{23} \\ p_1^{(2)} &= \pi_{11} + \pi_{21} \\ p_2^{(2)} &= \pi_{12} + \pi_{22} \\ p_3^{(2)} &= \pi_{13} + \pi_{23} \end{aligned} \tag{3.17}$$

where π_{ks}, lying in the range $[0, 1]$, are probabilities. The motivation behind the decomposition will be given in a bit. We note a few important aspects of this decomposition. The probabilities π_{ks} are normalized, since

$$\sum_{s=1}^{3} \sum_{k=1}^{2} \pi_{ks} = \sum_s p_s^{(v)} = 1, \tag{3.18}$$

for $v \in \{1, 2\}$. The probability $p_k^{(1)}$ is obtained by summing π_{ks} over index s, and $p_s^{(2)}$ is obtained by summing π_{ks} over index k. Lastly, and most importantly, the decomposition has the symmetry that π_{ks} enters in the expansion of both $p_k^{(1)}$ and $p_s^{(2)}$. Using this decomposition we can compute the total behaviour B as,

$$\begin{aligned} B = \begin{pmatrix} B^{(1)} \\ B^{(2)} \end{pmatrix} = \begin{pmatrix} \sum_{s=1}^{2} M_s^{(1)} p_s^{(1)} \\ \sum_{s=1}^{3} M_s^{(2)} p_s^{(2)} \end{pmatrix} &= \begin{pmatrix} \sum_{s=1}^{2} M_s^{(1)} \sum_{k=1}^{3} \pi_{sk} \\ \sum_{s=1}^{3} M_s^{(2)} \sum_{k=1}^{2} \pi_{ks} \end{pmatrix} \\ &= \sum_{k=1}^{2} \sum_{s=1}^{3} \pi_{ks} \begin{pmatrix} M_k^{(1)} \\ M_s^{(2)} \end{pmatrix}, \end{aligned} \tag{3.19}$$

and B is given by a convex sum over the vectors $\begin{pmatrix} M_k^{(1)T} & M_s^{(2)T} \end{pmatrix}^T$. We can form a table with the rows corresponding to $\begin{pmatrix} M_k^{(1)T} & M_s^{(2)T} \end{pmatrix}$ for different k and s,

1_x		2_x		
1_a	2_a	1_a	2_a	
1	0	1	0	π_{11}
1	0	0	1	π_{12}
1	0	0	0	π_{13}
0	1	1	0	π_{21}
0	1	0	1	π_{22}
0	1	0	0	π_{23}

(3.20)

where the shading indicates the input, 1_x or 2_x. That is, the shading indicates whether this part of the row comes from $M_k^{(1)T}$ or $M_s^{(2)T}$. To the far right we show the probability π_{ks} associated with the vector $\begin{pmatrix} M_k^{(1)T} & M_s^{(2)T} \end{pmatrix}^T$ making up the row. We see that the symmetry of the decomposition in Eq. 3.17, results in the behaviour B being a convex sum over all combinations of the scenarios associated with input 1_x and input 2_x. These combinations are *counter-factual*, for the vector $\begin{pmatrix} M_k^{(1)T} & M_s^{(2)T} \end{pmatrix}^T$ refers to the idea, that if you had given input 1_x you would have been in scenario k, and if you had given input 2_x you would have been in scenario s. However, in all experimental runs we can only either give input 1_x or 2_x, never both. For this reason we will refer to the decomposition Eq. 3.17 as a counter-factual decomposition, and we refer to table 3.20 as a counter-factual table. π_{ks} can then be interpreted as the probability that the counter-factual scenario $\begin{pmatrix} M_k^{(1)T} & M_s^{(2)T} \end{pmatrix}^T$ occur.

The decomposition in Eq. 3.17 has a straightforward interpretation if our measurement can be thought of as revealing the pre-existing properties λ of some object(s) S. Then π_{ks} is simply the probability, that the properties λ were such, that if we give input 1_x we obtain scenario k, and if we give input 2_x then we obtain scenario s. The probability of obtaining scenario v given input n_x, $p_v^{(n)}$, is given by the probability of S having any set of properties that would yield scenario v given input n_x. For example, scenario 1 for input 1_x is observed, if λ is such that if you give input 1_x you get scenario 1, and if you give input 2_x you obtain either scenario 1, 2 or 3. It follows that,

$$p_1^{(1)} = \pi_{11} + \pi_{12} + \pi_{13}, \tag{3.21}$$

and in general we obtain,

$$\begin{aligned} p_s^{(1)} &= \sum_{k=1}^{3} \pi_{sk} \\ p_s^{(2)} &= \sum_{k=1}^{2} \pi_{ks} \end{aligned} \tag{3.22}$$

which is the decomposition used in Eq. 3.17. Then as before, it follows that the behaviour can be described by Eq. 3.19. π_{ks} can then be understood as the frequency by which the properties λ correspond to the counter-factual scenario $\begin{pmatrix} M_k^{(1)T} & M_s^{(2)T} \end{pmatrix}^T$.

3.2 The Clauser-Horne inequalities

We then examine an experiment with 2 inputs x and y. x is assigned one of two numbers, 1 or 2, dependent on some physical condition being met. Likewise y is either 1 or 2. We will refer to a pair of inputs x, y as a context. We consider 4 possible contexts labelled as c_{11}, c_{12}, c_{21} and c_{22}. The four possible contexts are then given by,

$$\begin{aligned} c_{11}: &\quad 1_x, 1_y \\ c_{12}: &\quad 1_x, 2_y \\ c_{21}: &\quad 2_x, 1_y \\ c_{22}: &\quad 2_x, 2_y \end{aligned} \tag{3.23}$$

We have two outputs symbolized by the variables a and b. In each round of experiment the variables a and b are set to particular integers, dependent on some physical condition being met. For each of the 4 contexts c_k we measure the frequencies $p_s^{(k)}$ of the following scenarios,

1_b	$1_a, 1_b$	$1_x, 1_y$
0	0	$p_1^{(11)}$
1	0	$p_2^{(11)}$
1	1	$p_3^{(11)}$

1_a	$1_a, 1_b$	$2_x, 1_y$
0	0	$p_1^{(21)}$
1	0	$p_2^{(21)}$
1	1	$p_3^{(21)}$

1_a	$1_a, 1_b$	$1_x, 2_y$
0	0	$p_1^{(12)}$
1	0	$p_2^{(12)}$
1	1	$p_3^{(12)}$

1_b	$1_a, 1_b$	$2_x, 2_y$
0	0	$p_1^{(22)}$
1	0	$p_2^{(22)}$
1	1	$p_3^{(22)}$

where the elements of column 1_a for example, take the value 1 if the event $a = 1$ occurs in that scenario, and 0 if it doesn't. $1_a, 1_b$ should be understood as the event where both 1_a and 1_b occur. Note that for each table the set of scenarios is complete, i.e. one of the scenarios must occur in each experimental run. We derive a matrix from the above tables,

$$M = \begin{pmatrix} 0 & 0 \\ 1 & 0 \\ 1 & 1 \end{pmatrix}^T = \begin{pmatrix} 0 & 1 & 1 \\ 0 & 0 & 1 \end{pmatrix}. \tag{3.24}$$

We let M_s be the s'th column of M. We define the behaviours for each context,

$$B^{(11)} = \begin{pmatrix} p(1_b|1_x, 1_y) \\ p(1_a, 1_b|1_x, 1_y) \end{pmatrix} \quad , \quad B^{(12)} = \begin{pmatrix} p(1_a|1_x, 2_y) \\ p(1_a, 1_b|1_x, 2_y) \end{pmatrix} \tag{3.25}$$

$$B^{(21)} = \begin{pmatrix} p(1_a|2_x, 1_y) \\ p(1_a, 1_b|2_x, 1_y) \end{pmatrix} \quad , \quad B^{(22)} = \begin{pmatrix} p(1_b|2_x, 2_y) \\ p(1_a, 1_b|2_x, 2_y) \end{pmatrix} \tag{3.26}$$

As before we propose a counter-factual decomposition of the observed relative frequencies,

$$\begin{aligned} p_s^{(11)} &= \sum_{n,m,k=1}^{3} \pi_{s,n,m,k} \\ p_s^{(12)} &= \sum_{n,m,k=1}^{3} \pi_{n,s,m,k} \\ p_s^{(21)} &= \sum_{n,m,k=1}^{3} \pi_{n,m,s,k} \\ p_s^{(22)} &= \sum_{n,m,k=1}^{3} \pi_{n,m,k,s} \end{aligned} \tag{3.27}$$

where $\pi_{s,n,m,k}$ are counter-factual probabilities $0 \leq \pi_{s,n,m,k} \leq 1$ and the normalization $\sum_{s=1}^{3} p_s^{(k)} = 1$ implies the normalization $\sum_{s,n,m,k=1}^{3} \pi_{s,n,m,k} = 1$. Then we can expand the total behaviour B as,

$$\begin{aligned} B = \begin{pmatrix} B^{(11)} \\ B^{(12)} \\ B^{(21)} \\ B^{(22)} \end{pmatrix} = \begin{pmatrix} \sum_{s=1}^{3} M_s p_s^{(11)} \\ \sum_{s=1}^{3} M_s p_s^{(12)} \\ \sum_{s=1}^{3} M_s p_s^{(21)} \\ \sum_{s=1}^{3} M_s p_s^{(22)} \end{pmatrix} &= \begin{pmatrix} \sum_{n,m,k,s=1}^{3} M_s \pi_{s,n,m,k} \\ \sum_{n,m,k,s=1}^{3} M_s \pi_{n,s,m,k} \\ \sum_{n,m,k,s=1}^{3} M_s \pi_{n,m,s,k} \\ \sum_{n,m,k,s=1}^{3} M_s \pi_{n,m,k,s} \end{pmatrix} \\ &= \sum_{n,m,k,s=1}^{3} \pi_{s,n,m,k} \begin{pmatrix} M_s \\ M_n \\ M_m \\ M_k \end{pmatrix}. \end{aligned} \tag{3.28}$$

As before we have all counter-factual mixes of the various possible scenarios associated with the 4 contexts. Furthermore, the behaviour B is described by a convex sum over the possible counter-factual scenarios $\begin{pmatrix} M_s^T & M_n^T & M_m^T & M_k^T \end{pmatrix}^T$. This convex sum can be associated with the counter-factual table,

$1_x, 1_y$		$1_x, 2_y$		$2_x, 1_y$		$2_x, 2_y$		
1_b	$1_a, 1_b$	1_a	$1_a, 1_b$	1_a	$1_a, 1_b$	1_b	$1_a, 1_b$	
0	0	0	0	0	0	0	0	π_{1111}
0	0	0	0	0	0	1	0	π_{1112}
0	0	0	0	0	0	1	1	π_{1113}
0	0	0	0	1	0	0	0	π_{1121}
0	0	0	0	1	0	1	0	π_{1122}
⋮	⋮	⋮	⋮	⋮	⋮	⋮	⋮	⋮

which consists of 81 counter-factual scenarios in total.
We will now make an important assumption. We assume that there can be no correlation between x and b, nor between y and a, in any given counter-factual scenario. We will refer to this as the independence assumption. Under this assumption we must assign probability zero to counter-factual scenarios such as,

$1_x, 1_y$		$1_x, 2_y$		$2_x, 1_y$		$2_x, 2_y$		
1_b	$1_a, 1_b$	1_a	$1_a, 1_b$	1_a	$1_a, 1_b$	1_b	$1_a, 1_b$	
0	0	0	0	0	0	1	1	π_{1113}
0	0	0	0	1	0	1	0	π_{1122}
0	0	0	0	1	1	0	0	π_{1131}
⋮	⋮	⋮	⋮	⋮	⋮	⋮	⋮	⋮

(3.29)

For the scenario in the first row, if input y does not correlate with output a, then the event $1_a|2_x, 1_y$ should occur. Likewise for the scenario in the second row, the event $1_a, 1_b|2_x, 2_y$ should occur. In the third row the event $1_b|1_x, 1_y$ should occur, supposing that input x is not correlated with the output b.
One finds that under the independence assumption, an input x must match to an output a in a given counter-factual scenario. Likewise, an input y must match to an output b in a given counter-factual scenario. We can match two possible outputs, $a = 1$ or $a \neq 1$, to inputs 1_x and 2_x. Likewise, we can match two possible outputs, $b = 1$ or $b \neq 1$, to inputs 1_y and 2_y. We thereby obtain 2^4 possibilities. We find that these 16 counter-factual scenarios are,

$1_x, 1_y$		$1_x, 2_y$		$2_x, 1_y$		$2_x, 2_y$		
1_b	$1_a, 1_b$	1_a	$1_a, 1_b$	1_a	$1_a, 1_b$	1_b	$1_a, 1_b$	
0	0	0	0	0	0	0	0	π_1
0	0	0	0	0	0	1	0	π_2
0	0	0	0	1	0	0	0	π_3
0	0	1	0	0	0	0	0	π_4
1	0	0	0	0	0	0	0	π_5
0	0	0	0	1	0	1	1	π_6
1	0	0	0	1	1	0	0	π_7
0	0	1	1	0	0	1	0	π_8
1	1	1	0	0	0	0	0	π_9
1	0	0	0	0	0	1	0	π_{10}
0	0	1	0	1	0	0	0	π_{11}
1	1	1	0	1	1	0	0	π_{12}
0	0	1	1	1	0	1	1	π_{13}
1	0	0	0	1	1	1	1	π_{14}
1	1	1	1	0	0	1	0	π_{15}
1	1	1	1	1	1	1	1	π_{16}

and for simplicity we enumerate the associated probabilities π_k from 1 to 16. Under the independence assumption, we have that the marginal $p(1_b|1_x, 1_y)$ is independent of x, so $p(1_b|1_x, 1_y) = p(1_b|1_y)$. Similar arguments can be made for the remaining marginals. We can then compute the behaviour B as the convex sum,

$$\begin{pmatrix} p(1_b|1_y) \\ p(1_a,1_b|1_x,1_y) \\ p(1_a|1_x) \\ p(1_a,1_b|1_x,2_y) \\ p(1_a|2_x) \\ p(1_a,1_b|2_x,1_y) \\ p(1_b|2_y) \\ p(1_a,1_b|2_x,2_y) \end{pmatrix} = \begin{pmatrix} 0&0&0&0&1&0&1&0&1&1&0&1&0&1&1&1 \\ 0&0&0&0&0&0&0&0&1&0&0&1&0&0&1&1 \\ 0&0&0&1&0&0&0&1&1&0&1&1&1&0&1&1 \\ 0&0&0&0&0&0&0&1&0&0&0&0&1&0&1&1 \\ 0&0&1&0&0&1&1&0&0&0&1&1&1&1&0&1 \\ 0&0&0&0&0&0&1&0&0&0&0&1&0&1&0&1 \\ 0&1&0&0&0&1&0&1&0&1&0&0&1&1&1&1 \\ 0&0&0&0&0&1&0&0&0&0&0&0&1&1&0&1 \end{pmatrix} \begin{pmatrix} \pi_1 \\ \pi_2 \\ \pi_3 \\ \pi_4 \\ \vdots \\ \pi_{14} \\ \pi_{15} \\ \pi_{16} \end{pmatrix}$$

$$0 \leq \pi_k \leq 1 \quad , \quad \sum_k \pi_k = 1. \tag{3.30}$$

This polytope is referred to as a Bell polytope, and we may eliminate the variables π_k from the above system of linear equalities and inequalities using Fourier-Motzkin elimination. We perform the elimination in the program PORTA [25], and obtain a set of inequalities of the form,

$$\begin{gathered} p(1_a,1_b|n_x,k_y) \geq 0 \quad , \quad p(1_a|n_x) + p(1_b|k_y) - p(1_a,1_b|n_x,k_y) \leq 1 \\ p(1_a,1_b|n_x,k_y) \leq p(1_a|n_x) \quad , \quad p(1_a,1_b|n_x,k_y) \leq p(1_b|k_y) \end{gathered} \tag{3.31}$$

where $n, k \in \{1, 2\}$, and an additional four inequalities,

$$\begin{aligned} -1 \leq \; & p(1_a,1_b|1_x,1_y) + p(1_a,1_b|1_x,2_y) + p(1_a,1_b|2_x,1_y) \\ & - p(1_a,1_b|2_x,2_y) - p(1_a|1_x) - p(1_b|1_y) \leq 0 \\ -1 \leq \; & p(1_a,1_b|1_x,1_y) + p(1_a,1_b|1_x,2_y) - p(1_a,1_b|2_x,1_y) \\ & + p(1_a,1_b|2_x,2_y) - p(1_a|1_x) - p(1_b|2_y) \leq 0 \\ -1 \leq \; & p(1_a,1_b|1_x,1_y) - p(1_a,1_b|1_x,2_y) + p(1_a,1_b|2_x,1_y) \\ & + p(1_a,1_b|2_x,2_y) - p(1_a|2_x) - p(1_b|1_y) \leq 0 \\ -1 \leq \; & -p(1_a,1_b|1_x,1_y) + p(1_a,1_b|1_x,2_y) + p(1_a,1_b|2_x,1_y) \\ & + p(1_a,1_b|2_x,2_y) - p(1_a|2_x) - p(1_b|2_y) \leq 0, \end{aligned} \tag{3.32}$$

these last four inequalities, first given in [26] in the equivalent correlator form, are called Clauser-Horne inequalities in the literature [20]. The Clauser-Horne inequalities are examples of what is known as Bell inequalities. Together with the inequalities Eq. 3.31, the Clauser-Horne inequalities provide a representation of the Bell polytope given in Eq. 3.30.

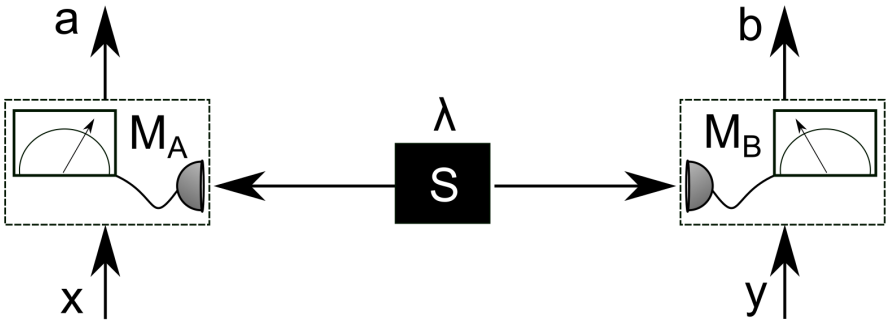

Figure 3.2: *A source S with properties λ acts on two measurement stations M_A and M_B, either through the emission of some objects or through action at a distance.*

We will now consider an experiment with two measurement devices M_A and M_B, and a source S, arranged as sketched in Fig. 3.2. We will assume that at some space-time coordinate τ_λ, defined w.r.t to some reference frame, the source S is characterized by having properties λ (see Fig. 3.3). It is the properties λ we want to measure. We let the measurement outcome obtained by device M_A be given by the variable a, and likewise b describes the output of the device M_B. x is the setting (input) of M_A, and y is the setting of M_B. We will assume that the input x is defined at space-time point τ_x, and the input y is defined at the space-time point τ_y. The outputs a and b are obtained at space-time points τ_a and τ_b respectively.

We then make another important assumption. We assume that in a particular round of experiment, the properties λ correspond to a particular counter-factual scenario. That is, in any given round of experiment, λ is such that a particular input x, y maps to a particular output a, b, with this mapping being defined for all possible inputs. Then, as explained at the end of section 3.1, the decomposition of the behaviour Eq. 3.28 should be understood as stating, that with probability $\pi_{s,n,m,k}$, the properties λ were such that we obtain the counter-factual scenario $\begin{pmatrix} M_s^T & M_n^T & M_m^T & M_k^T \end{pmatrix}^T$. The independence assumption can then be justified when the experimental events are positioned as shown in Fig. 3.3. According to the theory of special relativity, no signal can travel faster than the speed of light [27]. This suggests that an event at τ_a cannot be affected by an event at τ_y, since τ_a is outside of the forward light-cone of τ_y. For the same reason, an event at τ_b cannot be affected by an event at τ_x. Assuming that the theory of special relativity holds in each round of experiment, then the properties λ realized in a round of experiment must be constrained by the theory. So the counter-factual scenario associated to particular properties λ, must be constrained so that there is no correlation between x and b, nor between y and a. This is the content of the independence assumption.

Nevertheless, even though the events are ordered as in Fig. 3.3, we can for-

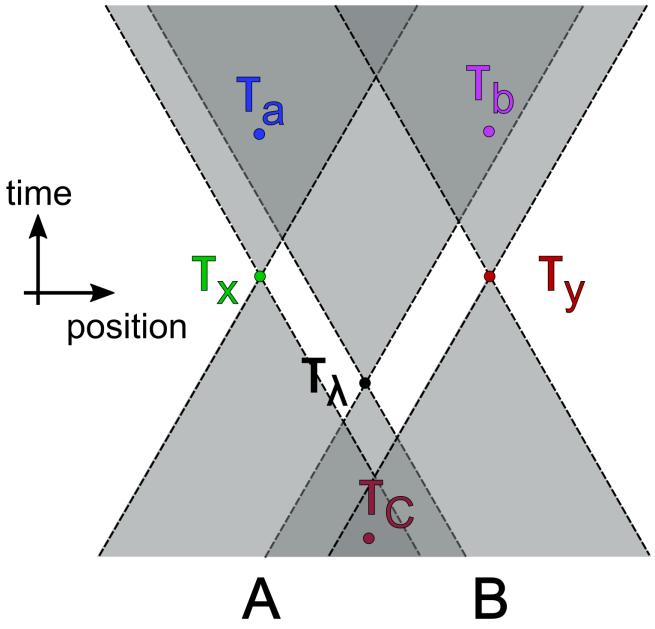

Figure 3.3: *A particular ordering of experimentally relevant events. The dotted cones are light-cones.* τ_x *is where setting* x *is chosen,* τ_a *is where outcome* a *is obtained,* τ_y *is where setting* y *is chosen,* τ_b *is where outcome* b *is obtained.* τ_λ *is where the properties of* S *are* λ*.* τ_C *is defined in the text.*

mulate conditions that would cause the independence assumption to fail. The first possibility is that nature is *non-local* [28]. Influences, which apparently travel faster than the speed of light, connect input x to the output b, and the input y to the output a. It follows that we were wrong to exclude scenarios such as those listed in table 3.29. However, these influences cannot be controlled for telegraphic purposes, for the marginal distribution of a remains independent of y according to quantum mechanics, and the marginal distribution of b remains independent of x [4]. Another possibility is that nature is *acausal*, and colliding systems are correlated both after *and* prior to their collision. Acausal physics is discussed in [29]–[31]. Hamilton's principle and the advanced potentials in electromagnetism [27] are examples of acausal concepts in physics. Within an acausal model x and λ, located at τ_x and τ_λ respectively, can be correlated in a given experimental run due to the measurement event located at τ_a. Since b can be correlated with λ, this then implies that b can be correlated with input x in a given experimental run, and we were wrong to exclude counter-factual scenarios such as those listed in table 3.29.

It was demonstrated in a sequence of experimental works [32]–[34], that the Clauser-Horne-Shimony-Holt (CHSH) inequalities are violated by nature. A violation of the CHSH inequalities is equivalent to a violation of the Clauser-Horne inequalities given above [7]. For this reason, it seems that we are forced to accept that one of the above possibilities must be true. However, we note that at least two other possible explanations for the violation remains. It is possible that the counter-factual scenarios used to decompose the behaviour, cannot be interpreted as corresponding to something physical. They are purely mathematical constructs, and we can therefore not condition them on physical laws, such as the theory of special relativity. The independence assumption can therefore not be justified. A second possibility is the existence of a *common cause*, C, located at the space-time point τ_C (see Fig. 3.3), in the backward light cone of τ_x, τ_y, τ_a and τ_b. There could be a common cause that determined the experimenters to choose inputs x and y, and determined the outputs a and b. Clearly then, any experimental record can be produced, including one that violates one of the Clauser-Horne inequalities.

3.3 The no-signalling polytope

Suppose we perform the experiment sketched in Fig 3.2, and obtain probabilities $p(a, b|x, y)$ for the co-occurrence of outcomes a and b, given that the physicists A and B (operating M_A and M_B respectively) gave inputs x and y. We can then compute the marginal distribution of a,

$$p(a|x, y) = \sum_b p(a, b|x, y). \tag{3.33}$$

Supposing the marginal distribution $p(a|x,y)$ depends on setting y, we see that if A and B share many copies of the system they are measuring on, and B always measure using the same setting y, then A can infer setting y from comparing the observed marginal distribution $p(a|x,y)$ to a known theoretical model. But what if B measured using setting y *after* A measured ? Then A would be able to predict which setting B is going to use. If A then tells B to use another setting, we arrive at a paradox. Hence the above marginal cannot generically depend on setting y, it can only do so if B measures before A.
It is easily seen that the linear operator algebra of quantum mechanics ensures that the marginal $p(a|x,y)$ is always independent of y. Let $\hat{P}_A(a,x)$ be the projector onto the state associated with outcome a for setting x, then

$$p(a,b|x,y) = \mathrm{Tr}_{\mathrm{AB}}\left[\rho \hat{P}_A(a,x)\hat{P}_B(b,y)\right], \tag{3.34}$$

where ρ is the quantum state shared by A and B. We may compute the marginal,

$$p(a|x,y) = \sum_b p(a,b|x,y) = \mathrm{Tr}_{\mathrm{AB}}\left[\rho \hat{P}_A(a,x)\sum_b \hat{P}_B(b,y)\right], \tag{3.35}$$

provided that some outcome must occur, we have $\sum_b \hat{P}_B(b,y) = 1$, and we can conclude,

$$p(a|x,y) = \mathrm{Tr}_{\mathrm{A}}\left[\mathrm{Tr}_{\mathrm{B}}\left[\rho\right]\hat{P}_A(a,x)\right], \tag{3.36}$$

which is clearly independent of y. So we find,

$$p(a|x,y) = p(a|x). \tag{3.37}$$

This constraint on the marginal is called *no-signalling*, for its violation would allow B to send a message to A simply by choosing a particular setting y [35]. We write up the no-signalling conditions together with conditions of normalization and positivity,

$$\sum_b p(a,b|x,y) = \sum_b p(a,b|x,y') \quad , \quad \sum_a p(a,b|x,y) = \sum_a p(a,b|x',y) \tag{3.38}$$

$$\sum_{a,b} p(a,b|x,y) = 1 \quad , \quad 0 \leq p(a,b|x,y) \leq 1, \tag{3.39}$$

which should hold for all inputs x, x', y, y', and outputs a, b. We see that the probabilities $p(a,b|x,y)$ are constrained by linear equalities and inequalities, hence the no-signalling conditions define a convex polytope. In summary, microscopic systems can yield behaviours that are outside the Bell polytope, but they are always inside the no-signalling polytope.

3.4 More than two participants

An important generalization of the CHSH inequalities to the case with more than two participants (parties for short) was described by Werner and Wolf in [36]. The inequality carries the name the Werner-Wolf-Weinfurter-Zukowski-Brukner inequality, or W^{3}ZB for short. The inequality applies to an experiment with N inputs and N outputs, where each input can take two values, and likewise each output can take two values. We denote the inputs as x_p and the outputs as a_p, with $p \in \{A, B, C, \cdots\}$. We refer to each letter $A, B, \ldots$ as a party, giving N parties in total. Each input can be 0 or 1, and each output can be 0 or 1. We let x be a vector of the inputs, i.e. $x = \begin{pmatrix} x_A & x_B & \cdots \end{pmatrix}$. We let a be a vector of the outputs $a = \begin{pmatrix} a_A & a_B & \cdots \end{pmatrix}$. We will be using binary strings of length N, and we order these numerically so that z_k is the binary string corresponding to the number k. So for example with $N = 4$,

$$z_3 = \begin{pmatrix} 0 & 0 & 1 & 1 \end{pmatrix}. \tag{3.40}$$

We denote the set of all binary strings of length N as B_N.
The counter-factual table corresponding to the experiment has the columns,

$x = z_1$			$x = z_2$			$\cdots$	
1_{a_A}	1_{a_B}	$\cdots$	1_{a_A}	1_{a_B}	$\cdots$	$\cdots$	
0	0	0	0	0	0	$\cdots$	π_0
$\vdots$	$\vdots$	$\vdots$	$\vdots$	$\vdots$	$\vdots$	$\cdots$	$\vdots$

(3.41)

The W^{3}ZB inequality can then be derived from the assumption that input x_p can only correlate with output a_p in a given counter-factual scenario. We introduce a vector for each p, $\lambda_p = \begin{pmatrix} \lambda_p^{(0)} & \lambda_p^{(1)} \end{pmatrix}$, where $\lambda_p^{(n)} \in \{0, 1\}$. We gather these vectors in a list $\lambda = \begin{pmatrix} \lambda_A & \lambda_B & \cdots \end{pmatrix}$. We introduce the function,

$$f(x_p, \lambda_p) = \delta(x_p, 0)\lambda_p^{(0)} + \delta(x_p, 1)\lambda_p^{(1)}. \tag{3.42}$$

We can then construct a vector $f(x, \lambda)$,

$$f(x, \lambda) = \begin{pmatrix} f(x_A, \lambda_A) & f(x_B, \lambda_B) & \cdots \end{pmatrix} \tag{3.43}$$

For each λ we can then construct a counter-factual scenario $T(\lambda)$ (a row of table 3.41) that is consistent with the assumption that a_p can only correlate with x_p,

$$T(\lambda) = \begin{pmatrix} f(z_1, \lambda) & f(z_2, \lambda) & \cdots \end{pmatrix}. \tag{3.44}$$

This counter-factual scenario is associated with the probability $p(\lambda)$. All counter-factual scenarios allowed under our assumption can be constructed in this way, that

is by choosing different lists λ. Summing over all possible λ, we must then have the normalization,

$$\sum_{\lambda} p(\lambda) = 1$$
$$p(\lambda) \geq 0. \tag{3.45}$$

Then the probability of obtaining a given inputs x, that is $p(a|x)$, is given by the probability of obtaining any λ where $f(x,\lambda) = a$. This probability is given by,

$$p(a|x) = \sum_{\lambda} p(\lambda) \prod_{p\in\{A,B,C,\ldots\}} \left[\delta(x_p,0)\delta(a_p,\lambda_p^{(0)}) + \delta(x_p,1)\delta(a_p,\lambda_p^{(1)})\right], \tag{3.46}$$

where $\delta(x,y)$ is the Kronecker delta function in x and y. Now comes the crucial trick, we compute the N party correlators,

$$M(x) = \sum_{a\in B_N} p(a|x) \prod_{p\in\{A,B,C,\ldots\}} \left[\delta(a_p,0) - \delta(a_p,1)\right], \tag{3.47}$$

i.e. if a_p is 0 we multiply by $+1$ and if a_p is 1 we multiply by -1. The sum over a runs over the binary strings z_k. Inserting Eq. 3.46 we obtain,

$$M(x) = \sum_{\lambda} M(x,\lambda)p(\lambda), \tag{3.48}$$

$$M(x,\lambda) = \sum_{a\in B_N} \prod_{p\in\{A,B,C,\ldots\}} \left[\delta(x_p,0)\delta(a_p,\lambda_p^{(0)}) + \delta(x_p,1)\delta(a_p,\lambda_p^{(1)})\right] \left[\delta(a_p,0) - \delta(a_p,1)\right] \tag{3.49}$$

We then evaluate $M(x,\lambda)$,

$$\begin{aligned} M(x,\lambda) &= \sum_{a\in B_N} \prod_{p\in\{A,B,C,\ldots\}} \left[\delta(x_p,0)\delta(a_p,\lambda_p^{(0)}) + \delta(x_p,1)\delta(a_p,\lambda_p^{(1)})\right] \left[\delta(a_p,0) - \delta(a_p,1)\right] \\ &= \sum_{a\in B_N} \prod_{p\in\{A,B,C,\ldots\}} \big[\delta(x_p,0)\delta(a_p,\lambda_p^{(0)})\delta(a_p,0) - \delta(x_p,0)\delta(a_p,\lambda_p^{(0)})\delta(a_p,1) \\ &\qquad +\delta(x_p,1)\delta(a_p,\lambda_p^{(1)})\delta(a_p,0) - \delta(x_p,1)\delta(a_p,\lambda_p^{(1)})\delta(a_p,1)\big], \end{aligned} \tag{3.50}$$

breaking up the sum we can move it under the product operator,

$$\begin{aligned}
&= \prod_{p\in\{A,B,C,\ldots\}} \sum_{a_p\in B_1} \big[\delta(x_p,0)\delta(a_p,\lambda_p^{(0)})\delta(a_p,0) - \delta(x_p,0)\delta(a_p,\lambda_p^{(0)})\delta(a_p,1) \\
&\qquad\qquad +\delta(x_p,1)\delta(a_p,\lambda_p^{(1)})\delta(a_p,0) - \delta(x_p,1)\delta(a_p,\lambda_p^{(1)})\delta(a_p,1)\big] \\
&= \prod_{p\in\{A,B,C,\ldots\}} \big[\delta(x_p,0)\delta(\lambda_p^{(0)},0) - \delta(x_p,0)\delta(\lambda_p^{(0)},1) \\
&\qquad\qquad +\delta(x_p,1)\delta(\lambda_p^{(1)},0) - \delta(x_p,1)\delta(\lambda_p^{(1)},1)\big] \\
&= \prod_{p\in\{A,B,C,\ldots\}} \left[\delta(x_p,0)(-1)^{\lambda_p^{(0)}} + \delta(x_p,1)(-1)^{\lambda_p^{(1)}}\right] \\
&= \prod_{p\in\{A,B,C,\ldots\}} (-1)^{\lambda_p^{(0)}} \left[\delta(x_p,0) + \delta(x_p,1)(-1)^{\lambda_p^{(0)}+\lambda_p^{(1)}}\right] \qquad (3.51)
\end{aligned}$$

Defining the vectors $\lambda^{(0)} = \begin{pmatrix}\lambda_A^{(0)} & \lambda_B^{(0)} & \cdots\end{pmatrix}$ and $\lambda^{(1)} = \begin{pmatrix}\lambda_A^{(1)} & \lambda_B^{(1)} & \cdots\end{pmatrix}$ we can perform the multiplication and obtain,

$$M(x,\lambda) = (-1)^{|\lambda^{(0)}|_1}(-1)^{\langle\lambda^{(0)}+\lambda^{(1)},x\rangle}. \qquad (3.52)$$

where $|\lambda^{(0)}|_1 = \sum_p \lambda_p^{(0)}$, and we've defined the inner product, $\langle\lambda^{(0)}+\lambda^{(1)},x\rangle = \sum_p \left(\lambda_p^{(0)}+\lambda_p^{(1)}\right)x_p$. Evidently we find that $M(x,\lambda)$ is uniquely defined by the number, $s = (-1)^{|\lambda^{(0)}|_1}$, and the binary vector $b = \lambda^{(0)} + \lambda^{(1)} \pmod 2$. We can then write,

$$M(x,\lambda) = M(x,s,b) = s(-1)^{\langle b,x\rangle}. \qquad (3.53)$$

We can group the scenarios λ corresponding to the same s and b, and perform the sum in Eq. 3.48 over s and b instead,

$$M(x) = \sum_{s\in\{-1,1\}} \sum_{b\in B_N} M(x,s,b)p(s,b), \qquad (3.54)$$

where we've defined,

$$p(s,b) = \sum_{\lambda\in\Omega(s,b)} p(\lambda) \qquad (3.55)$$

and $\Omega(s,b)$ is the domain over λ for which $(-1)^{|\lambda^{(0)}|} = s$ and $\lambda^{(0)}+\lambda^{(1)} \pmod 2 = b$. Expanding the summand,

$$M(x) = \sum_{s\in\{-1,1\}} s \sum_{b\in B_N} (-1)^{\langle b,x\rangle} p(s,b), \qquad (3.56)$$

we multiply both sides by $2^{-N}(-1)^{\langle x,y\rangle}$ where y is a binary vector of length N, and then we sum x over B_N. The left side of Eq. 3.56 yields the transformed correlator,

$$\tilde{M}(y) = 2^{-N} \sum_{x \in B_N} (-1)^{\langle x,y\rangle} M(x), \tag{3.57}$$

whereas the right side of Eq. 3.56 becomes,

$$\begin{aligned} & 2^{-N} \sum_{s\in\{-1,1\}} s \sum_{b\in B_N} p(s,b) \sum_{x\in B_N} (-1)^{\langle x,y+b\rangle} \\ &= \sum_{s\in\{-1,1\}} s \sum_{b\in B_N} p(s,b)\delta(y,b) \\ &= \sum_{s\in\{-1,1\}} sp(s,y). \end{aligned} \tag{3.58}$$

So we can express the transformed correlators as,

$$\tilde{M}(y) = \sum_{s\in\{-1,1\}} sp(s,y). \tag{3.59}$$

To understand this equation in more detail, we sketch the associated matrix equation. Enumerating the possible y as y_n, we have,

$$\begin{aligned} \begin{pmatrix} \tilde{M}(y_0) \\ \tilde{M}(y_1) \\ \tilde{M}(y_2) \\ \vdots \end{pmatrix} &= \begin{pmatrix} 1 \\ 0 \\ 0 \\ \vdots \end{pmatrix} p(1,y_0) + \begin{pmatrix} -1 \\ 0 \\ 0 \\ \vdots \end{pmatrix} p(-1,y_0) \\ &\quad + \begin{pmatrix} 0 \\ 1 \\ 0 \\ \vdots \end{pmatrix} p(1,y_1) + \begin{pmatrix} 0 \\ -1 \\ 0 \\ \vdots \end{pmatrix} p(-1,y_1) + \cdots \end{aligned} \tag{3.60}$$

and so forth. Examining the octahedron sketched in Fig. 3.4 we see that the octahedron is formed by the convex sum of the vertices

$$\{\begin{pmatrix}1 & 0 & 0\end{pmatrix}, \begin{pmatrix}-1 & 0 & 0\end{pmatrix}, \begin{pmatrix}0 & 1 & 0\end{pmatrix}, \begin{pmatrix}0 & -1 & 0\end{pmatrix}, \begin{pmatrix}0 & 0 & 1\end{pmatrix}, \begin{pmatrix}0 & 0 & -1\end{pmatrix}\}. \tag{3.61}$$

Hence we see that the convex sum in Eq. 3.60 is in fact the generalization of the octahedron to 2^N dimensions. Such a convex polytope is called a cross polytope.

The 2^N dimensional cross polytope can be defined by the inequality [24],

$$\sum_{m=0}^{2^N-1} |\tilde{M}(y_m)| \leq 1. \tag{3.62}$$

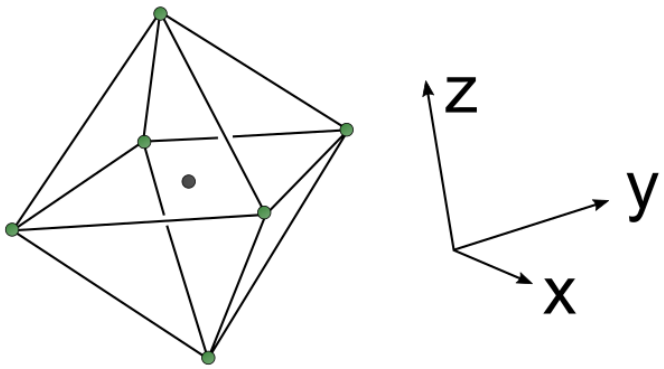

Figure 3.4: *Sketch of an octahedron.*

If we express $\tilde{M}(y)$ in terms of $M(x)$ we obtain from Eq. 3.62,

$$2^{-N} \sum_{y \in B_N} \left| \sum_{x \in B_N} (-1)^{\langle x,y \rangle} M(x) \right| \leq 1 \tag{3.63}$$

which is called the W^{3}ZB inequality.
Note that we can add a minus in front of any selection of the terms $|\tilde{M}(y_m)|$ in Eq. 3.62 and the inequality will still be valid. Hence Eq. 3.62 also implies all the inequalities,

$$\sum_{m=0}^{2^N-1} s_m \tilde{M}(y_m) \leq 1 \tag{3.64}$$

with $s_m \in \{-1, 1\}$. One can easily verify that the above 2^{2^N} inequalities are obeyed by all vertices of the cross polytope, and that for each inequality we obtain equality for 2^N vertices. These 2^N vertices define a facet of the cross polytope associated to each inequality.

Chapter 4

Proposal for a long-distance nonlocality test with entanglement swapping and displacement-based measurements

We now present the paper *Proposal for a long-distance nonlocality test with entanglement swapping and displacement-based measurements* [9]. This paper was authored by Anders J. E. Bjerrum, Jonatan B. Brask, Jonas S. Neergaard-Nielsen, and Ulrik L. Andersen. The paper was published in Physical Review A with the reference Phys. Rev. A 107, 052611 (2023).
A section has been attached to the end of the paper, describing how to convert the non-linear W^3ZB inequality into linear inequalities for particular cases.

4.1 Abstract

We analyze an all-optical setup which enables Bell-inequality violation over long distances by exploiting probabilistic entanglement swapping. The setup involves only two-mode squeezers, displacements, beamsplitters, and on/off detectors. We describe how events must be arranged to close both the detection and locality loopholes. We analyze a scenario with dichotomic inputs and outputs, and check the robustness of the Bell inequality violation for up to 6 parties, with respect to phase-, amplitude-, and dark-count noise, as well as loss.

4.2 Introduction

As pointed out already by Boole in his work on probability theory, logical relations between observable events imply inequalities for the probabilities of their occur-

rence [20], [37]. Bell later demonstrated that the inequalities implied by a local causal realist description of nature can be violated within quantum mechanics [21], [38], implying that quantum mechanics cannot be recast as a local realist theory. Subsequent experimental investigations by Clauser, Aspect and their collaborators [32], [33], [39] confirmed the nonlocal predictions of quantum mechanics, and nonlocality gradually became accepted as an aspect of nature. These early experiments were however not loophole-free, and while loophole-free violations have since been realised [34], [40]–[42], it still remains experimentally challenging, with loss and detector inefficiencies being some of the main obstacles [43].

Loopholes constitute ways in which nature, or an eavesdropper, can arrange experimental outcomes, such that an experiment appears nonlocal, while in reality it is not. The detection loophole is relevant when inconclusive measurements are discarded from the experimental data [7]. Such inconclusive measurements typically occur due to losses during transmission of the particles, or non-unit efficiency of the detectors. It has been demonstrated that discarding inconclusive measurement rounds renders it possible to violate a Bell inequality using classical optics [44]. The locality loophole is present if measurements are performed such that a sub-luminal signal can transfer information between measurement stations during a measurement sequence. Such a sequence includes the act of choosing a measurement basis, and performing the measurement in this basis. The locality loophole can be closed by separating the measurement stations and keeping the duration of the measurement sequence short. However, this separation tends to induce losses and noise in the state shared by the participants of the experiment, and these losses tend to make the shared quantum state local, i.e. it cannot be used to demonstrate a Bell inequality violation.

In spite of these difficulties, the utilization of nonlocality is now moving from fundamental science towards practical applications, where the provable nonlocality of a quantum state is used in device-independent protocols to certify the security of a cryptographic key [8], [45]–[49]. Crucial to the realization of device-independent quantum key distribution is the ability to close relevant loopholes, and to demonstrate the violation of Bell inequalities across distances relevant for telecommunication.

In this work we propose an experiment capable of violating a Bell inequality when the parties are separated by channels of low transmission. Our experiment is designed to be capable of closing the detection and locality loopholes, and invokes only standard quantum optics tools, such as two-mode squeezers, displacements, and click detectors (on/off detectors). A sketch of the setup with N parties is shown in Fig. 4.1. The proposed experiment is inspired by the setup in [50], in which displacement-based measurements are used to demonstrate a Bell inequality vio-

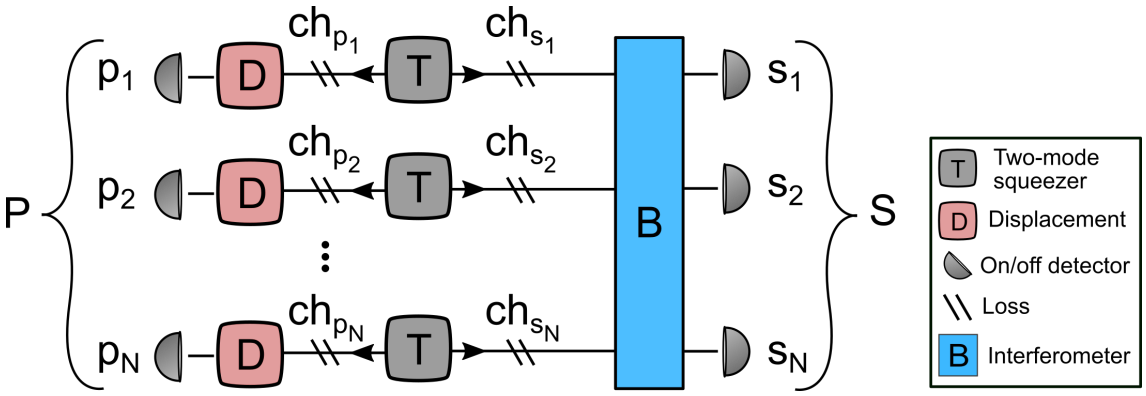

Figure 4.1: *Sketch of the analysed setup with N parties. The left-going modes are labelled p_n and the right-going modes are labelled s_n. A detector associated with a mode is given the same label as that mode. The measurement performed by the detectors in S effectively swaps the N bipartite entangled states, from the two-mode squeezers, into an N-mode entangled state. ch abbreviates channel.*

lation. In our protocol, two-mode squeezers generate weakly squeezed two-mode squeezed vacuum states with half of each state sent a short distance to an on/off detector, and the other half sent to a distant interferometer B. The left-going modes in Fig. 4.1 are labelled p_n and the right-going modes are labelled s_n, we group them into two sets $P = \{p_1, p_2, \ldots, p_N\}$ and $S = \{s_1, s_2, \ldots, s_N\}$. We use the same label for a mode and the corresponding detector. Each of the N detectors in P is considered as a party, with the possible measurement outcomes, click or no click, corresponding to whether any light arrives at the detector or not. The interferometer B mixes the modes S, so that a photon arriving at one of the input ports of B, has an equal probability of triggering each of the detectors in S. We then require that only detector s_N clicks, and that the remaining detectors in S do not click. Hence our protocol is similar to an event-ready scheme [34], [42], [51] based on optical entanglement swapping [52]–[55], but without the need for quantum memories. Upon obtaining the correct measurement outcome at S, the measurement outcomes at the detectors in P are approximately the same as if the detectors measured the single-photon state $\frac{1}{\sqrt{N}}(|1,0,\ldots,0\rangle + |0,1,\ldots,0\rangle + |0,0,\ldots,1\rangle)$, in the limit of vanishing squeezing. However, due to the presence of dark counts at the detectors it is not optimal to operate the experiment in the limit of vanishing squeezing, and the analysed state will only be similar to a W state. The nonlocality of the W state was analysed in [50], [56]–[58], and we expect to see similar results for the state analysed in this work. However it is worth noting that the study in [57] focuses on single-run violations of locality, as opposed to the statistical violation analysed in this work. Moreover the measurements in [57] involved general qubit measurements, while we assume the more feasible displacement-based measurements.
Our work also differs in key aspects from the protocols in [50], [56], [58]. The pu-

rification step proposed in the present work is part of the state preparation, i.e. obtaining the correct measurement outcomes at S will mitigate loss incurred in the channels ch_s for suitable values of the squeezing parameters, while at the same time preparing a N-partite entangled state. In [56], [58] the authors do not introduce a heralded step to mitigate loss, limiting the distance over which nonlocality can be demonstrated. In [50] loss is mitigated by each party filtering their part of the state using a quantum scissor [59]. However, quantum scissors require single-photon sources making the idea increasingly less practical as we increase the number of parties. Our purification step does not involve quantum scissors, hence no single-photon sources are required for our scheme.

Note that the state preparation in our scheme generates a N-partite entangled state *after* the N parties have measured on their parts of the shared state. This implies that the parties must discard obtained measurement outcomes if the subsequent heralding measurement at S fails, and this opens the door for the detection loophole. However, as we will show in the following, it turns out to be possible to arrange the events of the protocol such that the detection loophole is closed.

Prior to each detector in P, either of two different displacements (D in Fig. 4.1) is applied to the field. These displacements make up the two different measurement settings. We write the displacement applied on mode $p \in P$ as $X_p^{(n_p)} = \begin{pmatrix} x_p^{(n_p)} & y_p^{(n_p)} \end{pmatrix}^T$, with $n_p \in (0,1)$ labelling which of two possible displacements is implemented (measurement setting). We assume that all parties are choosing between the same two displacements, when the phases of the N two-mode squeezers are the same. This assumption is invoked to simplify our analysis, and we found no advantage when deviating from it. The displacement operator for mode p is defined as,

$$D_p\left(X_p^{(n_p)}\right) = \exp\left[i(\hat{q}_p\, y_p^{(n_p)} - \hat{p}_p\, x_p^{(n_p)})\right], \tag{4.1}$$

where $\hat{q}_p$ and $\hat{p}_p$ are the quadrature operators for mode p. We follow the convention $[\hat{q}_k, \hat{p}_l] = 2i\delta_{kl}$. From the quadrature operators we obtain the annihilation operator, $\hat{a}_p = \frac{1}{2}(\hat{q}_p + i\hat{p}_p)$. The coherent state generated by the displacement $X_p^{(n_p)}$, i.e. the state, $|X_p^{(n_p)}\rangle = D_p\left(X_p^{(n_p)}\right)|0\rangle$, is centred on the coordinates $\begin{pmatrix} q_p & p_p \end{pmatrix} = \begin{pmatrix} 2x_p^{(n_p)} & 2y_p^{(n_p)} \end{pmatrix}$ in phase space. We associate a click at a detector with the value 1, and no click with the value -1. The observable associated with detector p is then given by,

$$M_p = (I_p - |0\rangle_p\langle 0|) - |0\rangle_p\langle 0| \tag{4.2}$$

$$= I_p - 2\,|0\rangle_p\langle 0|\,, \tag{4.3}$$

where I_p is the identity operator associated with mode p. We may transfer the displacement applied prior to detector p onto the observable to obtain,

$$M_p^{(n_p)} = I_p - 2\,|-X_p^{(n_p)}\rangle_p\langle -X_p^{(n_p)}|\,. \tag{4.4}$$

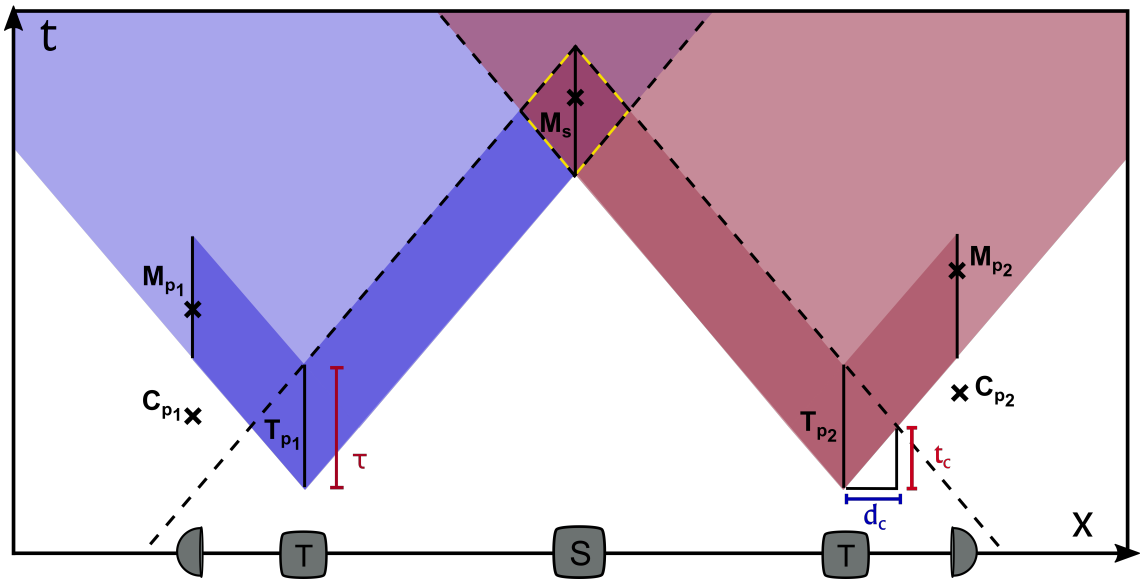

Figure 4.2: *Space-time diagram of a loophole-free experiment with two parties, showing the space-time ordering of important events (marked by ×). The events T_{p_1} and T_{p_2} correspond to the generation of two-mode squeezed vacuum. C_{p_1} and C_{p_2} are the events where p_1 and p_2 decide their measurement settings. M_{p_1} and M_{p_2} correspond to events where p_1 and p_2 measure. M_s correspond to the event where s_1 and s_2 measure. At the bottom we sketch the experimental setup (compare with Fig. 4.1), where S corresponds to the swap following the interferometer B.*

We attempt to violate the W^{3}ZB (Werner-Wolf-Weinfurter-Żukowski-Brukner) inequality [36], [60], [61],

$$2^{-N} \sum_b \left| \sum_n (-1)^{\langle b,n \rangle} \langle M^{(n)} \rangle \right| \leq 1. \tag{4.5}$$

b and n are binary lists of length N, and the sums run over all possible binary lists. $\langle b, n \rangle$ is the dot product between b and n. The entries of n label the measurement settings of the involved parties. $\langle M^{(n)} \rangle$ is the correlator given by the product $\langle M^{(n)} \rangle = \langle \prod_p M_p^{(n_p)} \rangle$. We will refer to the left side of Eq. 4.5 as the Bell value of the W^{3}ZB inequality. The maximal violation of the W^{3}ZB inequality increases with the number of parties [62]. We therefore expect that when some loss and noise does not scale with the number of parties, then a violation of a W^{3}ZB inequality with more parties is more robust against this loss and noise, as compared to a W^{3}ZB inequality with fewer parties.

To close both the locality and detection loophole with two parties, p_1 and p_2, we require that the events of the experiment are positioned as shown in the space-

time diagram in Fig. 4.2. The events T_{p_1} and T_{p_2} correspond to the generation of two-mode squeezed vacuum for party p_1 and party p_2 respectively. These events occur along a temporal (vertical) line, since the light emitted from the source has a finite duration τ. For this reason there exists at each position x a duration of time where we expect the light to arrive with very high probability, this is marked with a darker shaded area. The measurements by p_1 and p_2 are labelled M_{p_1} and M_{p_2} respectively. M_s correspond to the event where s_1 and s_2 measure. The choosing of measurement setting is labelled C_{p_1} and C_{p_2}. The measurements M_{p_1} and M_{p_2} collapse the temporal width of the pulses, as illustrated in the figure by an $\times$. The swap M_s occurs with very high probability along the vertical black line inside the central black and yellow dashed diamond. The backwards light cone for a swapping event will then typically be bounded by the dashed backwards light cone.

To close the detection loophole, p_1 and p_2 must choose their measurement settings at a time and place such that information about their choices cannot influence the swapping measurement M_s via a sub-luminal signal. If the experiment is executed in this way, then we anticipate that an eavesdropper cannot tamper with the swap to falsify nonlocal correlations [63]. Most swapping events will obey this requirement if C_{p_1} and C_{p_2} are outside the dotted backward time cone shown in Fig. 4.2. The critical distance d_c, which is the characteristic distance the event C_{p_2} must be separated from the two-mode squeezer T_{p_2}, can be found by geometric arguments as $d_c = (1/2)c\tau$, and is associated with a waiting time $t_c = (1/2)\tau$. Ideally p_2 could make her choice of measurement setting at a distance d_c from T_{p_2}, at a time t_c after the light started to be emitted from the squeezer. Then her choice would most likely not be able to influence the swap M_s, while at the same time ensuring that the light pulse has not passed by her yet.

The experimental constraints discussed above generalize to the scenario where N parties attempt to obtain a Bell inequality violation, while closing the detection and locality loophole. That is, the parties should ensure that the events C_{p_n} are outside the backward timecone for the swapping event M_s. However, one should also ensure that the parties are sufficiently distant from each other, so that information on the choice of measurement setting and outcome cannot travel between parties during a measurement sequence.

4.3 Model

We now give an outline of how we model the optical field, and how we include experimental imperfections in our analysis. A full description can be found in appendix A1. The fields generated by the two-mode squeezers are distributed in time and space according to some mode functions [2]. The amplitudes of these modes are quantum uncertain with Gaussian statistics described by a covariance matrix σ with

elements $\sigma_{kl} = 1/2\langle\{Q_k, Q_l\}\rangle - \langle Q_k\rangle\langle Q_l\rangle$, where $\{.,.\}$ denotes the anti-commutator and $Q = Q_P \oplus Q_S$, where $Q_P = \bigoplus_{p\in P}\begin{pmatrix}\hat{q}_p & \hat{p}_p\end{pmatrix}$ with $Q_S = \bigoplus_{s\in S}\begin{pmatrix}\hat{q}_s & \hat{p}_s\end{pmatrix}$ [16]. The corresponding density matrix, also describing the statistics of the field, is denoted ρ. We denote the squeezing parameter of the N squeezers as r and introduce the symbols, $a = \sinh(2r)$ and $v = \cosh(2r)$. The covariance matrix of the 2N modes can be written as,

$$\sigma = \begin{pmatrix} v\mathbf{I} & \mathbf{R}_\phi \\ \mathbf{R}_\phi & v\mathbf{I}\end{pmatrix}, \tag{4.6}$$

where $\mathbf{I}$ is the identity matrix of dimension 2N and $\mathbf{R}_\phi$ is the block diagonal matrix,

$$\mathbf{R}_\phi = \bigoplus_p \begin{pmatrix} a\cos(\phi_p) & -a\sin(\phi_p) \\ -a\sin(\phi_p) & -a\cos(\phi_p)\end{pmatrix}, \tag{4.7}$$

where ϕ_p is the phase angle of the squeezer for party p. The expectation value of the field amplitude is assumed zero. The Wigner characteristic function corresponding to ρ is given by $\chi_\rho(\Lambda) = \exp[-(1/2)\Lambda^T\Omega\sigma\Omega^T\Lambda]$ where Λ is a vector of conjugate quadratures (the Fourier transform dual to the quadratures) for the modes P and S, i.e. $\Lambda = \Lambda_P \oplus \Lambda_S$, where $\Lambda_P = \bigoplus_{p\in P}\Lambda_p$ and $\Lambda_S = \bigoplus_{s\in S}\Lambda_s$. The conjugate quadratures for mode k is a vector $\Lambda_k = \begin{pmatrix}\lambda_{kx} & \lambda_{ky}\end{pmatrix}^T$. We have also introduced the symplectic form $\Omega = \bigoplus_{k=1}^{2N}\omega$, where ω is the antisymmetric matrix,

$$\omega = \begin{pmatrix} 0 & 1 \\ -1 & 0\end{pmatrix}. \tag{4.8}$$

The modes S are then mixed on the interferometer B, and we assume that the corresponding mode functions are identical and have a high overlap at the beamsplitters making up the interferometer. Let $\hat{a}_s$ be the amplitude operator for a mode $s \in S$, the interferometer B is assumed to generate the Bogoliubov transformation,

$$\begin{pmatrix}\hat{a}_{s_1}\\ \hat{a}_{s_2}\\ \hat{a}_{s_3}\\ \vdots \\ \hat{a}_{s_N}\end{pmatrix} \to \frac{1}{\sqrt{N}}\begin{pmatrix} 1 & e^{i\frac{2\pi}{N}} & e^{i2\frac{2\pi}{N}} & \dots & e^{i(N-1)\frac{2\pi}{N}} \\ 1 & e^{i2\frac{2\pi}{N}} & e^{i4\frac{2\pi}{N}} & \dots & e^{i2(N-1)\frac{2\pi}{N}} \\ 1 & e^{i3\frac{2\pi}{N}} & e^{i6\frac{2\pi}{N}} & \dots & e^{i3(N-1)\frac{2\pi}{N}} \\ \vdots & \vdots & \vdots & \ddots & \vdots \\ 1 & 1 & 1 & \dots & 1\end{pmatrix}\begin{pmatrix}\hat{a}_{s_1}\\ \hat{a}_{s_2}\\ \hat{a}_{s_3}\\ \vdots \\ \hat{a}_{s_N}\end{pmatrix} \tag{4.9}$$

We condition the state on obtaining a click at detector s_N and no clicks at the remaining detectors, thereby heralding the conditional state ρ_c of modes P. The projector corresponding to this event is $\hat{\Pi}_c = \left(\prod_{s\in\bar{S}}|0\rangle_s\langle 0|\right)(I_{s_N} - |0\rangle_{s_N}\langle 0|)$, where $\bar{S}$ is the set $\bar{S} = S\backslash\{s_N\}$. The conditional state is obtained as $\rho_c = \mathrm{Tr}_S[\rho\hat{\Pi}_c]/P(C)$, where $P(C)$ is the normalization, i.e. the probability of obtaining the measurement

outcomes heralding a successful swap. $\hat{\Pi}_c$ has the characteristic function,

$$\begin{aligned}\chi_c(\Lambda_S) &= \mathrm{Tr}\left[\hat{\Pi}_c D_S(\Lambda_S)\right] \\ &= E(\Lambda_{\bar{S}}) \cdot \left(\pi\delta^{(2)}(\Lambda_{s_N}) - E(\Lambda_{s_N})\right),\end{aligned} \tag{4.10}$$

where

$$E(\Lambda_j) = \exp\left[-\frac{1}{2}\Lambda_j^T \Lambda_j\right], \tag{4.11}$$

and $\delta^{(2)}(\Lambda_j)$ is a delta function. We obtain the characteristic function of the conditional state through integration,

$$\chi_{\rho_c}(\Lambda_P) = \frac{1}{\pi^N P(C)} \int_{\mathbb{R}^{2N}} \chi_\rho(\Lambda)\chi_c(-\Lambda_S) d^{2N}\Lambda_S. \tag{4.12}$$

We then compute the Bell value of the W^{3}ZB inequality by evaluating the expectation values $\langle M^{(n)}\rangle = \langle \prod_{p\in P} M_p^{(n_p)}\rangle$, for each setting n. This is done via the integral [1],

$$\begin{aligned}\left\langle \prod_{p\in P} M_p^{(n_p)} \right\rangle &= \mathrm{Tr}\left\{\rho_c \prod_{p\in P} M_p^{(n_p)}\right\} \\ &= \frac{1}{\pi^N}\int_{\mathbb{R}^{2N}} \chi_{\rho_c}(-\Lambda_P)\chi_M\left(\Lambda_P, X_P\right) d^{2N}\Lambda_P,\end{aligned} \tag{4.13}$$

where $\chi_M\left(\Lambda_P, X_P\right)$ is the characteristic function associated with the observable $\prod_{p\in P} M_p^{(n_p)}$. X_P is a vector of the displacements applied prior to the detectors, $X_P = \bigoplus_{p\in P} X_p^{(n_p)}$. A closed form expression for $\langle \prod_{p\in P} M_p^{(n_p)}\rangle$ can be found in appendix A1.

Noise model

We now outline how we describe noise relevant to the experiment. We will include dark-counts in the detectors, loss in the channels, phase noise in the channels and measurements, and finally, amplitude noise in the measurements. Amplitude and phase noise during measurement are expected to arise if imperfect displacements are applied.

We include dark-counts in our measurement model by adding a noise term to the observable. Given that p_d is the probability of getting a dark-count at a given detector, then we measure the observable,

$$\begin{aligned}M_p^{(n_p)} &= (1-p_d)\left[I_p - 2\left|-X_p^{(n_p)}\right\rangle_p\left\langle -X_p^{(n_p)}\right|\right] + p_d I_p \\ &= I_p - 2(1-p_d)\left|-X_p^{(n_p)}\right\rangle_p\left\langle -X_p^{(n_p)}\right|.\end{aligned} \tag{4.14}$$

If a given detector in S is triggered by a dark-count with probability p_d, then the swap results in the transformation (see appendix A1),

$$\rho \to \rho_c = \frac{1}{P(C)} \mathrm{Tr}_S \left[\rho \widetilde{\Pi}_c \right]. \tag{4.15}$$

We have introduced the operator $\widetilde{\Pi}_c$,

$$\widetilde{\Pi}_c = (1-p_d)^{N-1} \left(\prod_{s \in \bar{S}} |0\rangle_s\langle 0| \right) \cdot \left(I_{s_N} - (1-p_d) |0\rangle_{s_N}\langle 0| \right). \tag{4.16}$$

We now describe how channel loss and detector efficiency is included in our model. Given that channel ch_{p_n} has transmission η_{p_n} and channel ch_{s_k} has transmission η_{s_k}, we model loss by a Gaussian map acting on the covariance matrix σ as [1],

$$\sigma \to G_\eta^{1/2} \sigma G_\eta^{1/2} + (I - G_\eta), \tag{4.17}$$

with the diagonal matrix $G_\eta = G_{\eta_P} \oplus G_{\eta_S}$, where $G_{\eta_P} = \mathrm{Diag}\left[\bigoplus_{p \in P} \begin{pmatrix} \eta_p & \eta_p \end{pmatrix} \right]$ and $G_{\eta_S} = \mathrm{Diag}\left[\bigoplus_{s \in S} \begin{pmatrix} \eta_s & \eta_s \end{pmatrix} \right]$. We will assume that η_{p_n} equals η_P, i.e. the channels $\mathrm{ch_P} = \{\mathrm{ch}_{p_1}, \mathrm{ch}_{p_2}, \ldots, \mathrm{ch}_{p_N}\}$ have the same transmission. Likewise we assume that η_{s_k} equals η_S. η_d is the efficiency of a detector, and $1-\eta_d$ is the loss of the detector. Given that η_d is the same for all detectors in S, detector loss can then be commuted through B and absorbed into the transmission of the channels $\mathrm{ch_S} = \{\mathrm{ch}_{s_1}, \mathrm{ch}_{s_2}, \ldots, \mathrm{ch}_{s_N}\}$. Likewise, the detector loss in P can be shifted to be prior to the displacements, if we attenuate the magnitude of the displacements by the factor $\sqrt{\eta_d}$.
We now turn to the problem of how to model phase noise. A phase perturbation of the state ρ, e.g. caused by environmental disturbance, can be modelled as a stochastic rotation in phase space,

$$\rho = \int d^N \boldsymbol{\theta} P(\boldsymbol{\theta}) R(\boldsymbol{\theta}) \rho_0 R(-\boldsymbol{\theta}), \tag{4.18}$$

where ρ_0 is the unperturbed state, and $\boldsymbol{\theta}$ is a vector of stochastic rotation angles θ_p for $p \in P$, each being a perturbation on the phase of the corresponding mode. Note that phase noise acting on channels $\mathrm{ch_S}$ is shifted to act on channels $\mathrm{ch_P}$ instead. $R(\boldsymbol{\theta})$ is the rotation operator $R(\boldsymbol{\theta}) = \prod_{p \in P} R_p(\theta_p)$. $R_{p_n}(\theta_{p_n})$ is applied just prior to the displacement operation on mode p_n, and includes phase noise resulting from propagation in the channels $\mathrm{ch}_{\mathtt{p}_n}$ and $\mathrm{ch}_{\mathtt{s}_n}$, and also the phase noise in the subsequent displacement operation. We make the assumption that the angles $\boldsymbol{\theta}$ are uncorrelated, and model the probability density $P(\boldsymbol{\theta})$ as a product of normal distributions for each angle θ_p. The variance of θ_p is labelled as V_θ, and is the same for all modes. The correlated phase noise resulting from the interferometer B cannot be entirely captured by this simple model, but we expect that our model is sufficiently

η_P	η_S	σ_A	σ_θ	p_d
0.9	0.2	3/100	100 mrad	1/10000

Table 4.1: *Standard settings for noise parameters. η_P is the transmission of the channels $ch_{\mathbf{p}}$ ($ch_{\mathbf{p}_1}$, $ch_{\mathbf{p}_2}$ etc.). η_S is the transmission of channels $ch_{\mathbf{s}}$. σ_A is the standard deviation of the relative amplitude distribution ($\sigma_A^2 = V_A$). σ_θ is the standard deviation of the phase angle distribution ($\sigma_\theta^2 = V_\theta$). p_d is the probability of getting a dark-count at a given detector (e.g. p_n or s_n) during the measurement interval (which is assumed to be τ in our analysis).*

close to reality to indicate the sensitivity of the experiment toward phase noise. We furthermore assume that the angles θ_p are small, allowing us to approximate the rotation of a coherent state by a small linear translation in phase space.
Finally, we describe how we model amplitude noise. Amplitude noise arises from an imperfect displacement and is modelled similarly to phase noise, with the rotation operator in Eq. 4.18 replaced by a displacement operator. The stochastic displacement on mode p is given relative to the displacement $X_p^{(n_p)}$ applied on mode p, i.e. for mode p we obtain the stochastic displacement $\epsilon_p X_p^{(n_p)}$, where ϵ_p is referred to as the relative amplitude. We assume that the relative amplitudes ϵ_p are normal, independent and identically distributed, with variance V_A. A more detailed description of the noise model can be found in appendix A1.

4.4 Results and Discussion

We compute Bell values under varying experimental conditions. In order to obtain realistic values we must include in the model reasonable experimental errors. We choose the noise parameters shown in Table 4.1. Unless otherwise stated, these are the values used for the noise parameters throughout our analysis. E.g. if we vary η_P, as is done in Fig. 4.6, then the remaining noise parameters are set at the values listed in Table 4.1.

We maximize the violation of the W^{3}ZB inequality in the squeezing parameter r. The Bell value as a function of r, for the optimal choice of measurement settings, is shown in Fig. 4.3. We clearly observe that there exists an optimal squeezing value for which the Bell value is maximized, and that the optimal squeezing depends on the number of parties. We also observe that the maximal Bell value increases for more parties, until 6 parties, at which point the maximal Bell value decreases for more parties.

While the correlations between all parties lead to a violation of the W^{3}ZB inequality at the optimal squeezing, we find that, for up to 4 parties, the marginal outcome probabilities describing any subgroup of parties are inside the Bell poly-

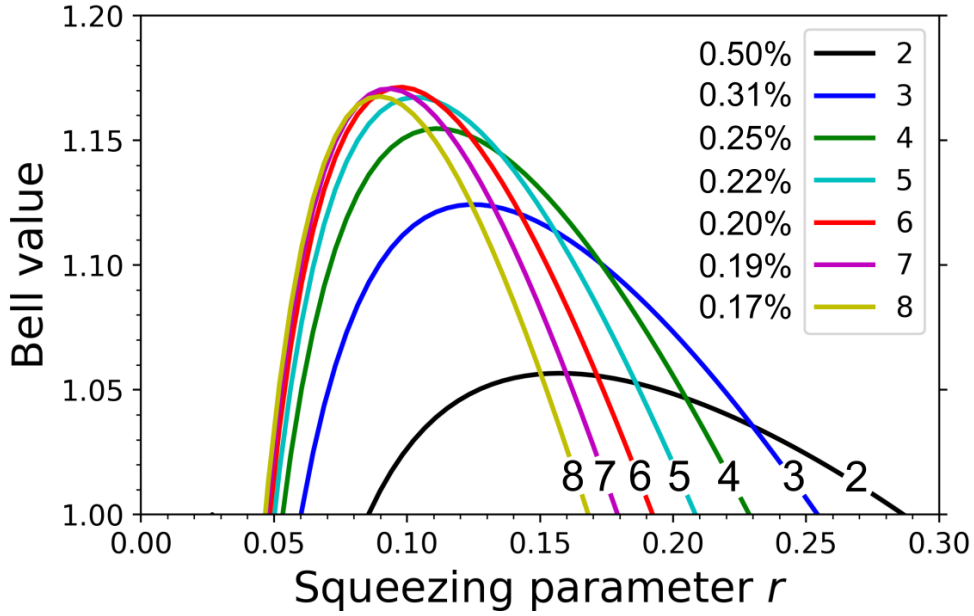

Figure 4.3: *Bell value of the W^3ZB inequality against the squeezing parameter r for different number of parties. The annotation and legend gives the number of parties. The Bell value is computed for the optimal measurement settings at the given value of r. We observe a maximum in the Bell value at a particular squeezing. Next to the legend we list the probability $P(C)$ that an experiment succeeds with that number of parties, at the corresponding optimal value of r (the value of r giving the largest Bell value).*

tope, with the used measurement settings. This was evidenced by a linear program (see appendix A2), and indicates that in these cases nonlocality results from correlations between *all* parties. An exception can occur for 5 parties if η_P is above 97%, and for 6 parties if η_P is above 91%, with the used measurement settings. In these cases a Bell inequality can be broken with a subgroup of 4 and 5 parties respectively.

We find the optimal displacements (measurement settings), at the optimal squeezing, for which the violation is maximized. The optimal displacement for party p_1 and another party p_n, are shown in Fig. 4.4. The phase angles of the two-mode squeezers belonging to p_1 and p_n respectively, are labelled as ϕ_{p_1} and ϕ_{p_n}. $m_0^{(p_1)}$ and $m_1^{(p_1)}$ are the displacements used by party p_1, whereas $m_0^{(p_n)}$ and $m_1^{(p_n)}$ are the displacements used by party p_n. $m_0^{(p_1)}$ and $m_0^{(p_n)}$ have the same magnitude, but the displacements are directed along different quadrature axes at an angle $\phi_{p_1} - \phi_{p_n}$, likewise for $m_1^{(p_1)}$ and $m_1^{(p_n)}$. So the displacements used by a given party p_n will be determined by the phase angle of their squeezer ϕ_{p_n}. The magnitudes of $m_0^{(p_n)}$ and $m_1^{(p_n)}$ depend on the number of parties and are listed in Table 4.2. The overall orientation of the quadrature axes is arbitrary, i.e. we can freely rotate Fig. 4.4, as long as the angle between displacements remain unchanged. In this sense, the displacements used by party p_1 serve as a reference from which we can define the displacements to be used by the remaining parties.

We note that the optimum in squeezing, seen in Fig. 4.3, is the result of a competition between the dark-count rate and the multi-photon generation rate. A dark-count would render the measurements by the parties uncorrelated, thereby lowering the Bell value. This indicates that it is preferable to have high squeezing, so that photons from the optical field outnumber the dark-counts. However, the click detectors in S cannot distinguish between 1 or more photons. Multi-photon emission from the two-mode squeezers therefore create mixedness in the conditional state generated by the swap, and this mixedness weakens the correlations between the measurement outcomes obtained by the parties. This mixedness can be avoided by lowering the degree of squeezing, so that on average less than one photon reaches the detectors in S. As a result, there is some amount of squeezing where the combined detrimental effect of dark-counts and multi-photon generation is minimized. As we increase the number of parties, the presence of dark-counts becomes more detrimental due to the increased number of detectors, and the lower probability of a successful swap $P(C)$. This is the cause of the decrease in maximal Bell value for 7 and 8 parties, as compared to the case with 6 parties.

We investigate the sensitivity of the experiment toward the probability of a dark-count at a given detector in S, the result can be seen in Fig. 4.5 (left) for different number of parties. The probability of a dark-count at a given detector in P is fixed at 0.01%. A dark-count at detector s_N would mistakenly herald nonlocal

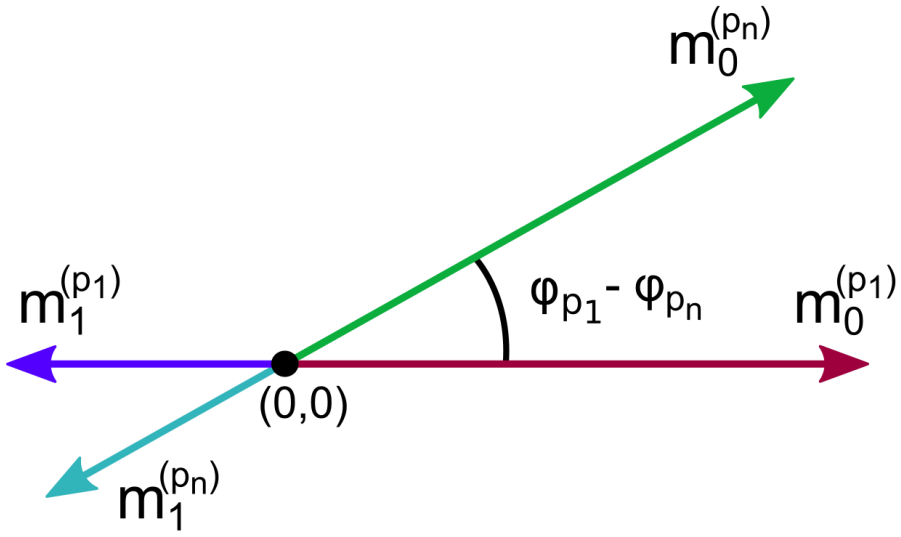

Figure 4.4: *We show the orientation of the optimal displacements (measurement settings) that the parties p_1 and p_n should use to obtain a maximal violation of the W^3ZB inequality. $m_0^{(p_1)}$ and $m_1^{(p_1)}$ are the displacements used by party p_1, whereas $m_0^{(p_n)}$ and $m_1^{(p_n)}$ are the displacements used by party p_n (any party). p_n's displacements should be at the angle $\phi_{p_1} - \phi_{p_n}$ relative to p_1's displacements, where ϕ_{p_1} and ϕ_{p_n} are the phase angles of the two-mode squeezers belonging to p_1 and p_n. The magnitudes of $m_0^{(p_n)}$ and $m_1^{(p_n)}$ depend on the number of parties and are listed in Table 4.2.*

No. of Parties	m_0	m_1
2	0.59	-0.18
3	0.47	-0.20
4	0.41	-0.19
5	0.37	-0.18
6	0.33	-0.17

Table 4.2: *Magnitudes of the optimal displacements shown in Fig. 4.4 for the optimal value of r. If the detector transmission is η_d, then the magnitudes should be multiplied by $1/\sqrt{\eta_d}$.*

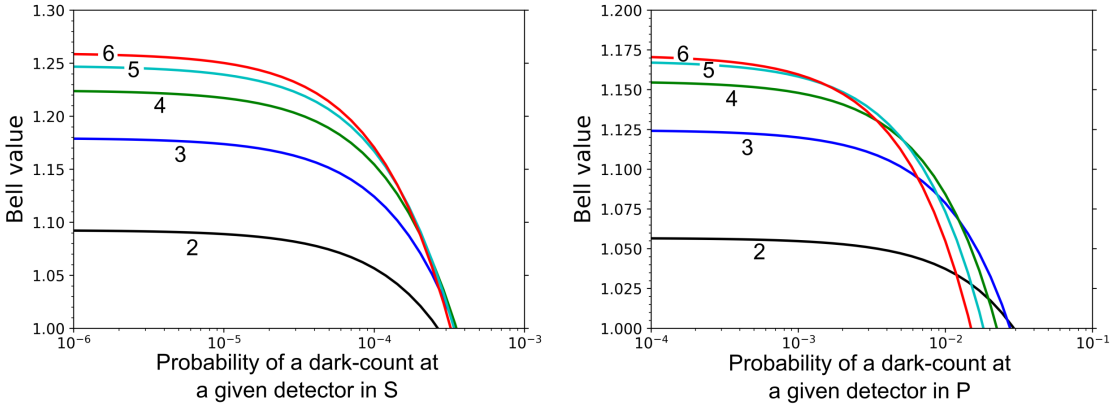

Figure 4.5: ***Left**: Bell value of the W^3ZB inequality against the probability of a dark-count at a given detector in S during the measurement interval. The annotation indicates the number of parties.* ***Right**: Bell value of the W^3ZB inequality against the probability of a dark-count at a given detector in P during the measurement interval.*

correlations between the detectors in P, when no such correlations actually exists. This erroneous heralding significantly lowers the calculated Bell value. The Bell value is found to rapidly decrease around 0.02%. At this point, the probability of getting a dark-count is no longer insignificant compared with the probability of generating the conditional state, which is in the range 0.2% to 0.5%, depending on the number of parties (see Fig. 4.3). For the case of 2 parties, the decrease in Bell value proceeds a bit slower, however the lower initial Bell value (1.09) results in the curve reaching the classical limit of 1 at smaller dark-count probabilities. The drop in Bell value for increasing probability of a dark-count, is in part due to the squeezing no longer being optimal. However, our calculations indicate that if p_d exceeds 0.05%, then the experiment cannot be used to violate the W^3ZB inequality, given the remaining errors (Table 4.1), even at the corresponding optimal squeezing and measurement settings, and for any number of parties.
We also analyse the robustness of the Bell inequality violation against the probability of a dark-count at a given detector in P, while the probability of a dark-count at a given detector in S is fixed at 0.01%. A plot of this is shown in Fig. 4.5 (right), and clearly illustrates that the violation is highly robust against this probability.

The impact of loss on the Bell value of the W^3ZB inequality is shown in Fig. 4.6 and Fig. 4.7. In Fig. 4.6 we vary the transmission η_P, and show how the Bell value changes. The transmission at which the Bell value drop below one, lowers as we increase the number of parties. This indicates that a demonstration of nonlocality might be easier to realize when using more parties. In Fig. 4.7 we show the dependence of the Bell value on the transmission η_S. We observe that the Bell value is

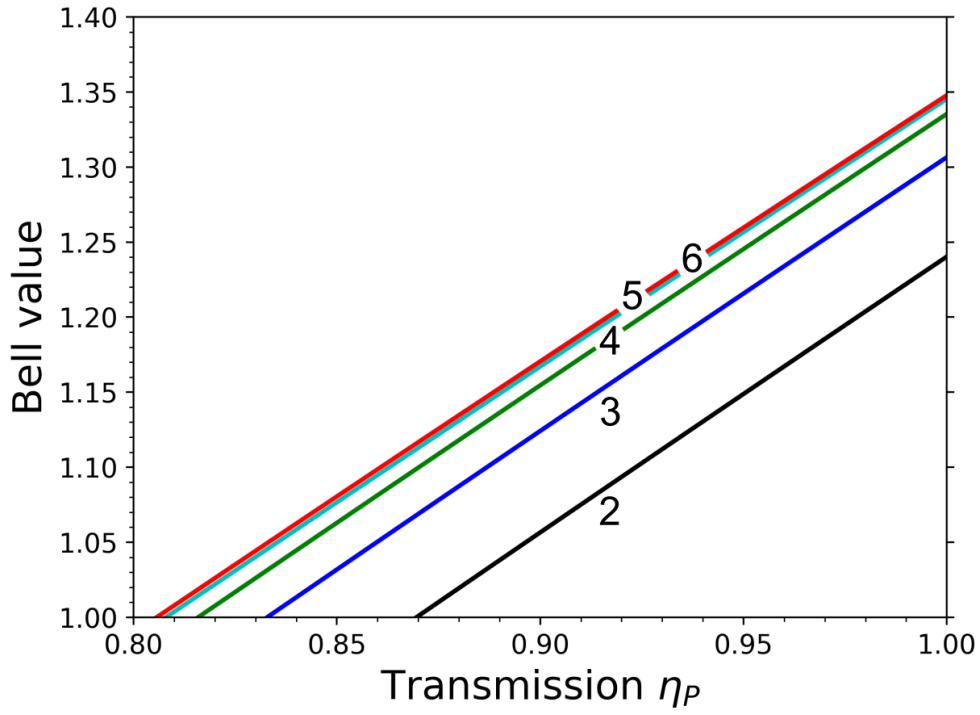

Figure 4.6: *We plot how the Bell value of the W^3ZB inequality depends on the transmission of the channels ch_P, connecting the two-mode squeezers to the detectors in P. The annotation indicates the number of parties.*

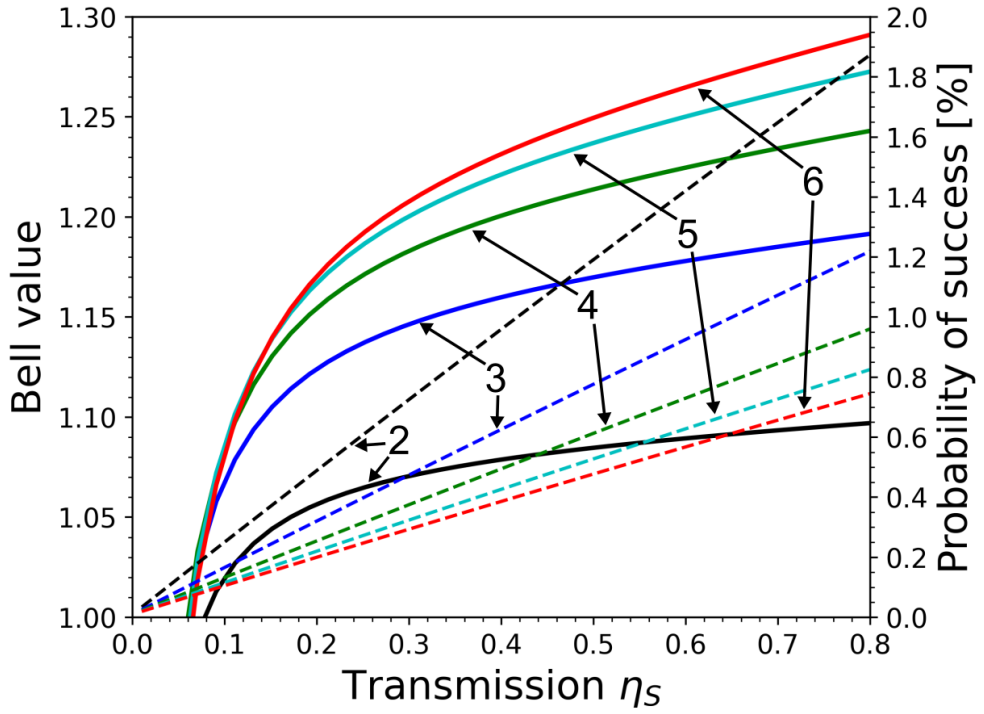

Figure 4.7: *We plot how the Bell value of the W^3ZB inequality depends on the transmission of the channels ch_S, connecting the two-mode squeezers to the swapping detectors S. The annotation indicates the number of parties. The solid curves correspond to Bell values and match the left y-axis. The dashed curves are the corresponding probabilities of generating the conditional state $P(C)$, these drop as we lower the transmission η_S.*

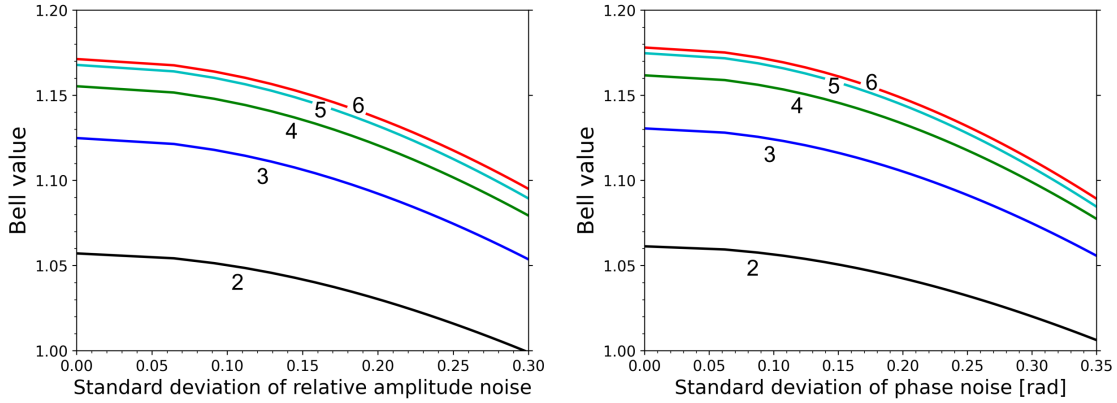

Figure 4.8: ***Left**: We plot how the Bell value of the W^3ZB inequality depends on amplitude noise (σ_A). The annotation indicates the number of parties.* ***Right**: We plot how the Bell value depends on the phase noise (σ_θ).*

only weakly dependent on this transmission until a critical point around a transmission of 10 %. The probability $P(C)$ of successfully generating the conditional state, heralded by detector s_N clicking and the remaining detectors in S staying silent, is seen to drop linearly for decreasing transmission. If we assume a fiber loss of 0.3 dB/km, we find that a transmission of 10 % corresponds to approximately 30 km. The maximal achievable separation between two parties will then be around 60 km.

We then check the sensitivity of the experiment against phase and amplitude noise. The result is shown in Fig. 4.8. In Fig. 4.8 (left) we plot the Bell value against the standard deviation of the relative amplitude distribution, σ_A. In Fig. 4.8 (right) we plot the Bell value against the standard deviation of the phase distribution, σ_θ. We observe that the Bell value is not very sensitive to amplitude and phase noise. This implies that the optimal displacements, shown in Table 4.2 and Fig. 4.4, are not so strict, and that slight deviations from these displacements are acceptable.

4.5 Conclusion

We have proposed an experiment for demonstrating nonlocality with multiple parties separated by a set of lossy channels. The experiment utilizes only standard quantum optical elements, including on/off detectors, beamsplitters, two-mode squeezers and displacements. We have given a detailed account of how loss impact the experiment, and identified critical values for channel transmissions, required for a Bell inequality violation with dichotomic inputs and outputs. We found that the experiment is

very robust against loss in the channels connecting the parties ($\mathrm{ch_S}$), allowing for transmissions as low as 10%. On the other hand, our calculations indicate that the nonlocality of the experiment is strongly impacted by loss in the channels connecting the two-mode squeezer of each party, to the detector associated with that party (channels $\mathrm{ch_P}$). However, we found that the experiment could be made more robust against loss in channels $\mathrm{ch_P}$, if the number of parties is increased. With 4 parties we found that the $\mathrm{W^3ZB}$ inequality could be violated for transmissions of channels $\mathrm{ch_P}$ as low as 82%. For an experiment with 4 or fewer parties, we found that the marginal outcome probabilities for all possible subgroups were inside the Bell polytope, with the used measurement settings.

Due to the heralded nature of the experiment, it is very sensitive toward dark-counts at the heralding detector. Our calculations indicate that the probability of a dark-count at a given detector during a measurement must not be much higher than 1 in 10000, or the experiment fails. We then examined the influence of amplitude and phase noise, and found that the experiment is quite robust against these noise sources. The phase noise could be as high as several hundred milliradians, and the relative amplitude noise could be in excess of 25%.

4.6 Acknowledgment

This work was supported by the European Union's Horizon Europe research and innovation programs under the project "Quantum Security Networks Partnership" (QSNP, grant agreement No 101114043) and the Danish National Research Foundation, Center for Macroscopic Quantum States (bigQ, DNRF142) and research grant (40864) from VILLUM FONDEN.

4.7 Appendix

4.7.1 A1

The state ρ is generated by N two-mode squeezers, and occupy the modes S and P. The characteristic function of ρ is given by $\chi_\rho(\Lambda) = \exp[-(1/2)\Lambda^T\Omega\sigma\Omega^T\Lambda]$ where Λ is a vector of conjugate quadratures for the modes in S and P. We introduce the following decomposition of the covariance matrix of ρ,

$$\sigma = \begin{pmatrix} \sigma_P & K_{\bar{S}} & K_{s_N} \\ K_{\bar{S}}^T & \sigma_{\bar{S}} & C \\ K_{s_N}^T & C^T & \sigma_{s_N} \end{pmatrix}. \tag{4.19}$$

We also introduce the matrices,

$$K_S = \begin{pmatrix} K_{\bar{S}} \, K_{s_N} \end{pmatrix}, \quad \sigma_S = \begin{pmatrix} \sigma_{\bar{S}} & C \\ C^T & \sigma_{s_N} \end{pmatrix}. \tag{4.20}$$

The subscript refer to the modes described by the relevant submatrix, i.e. $\sigma_{\bar{S}}$ describes the marginal distribution of the modes $\bar{S} = S \backslash \{s_N\}$.
The modes in S are mixed in the interferometer B, described by the Bogoliubov transformation in Eq. 4.9. We then condition the state on obtaining a click at detector s_N and no click at the remaining detectors in S (this is referred to as a swap). If the detectors in S are triggered by a dark-count with probability p_d, then the swap might herald success under three different conditions,

1. No dark-counts occur. Light reaches detector s_N and no light reaches the remaining detectors in S. This event is associated with the projector $\hat{\Pi}_1 = \left(\prod_{s\in\bar{S}} |0\rangle_s\langle 0|\right)(I_{s_N} - |0\rangle_{s_N}\langle 0|)$.
2. A dark-count occurs at detector s_N. Light reaches detector s_N and no light reaches the remaining detectors in S. This event is associated with the projector $\hat{\Pi}_1 = \left(\prod_{s\in\bar{S}} |0\rangle_s\langle 0|\right)(I_{s_N} - |0\rangle_{s_N}\langle 0|)$.
3. A dark-count occurs at detector s_N. No light reaches any detectors in S. This event is associated with the projector $\hat{\Pi}_2 = \prod_{s\in S} |0\rangle_s\langle 0|$.

Let $P(\hat{\Pi}_n|C)$ be understood as the probability that the event $\hat{\Pi}_n$ occur, given that detectors S herald a successful swap C. $P(\hat{\Pi}_n) = \mathrm{Tr}\left[\hat{\Pi}_n\rho\right]$ is the prior probability that the event $\hat{\Pi}_n$ occurs. The swap then transform the state ρ into the conditional

state ρ_c as,

$$\begin{aligned}
&\rho \to \rho_c \\
&= \mathrm{Tr}_S \left[P(\hat{\Pi}_1|C) \frac{\hat{\Pi}_1 \rho \hat{\Pi}_1}{P(\hat{\Pi}_1)} + P(\hat{\Pi}_2|C) \frac{\hat{\Pi}_2 \rho \hat{\Pi}_2}{P(\hat{\Pi}_2)} \right] \\
&= \mathrm{Tr}_S \left[\rho \left(P(\hat{\Pi}_1|C) \frac{\hat{\Pi}_1}{P(\hat{\Pi}_1)} + P(\hat{\Pi}_2|C) \frac{\hat{\Pi}_2}{P(\hat{\Pi}_2)} \right) \right].
\end{aligned} \tag{4.21}$$

By Bayes' theorem we have,

$$\frac{P(\hat{\Pi}_n|C)}{P(\hat{\Pi}_n)} = \frac{P(C|\hat{\Pi}_n)}{P(C)}, \tag{4.22}$$

which gives another expression for ρ_c,

$$\begin{aligned}
\rho_c &= \mathrm{Tr}_S \left[\rho \left(\frac{P(C|\hat{\Pi}_1)}{P(C)} \hat{\Pi}_1 + \frac{P(C|\hat{\Pi}_2)}{P(C)} \hat{\Pi}_2 \right) \right] \\
&= \frac{1}{P(C)} \mathrm{Tr}_S \left[\rho \widetilde{\Pi}_c \right]
\end{aligned} \tag{4.23}$$

Where we have introduced the operator $\widetilde{\Pi}_c$,

$$\widetilde{\Pi}_c = P(C|\hat{\Pi}_1)\hat{\Pi}_1 + P(C|\hat{\Pi}_2)\hat{\Pi}_2 \tag{4.24}$$

The probability of the swap being heralded as successful, given that the event $\hat{\Pi}_1$ occur, is given by $P(C|\hat{\Pi}_1) = (1-p_d)^N + (1-p_d)^{N-1} p_d$, i.e. the swap will succeed as long as no dark-count triggers any detector other than s_N. If no light reaches any detectors in S, then the swap can only be heralded as successful if a dark-count triggers detector s_N, so $P(C|\hat{\Pi}_2) = (1-p_d)^{N-1} p_d$. Then we have,

$$\begin{aligned}
\widetilde{\Pi}_c &= (1-p_d)^N \hat{\Pi}_1 + (1-p_d)^{N-1} p_d (\hat{\Pi}_1 + \hat{\Pi}_2) \\
&= (1-p_d)^{N-1} \left(\prod_{s \in \bar{S}} |0\rangle_s \langle 0| \right) \left[I_{s_N} - (1-p_d) |0\rangle_{s_N} \langle 0| \right]
\end{aligned} \tag{4.25}$$

Different number of photons could *in principle* be distinguishable by the detector, even if the experimenter cannot distinguish the detector states sufficiently well to obtain this information. We define a projector onto Fock states, $\hat{\Pi}^{(n)} = \left(\prod_{s \in \bar{S}} |0\rangle_s \langle 0| \right) |n\rangle_{s_N} \langle n|$. If different Fock states are in principle distinguishable, then

the transformation of ρ, conditioned on the swap, ought to be,

$$\begin{aligned}\rho &\to \mathrm{Tr}_S\left[\sum_{n=0}^{\infty} P\left(\hat{\Pi}^{(n)}|C\right)\frac{\hat{\Pi}^{(n)}\rho\hat{\Pi}^{(n)}}{P\left(\hat{\Pi}^{(n)}\right)}\right]\\ &= \mathrm{Tr}_S\left[\rho\sum_{n=0}^{\infty}\frac{P\left(\hat{\Pi}^{(n)}|C\right)}{P\left(\hat{\Pi}^{(n)}\right)}\hat{\Pi}^{(n)}\right]\end{aligned} \tag{4.26}$$

Using Bayes' theorem we have,

$$\begin{aligned}&= \frac{1}{P(C)}\mathrm{Tr}_S\left[\rho\sum_{n=0}^{\infty}P\left(C|\hat{\Pi}^{(n)}\right)\hat{\Pi}^{(n)}\right]\\ &= \frac{1}{P(C)}\mathrm{Tr}_S\left[\rho\widetilde{\Pi}'_c\right]\end{aligned} \tag{4.27}$$

We then make the assumption that,

$$P\left(C|\hat{\Pi}^{(n)}\right) = \begin{cases}(1-p_d)^N + (1-p_d)^{N-1}p_d, & \text{if } n>0\\ (1-p_d)^{N-1}p_d, & \text{if } n=0\end{cases} \tag{4.28}$$

Under this assumption one can show that $\widetilde{\Pi}'_c = \widetilde{\Pi}_c$, and it doesn't matter whether we use the transformation in Eq. 4.21 or in Eq. 4.26.
The characteristic function of $\widetilde{\Pi}_c$ is given by,

$$\begin{aligned}&\chi_c(\Lambda_S) = \mathrm{Tr}_S\left[\widetilde{\Pi}_c D_S(\Lambda_S)\right]\\ &= (1-p_d)^{N-1}E(\Lambda_{\bar{S}})\cdot\left(\pi\delta^{(2)}(\Lambda_{s_N}) - (1-p_d)E(\Lambda_{s_N})\right)\end{aligned} \tag{4.29}$$

Then we have that,

$$\begin{aligned}&\rho_c = \frac{1}{P(C)}\mathrm{Tr}_S[\rho\widetilde{\Pi}_c] =\\ &\frac{1}{P(C)}\int_{\mathbb{R}^{4N}} D_P(-\Lambda_P)\chi_\rho(\Lambda_P,\Lambda_S)\chi_c(-\Lambda_S)\frac{d^{4N}\Lambda}{\pi^{2N}}.\end{aligned} \tag{4.30}$$

In evaluating the above expression we have used Glauber's formula [1] to express ρ and $\widetilde{\Pi}_c$ in terms of their characteristic functions (χ_ρ and χ_c),

$$\hat{O} = \int_{\mathbb{R}^{2n}}\frac{d^{2n}B}{\pi^n}\chi_O(B)D^\dagger(B), \tag{4.31}$$

where n is the number of modes. We also used the facts,

$$\mathrm{Tr}_i[D(\Lambda_i)] = \pi\delta^{(2)}(\Lambda_i) \tag{4.32}$$

$$D(\Lambda_i)D(\Lambda_j) = D(\Lambda_i + \Lambda_j)\exp[-i\Lambda_i^T \omega \Lambda_j] \tag{4.33}$$

From Eq. 4.30 we may read off the characteristic function of the conditional state ρ_c,

$$\chi_{\rho_c}(\Lambda_P) = \frac{1}{\pi^N P(C)} \int_{\mathbb{R}^{2N}} \chi_\rho(\Lambda_P, \Lambda_S)\chi_c(-\Lambda_S) d^{2N}\Lambda_S. \tag{4.34}$$

Inserting the expressions for χ_ρ and χ_c, we may evaluate the conditional state as,

$$\chi_{\rho_c}(\Lambda_P) = \frac{(1-p_d)^{N-1}}{P(C)} \left[\chi_{\bar{S}}(\Lambda_P) - (1-p_d)\chi_S(\Lambda_P)\right]. \tag{4.35}$$

$\chi_{\bar{S}}$ and χ_S are Gaussian and respectively given by

$$\begin{aligned}
\chi_{\bar{S}}(\Lambda_P) &= \frac{1}{\pi^N} \int_{\mathbb{R}^{2N}} \chi_\rho(\Lambda_P, \Lambda_S) E(\Lambda_{\bar{S}}) \pi\delta^{(2)}(\Lambda_{s_N}) d^{2N}\Lambda_S \\
&= 2^{N-1} ||\gamma_{\bar{S}}||^{-1/2} E\left[V_{\bar{S}}, 0\right](\Lambda_P) \qquad (4.36) \\
\chi_S(\Lambda_P) &= \frac{1}{\pi^N} \int_{\mathbb{R}^{2N}} \chi_\rho(\Lambda_P, \Lambda_S) E(\Lambda_S) d^{2N}\Lambda_S \\
&= 2^N ||\gamma_S||^{-1/2} E\left[V_S, 0\right](\Lambda_P). \qquad (4.37)
\end{aligned}$$

Where the brackets $||.||$ refer to the determinant and,

$$\begin{aligned}
E\left[V, \bar{x}\right](B) &= \exp\left[-\frac{1}{2} B^T \Omega V \Omega^T B - i(\Omega\bar{x})^T B\right], \\
\gamma_{\bar{S}} &= \sigma_{\bar{S}} + I, \quad \gamma_S = \sigma_S + I, \\
V_{\bar{S}} &= \sigma_P - K_{\bar{S}}\, \gamma_{\bar{S}}^{-1}\, K_{\bar{S}}^T, \\
V_S &= \sigma_P - K_S\, \gamma_S^{-1}\, K_S^T.
\end{aligned} \tag{4.38}$$

The normalization $P(C)$ can be obtained by demanding that $\chi_{\rho_c}(\Lambda_P = 0) = 1$. $E\left[V, \bar{x}\right](B)$ is the characteristic function of a Gaussian state with covariance matrix V and centred on position $\bar{x}$ in phase space.

We now derive a closed-form expression for the correlator $\langle \prod_{p\in P} M_p^{(n_p)} \rangle$, describing correlations between the measurement outcomes obtained by the N parties. The characteristic function of the observable $\prod_{p\in P} M_p^{(n_p)}$ is given by,

$$\begin{aligned}
&\chi_M(\Lambda, X_P) \\
&= \prod_{p\in P} \left\{\pi\delta^{(2)}(\Lambda_p) - 2(1-p_d) E\left[I, -2X_p^{(n_p)}\right](\Lambda_p)\right\}.
\end{aligned} \tag{4.39}$$

As we will show in the next section, when amplitude or phase noise is present, then we should instead use the characteristic function,

$$\begin{aligned}&\chi_M\left(\Lambda_P, X_P\right)\\&=\prod_{p\in P}\left\{\pi\delta^{(2)}\left(\Lambda_p\right)-2(1-p_d)E\left[\Delta_p^{(n_p)},-2X_p^{(n_p)}\right]\left(\Lambda_p\right)\right\},\end{aligned}\tag{4.40}$$

where $\Delta_p^{(n_p)}$ is the covariance matrix describing a noisy displacement for party p. We form the covariance matrix Δ_P, describing the statistics of the noisy displacements for all N modes. We assume no correlation between noise in different modes, and Δ_P is therefore block diagonal. The above product is rewritten as a sum over products,

$$\chi_M\left(\Lambda_P, X_P\right)=\sum_d[-2(1-p_d)]^{|d|}\prod_{p\in P}K_p^{(d_p)},\tag{4.41}$$

where the sum runs over all binary lists $d=(d_{p_1},d_{p_2},\ldots,d_{p_N})$. $|d|$ is the sum of d, i.e. the number of ones in the list. $K_p^{(d_p)}$ is the piecewise characteristic function defined as,

$$K_p^{(d_p)}=\begin{cases}\pi\delta^2\left(\Lambda_p\right) & \text{if } d_p=0\\ E\left[\Delta_p^{(n_p)},-2X_p^{(n_p)}\right]\left(\Lambda_p\right) & \text{if } d_p=1\end{cases}.\tag{4.42}$$

Given a Gaussian state ρ_G with characteristic function $E[\sigma_G,0](\Lambda_P)$, we evaluate the expectation value of the observable,

$$\begin{aligned}&f\left(\sigma_G,X_P\right)=\mathrm{Tr}\left\{\rho_G\prod_{p\in P}M_p^{(n_p)}\right\}\\&=\frac{1}{\pi^N}\int_{\mathbb{R}^{2N}}E[\sigma_G,0](-\Lambda_P)\chi_M\left(\Lambda_P,X_P\right)d^{2N}\Lambda_P\\&=\sum_d[-8\pi(1-p_d)]^{|d|}G\left[\sigma_G^{(d)}+\Delta_P^{(d)},0\right]\left(2X_P^{(d)}\right)\end{aligned}\tag{4.43}$$

$\sigma_G^{(d)}$ is the submatrix of σ_G containing all the modes where d is 1, i.e. if $d=(1,0,1,1)$ then we extract the covariance matrix describing the marginal distribution of modes p_1, p_3 and p_4. Likewise, we have for the present example $\Delta_P^{(d)}=\mathrm{Diag}\left(\Delta_{p_1}^{(n_{p_1})},\Delta_{p_3}^{(n_{p_3})},\Delta_{p_4}^{(n_{p_4})}\right)$ and $X_P^{(d)}=X_{p_1}^{(n_{p_1})}\bigoplus X_{p_3}^{(n_{p_3})}\bigoplus X_{p_4}^{(n_{p_4})}$. We have also defined the normal distribution, $G[V,\bar{x}](X)=\left[(2\pi)^D\|V\|\right]^{-1/2}e^{-\frac{1}{2}(X-\bar{x})^TV^{-1}(X-\bar{x})}$, where D is the dimension of V. Applying this result to the conditional state, which

is a sum of two Gaussians, we obtain

$$\begin{aligned}\left\langle \prod_{p\in P} M_p^{(n_p)} \right\rangle &= \mathrm{Tr}\left\{ \rho_c \prod_{p\in P} M_p^{(n_p)} \right\} \\ &= \frac{(1-p_d)^{N-1}}{P(C)} \Big[2^{N-1} \left\|\gamma_{\bar{S}}\right\|^{-\frac{1}{2}} f\left(V_{\bar{S}}, X_P\right) \\ &-2^N (1-p_d) \left\|\gamma_S\right\|^{-\frac{1}{2}} f\left(V_S, X_P\right) \Big]. \end{aligned} \tag{4.44}$$

Which is a closed-form expression for the correlator of the measurements.

Loss

A Gaussian transformation transforms the quadrature operators as $Q \to SQ + d$, where S is a symplectic matrix, i.e. $S\Omega S^T = \Omega$, and d is a displacement [1], [16]. Correspondingly, one can show that under a Gaussian transformation, the characteristic function transforms as,

$$\chi(\Lambda) \to \exp\left[id^T \Omega \Lambda \right] \chi(S^{-1}\Lambda). \tag{4.45}$$

We note that $S^{-1} = \Omega^T S^T \Omega$. We model loss, acting on the optical modes of the system, by mixing said modes with a set of empty (groundstate) environmental modes, and subsequently trace out the environmental modes. Let the modes be ordered as $\Lambda = \Lambda_P \oplus \Lambda_S \oplus \Lambda_E$, where Λ_E are the conjugate quadratures for the environmental modes. We assume there is one environmental mode for each system mode (S, P). The system modes and environmental modes are mixed using beamsplitter interactions, described by the symplectic matrix U_η,

$$U_\eta = \begin{pmatrix} G_\eta^{1/2} & -\sqrt{I - G_\eta} \\ \sqrt{I - G_\eta} & G_\eta^{1/2} \end{pmatrix}, \tag{4.46}$$

By using Eq. 4.31, Eq. 4.45, and U_η, we obtain the map corresponding to loss acting on the system modes. This map transforms the characteristic function as,

$$\chi(\Lambda) \to \chi\left(G_\eta^{1/2}\Lambda\right) \exp\left[-\frac{1}{2} \Lambda^T (I - G_\eta) \Lambda \right], \tag{4.47}$$

Eq. 4.17 can be derived from this mapping, and it can also be used to show that detector loss can be commuted through the interferometer B, given that all detectors have the same efficiency.

Phase and amplitude noise

We now evaluate the effect of phase and amplitude noise on the computed correlators. Given that the optical state ρ is perturbed in phase by the environment,

we model this by stochastic rotations in phase space $\rho = \int d^N\boldsymbol{\theta} P(\boldsymbol{\theta}) R(\boldsymbol{\theta}) \rho_0 R(-\boldsymbol{\theta})$. Where ρ_0 is the unperturbed state, $\boldsymbol{\theta} = \left(\theta_{p_1}\theta_{p_2}\ldots\theta_{p_N}\right)$ is a vector of stochastic rotation angles, and $R(\boldsymbol{\theta})$ is the rotation operator $R(\boldsymbol{\theta}) = \prod_{p\in P} R_p(\theta_p)$. We shift this stochastic rotation from the state onto the observable:

$$\begin{aligned}
&\left\langle \prod_{p\in P} M_p^{(n_p)} \right\rangle = \mathrm{Tr}\left\{ \prod_{p\in P} M_p^{(n_p)} \rho \right\} \\
&= \mathrm{Tr}\left\{ \prod_{p\in P} M_p^{(n_p)} \int d^N\boldsymbol{\theta} P(\boldsymbol{\theta}) R(\boldsymbol{\theta}) \rho_0 R(-\boldsymbol{\theta}) \right\} \\
&= \mathrm{Tr}\left\{ \int d^N\boldsymbol{\theta} P(\boldsymbol{\theta}) R(-\boldsymbol{\theta}) \prod_{p\in P} M_p^{(n_p)} R(\boldsymbol{\theta}) \rho_0 \right\} \\
&= \mathrm{Tr}\left\{ \prod_{p\in P} \int d\theta_p P(\theta_p) R_p(-\theta_p) M_p^{(n_p)} R_p(\theta_p) \rho_0 \right\} \\
&= \mathrm{Tr}\left\{ \prod_{p\in P} \widetilde{M}_p^{(n_p)} \rho_0 \right\}
\end{aligned} \tag{4.48}$$

Where $\widetilde{M}_p^{(n_p)}$ is the noisy observable. By factorizing the probability as $P(\boldsymbol{\theta}) = \prod_{p\in P} P(\theta_p)$, we have tacitly assumed that there is no correlation in the phase noise acting on different modes. Inserting the expression for the observable $M_p^{(n_p)}$, we have

$$\begin{aligned}
&R_p(-\theta_p) M_p^{(n_p)} R_p(\theta_p) \\
&= I_p - 2(1-p_d) R_p(-\theta_p) \left|-X_p^{(n_p)}\right\rangle_p \left\langle -X_p^{(n_p)}\right| R_p(\theta_p)
\end{aligned} \tag{4.49}$$

For a coherent state $|-X_p^{(n_p)}\rangle$, we have that a small rotation is identical to a displacement acting orthogonal to the amplitude vector $-X_p^{(n_p)}$. An orthogonal vector can be constructed by acting with the symplectic form: $-\omega(-X_p^{(n_p)})$. With this in mind, we make the substitution:

$$R_p(\theta_p) \to D_p\left(\theta_p \omega X_p^{(n_p)}\right) \tag{4.50}$$

Imprecision in the measurement process, such as a noisy displacement, might lead to noise in the amplitude. We include this by also applying a stochastic displacement along the amplitude vector $X_p^{(n_p)}$. This stochastic displacement is given as a fraction ϵ_p of the amplitude vector $X_p^{(n_p)}$, i.e. the stochastic displacement is $\epsilon_p X_p^{(n_p)}$. ϵ_p is referred to as the relative amplitude. The noisy observable for party p is then given

as,

$$\begin{aligned}
&\widetilde{M}_p^{(n_p)} = \\
&\int d\theta_p d\epsilon_p P\left(\theta_p, \epsilon_p\right) D_p\left(-\theta_p \omega X_p^{(n_p)}\right) D_p\left(-\epsilon_p X_p^{(n_p)}\right) M_p^{(n_p)} D_p\left(\epsilon_p X_p^{(n_p)}\right) D_p\left(\theta_p \omega X_p^{(n_p)}\right) \\
&= I - 2\left(1 - p_d\right) \int P\left(\theta_p, \epsilon_p\right) \cdot \left|-\left(1 + \epsilon_p + \theta_p \omega\right) X_p^{(n_p)}\right\rangle \left\langle-\left(1 + \epsilon_p + \theta_p \omega\right) X_p^{(n_p)}\right| d\theta_p d\epsilon_p \\
&= I - 2(1 - p_d)\beta_p^{(n_p)}
\end{aligned} \tag{4.51}$$

$P\left(\theta_p, \epsilon_p\right)$ is the distribution over displacements, and we have introduced the state,

$$\beta_p^{(n_p)} = \int P\left(\theta_p, \epsilon_p\right) \cdot \left|-\left(1 + \epsilon_p + \theta_p \omega\right) X_p^{(n_p)}\right\rangle \left\langle-\left(1 + \epsilon_p + \theta_p \omega\right) X_p^{(n_p)}\right| d\theta_p d\epsilon_p. \tag{4.52}$$

We model $P\left(\theta_p, \epsilon_p\right)$ as a Gaussian, given by

$$P\left(\theta_p, \epsilon_p\right) = \left[(2\pi)^2 \left\|\Sigma_p\right\|\right]^{-1/2} \exp\left[-\frac{1}{2}\begin{pmatrix}\epsilon_p & \theta_p\end{pmatrix} \Sigma_p^{-1} \begin{pmatrix}\epsilon_p \\ \theta_p\end{pmatrix}\right]. \tag{4.53}$$

The covariance matrix is chosen to be diagonal

$$\Sigma_p = \begin{pmatrix} V_A & 0 \\ 0 & V_\theta \end{pmatrix}. \tag{4.54}$$

V_A and V_θ are the relative amplitude and phase angle variances respectively. $\beta_p^{(n_p)}$ has a characteristic function given by,

$$\begin{aligned}
\chi_{\beta_p^{(n_p)}} &= \mathrm{Tr}\left\{\beta_p^{(n_p)} D_p\left(\Lambda_p\right)\right\} \\
&= \int P\left(\theta_p, \epsilon_p\right) \cdot E\left[I, -\left(1 + \epsilon_p + \theta_p \omega\right) 2X_p^{(n_p)}\right]\left(\Lambda_p\right) d\theta_p d\epsilon_p \\
&= E\left[I + V_A\left(2X_p^{(n_p)}\right) \otimes \left(2X_p^{(n_p)}\right)^T + V_\theta\left(\omega^T 2X_p^{(n_p)}\right) \otimes \left(\omega^T 2X_p^{(n_p)}\right)^T, -2X_p^{(n_p)}\right]\left(\Lambda_p\right).
\end{aligned} \tag{4.55}$$

So the effect of amplitude and phase noise is to broaden the phase space distribution of $\beta_p^{(n_p)}$ along $2X_p^{(n_p)}$ and $\omega^T 2X_p^{(n_p)}$. We define the covariance matrix of the state $\beta_p^{(n_p)}$ as $\Delta_p^{(n_p)}$,

$$\begin{aligned}
\Delta_p^{(n_p)} &= I + V_A\left(2X_p^{(n_p)}\right) \otimes \left(2X_p^{(n_p)}\right)^T \\
&\quad + V_\theta\left(\omega^T 2X_p^{(n_p)}\right) \otimes \left(\omega^T 2X_p^{(n_p)}\right)^T
\end{aligned} \tag{4.56}$$

4.7.2 A2

Let n be a binary list of measurement settings, and g a binary list of measurement outcomes for the detectors in P, where click corresponds to 1 and no click corresponds to 0. We may then compute the probability of obtaining the outcomes g using the characteristic function χ_{ρ_c}. This probability is given by the expression,

$$P_Q(g|n) = \frac{(1-p_d)^{N-1}}{P(C)} \Big[2^{N-1} \left\| \gamma_{\bar{S}} \right\|^{-\frac{1}{2}} h_g\left(V_{\bar{S}}\right) - 2^N (1-p_d) \left\| \gamma_S \right\|^{-\frac{1}{2}} h_g\left(V_S\right) \Big], \tag{4.57}$$

where

$$h_g(V) = \left[4\pi (1-p_d)\right]^{|\bar{g}|} \sum_b \left[-4\pi (1-p_d)\right]^{|b|} G\left[V^{(b+\bar{g})} + \Delta_P^{(b+\bar{g})}, 2X_P^{(b+\bar{g})} \right]. \tag{4.58}$$

$\bar{g}$ is the negation of g, i.e. we replace 1 by 0 and vice versa. The measurement settings n define the arrays Δ_P and X_P. The sum runs over all binary lists b of length N, satisfying the constraint that b takes the value zero in positions where g takes the value zero. E.g. if $g = \left(1,0,0,1\right)$, then the sum would run over the lists $b \in \left\{ \left(0,0,0,0\right), \left(1,0,0,0\right), \left(0,0,0,1\right), \left(1,0,0,1\right) \right\}$. $V^{(b+\bar{g})}$ is the submatrix of the covariance matrix V, containing all the modes where the vector $b+\bar{g}$ takes the value 1, e.g. if $b+\bar{g} = \left(0,1,1,1\right)$ then the marginal covariance matrix describing modes p_2, p_3 and p_4 is extracted. Marginal probabilities for a subset of parties A can be extracted from $P_Q(g|n)$ by summing over outcomes for the remaining parties B. The measurement settings for subset B should be fixed during this summation, however the choice of settings for B is arbitrary owing to the no-signalling property of quantum mechanics [7].

We then want to determine whether the array $P_Q(g|n)$ can be expressed as a convex sum of local response functions. Let $L\left(g_p|n_p,\lambda_k\right)$ be the local response function for party p, determined by the hidden variables λ_k. The response function gives the probability of party p obtaining a particular outcome g_p, given the measurement setting n_p and hidden variables λ_k. We determine whether there exists a set of coefficients c_k such that [7]:

$$\begin{aligned} P_Q(g|n) &= \sum_k c_k \prod_{p\in P} L\left(g_p|n_p,\lambda_k\right) \\ \sum_k c_k &= 1 \\ c_k &\geq 0 \end{aligned} \tag{4.59}$$

c_k is interpreted as the probability that the hidden variables λ_k are shared by the parties in a given measurement round. We use the set of deterministic response functions, i.e. each response function can be written as a Kronecker delta function,

$$L\left(g_p|n_p,\lambda_k\right)=\delta(g_p,g_{n_p,\lambda_k}) \tag{4.60}$$

g_p is a potential outcome for party p and g_{n_p,λ_k} is the outcome that is actually obtained, given the hidden variables λ_k and the setting n_p. Whether the set of requirements in Eq. 4.59 allows for a solution or not, is determined using the linprog module of the SciPy 1.8.1 package in Python. When no solution is present, we know that the array of probabilities $P_Q(g|n)$, determined by the quantum state, does not admit a local hidden variable model. In this case $P_Q(g|n)$ lies outside the Bell polytope. However, when a solution *is* present we know that the system can be described by a local hidden variable model, and no Bell inequality can be violated.

4.8 Converting the nonlinear W^{3}ZB inequality into linear inequalities

The nonlinear W^{3}ZB inequality is equivalent to a large set of linear inequalities, as described by Eq. 3.64, and we now seek to identify which of these linear inequalities are in fact broken by the analyzed experiment. We let $M(s)$ be the correlators of the experiment for different binary vectors of settings s, with the setting of p_1 being leftmost in the binary list s. We define the vector M with elements,

$$M=\begin{pmatrix}M(s_0) & M(s_1) & M(s_2) & \cdots\end{pmatrix}^T. \tag{4.61}$$

As before, s_k is the binary string of length N (the number of parties) corresponding to the integer k.

We want to find the linear inequality which is the most resilient toward loss in channels ch_p, since it is already difficult to achieve the required transmissions of 81-87 %. We might go about this task by searching systematically through the inequalities given in Eq. 3.64, however we run into the problem that with 5 participants the number of inequalities to search through is $2^{2^5}\approx 4.3\times 10^9$, which is rather cumbersome. Then an alternative strategy could be to decrease the transmission η_p until the linear program,

$$M=\sum_\lambda M(\lambda)p(\lambda) \quad , \quad p(\lambda)\geq 0 \quad , \quad \sum_\lambda p(\lambda)=1 \tag{4.62}$$

has a solution, with

$$M(\lambda)=\begin{pmatrix}M(s_0,\lambda) & M(s_1,\lambda) & M(s_2,\lambda) & \cdots\end{pmatrix}^T. \tag{4.63}$$

where $M(s,\lambda)$ is defined in Eq. 3.52. At the point where a solution becomes possible, the correlators M are given by a convex combination of the vertices $M(\lambda)$ making up the relevant facet, and these vertices are readily identified by solving the linear program. Labelling these vertices as v_k, we subtract one of these, labelled as v_1, from the rest. We then combine the resulting displacement vectors in a matrix,

$$V = \begin{pmatrix} (v_2 - v_1)^T \\ (v_3 - v_1)^T \\ \vdots \end{pmatrix}. \tag{4.64}$$

If we let $v_\perp$ belong to the null space of V,

$$V v_\perp = 0, \tag{4.65}$$

then the facet inequality is,

$$\langle v_\perp, M \rangle \leq \langle v_\perp, v_1 \rangle \tag{4.66}$$

and equality is obtained for M contained in the facet. Clearly this strategy does not always work, since M might end up in a hyperedge of the polytope instead of a hyperplane when we decrease η_p. Nevertheless we succeed in finding linear relevant facet inequalities in the case of 2,3,4,5 and 6 parties. We list the relevant facet inequality for 2-5 parties below, with the inequality being the one that is the most resilient toward loss in channels ch_p:

2 parties:

$$+\frac{1}{2}M(0,0) - \frac{1}{2}M(0,1) - \frac{1}{2}M(1,0) - \frac{1}{2}M(1,1) \leq 1 \tag{4.67}$$

3 parties:

$$-\frac{1}{2}M(0,0,0) + \frac{1}{2}M(0,1,1) + \frac{1}{2}M(1,0,1) + \frac{1}{2}M(1,1,0) \leq 1 \tag{4.68}$$

4 parties:

$$\begin{aligned} &+\frac{3}{8}M(0,0,0,0) + \frac{1}{8}M(0,0,0,1) + \frac{1}{8}M(0,0,1,0) - \frac{1}{8}M(0,0,1,1) + \frac{1}{8}M(0,1,0,0) \\ &- \frac{1}{8}M(0,1,0,1) - \frac{1}{8}M(0,1,1,0) - \frac{3}{8}M(0,1,1,1) + \frac{1}{8}M(1,0,0,0) - \frac{1}{8}M(1,0,0,1) \\ &- \frac{1}{8}M(1,0,1,0) - \frac{3}{8}M(1,0,1,1) - \frac{1}{8}M(1,1,0,0) - \frac{3}{8}M(1,1,0,1) - \frac{3}{8}M(1,1,1,0) \\ &+ \frac{3}{8}M(1,1,1,1) \leq 1 \end{aligned} \tag{4.69}$$

5 parties:

$$
\begin{aligned}
&-\frac{1}{4}M(0,0,0,0,0)-\frac{1}{8}M(0,0,0,0,1)-\frac{1}{8}M(0,0,0,1,0)-\frac{1}{8}M(0,0,1,0,0)\\
&+\frac{1}{8}M(0,0,1,1,1)-\frac{1}{8}M(0,1,0,0,0)+\frac{1}{8}M(0,1,0,1,1)+\frac{1}{8}M(0,1,1,0,1)\\
&+\frac{1}{8}M(0,1,1,1,0)+\frac{1}{4}M(0,1,1,1,1)-\frac{1}{8}M(1,0,0,0,0)+\frac{1}{8}M(1,0,0,1,1)\\
&+\frac{1}{8}M(1,0,1,0,1)+\frac{1}{8}M(1,0,1,1,0)+\frac{1}{4}M(1,0,1,1,1)+\frac{1}{8}M(1,1,0,0,1)\\
&+\frac{1}{8}M(1,1,0,1,0)+\frac{1}{4}M(1,1,0,1,1)+\frac{1}{8}M(1,1,1,0,0)+\frac{1}{4}M(1,1,1,0,1)\\
&+\frac{1}{4}M(1,1,1,1,0)-\frac{5}{8}M(1,1,1,1,1)\leq 1 \qquad (4.70)
\end{aligned}
$$

These inequalities are broken until the critical transmissions given in Fig. 4.6 are reached.

Chapter 5

Quantum repeater using two-mode squeezed states and atomic noiseless amplifiers

We now present the paper *Quantum repeater using two-mode squeezed states and atomic noiseless amplifiers* [10]. This paper was authored by Anders J. E. Bjerrum, Jonatan B. Brask, Jonas S. Neergaard-Nielsen, and Ulrik L. Andersen. The paper was published in Physical Review A with the reference Phys. Rev. A 107, 042606 (2023).

5.1 Abstract

We perform a theoretical investigation into how a two-mode squeezed vacuum state, that has undergone photon loss, can be stored and purified using noiseless amplification with a collection of solid-state qubits. The proposed method may be used to probabilistically increase the entanglement between the two parties sharing the state. The proposed amplification step is similar in structure to a set of quantum scissors. However, in this work the amplification step is realized by a state transfer from an optical mode to a set of solid-state qubits, which act as a quantum memory. We explore two different applications, the generation of entangled many-qubit registers, and the construction of quantum repeaters for long-distance quantum key distribution.

5.2 Introduction

Quantum communication is the act of distributing quantum states in a network [64]. It enables the generation of secret encryption keys [65], and perhaps, the establishment of a fully fault-tolerant quantum internet [66], [67]. The different nodes of the

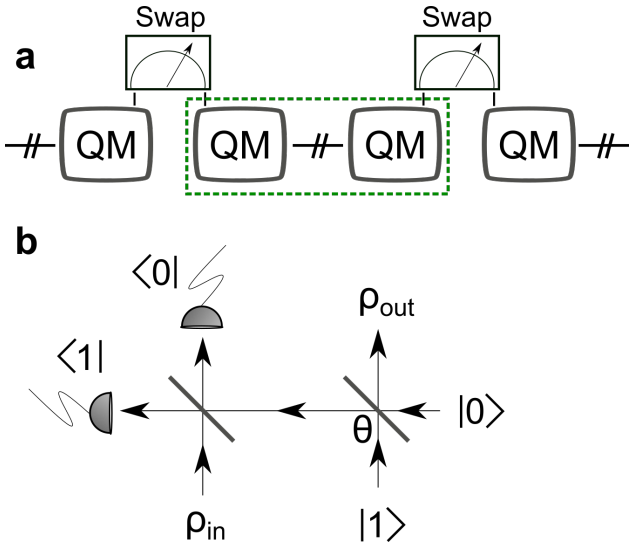

Figure 5.1: ***a**: Repeater scheme with entanglement swaps (meters) acting on sets of quantum memories (QM) separated by lossy channels. A single repeater segment is enclosed by a dashed green box, and will include a purification step.* ***b**: Layout of a quantum scissor. The left beamsplitter is balanced (50:50) and the right beamsplitter is tunable with transmission* $\cos(\theta)^2$*. The transmission may be tuned to purify the state* ρ_{in} *at the single photon level.*

network are usually connected by photonic communication channels owing to the weak influence of the environment on the coherence of optical photons. However, photons suffer from propagation loss with the probability of successful transmission decaying exponentially with distance.

The exponential scaling can be mitigated using quantum repeater nodes between the sender and receiver stations leading to polynomial [52], [68] or even constant-rate scaling [69] for schemes based on error correction. We consider a quantum repeater architechture with two-way classical communication and without error correction, as originally envisioned [52], [68]. In this scheme, entanglement between parties is established by first distributing and purifying entangled states over shorter segments. These entangled segments then undergo a series of entanglement swaps, ultimately generating entanglement between the parties (see Fig. 5.1a). However, due to the probabilistic nature of the purification protocol, quantum memories must be placed at each repeater node. Many different platforms have been considered for memories in quantum repeaters including atomic ensembles [70], trapped ions [71], solid-state systems [72], and mechanical resonators [73]. The basic structure of all quantum repeaters is largely independent of the type of memory employed, however.

One intriguing approach for the probabilistic purification of a quantum state is

the protocol of noiseless linear amplification [59]. It has mainly been applied in continuous-variable (CV) quantum repeater schemes to enable long-distance distribution of quadrature and photon-number entanglement [74]–[80] (see also [81] for a different approach). In its simplest form, the noiseless linear amplifier consists of a single quantum scissor scheme [82] illustrated in Fig. 5.1b. A single photon is split on a beam splitter to form an entangled state which is subsequently used to purify an input state ($\rho_{\mathtt{in}}$) via quantum teleportation in a truncated two-dimensional Hilbert space. The achieved purification can be understood intuitively through the fact, that the projective measurement of the photon-detectors lower the entropy of the system, while the effectuated quantum teleportation preserve the coherences of the input state. By combining quantum scissor operations with quantum memories and entanglement swapping via Bell measurements, a quantum repeater network can be established. In previous CV quantum repeater protocols, the quantum scissors, the quantum memories and the Bell measurements are typically considered as being individual and independent physical elements.
In the present work we show that by using light-matter entangled states (for example generated by Nitrogen-Vacancy centers in diamond [83]–[85]), it is possible to perform noiseless linear amplification and storage of the quantum state in a single operation. In section 5.3 we introduce the operation of noiseless linear amplification based on a photo-active qubit. We first consider the case with a single qubit, similar to a single quantum scissor operation, and subsequently generalize it to multiple qubits to explore the effect of noiseless linear amplification in a larger Hilbert space. In section 5.4 we investigate the entanglement generated by our protocol and measure it using the negativity. In section 5.5 we then introduce the structure of the quantum repeater scheme, including entanglement swapping. In section 5.6 we present the results in terms of secret key rates and Bell inequality violations.

5.3 Analysis of a single repeater segment

We start by presenting the repeater segment that forms the core of the quantum repeater protocol. It corresponds to the part of the repeater array enclosed by a green dotted box in Fig. 5.1a and is schematically shown in Fig. 5.2 with a single solid state qubit (diamond) in each register. Our repeater scheme is based on the distribution of two-mode squeezed vacuum states followed by noiseless linear amplification and memorization by means of a photo-active three-level atomic systems. The basic idea is that the atomic systems produce spin-photon entanglement to be used as the resource for heralded noiseless amplification similar to the all-optical approach in Fig. 5.1b where single-photon entanglement is used as the resource. However, in contrast to the pure optical approach in Fig. 5.1b where the state is teleported onto another optical mode, in our scheme the state is teleported (and truncated) into a spin degree of freedom of the atomic system, and thus directly memorized after purification. While the atomic system could be realised by many

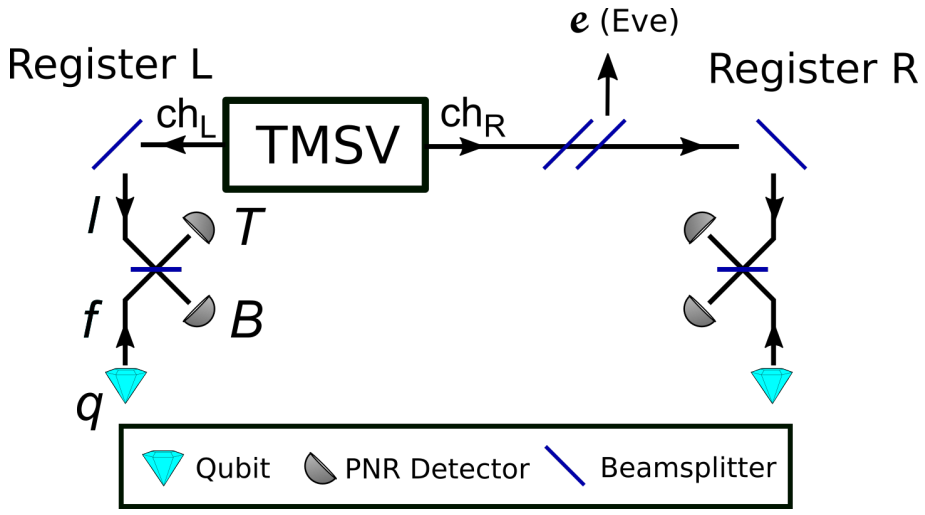

Figure 5.2: *Layout of the entanglement-sharing scheme, with a single qubit in each register (quantum memory).* **e** *is an environmental mode that couples to the fiber. The drawn setup corresponds to a repeater segment (the green dotted box in Fig. 5.1)*

different physical systems, here we focus on the Nitrogen-Vacancy center (NV). In this case the information is stored in the electronic spin degree of freedom of the NV center but it can also be swapped to a nearby (and very long-lived) ^{13}C nuclear spin [84]. In addition to extending the lifetime, the swap also free up the electronic spin for a subsequent entangling round and it allows for entanglement swapping to be carried through Bell measurements between the electronic and nuclear spins (as discussed in section 5.5).

A two-mode squeezed vacuum (TMSV) state shares quadrature and photon number correlations between the left (L) and right (R) registers. The TMSV state is expressed in the photon-number basis as

$$|\texttt{TMSV}\rangle = \sum_{n=0}^{\infty} c_n \, |n, n\rangle \, , \tag{5.1}$$

where the amplitudes c_n are the Fock-state amplitudes

$$c_n = (-e^{i\phi})^n \sqrt{\frac{\langle n \rangle^n}{(1 + \langle n \rangle)^{n+1}}}, \tag{5.2}$$

$\langle n \rangle$ is average photon number in each of the two modes and ϕ is the phase.

The register qubits have a dark state ($|0\rangle_q$) and a bright state ($|1\rangle_q$). The bright state emits a single photon into the optical mode f when excited by some external mechanism, such as a driving laser, whereas the dark state never emits a photon.

We initialize the qubit q and optical mode f in the state

$$|q,f\rangle = \cos(\theta)\,|0\rangle_q\,|0\rangle_f + \sin(\theta)\,|1\rangle_q\,|0\rangle_f\,, \tag{5.3}$$

with $|0\rangle_f$ being the optical vacuum state. Then we assume we can excite the qubit such that it emits a photon if it is in the bright state, thereby preparing the state

$$\cos(\theta)\,|0\rangle_q\,|0\rangle_f + \sin(\theta)\,|1\rangle_q\,|1\rangle_f\,. \tag{5.4}$$

States such as this one were produced experimentally using a NV center in ref. [86]. We assume that the photons of the TMSV field are indistinguishable from the photons emitted by the qubits. Realistically, this may be a challenge to achieve, but can in principle be done with proper light source engineering and filtering. At each register the TMSV field is mixed with the field emitted by the register qubit on a balanced beamsplitter. Two photon-number-resolving detectors (PNR detectors) measure the outputs of the beamsplitter, and events where exactly one photon is detected at each register are considered successful. If we assume no loss in channels ch_L and ch_R, then the qubit registers are projected into the entangled state

$$\begin{aligned}|\psi\rangle = \frac{1}{2}c_1\cos(\theta_L)\cos(\theta_R)\,|00\rangle + \\ \frac{1}{2}c_0\sin(\theta_L)\sin(\theta_R)\,|11\rangle\,,\end{aligned} \tag{5.5}$$

where θ_L and θ_R are the superposition angles given in Eq. 5.3, for the left and right qubit respectively. We note that $4\,\langle\psi|\psi\rangle$ will correspond to the probability that the projective measurements (photon detection) in register L and R succeed. The factor of 4 originates from the fact that the projective measurement can succeed in 2 different ways at both registers, i.e. either the top (T) or bottom (B) detector can register a single photon. We note that whether the bottom or top detector clicks, will influence the phase of the quantum state, and we assume that this is corrected for.

We then set the transmission of channel $\mathrm{ch}_\mathtt{R}$, connecting the TMSV source and register R, to η_R. We will for now assume that the channel $\mathrm{ch}_\mathtt{L}$ is lossless. We find that under these conditions, the density matrix describing register L and R, is given by

$$\rho = \frac{\mathcal{K}_1}{4}\begin{pmatrix} |c_1|^2\eta_R c_L^2 c_R^2 & 0 & 0 & c_1c_0^*\sqrt{\eta_R}s_Rs_Lc_Rc_L \\ 0 & |c_1|^2(1-\eta_R)c_L^2s_R^2 & 0 & 0 \\ 0 & 0 & 0 & 0 \\ c_1^*c_0\sqrt{\eta_R}s_Rs_Lc_Rc_L & 0 & 0 & |c_0|^2s_L^2s_R^2 \end{pmatrix}, \tag{5.6}$$

Where $s_L = \sin(\theta_L)$, $s_R = \sin(\theta_R)$, $c_L = \cos(\theta_L)$, and $c_R = \cos(\theta_R)$. A derivation of this result can be found in Appendix A. The basis vectors describing the

state are $|0\rangle_L|0\rangle_R$, $|0\rangle_L|1\rangle_R$, $|1\rangle_L|0\rangle_R$, $|1\rangle_L|1\rangle_R$. Eg. the matrix element $\rho_{22} = \frac{\mathcal{K}_1}{4}|c_1|^2(1-\eta_R)\cos(\theta_L)^2\sin(\theta_R)^2$ corresponds to the state $|0\rangle_L|1\rangle_R\langle 0|_L\langle 1|_R$. $\mathcal{K}_1$ is the normalization and $4/\mathcal{K}_1$ will be the probability that the projective measurements in register L and R succeed.
The diagonal term ρ_{22} describes the situation where a photon is lost in the right channel. Suppose that the TMSV source emits a single photon into both ch_L and ch_R, and that the photon is lost from channel ch_R. Then a successful measurement at register R and L implies that the qubit in register L is in the dark state ($|0\rangle_L$), and that the qubit in register R is in the bright state ($|1\rangle_R$).
In section 5.4 we show that tuning of the angles θ_L and θ_R, can increase (or decrease) the entanglement shared between the two registers, in a similar fashion as a pair of quantum scissors would.

In the architecture discussed above and illustrated in Fig. 5.2, the amount of distributed and purified entanglement is limited due to the restricted four-dimensional Hilbert space spanned by the two qubits. To circumvent this limitation we consider an expanded version of the two registers where every register now comprises several qubits and thus enlarges the dimensionality of the quantum memory. The setup can be seen in Fig. 5.3. At the left register the TMSV state is split evenly into the N arms of the register. Concurrently with this splitting of the TMSV, we excite the qubits, such that they will emit a photon if they are in the bright state. Again, PNR detectors measure on the output, and events where exactly one photon is detected in each of the N register arms, are considered successful. Conditioned on all the measurements succeeding, we obtain correlations between the number of bright-state qubits in the left register, and the number of photons in the right part of the TMSV state. Repeating the procedure at the right register ultimately creates entanglement between the two registers.

Our analysis, given in appendix A, reveals that the quantum state of the two many-qubit registers, when assuming no loss in the connecting channel, is given by

$$|\alpha\rangle = \mathcal{N}_N \sum_{n=0}^{N} c_n \Delta(n,\theta_L)\Delta(n,\theta_R)\,|\mathbf{I}_{N-n}\rangle_L\,|\mathbf{I}_{N-n}\rangle_R \tag{5.7}$$

The subscript R/L indicates whether we are referring to the qubits in the left (L) or right (R) register. The superposition angle $\theta_{R/L}$ is assumed to be the same for all qubits in the same register. The vectors $|\mathbf{I}_{N-n}\rangle$ are even superpositions of all states containing $N-n$ bright state qubits and n dark state qubits:

$$|\mathbf{I}_{N-n}\rangle = \binom{N}{n}^{-1/2} \sum_{\mathbf{i}_{N-n}} |\mathbf{i}_{N-n}\rangle \tag{5.8}$$

where the sum runs over binary lists $\mathbf{i}_{N-n}$ of length N with $N-n$ ones. $\mathcal{N}_N$ is the

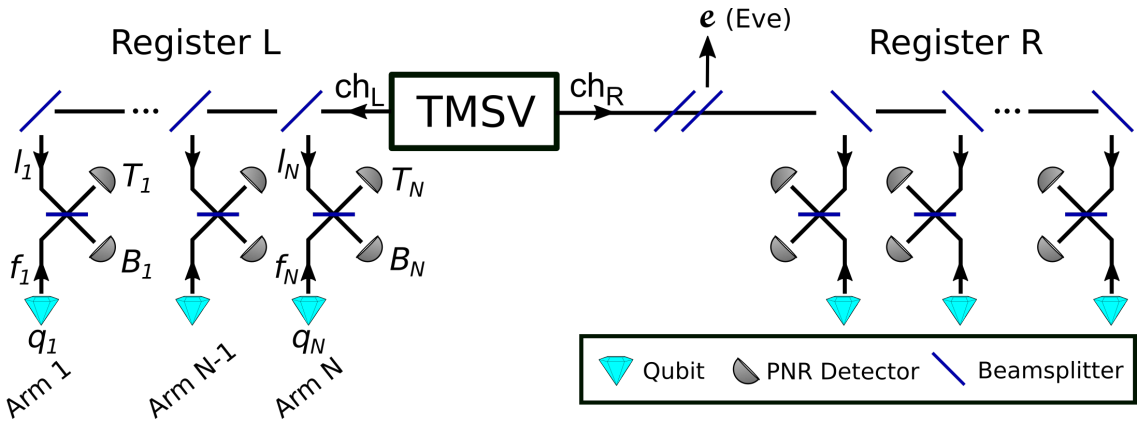

Figure 5.3: *Layout of the entanglement-sharing scheme investigated in this work. Entanglement is distributed to the atomic qubits consituting register R and L via a two-mode squeezed vacuum state.*

normalization, given by

$$\mathcal{N}_N^{-2} = \sum_{m=0}^{N} |c_m|^2 |\Delta(m, \theta_L)|^2 |\Delta(m, \theta_R)|^2 \tag{5.9}$$

The value of $\mathcal{N}_N^{-2}$ reflects the probability that the entanglement sharing scheme succeeds. The amplitude $\Delta(n, \theta)$ is

$$\Delta(n, \theta) = \sqrt{\frac{N!}{2^N N^n (N-n)!}} \beta(n, \theta), \tag{5.10}$$

where $\beta(n, \theta)$ is

$$\beta(n, \theta) = \cos(\theta)^n \sin(\theta)^{N-n} \tag{5.11}$$

When including loss in both channels, we find the density matrix describing the two registers to be:

$$\rho = \sum_{n,m=0}^{\infty} \sum_{l,r=0}^{\min(n,m)} \Lambda(n, m, l, r) \cdot \tag{5.12}$$
$$|\mathbf{I}_{N-n+l}\rangle_L \langle \mathbf{I}_{N-m+l}| \otimes |\mathbf{I}_{N-n+r}\rangle_R \langle \mathbf{I}_{N-m+r}|$$

This density matrix is not normalized, and the norm should be interpreted as the probability that entanglement sharing succeeds. The matrix elements are given by

$$\begin{aligned} \Lambda(n, m, l, r) = {} & c_n c_m^* \epsilon_R(n, r) \epsilon_L(n, l) \epsilon_R(m, r)^* \epsilon_L(m, l)^* \\ & \Delta(n-l, \theta_L) \Delta(n-r, \theta_R) \Delta(m-l, \theta_L)^* \Delta(m-r, \theta_R)^* \\ & \Theta(N+l-n) \Theta(N+r-n) \Theta(N+l-m) \Theta(N+r-m), \end{aligned} \tag{5.13}$$

where $\Theta(x)$ is the step function,

$$\Theta(x) = \begin{cases} 1 & \text{if } x \geq 0 \\ 0 & \text{if } x < 0 \end{cases} \tag{5.14}$$

$\epsilon(n, l)$ is related to the transmission of the channel, $\eta_{R/L}$ (for $\mathrm{ch_L}$ and $\mathrm{ch_R}$), through the relation,

$$\epsilon_{R/L}(n, l) = \sqrt{\binom{n}{n-l}} \eta_{R/L}^{(n-l)/2} (1 - \eta_{R/L})^{l/2} \tag{5.15}$$

5.4 Entanglement of the Registers

Based on the above analysis, we now evaluate the amount of entanglement between the two registers using negativity as the measure of entanglement. The negativity is defined as the absolute value of the sum of negative eigenvalues of the partial transpose of the density matrix, and can be shown to be an entanglement monotone [87]. If we have the density matrix ρ, then the partial transpose with respect to Alice's subsystem, ρ^{T_A}, has the matrix elements $\langle i_A, j_B|\rho^{T_A}|k_A, l_B\rangle = \langle k_A, j_B|\rho|i_A, l_B\rangle$. Given that ρ^{T_A} has the negative eigenvalues μ_i, then the negativity of the state ρ is defined as

$$\mathbb{N}(\rho) = \left| \sum_i \mu_i \right| \tag{5.16}$$

The negativity is the same regardless of which party was transposed, since $(\rho^{T_A})^T = \rho^{T_B}$. We will first assume the channels to be loss-free, in which case the superposition angles, θ_R and θ_L, are set to the same value due to symmetry. The average number of photons $\langle n \rangle$ per party in the TMSV state is fixed at 0.5. In Fig. 5.4 we plot the negativity as a function of the angle, $\theta_R = \theta_L$, for a different number of atomic qubits at each register. We clearly observe a strong dependency on the superposition angle.

We then fix θ_L at the value corresponding to the largest negativity, as inferred from Fig. 5.4, and lower the transmission of the right channel ($\mathrm{ch_R}$). We allow θ_R to change and find the angle that maximizes the negativity at different transmissions. The result can be seen in Fig. 5.5a. We find that as the channel transmission, η_R, is reduced, the angle θ_R must be changed to maximize the negativity. This can be understood from the fact that a low transmission reduces the probability that photons arrive at the right register. This in turn implies, that a successful measurement outcome at the photodetectors, was entirely due to light emitted from bright state qubits at the register. This lowers the negativity of the two registers since they approach a separable state. However, this effect can be counteracted by lowering

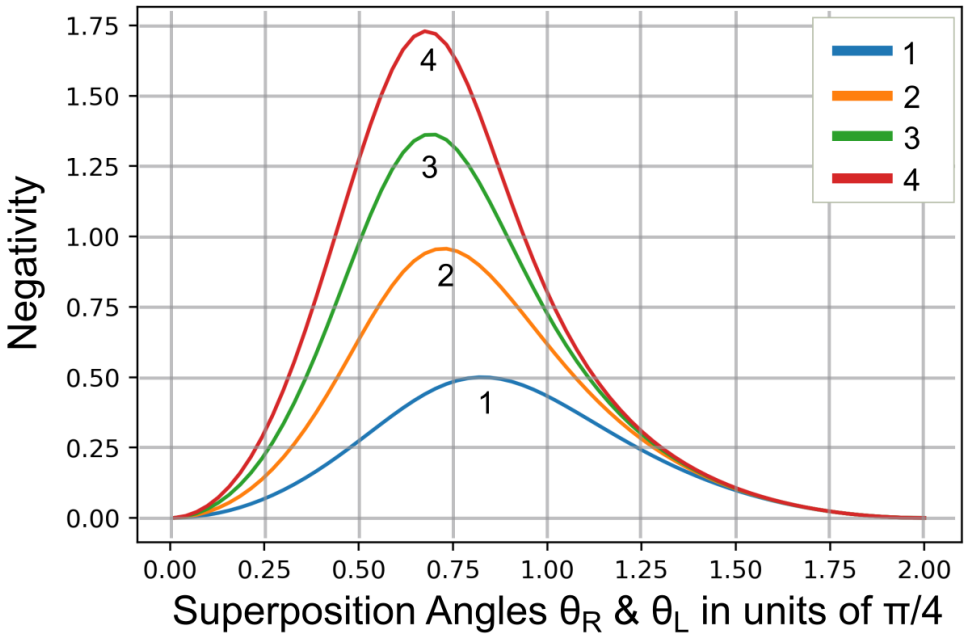

Figure 5.4: *The negativity of the two registers as a function of the superposition angle $\theta = \theta_R = \theta_L$. The different plots correspond to different number of qubits in the registers. The average number of photons $\langle n \rangle$ emitted by the TMSV source into each channel is fixed at 0.5. The superposition angle θ is shown along the x-axis in units of $\pi/4$.*

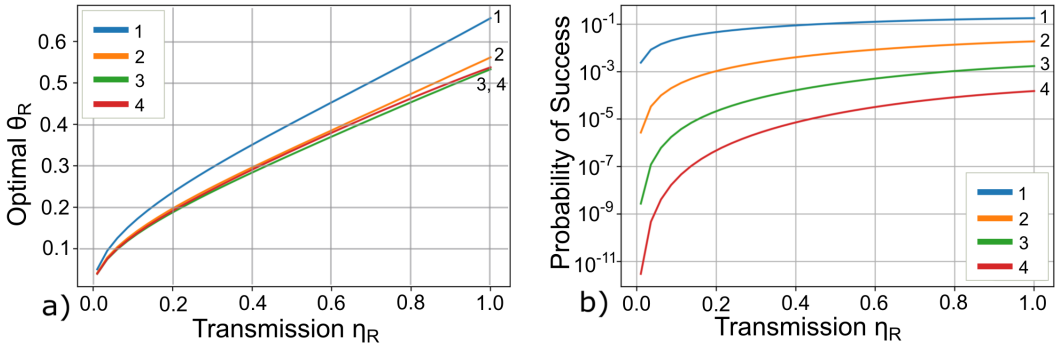

Figure 5.5: ***a:*** *The choice of θ_R (in radians) that maximizes the negativity of the two registers for a given loss in channel ch_R. We have fixed $\langle n \rangle$ at 0.5. The legend and plot label indicates the number of qubits in each register.* ***b:*** *We plot the probability of the measurements at all the photodetectors succeeding, at the optimal value of θ_R. The legend and plot label indicates the number of qubits in each register.*

the probability that the qubits are in the bright state, which is exactly what is done by lowering θ_R.

The probability that the measurement outcomes at the photodetectors correspond to successful entanglement sharing, at the optimal value of θ_R, is shown Fig. 5.5b. We observe that the probability of success decreases exponentially in the number of qubits in the registers, and super-exponentially for decreasing transmission. The super-exponential decrease in the probability of success, is caused by the scheme compensating for a low η_R by lowering θ_R. This implies that our entanglement sharing scheme will be practically infeasible at low transmissions and for registers with many qubits.

In Fig. 5.6 we show how the negativity of the state shared by the registers depend on the transmission of channel ch_R. The negativity is computed at the optimal value of θ_R. For reference we plot the negativity of the TMSV state used to share entanglement between the registers. We observe that for low transmission, the registers have a higher negativity than the TMSV state. This is caused by the noiseless amplification process. Of course, this comes at a cost of probability, with experiments performed at low transmissions (η_R) having a very low probability of success. On the other hand, when the transmission is high and the registers comprise only one or two qubits, the negativity is in fact decreased by the noiseless amplification process. This is due to the truncation of the Hilbert space, and this effect is mitigated by increasing the number of qubits in the registers.

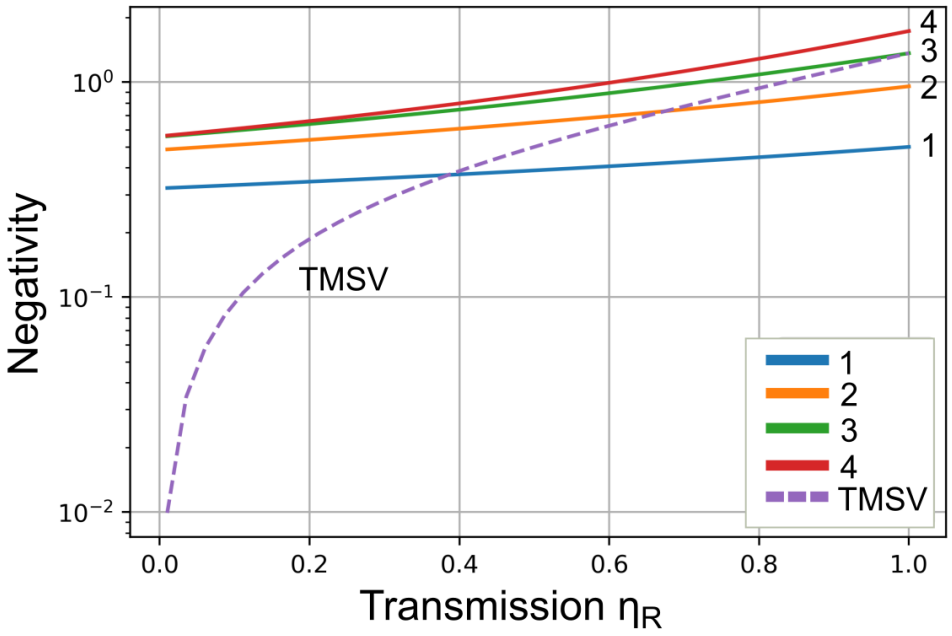

Figure 5.6: *We plot how the negativity depends on the transmission of the channel connecting the registers. The negativity is computed at the optimal value of θ_R shown in Fig. 5.5a. The average number of photons emitted by the TMSV source $\langle n \rangle$ into each channel is fixed at 0.5. The plot label and legend indicates the number of qubits in each register.*

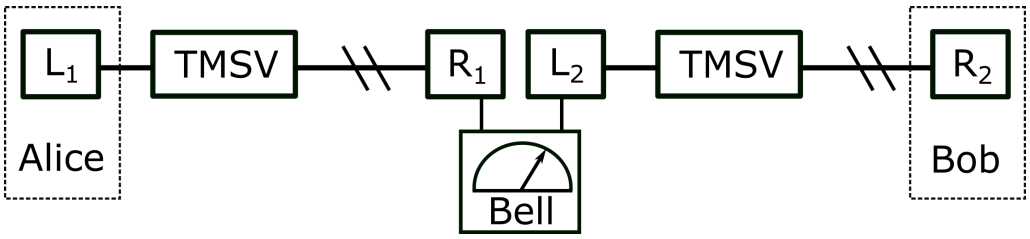

Figure 5.7: *We generate two pair of entangled registers and label them as L_1, R_1, L_2, and R_2. We assume we can perform a joint measurement on register R_1 and L_2.*

5.5 Connecting the Segments via Deterministic Entanglement Swapping

Having established that the superposition angle θ can be used to increase the negativity between registers, we investigate the possibility of using these registers as a memory unit in a quantum repeater. We will focus our analysis on the case of 1 qubit per register. This case is the most relevant considering current technological limitations. We now show how entanglement swapping between single-qubit registers is performed. Suppose we have 4 registers, as shown in Fig. 5.7, pairwise entangled in the state ρ given by Eq. 5.12 with $N = 1$. The total state Ω is then a product of two of such states $\Omega = \rho \otimes \rho$. We label the registers as L_1, R_1, L_2, and R_2. We assume we can perform a deterministic Bell measurement on the registers R_1 and L_2. We may join several pairs of registers in series to form a repeater array as shown in Fig. 5.8a.

We propose that a repeater node (eg. R_1 and L_2) could consist of two closely situated (coupled) NV centers, on which we can perform a joint Bell measurement, and we will analyze the repeater based on this assumption. However, we note that the qubits making up a repeater node could also be realized as the electronic spin of a NV center and the spin of a nearby ^{13}C atom coupled to the NV center. In this case, the repeater protocol would have to be realized step-wise. Eg. referring to Fig. 5.8a, repeater segment 1 would establish entanglement between the NV centers at Alice and node 1, and the entangled state would then be transferred to ^{13}C atoms at Alice and node 1. These nuclear qubits make up L_1 and R_1. Simultaneously with this, entanglement would be generated between ^{13}C atoms at node 2 and at Bob using repeater segment 3. These nuclear qubits would in turn make up L_3 and R_3. Entanglement is then shared between NV centers at node 1 and node 2 using repeater segment 2, these electronic qubits make up L_2 and R_2. A swap is then performed on the NV center and ^{13}C nuclear spin at both node 1 and 2, thereby generating an entangled state between Alice and Bob's ^{13}C nuclear spins. The idea is sketched for a longer repeater in Fig. 5.8b. State transfer between the electronic spin and a coupled ^{13}C nuclear spin was experimentally demonstrated

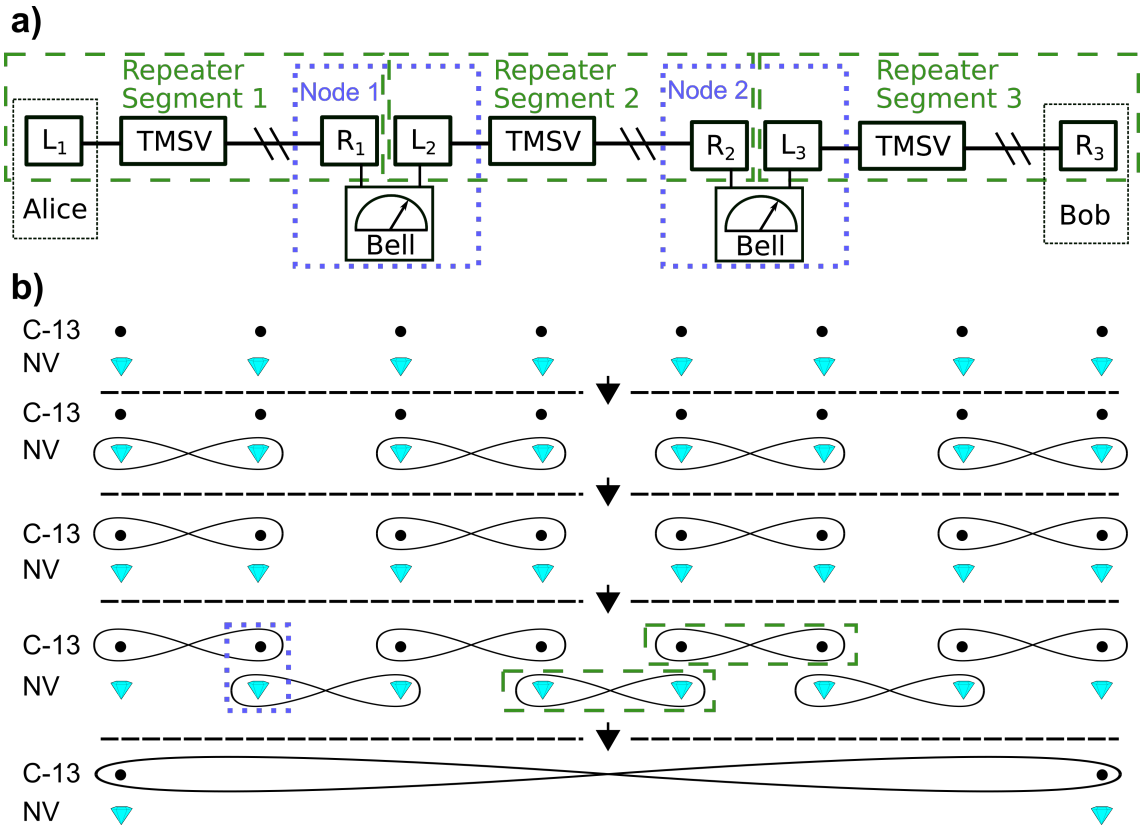

Figure 5.8: ***a**: We refer to a pair of registers connected by a TMSV state as a repeater segment. Pairs of registers capable of undergoing an entanglement swap forms a repeater node. We may combine repeater segments sequentially to form a repeater, here shown with 3 repeater segments connecting Alice and Bob. Segments are highlighted with an enveloping green dashed box, and nodes are indicated with a blue dotted box.* ***b**: If we interpret the two qubits in a given node as an NV-center and a nearby coupled ^{13}C nuclear spin, then the repeater chain must run step-wise as sketched. The involved steps are separated by a dotted line and an arrow, moving from top to bottom. Entanglement between two qubits is indicated by an enveloping loop. We highlight two repeater segments with a green dashed box, and a node in a blue dotted box. In the final step, entanglement swapping is performed at all the nodes, generating an entangled state between Alice and Bob.*

in [88]. Their protocol realizes a rotation of either the electronic or nuclear spin, controlled by the state of the other spin. This enables a CNOT gate, and combined with the ability to rotate the spins, facilitates a state transfer between the spins (see also [89], [90]). The same operations enable the realization of a Bell measurement on the two spins, and this was experimentally realized with a ^{14}N nuclear spin in [91].

Performing entanglement swapping at all the nodes, we find the normalized density matrix after s swaps:

$$\rho_s = \left[2 + (s+1)(\eta^{-1}-1)\tan(\theta_R)^2\right]^{-1} \begin{pmatrix} 1 & 0 & 0 & \left(-e^{i\phi}\right)^{s+1} \\ 0 & (s+1)(\eta^{-1}-1)\tan(\theta_R)^2 & 0 & 0 \\ 0 & 0 & 0 & 0 \\ \left(-e^{-i\phi}\right)^{s+1} & 0 & 0 & 1 \end{pmatrix} \tag{5.17}$$

Here we assumed that all s Bell measurements projected onto the state ,

$$|\psi\rangle = \frac{1}{\sqrt{2}}\left(|0_{R_n}0_{L_{n+1}}\rangle + |1_{R_n}1_{L_{n+1}}\rangle\right). \tag{5.18}$$

The derivation can be found in appendix A. We note that the matrix element corresponding to loss, $((s+1)(\eta^{-1}-1)\tan(\theta_R)^2)$, grows linearly in the number of swaps, and will dominate after many swaps. Of course, other Bell measurement outcomes than the one considered here will occur. In our reported results we sample swaps fairly according to the probability at which they occur.

5.6 Performance of the Quantum Repeater

Having described the construction of the entire quantum repeater scheme, we will now discuss its performance in terms of its ability to generate a secret key between two parties. We will assume that Alice is the reconcilliator. We will also analyze the possibility of violating a Bell inequality, which will enable device independent quantum key distribution (DI-QKD). As is derived in Appendix A, when we decrease θ_R we increase the purity of the state shared by the single qubit registers, however this comes at a cost of a lower probability of success. In a realistic scenario, the experimenter has a finite number of attempts to set up her repeater channel. If the scheme has not succeeded within this number of attempts it might be impractical to use the scheme for sharing secret keys, due to the long waiting time. We take this into account by defining some number of attempts available to the experimenter, A. Mathematically we impose the constraint that the average experiment succeeds in A attempts.
Let p be the probability that each pair of registers (L_n, R_n) successfully generate the shared state given in Eq. 5.12. In order for the whole repeater array to succeed in

A attempts on average, then p must necessarily be related to A. The exact relation is given in Appendix C Eq. 5.82. We determine p numerically from A and insert it into Eq. 5.66 so that we may determine the optimal values of θ_R, θ_L and $\langle n \rangle$. We then compute the secret key rate for various values of A. An expression for the secret key rate is derived in Appendix B and C, and given by Eq. 5.83. The secret key rate can be seen in Fig. 5.9 as a function of distance (assuming a fiber loss rate of 0.2dB/km). Our calculations imply that the proposed setup, under the assumed idealizations, might beat the point-to-point capacity bound (also known as the PLOB bound [92]) at roughly 130 km. However, one should keep in mind that the repeater requires extensive two-way classical communication between segments, and key exchange is expected to be slow.

In order to compute the key rates presented in Fig. 5.9, we have numerically optimized a number of repeater parameters, including the length of a single segment, the mean photon number of the TMSV, and the angles, θ_L and θ_R. The length of a repeater segment was set to 10 km. This distance was found to be optimal as revealed by the scans shown in Appendix D Fig. 5.13. Note that the performance only varies weakly with the segment length. The optimal value of $\langle n \rangle$ as a function of the distance is shown in Appendix D Fig. 5.14. The optimal values of θ_L and θ_R are also shown in Appendix D, in Fig. 5.15 and Fig. 5.16 respectively.

5.6.1 Bell Inequality Violation and Device-Independent QKD

Device independence represents an ultimate level of security where minimal trust is placed in the implementation of the QKD protocol. A prerequisite for a device independent proof of security is that Alice and Bob (the end points of the repeater) can violate a Bell inequality with their shared 2 qubit state, and that the violation coincide with what they expect based on the quality of the channel in use [49], [93]. We follow the device independent protocol presented in [8]. We note that Alice is the reconcilliator in our scheme. Alice measures one of the operators

$$\begin{aligned} M_A^{(1)} &= \sigma_x, \\ M_A^{(2)} &= \sigma_z. \end{aligned} \tag{5.19}$$

Whereas Bob measures one of the operators

$$\begin{aligned} M_B^{(0)} &= \sigma_x, \\ M_B^{(1)} &= (\sigma_x + \sigma_z)/\sqrt{2}, \\ M_B^{(2)} &= (\sigma_x - \sigma_z)/\sqrt{2}. \end{aligned} \tag{5.20}$$

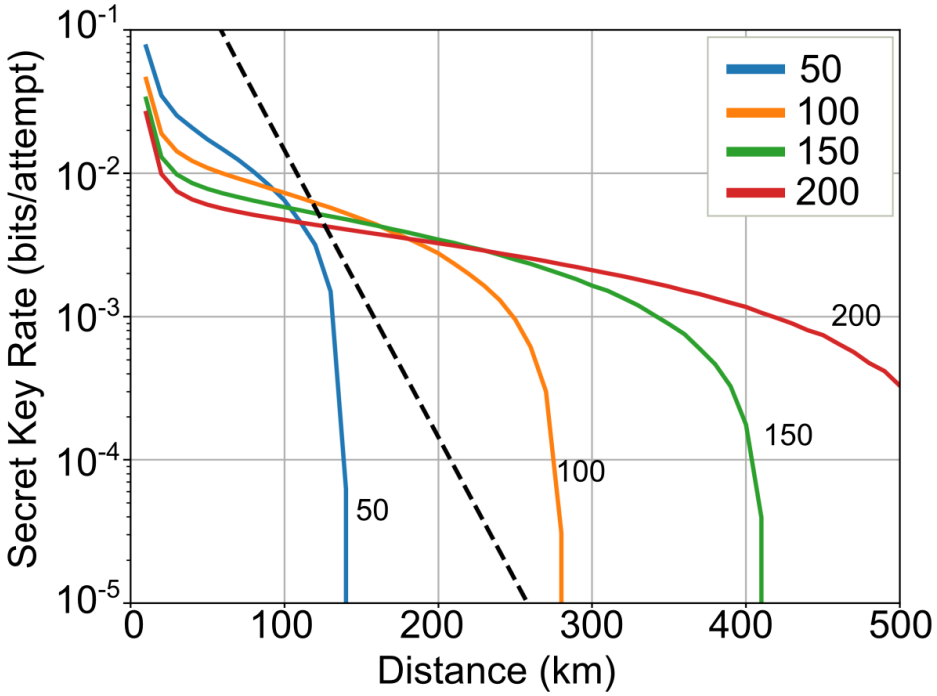

Figure 5.9: *Plot of the secret key rate obtained with 1 qubit per register against the distance between the two participants attempting to share a secret key. Alice is the reconcilliator. The secret key rate is computed for different number of allowed attempts A (legend and plot label). We assume a loss of 0.2 db/km. Each curve is an average over 15 calculations, where each calculation might differ due to the Bell measurement outcomes realized at each swap. The separation of two registers, forming a repeater segment, is 10 km. For reference we plot the PLOB bound [92] as a dotted black line.*

A key can be extracted when Alice happens to measure $M_A^{(1)}$ and Bob happens to measure $M_B^{(0)}$. If Bob measures either $M_B^{(1)}$ or $M_B^{(2)}$, then these measurement outcomes are announced and compared with Alice's measurement outcomes. From this comparison one can compute the value of the CHSH inequality,

$$\begin{aligned} S =& \langle M_A^{(1)} M_B^{(1)} \rangle + \langle M_A^{(1)} M_B^{(2)} \rangle \\ &+ \langle M_A^{(2)} M_B^{(1)} \rangle - \langle M_A^{(2)} M_B^{(2)} \rangle \leq 2. \end{aligned} \tag{5.21}$$

A requirement for violating the CHSH inequality, and extracting a secret key, is that Alice and Bob keep track of what swaps occurred in the repeater, and perform appropriate corrections to the shared quantum state. In Fig. 5.10 to the left we plot the CHSH value S against the distance between Alice and Bob. We note that the critical distance, where S drops below the classical bound of 2, is similar to the distance at which the secret key rate (Fig. 5.9) vanishes for the same value of A. To investigate this connection further, we determine the distance at which the secret key rate vanishes for various values of A, and compare it with the distance at which the CHSH value drops below 2. The two resulting curves are shown as a function of A in Fig. 5.10 to the right. We note that both curves exhibit a nearly linear dependence on A, and that the two curves nearly coincide.
We compute the device-independent secret key as [8]

$$r \geq 1 - h(Q) - h\left(\frac{1 + \sqrt{(S/2)^2 - 1}}{2}\right), \tag{5.22}$$

and normalize by the required number of attempts to set up the repeater. The rate in Eq. 5.22, while first derived for collective attacks, by entropy accumulation also holds asymptotically for coherent attacks [47]. The quantum bit error rate Q (QBER) is defined as the probability that Alice and Bob get measurement outcomes that are in disagreement with what they expect, given that they measure $M_A^{(1)}$ and $M_B^{(0)}$. For example, they might obtain differing outcomes when they expect the same outcomes, as inferred from the shared quantum state. We have introduced the binary entropy function $h(x)$. The computed device-independent key rate can be seen in Fig. 5.11 to the left. To the right we show the corresponding values of Q. The device-independent key rate appear to be more sensitive to loss than the regular key rate (Fig. 5.9), and as a result, vanishes at shorter distances.

5.6.2 Robustness of the Scheme

We then investigate the robustness of the scheme toward various sources of error. We consider the following 4 errors: Loss in the left channel ($\mathrm{ch_L}$), loss when coupling the emission of the NV center to a fiber (channels f), dark counts at the detectors T and B, and finally, loss in the detectors T and B. It is difficult to obtain an analytic

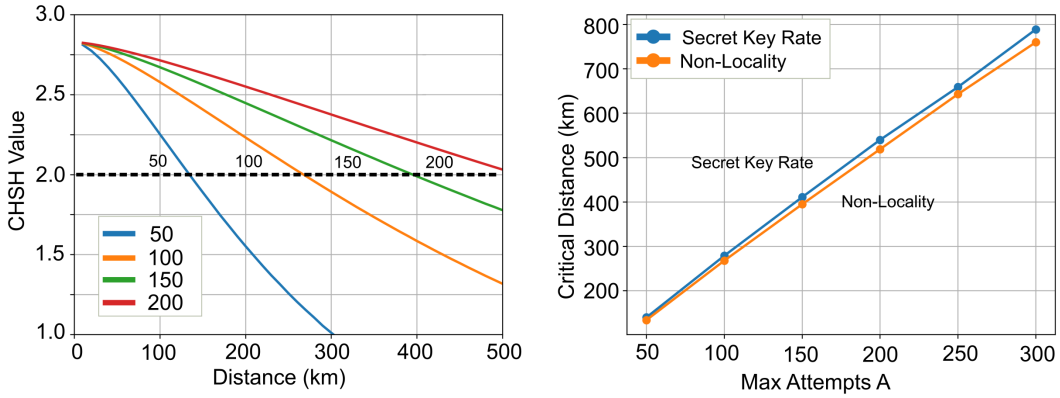

Figure 5.10: ***Left:*** *Plot of the CHSH value against the distance between the end points of the repeater. A CHSH value above 2 is inconsistent with a local model. The CHSH value is computed for different number of allowed attempts A (legend and plot label). Each curve is an average over 15 calculations.* ***Right:*** *We plot the critical distance at which the secret key rate vanishes, and the distance at which the CHSH value is equal to 2, against the number of allowed attempts A. We observe a nearly linear dependence on A and the curves are nearly identical.*

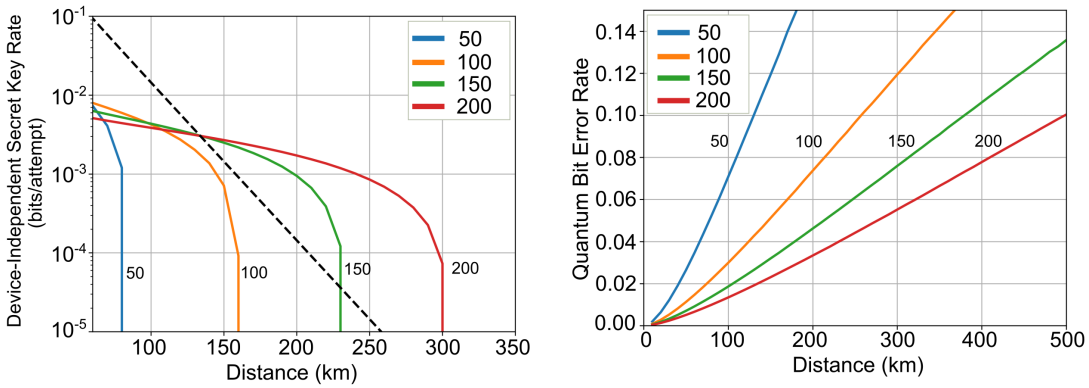

Figure 5.11: ***Left:*** *Device-independent secret key rate against the distance between the end points of the repeater. The rate is computed using Eq. 5.22. The PLOB bound is drawn as a black dotted line.* ***Right:*** *Quantum bit error rate (Q) against the distance. The quantum bit error rate is in our case defined as the probability that Alice and Bob get different outcomes given that they measure $M_A^{(1)}$ and $M_B^{(0)}$, that is $Q = P(a \neq b|10)$. The legend and curve annotation indicates the value of A.*

expression for the state when including these errors, due to the large number of sums involved. Therefore we turn to a numerical simulation using a custom Python module given on github [94]. We find that when including these errors in our model, it is advantageous to increase the distance of a repeater segment to 60 km, while also increasing A to 500. By increasing the length of a repeater segment, we decrease the required number of segments, and therefore the number of errors. Note that A will vary slightly as we change the error rates, and all key rates are normalized appropriately. The secret key rates obtained from our simulation can be seen in Fig. 5.12, from which one can gauge the sensitivity of the repeater toward various sources of error. Our calculations indicate, that in order to beat the PLOB bound, loss in channel ch_L should be kept below about one percent. Likewise, coupling loss from the NV center to the fiber should also be kept below about one percent. The loss in the detectors should be less than half a percent, and the probability of a dark count during a measurement should be less than $0.5 \cdot 10^{-4}$ ($0.5 \cdot 10^{-2}$ percent). We will not in the present work investigate the robustness of the scheme against noise and decoherence in the qubit memories. However, we expect that the probability of a bit flip must be kept below one percent. We base this expectation on the fact that coupling loss and loss in the channel ch_L, has an effect on the quantum state which strongly resemble a bit flip error. Another potential source of error is phase noise in the fibers connecting the repeater nodes. Phase noise will reduce the entanglement of a repeater segment, since the state shared by the registers become a mixture. We expect that the standard deviation of the phase noise in the state shared by Alice and Bob after entanglement swapping, will scale as $\sqrt{M}$ where M is the number of repeater segments. Hence, the tolerated phase noise per repeater segment will be $\delta/\sqrt{M}$, where δ is the tolerated phase noise for a repeater consisting of a single segment. δ is inferred from the particular QKD protocol in use, we estimate that $\delta = 200$ mrad corresponds to a quantum bit error rate of roughly 1%, when the phase noise is normally distributed with standard deviation δ, the details can be found in appendix E. Finally, we estimate that in order to beat the PLOB bound, the average number of thermal photons in the generated TMSV states must not be much higher than 10^{-3}. This is around 2 orders of magnitude smaller than the expected number of non-thermal photons, which is set to be on the order of 0.1. The details of the calculation can be found in appendix E.

5.7 Conclusion

We have analyzed a protocol for generating entanglement between a pair of multi-qubit registers, where entanglement is shared by distributing two-mode squeezed vacuum states followed by noiseless amplification using quantum scissor operations with atomic qubits. Underlying our analysis is the assumption that the qubits can occupy a bright and a dark state. With this in mind, we propose that these registers could be physically realized using NV centers in diamond. We found that

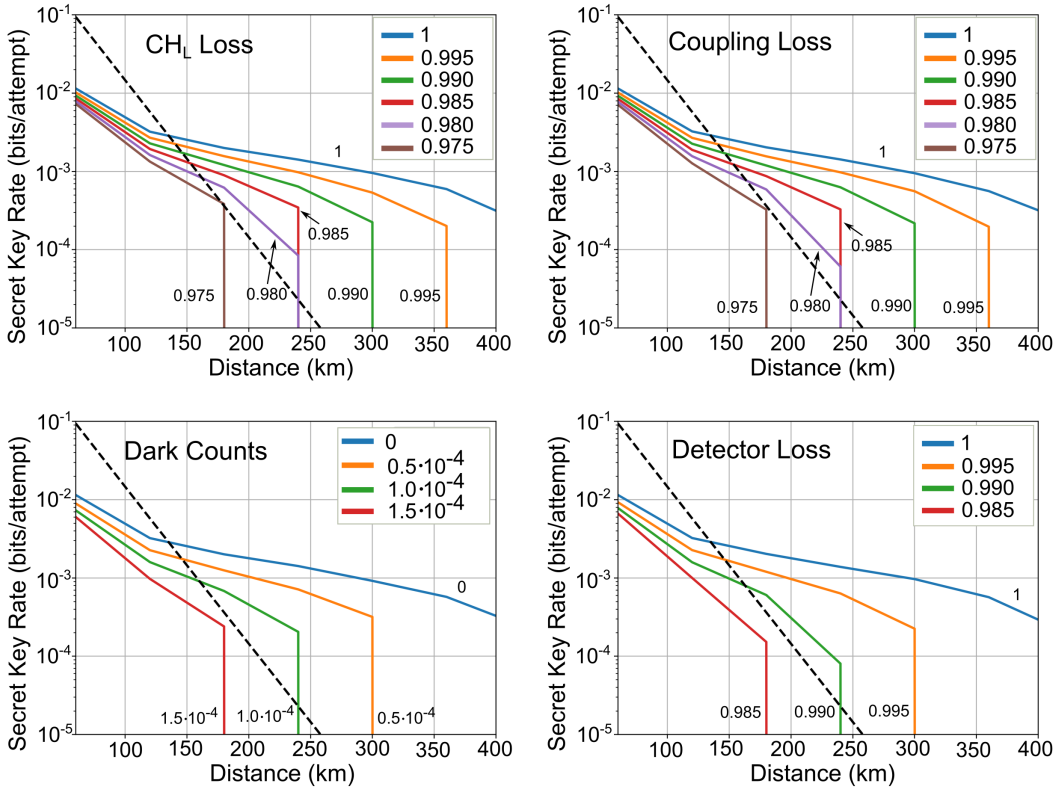

Figure 5.12: *We plot the secret key rate with varying imperfections in the repeater. The distance between repeater nodes is 60 km, and A (the expected number of attempts) is close to 500 for all plots. The plots are jagged due to the length of a repeater segment being 60 km. The PLOB bound is drawn as a black dotted line.* ***Top left:*** *We vary the transmission of the left channel (ch_L). The assumed transmission of ch_L is shown in the legend and plot label.* ***Top right:*** *We vary the transmission when coupling the emission of the NV center to a fiber. The assumed transmission is shown in the legend and plot label.* ***Bottom left:*** *We vary the probability of a dark count at the detectors T and B. The assumed probability is shown in the legend and plot label.* ***Bottom right:*** *We vary the loss of detectors T and B. The assumed fraction of light collected by the detectors, is shown in the legend and plot label.*

entanglement can be increased between the registers by purifying the shared state via tuning of the angles θ_L and θ_R, with $\sin(\theta_L)$ ($\sin(\theta_R)$) being the amplitude corresponding to qubits in the left (right) register being in the bright state. We found that with a single qubit per register it is possible to use the proposed protocol in a repeater, capable of beating the PLOB bound at around 130 km, under ideal conditions. We then gauged the sensitivity of the scheme against various sources of error. We found that in order to beat the PLOB bound, loss of emission from the NV centers should be kept below 1 percent, and loss in the channel ch_L should likewise be below 1 %. Loss in the detectors should be kept below 0.5 %, and the probability of a dark count during a measurement should be kept below $0.5 \cdot 10^{-2}$ %. We computed the value of the CHSH inequality for the analyzed setup, and found that at the distance where the secret key rate vanishes, it is also possible to construct a local hidden variable model for the measurement outcomes. Finally, using the computed CHSH value and the quantum bit error rate, we bounded the device-independent secret key rate of the repeater for a particular protocol.

5.8 Acknowledgment

We acknowledge the support of the Danish National Research Foundation through the Center for Macroscopic Quantum States (bigQ, DNRF0142).

5.9 Appendix

5.9.1 Generating Entangled Registers

We initialize the optical channels ($\mathrm{ch_L}$ and $\mathrm{ch_R}$) into a TMSV state:

$$|\psi\rangle = \sum_{n=0}^{\infty} c_n |n\rangle_L |n\rangle_R \tag{5.23}$$

The subscript L and R indicate whether we are referring to the left part of the state or the right part. The amplitudes are given by:

$$c_n = (-e^{i\phi})^n \sqrt{\frac{\langle n\rangle^n}{(1+\langle n\rangle)^{n+1}}} \tag{5.24}$$

Where $\langle n\rangle$ is the average number of photons in each arm of the TMSV state. In this work we consider the case where the phase ϕ is set to 0. Focusing on the left side of Figure 5.3. We split up the optical mode on N beamsplitters. We intend to split the optical field evenly among the N modes, to do this we use the transmission and reflection coefficients:

$$t_j = \sqrt{\frac{j-1}{j}}, \qquad r_j = \sqrt{\frac{1}{j}} \tag{5.25}$$

Where j is the number of the arm, starting from 1 at the leftmost arm. As a result, the amplitude operator for the left part of the TMSV, a_L, splits into the N arms as:

$$a_L \to \sqrt{\frac{1}{N}} \sum_{k=1}^{N} a_k \tag{5.26}$$

$|\psi\rangle$ then transforms as:

$$\begin{aligned} |\psi\rangle &= \sum_{n=0}^{\infty} c_n \frac{(a_L^\dagger)^n}{\sqrt{n!}} |0\rangle_L |n\rangle_R \\ &\to \sum_{n=0}^{\infty} c_n \frac{1}{\sqrt{n!}} \left(\sqrt{\frac{1}{N}}\right)^n (a_1^\dagger + a_2^\dagger + \cdots + a_N^\dagger)^n |0\rangle_l |n\rangle_R \end{aligned} \tag{5.27}$$

Note that we also propagated $|0\rangle_L$ to $|0\rangle_l$ with the latter being the empty l modes at the left register. Using the multinomial theorem, we may rewrite the ladder operator

product as:

$$\begin{aligned}
&(a_1^\dagger + a_2^\dagger + \cdots + a_N^\dagger)^n \left|0\right\rangle_l \\
&= \sum_{j_1+j_2+\cdots+j_N=n} \frac{n!}{j_1!j_2!\cdots j_N!} \left(a_1^\dagger\right)^{j_1} \left(a_2^\dagger\right)^{j_2} \cdots \left(a_N^\dagger\right)^{j_N} \left|0\right\rangle_l \\
&= \sum_{j_1+j_2+\cdots+j_N=n} \frac{n!\sqrt{j_1!}\sqrt{j_2!}\cdots\sqrt{j_N!}}{j_1!j_2!\cdots j_N!} \left|j_1, j_2, \cdots, j_N\right\rangle_l \\
&= \sum_{\mathbf{j}_n} \Omega_{\mathbf{j}_n} \left|\mathbf{j}_n\right\rangle_l
\end{aligned} \tag{5.28}$$

Where the final sum $\sum_{\mathbf{j}_n}$ runs over unique strings $\mathbf{j}_n = (j_1, j_2, \cdots, j_N)$ such that $j_1 + j_2 + \cdots + j_N = n$. E.g. if $n = 2$ and $N = 2$, then the sum runs over the states $\left|\mathbf{j}_2\right\rangle \in \{\left|2,0\right\rangle, \left|1,1\right\rangle, \left|0,2\right\rangle\}$. $\Omega_{\mathbf{j}_n}$ is the prefactor given by:

$$\Omega_{\mathbf{j}_n} = \frac{n!}{\sqrt{j_1!}\sqrt{j_2!}\cdots\sqrt{j_N!}} \tag{5.29}$$

Using this notation we then write $\left|\psi\right\rangle$ as:

$$\left|\psi\right\rangle = \sum_{n=0}^{\infty} c_n \frac{1}{\sqrt{n!}} \left(\sqrt{\frac{1}{N}}\right)^n \sum_{\mathbf{j}_n} \Omega_{\mathbf{j}_n} \left|\mathbf{j}_n\right\rangle_l \left|n\right\rangle_R \tag{5.30}$$

Meanwhile, we initialize the left registry in the state:

$$\left|L\right\rangle = \prod_{k=1}^{N} (\cos(\theta_L) \left|0\right\rangle_{q_k} \left|0\right\rangle_{f_k} + \sin(\theta_L) \left|1\right\rangle_{q_k} \left|1\right\rangle_{f_k}) \tag{5.31}$$

Where the notation $\left|0\right\rangle_{q_k} \left|0\right\rangle_{f_k}$ indicates that for arm k, the qubit (q_k) is in the state 0 and the fiber (f_k) coupled to the qubit is occupied by 0 photons.
We may then write $\left|L\right\rangle$ as:

$$\begin{aligned}
\left|L\right\rangle = &\sum_{a_1=\{0,1\}} \sum_{a_2=\{0,1\}} \cdots \sum_{a_N=\{0,1\}} \\
&\cos(\theta_L)^{(1-a_1)} \sin(\theta_L)^{a_1} \cdots \cos(\theta_L)^{(1-a_N)} \sin(\theta_L)^{a_N} \\
&\left|a_1\right\rangle_{q_1} \left|a_1\right\rangle_{f_1} \cdots \left|a_N\right\rangle_{q_N} \left|a_N\right\rangle_{f_N} \\
&= \sum_{\mathbf{a}} \beta(\mathbf{a}, \theta_L) \left|\mathbf{a}\right\rangle_q \left|\mathbf{a}\right\rangle_f
\end{aligned} \tag{5.32}$$

Where we've introduced a sum over binary lists $\sum_{\mathbf{a}}$ leaving the registry in a superposition of binary states $\left|\mathbf{a}\right\rangle_q \left|\mathbf{a}\right\rangle_f = \left|a_1\right\rangle_{q_1} \left|a_1\right\rangle_{f_1} \cdots \left|a_N\right\rangle_{q_N} \left|a_N\right\rangle_{f_N}$. We've also introduced the parameter $\beta(\mathbf{a}, \theta_L)$ to take the angle θ_L into account. We interact $\left|\psi\right\rangle$ and $\left|L\right\rangle$ using N beamsplitters acting on the l and f modes, we then measure

on these modes using the photon resolving detectors T and B for each arm. We assume a particular measurement outcome $(t_k, b_k)_k$, indicating that t_k photons are going to detector T_k and b_k photons are going to detector B_k in arm k. Subject to this measurement, the state transforms as:

$$\begin{aligned} |\psi\rangle |L\rangle \rightarrow \langle t_1|_{T_1} \langle b_1|_{B_1} U_1 \langle t_2|_{T_2} \langle b_2|_{B_2} U_2 \\ \cdots \langle t_N|_{T_N} \langle b_N|_{B_N} U_N |\psi\rangle |L\rangle \end{aligned} \tag{5.33}$$

Where U_k is the beamsplitter in arm k. The bra acting from the left then indicates the projective action of the photon resolving detectors.
The right part of the TMSV state is entangled with the left registry qubit k if $t_k + b_k = 1$ since the photon could then have come from either the TMSV state or the bright state of the qubit. Other measurement outcomes tend to yield information about the state of the registry and the TMSV state, and are expected to lower the entanglement, though this assumption could be explored further. In this work we will only accept measurement outcomes where $t_k + b_k = 1$ for all N arms of the registers.
To evaluate the above expression, we let the beamsplitters act on the bra. Eg. we examine:

$$\langle t_k|_{T_k} \langle b_k|_{B_k} U_k = (U_k^\dagger |t_k\rangle_{T_k} |b_k\rangle_{B_k})^\dagger \tag{5.34}$$

First let $t_k = 1$ and $b_k = 0$, we assume balanced beamsplitters:

$$U_k^\dagger |1\rangle_{T_k} |0\rangle_{B_k} = \frac{1}{\sqrt{2}} \left(|0\rangle_{f_k} |1\rangle_{l_k} + |1\rangle_{f_k} |0\rangle_{l_k} \right) \tag{5.35}$$

When we let $t_k = 0$ and $b_k = 1$, we get:

$$U_k^\dagger |0\rangle_{T_k} |1\rangle_{B_k} = \frac{1}{\sqrt{2}} \left(|0\rangle_{f_k} |1\rangle_{l_k} - |1\rangle_{f_k} |0\rangle_{l_k} \right) \tag{5.36}$$

As required by the reciprocity relations of the beamsplitter. Evidently, measuring $t_k = 0$ and $b_k = 1$ phase shifts registry qubit k by π if it is in the bright state (since the mode f_k is then occupied). We will assume that this phase shift can be corrected experimentally. For simplicity we examine the situation, where for all arms, we obtain the measurements $t_k = 1$ and $b_k = 0$. The measurement described by Eq. 5.33 then transforms the state as:

$$|\psi\rangle |L\rangle \rightarrow \left(\frac{1}{\sqrt{2}} \right)^N \prod_{k=1}^{N} (\langle 0|_{f_k} \langle 1|_{l_k} + \langle 1|_{f_k} \langle 0|_{l_k}) |\psi\rangle |L\rangle \tag{5.37}$$

Note that we haven't renormalized, and the norm of the state has been reduced.
Evidently, if mode l_k contains 1 photon, then mode f_k is vacant, and the qubit state

must be $|0\rangle_{q_k}$ (dark). Vice versa if mode l_k contains no photons. We rewrite the projective measurement as:

$$\prod_{k=1}^{N}(\langle 0|_{f_k}\langle 1|_{l_k}+\langle 1|_{f_k}\langle 0|_{l_k})=\sum_{\mathbf{m}}\langle\neg\mathbf{m}|_f\langle\mathbf{m}|_l \tag{5.38}$$

Where $\mathbf{m}$ is any binary list of length N. $\neg\mathbf{m}$ should be understood as the negation (not) of $\mathbf{m}$. Using Eq. 5.30, 5.32, 5.37, and 5.38, the result of the measurement is:

$$\begin{aligned}&|\psi\rangle|L\rangle\rightarrow|\alpha\rangle\\&=\left(\frac{1}{\sqrt{2}}\right)^N\sum_{n=0}^{\infty}\sum_{\mathbf{j}_n}\sum_{\mathbf{a}}\sum_{\mathbf{m}}c_n\frac{1}{\sqrt{n!}}\left(\frac{1}{\sqrt{N}}\right)^n\beta(\mathbf{a},\theta_L)\Omega_{\mathbf{j}_n}\langle\neg\mathbf{m}|_f|\mathbf{a}\rangle_f|\mathbf{a}\rangle_q\langle\mathbf{m}|_l|\mathbf{j}_n\rangle_l|n\rangle_R\end{aligned} \tag{5.39}$$

Since $\mathbf{m}$ is a binary list, then the overlap $\langle\mathbf{m}|_l|\mathbf{j}_n\rangle_l$ is only non-zero when the optical input from the TMSV state $\mathbf{j}_n$ is also binary. This implies:

$$\Omega_{\mathbf{j}_n}=n! \tag{5.40}$$

Conditioned on the overlap $\langle\mathbf{m}|_l|\mathbf{j}_n\rangle_l$ being non-zero, we see that $\mathbf{a}$ must be the negation of $\mathbf{j}_n$ so that $\langle\neg\mathbf{m}|_f|\mathbf{a}\rangle_f$ is also non-zero. This implies that the state shared between the right TMSV and the left registry after measurement is:

$$\begin{aligned}|\alpha\rangle=\left(\frac{1}{\sqrt{2}}\right)^N\sum_{n=0}^{N}\sum_{\mathbf{i}_n}c_n\left(\frac{1}{\sqrt{N}}\right)^n\\\beta(n,\theta_L)\sqrt{n!}|\neg\mathbf{i}_n\rangle_L|n\rangle_R\end{aligned} \tag{5.41}$$

Where $|\neg\mathbf{i}_n\rangle_L$ is the state of the qubits in the left register, and the sum runs over binary lists $\mathbf{i}_n$ of length N. $\mathbf{i}_n$ will contain n ones and $N-n$ zeros. $\mathbf{i}_n$ corresponds to the binary distribution of photons in the l_k modes prior to a successful measurement. The sum over n has been terminated at N, since no binary string $\mathbf{i}_n$ exist for $n>N$. We've also used the fact that:

$$\beta(\mathbf{a},\theta_L)=\beta(\neg\mathbf{i}_n,\theta_L)=\beta(n,\theta_L)=\cos(\theta_L)^n\sin(\theta_L)^{N-n} \tag{5.42}$$

We may perform the sum over $\mathbf{i}_n$ by introducing the vector:

$$\sum_{\mathbf{i}_n}|\neg\mathbf{i}_n\rangle_L=\binom{N}{n}^{1/2}|\mathbf{I}_{N-n}\rangle_L \tag{5.43}$$

Where $|\mathbf{I}_{N-n}\rangle_L$ is normalized and is an even superposition of all binary states containing $N-n$ bright state qubits and n dark state qubits. In terms of these vectors, we find that we may express $|\alpha\rangle$ as:

$$|\alpha\rangle = \left(\frac{1}{\sqrt{2}}\right)^N \sum_{n=0}^{N} c_n \left(\frac{1}{\sqrt{N}}\right)^n \beta(n,\theta_L) \sqrt{n!}\binom{N}{n}^{1/2} |\mathbf{I}_{N-n}\rangle_L |n\rangle_R \tag{5.44}$$

Comparing with the original TMSV state, we see that the left register transforms a Fock state as:

$$\begin{aligned} |n\rangle \rightarrow & \left(\frac{1}{\sqrt{2}}\right)^N \left(\frac{1}{\sqrt{N}}\right)^n \beta(n,\theta_L)\sqrt{n!}\binom{N}{n}^{1/2} |\mathbf{I}_{N-n}\rangle \\ & = \Delta(n,\theta_L) |\mathbf{I}_{N-n}\rangle \end{aligned} \tag{5.45}$$

Where

$$\Delta(n,\theta_L) = \left(\frac{1}{\sqrt{2}}\right)^N \binom{N}{n}^{1/2} \left(\frac{1}{\sqrt{N}}\right)^n \sqrt{n!}\beta(n,\theta_L) \tag{5.46}$$

Using this transform, and assuming no loss in the fiber, we may infer that storing the right part of the TMSV in the right register (see Fig. 5.3), results in the state:

$$|\alpha\rangle = \sum_{n=0}^{N} c_n \Delta(n,\theta_L)\Delta(n,\theta_R) |\mathbf{I}_{N-n}\rangle_L |\mathbf{I}_{N-n}\rangle_R \tag{5.47}$$

We may then compute the norm of the state of the two registers:

$$\langle\alpha|\alpha\rangle = \sum_{m=0}^{N} |c_m|^2 |\Delta(m,\theta_L)|^2 |\Delta(m,\theta_R)|^2 \tag{5.48}$$

The probability of successful entanglement sharing between the 2 registries is then this norm multiplied by the number of measurements that would yield an equivalent state. For each arm we have 2 detector outcomes, (0,1) or (1,0), that would yield a state equivalent to the one described above. The probability of successful entanglement sharing is then:

$$P_s = 2^N 2^N \langle\alpha|\alpha\rangle = 4^N \langle\alpha|\alpha\rangle \tag{5.49}$$

Performance with Loss

We initialize the optical channel in a TMSV state:

$$|\psi\rangle = \sum_{n=0}^{\infty} c_n |n\rangle_L |n\rangle_R \tag{5.50}$$

We send the right part of the TMSV through a lossy channel modelled by a beam-splitter with transmission amplitude $\sqrt{\eta_R}$. The transmission of the fiber is then given by η_R. Likewise we send the left part of the TMSV state through a lossy channel of transmission η_L The channels transforms the state as:

$$\begin{aligned}|\psi\rangle \rightarrow &\sum_{n=0}^{\infty}\sum_{l_R,l_L=0}^{n}\epsilon_R(n,l_R)\epsilon_L(n,l_L)c_n \\ &|n-l_L\rangle_L|n-l_R\rangle_R|l_L\rangle_{e_L}|l_R\rangle_{e_R}\end{aligned} \tag{5.51}$$

Where e_R is a loss channel. The loss amplitude is given as:

$$\epsilon_{R/L}(n,l_{R/L}) = \sqrt{\binom{n}{n-l_{R/L}}}\eta_{R/L}^{(n-l_{R/L})/2}(1-\eta_{R/L})^{l_{R/L}/2} \tag{5.52}$$

Inserting the Fock state transform Eq. 5.45, we arrive at the register state:

$$\begin{aligned}|\alpha\rangle = &\sum_{n=0}^{\infty}\sum_{l_L=0}^{n}\sum_{l_R=0}^{n}c_n\epsilon_L(n,l_L)\epsilon_R(n,l_R)\Delta(n-l_L,\theta_L) \\ &\Delta(n-l_R,\theta_R)\Theta(N+l_L-n)\Theta(N+l_R-n) \\ &|\mathbf{I}_{N-n+l_L}\rangle_L|\mathbf{I}_{N-n+l_R}\rangle_R|l_L\rangle_{e_L}|l_R\rangle_{e_R}\end{aligned} \tag{5.53}$$

Where we've introduced the step function:

$$\Theta(x) = \begin{cases}1 & \text{if } x \geq 0 \\ 0 & \text{if } x < 0\end{cases} \tag{5.54}$$

The step function takes into account that when more than N photons reach either registers, then the projective measurement fails.

The corresponding density matrix is:

$$\begin{aligned}\sigma = &\sum_{n=0}^{\infty}\sum_{m=0}^{\infty}\sum_{l_L=0}^{n}\sum_{k_L=0}^{m}\sum_{l_R=0}^{n}\sum_{k_R=0}^{m}c_nc_m^*\epsilon_R(n,l_R)\epsilon_L(n,l_L)\epsilon_R(m,k_R)^*\epsilon_L(m,k_L)^* \\ &\Delta(n-l_L,\theta_L)\Delta(n-l_R,\theta_R)\Delta(m-k_L,\theta_L)^*\Delta(m-k_R,\theta_R)^* \\ &\Theta(N+l_L-n)\Theta(N+l_R-n)\Theta(N+k_L-m)\Theta(N+k_R-m) \\ &|\mathbf{I}_{N-n+l_L}\rangle_L\langle\mathbf{I}_{N-m+k_L}|_L|\mathbf{I}_{N-n+l_R}\rangle_R\langle\mathbf{I}_{N-m+k_R}|_R|l_L\rangle_{e_L}\langle k_L|_{e_L}|l_R\rangle_{e_R}\langle k_R|_{e_R}\end{aligned} \tag{5.55}$$

We then trace out the loss channels, giving the state:

$$\begin{aligned}\rho = \mathrm{Tr}_e\sigma = &\sum_{n=0}^{\infty}\sum_{m=0}^{\infty}\sum_{l=0}^{\mathtt{min}(n,m)}\sum_{r=0}^{\mathtt{min}(n,m)}c_nc_m^*\epsilon_R(n,r)\epsilon_L(n,l)\epsilon_R(m,r)^*\epsilon_L(m,l)^* \\ &\Delta(n-l,\theta_L)\Delta(n-r,\theta_R)\Delta(m-l,\theta_L)^*\Delta(m-r,\theta_R)^* \\ &\Theta(N+l-n)\Theta(N+r-n)\Theta(N+l-m)\Theta(N+r-m) \\ &|\mathbf{I}_{N-n+l}\rangle_L\langle\mathbf{I}_{N-m+l}|_L|\mathbf{I}_{N-n+r}\rangle_R\langle\mathbf{I}_{N-m+r}|_R\end{aligned} \tag{5.56}$$

We define the matrix elements:

$$\begin{aligned}\Lambda(n,m,l,r) = c_n c_m^* \epsilon_R(n,r)\epsilon_L(n,l)\epsilon_R(m,r)^*\epsilon_L(m,l)^* \\ \Delta(n-l,\theta_L)\Delta(n-r,\theta_R)\Delta(m-l,\theta_L)^*\Delta(m-r,\theta_R)^* \\ \Theta(N+l-n)\Theta(N+r-n)\Theta(N+l-m)\Theta(N+r-m)\end{aligned} \tag{5.57}$$

Such that we may write the state as:

$$\rho = \sum_{n=0}^{\infty}\sum_{m=0}^{\infty}\sum_{l=0}^{\min(n,m)}\sum_{r=0}^{\min(n,m)} \Lambda(n,m,l,r)\left|\mathbf{I}_{N-n+l}\right\rangle_L\left\langle\mathbf{I}_{N-m+l}\right|_L\left|\mathbf{I}_{N-n+r}\right\rangle_R\left\langle\mathbf{I}_{N-m+r}\right|_R \tag{5.58}$$

One Qubit Per Register

In the following we will analyse the case of one sided loss. Loss is assumed to only occur between the TMSV source and the right register. If $N = 1$ then we have the density matrix:

$$\rho = \frac{1}{4}\begin{pmatrix} |c_1|^2\eta c_{\theta_L}^2 c_{\theta_R}^2 & 0 & 0 & c_1 c_0^*\sqrt{\eta}s_{\theta_R}s_{\theta_L}c_{\theta_R}c_{\theta_L} \\ 0 & |c_1|^2(1-\eta)c_{\theta_L}^2 s_{\theta_R}^2 & 0 & 0 \\ 0 & 0 & 0 & 0 \\ c_1^* c_0\sqrt{\eta}s_{\theta_R}s_{\theta_L}c_{\theta_R}c_{\theta_L} & 0 & 0 & |c_0|^2 s_{\theta_L}^2 s_{\theta_R}^2 \end{pmatrix} \tag{5.59}$$

where $c_{\theta_L} = \cos(\theta_L)$, $c_{\theta_R} = \cos(\theta_R)$, $s_{\theta_L} = \sin(\theta_L)$ and $s_{\theta_R} = \sin(\theta_R)$. If we use the above state for entanglement swapping via Bell measurements, there is an advantage in keeping the matrix elements ρ_{11} and ρ_{44} identical. If this is not the case, series of swaps will tend to make the state more separable and thereby diminish entanglement. This constraint implies:

$$|c_1|^2\eta\cos(\theta_L)^2\cos(\theta_R)^2 = |c_0|^2\sin(\theta_L)^2\sin(\theta_R)^2 \tag{5.60}$$

This implies a bond between θ_R and θ_L.

$$\tan(\theta_L)^2 = \tan(\theta_R)^{-2}\eta\frac{|c_1|^2}{|c_0|^2} \tag{5.61}$$

Utilizing the bond in Eq. 5.61 we may rewrite the density matrix as:

$$\rho = \frac{1}{4}\frac{\sin(\theta_R)^2|c_1|^2|c_0|^2\eta}{\tan(\theta_R)^2|c_0|^2+\eta|c_1|^2}\begin{pmatrix} 1 & 0 & 0 & -e^{i\phi} \\ 0 & (\eta^{-1}-1)\tan(\theta_R)^2 & 0 & 0 \\ 0 & 0 & 0 & 0 \\ -e^{-i\phi} & 0 & 0 & 1 \end{pmatrix} \tag{5.62}$$

We now want to choose the superposition angle θ_R such that the state is as entangled as possible. Evidently we have that if we suppress the loss term, corresponding to matrix element ρ_{22}, then the state of the qubits is a maximally entangled state. This suggests that we should make $\tan(\theta_R)^2$ as small as possible. However, there is one more condition to consider. The probability of the measurements at the photodetectors succeeding, which goes to zero in this limit where $\theta_R \to 0$. The probability of success is given by the trace of ρ:

$$P(\theta_R, \langle n \rangle; \eta) = \sin(\theta_R)^2 |c_1|^2 |c_0|^2 \frac{2\eta + (1-\eta)\tan(\theta_R)^2}{\tan(\theta_R)^2 |c_0|^2 + \eta |c_1|^2} \tag{5.63}$$

Where we take into account that the measurements at the photodetectors can succeed in 4 ways. The optimal choice of θ_R is then the choice that minimizes $\tan(\theta_R)^2$ subject to the condition that:

$$P(\theta_R, \langle n \rangle; \eta) \geq p \tag{5.64}$$

Where p is the minimum probability of success tolerated by the experimental setup. We may maximize $P(\theta_R, \langle n \rangle; \eta)$ in $\langle n \rangle$ for a given θ_R and η by choosing the squeezing of the TMSV source such that we have the equality:

$$\langle n \rangle = \sqrt{1 - \frac{\eta}{\eta + \tan\left(\theta_R\right)^2}} \tag{5.65}$$

Inserting the optimal choice of $\langle n \rangle$ into $P(\theta_R, \langle n \rangle; \eta)$ we obtain the probability $P(\theta_R; \eta)$. From numerical investigation we find that this probability depends on the angle θ_R in a complicated manner. However, for values of $|\theta_R|$ below ~ 0.66 we have that $P(\theta_R; \eta)$ decreases monotonically in $|\theta_R|$ for any value of η. In order to minimize $\tan(\theta_R)^2$ we require low values of θ_R, and so we expect to be below this angle. With this consideration, we may infer that the optimal choice of θ_R is obtained when:

$$P(\theta_R; \eta) = p \tag{5.66}$$

Which can be rewritten as a quartic polynomial equation in $z = \sqrt{1 - \frac{\eta}{\eta + \tan(\theta_R)^2}}$:

$$\begin{aligned} p + 2pz + \eta\left[p - 2\right] z^2 + p\left[2\eta - 2\right] z^3 \\ + \left[-p + (1+p)\eta + \eta^2\right] z^4 = 0 \end{aligned} \tag{5.67}$$

Which can be solved efficiently numerically and from which we can find θ_R.

Given that we've made the optimal choice of θ_R we can investigate how the state evolves under a sequence of swaps. Suppose we have 4 registers, as shown in Fig. 5.7, pairwise entangled in the state ρ given by Eq. 5.62. The total state Ω is then a

product of two of such states $\Omega = \rho \otimes \rho$. Obtaining the particular Bell measurement outcome corresponding to the ket $|\psi\rangle = \frac{1}{\sqrt{2}}(|0_{R_1}0_{L_2}\rangle + |1_{R_1}1_{L_2}\rangle)$ on registers R_1 and L_2, we obtain the state:

$$\rho_1 = \frac{1}{2}(\langle 0_{R_1}0_{L_2}| + \langle 1_{R_1}1_{L_2}|)\Omega(|0_{R_1}0_{L_2}\rangle + |1_{R_1}1_{L_2}\rangle) \tag{5.68}$$

We may evaluate ρ_1 by inserting ρ from Eq. 5.62. We obtain the unormalized state:

$$\rho_1 = \frac{1}{2}\left(\frac{1}{4}\frac{\sin(\theta_R)^2|c_1|^2|c_0|^2\eta}{\tan(\theta_R)^2|c_0|^2 + \eta|c_1|^2}\right)^2 \begin{pmatrix} 1 & 0 & 0 & \left(-e^{i\phi}\right)^2 \\ 0 & 2(\eta^{-1}-1)\tan(\theta_R)^2 & 0 & 0 \\ 0 & 0 & 0 & 0 \\ \left(-e^{-i\phi}\right)^2 & 0 & 0 & 1 \end{pmatrix} \tag{5.69}$$

Clearly the state is similar in structure to the original state, with the loss term having doubled in size relative to the other matrix elements. Continuing this, then after s swaps we obtain the unnormalized density matrix:

$$\rho_s = \left(\frac{1}{2}\right)^s \left(\frac{1}{4}\frac{\sin(\theta_R)^2|c_1|^2|c_0|^2\eta}{\tan(\theta_R)^2|c_0|^2 + \eta|c_1|^2}\right)^{s+1} \begin{pmatrix} 1 & 0 & 0 & \left(-e^{i\phi}\right)^{s+1} \\ 0 & (s+1)(\eta^{-1}-1)\tan(\theta_R)^2 & 0 & 0 \\ 0 & 0 & 0 & 0 \\ \left(-e^{-i\phi}\right)^{s+1} & 0 & 0 & 1 \end{pmatrix} \tag{5.70}$$

Of course, other Bell measurement outcomes than the one considered here will occur. We will numerically simulate swaps by drawing fairly from the four Bell measurement outcomes.

5.9.2 Secret Key Rate

Having established entanglement between registers we're interested in computing how large a shared secret key might be extractable from the density matrix. We will assume that Eve can perform a collective attack [16]. Given that Alice and Bob each measure their registry qubit, the secret information is then simply the mutual information between the observed outcomes (a and b) minus the information an eavesdropper might have of the outcome obtained by the reconcilliator x (Alice or Bob) [95]. The secret information is given by the Devetak-Winter formula [96]:

$$K = \beta I(a:b) - S(x:E) \tag{5.71}$$

Where β is the reconcilliation efficiency, that is, how large a part of the mutual information that can be distilled into a shared key. The mutual information between the measurement outcomes obtained by Alice and Bob is simply [4]:

$$I(a:b) = \sum_{a,b} P(a,b) \log_2 \left(\frac{P(a,b)}{P(a)P(b)} \right) \tag{5.72}$$

Where $P(a,b)$ is the probability of obtaining outcomes a and b, whereas $P(a)$ and $P(b)$ are the marginal probabilities of obtaining outcomes a and b respectively. $S(x:E)$ is the Holevo information which upper bounds the information Eve can obtain about the variable x given her measurement e [5]:

$$I(x:e) \leq S(x:E) \tag{5.73}$$

With the capital E indicating the state on which Eve has not yet measured. We will assume that Alice is the reconcilliator $x = a$. The Holevo value is given by

$$S(a:E) = S(\rho_E) - \sum_a P(a) S(\rho_E^a). \tag{5.74}$$

Where ρ_E^a is the state held by Eve subject to the condition that Alice measures a. Since Bob purifies the state ρ_E^a, we have that

$$S(\rho_E^a) = S(\rho_B^a). \tag{5.75}$$

Furthermore, since Alice and Bob purifies the state held by Eve

$$S(\rho_E) = S(\rho_{AB}). \tag{5.76}$$

So we may compute the Holevo value simply by knowing the state shared by Alice and Bob

$$S(a:E) = S(\rho_{AB}) - \sum_a P(a) S(\rho_B^a). \tag{5.77}$$

To obtain a secret key *rate*, we normalize K by the number of channel uses necessary to generate that secret key. The number of channel uses neccessary will be established in Appendix C. We will be assuming a reconcilliation efficiency β of 1, and that Alice and Bob either measure σ_x or σ_z (e.g. they could use the BB84 protocol). They can then extract a secret key from measurement rounds where their choice of basis coincide.

5.9.3 Trials Needed Before M Repeater Segments Succeed

In the previous sections we analyzed a single pair of registers, L_1 and R_1, and found the probability p with which we successfully generate the state ρ given in

Eq. 5.58, with p given by $4^N \mathrm{Tr}\rho$. Given p we will assume that the probability of successfully generating ρ after *exactly* n attempts, follows a geometric distribution, with probability mass function:

$$\mathrm{PMF}(n) = p(1-p)^{n-1} \tag{5.78}$$

The corresponding cumulative distribution function, which should be interpreted as the probability that ρ has been established in less than or exactly n attempts, is given by:

$$\mathrm{CDF}(n) = 1 - (1-p)^n \tag{5.79}$$

Now we will assume that we have a collection of M repeater segments, each repeater segment being a pair of registers, as shown in Fig. 5.8 a. We now want to compute how many attempts are necessary before all M repeater segments successfully generate the state ρ. The cumulative distribution for M repeaters attempting in parallel is simply the product:

$$\mathrm{CDF}_M(n) = [1 - (1-p)^n]^M \tag{5.80}$$

The probability of all repeaters having succeeded after exactly n attempts is then:

$$\begin{aligned} \mathrm{PDF}_M(n) &= \mathrm{CDF}_M(n) - \mathrm{CDF}_M(n-1) \\ &= [1-(1-p)^n]^M - [1-(1-p)^{n-1}]^M \\ &= \sum_{s=0}^{M} \binom{M}{s} (1-p)^{n\cdot s} \left[1 - (1-p)^{-s}\right] \end{aligned} \tag{5.81}$$

A similar formula may be found in [97].
We then fix p by demanding that the following relation is satisfied:

$$A = \sum_{n=1}^{\infty} n \cdot \mathrm{PDF}_M(n) \tag{5.82}$$

Implying that the average experiment succeeds in A attempts.
Assuming that a state ρ_M is generated from $M-1$ deterministic entanglement swaps using M repeater segments, and that a secret key K_M can be extracted from this state, we normalize this key by the number of attempts necessary to generate ρ_M. This gives us the secret key rate $\mathcal{K}_M$:

$$\mathcal{K}_M = \sum_{n=1}^{\infty} \frac{K_M}{n} \cdot \mathrm{PDF}_M(n) = K_M \sum_{n=1}^{\infty} \frac{\mathrm{PDF}_M(n)}{n} \tag{5.83}$$

Where K_M is computed from Eq. 5.71.

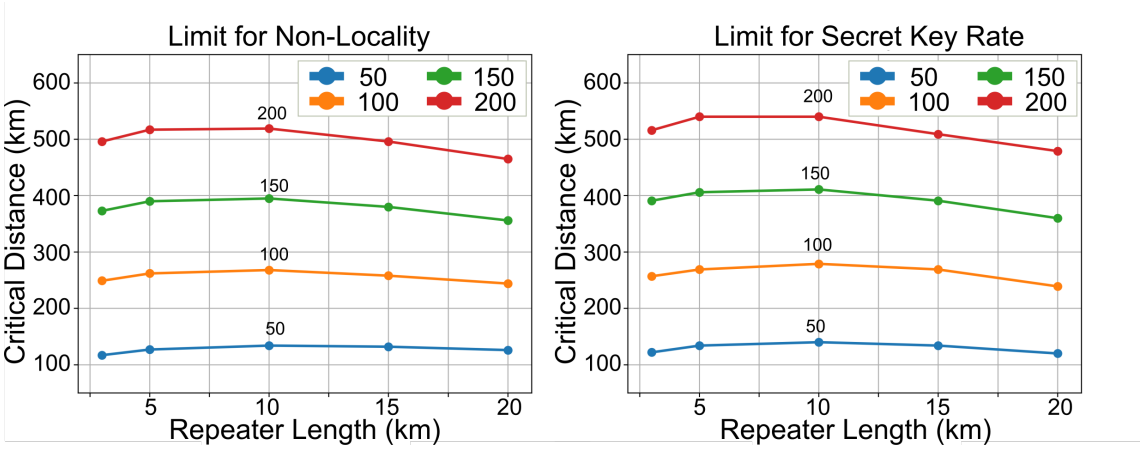

Figure 5.13: ***Left**: Plot of the distance where no Bell inequality can be violated for various register separations with 1 qubit per register. **Right**: Plot of the distance where the secret key rate vanishes for various register separations with 1 qubit per register. The legend and plot label indicates the expected number of attempts A.*

5.9.4 Optimal Parameters - 1 Qubit per Register

In Fig. 5.13 to the right we plot the critical distance at which the secret key rate vanishes, against the separation between registers making up a repeater segment. In Fig. 5.13 to the left we likewise show the critical distance at which the CHSH inequality is no longer broken, also against the separation between registers making up a repeater segment.
We then give the optimal average photon number, the optimal values of θ_L, and the optimal values of θ_R against the distance between the end points of the repeater. These are shown in Fig. 5.14, 5.15, and 5.16 respectively. Note that the length of a repeater segment was set to 10 km.

5.9.5 Phase and Thermal Noise

Phase noise in the optical fibers result in the optical TMSV state,

$$|\psi\rangle = \sum_{n=0}^{\infty} c_n e^{i\gamma n} |n\rangle_L |n\rangle_R \tag{5.84}$$

Where γ is a stochastic phase-shift of the state. γ is the combined phase-shift arising from phase noise in both arms of the TMSV state. γ can be absorbed into c_n, and in the case of 1 qubit in each register, we obtain the density matrix describing the

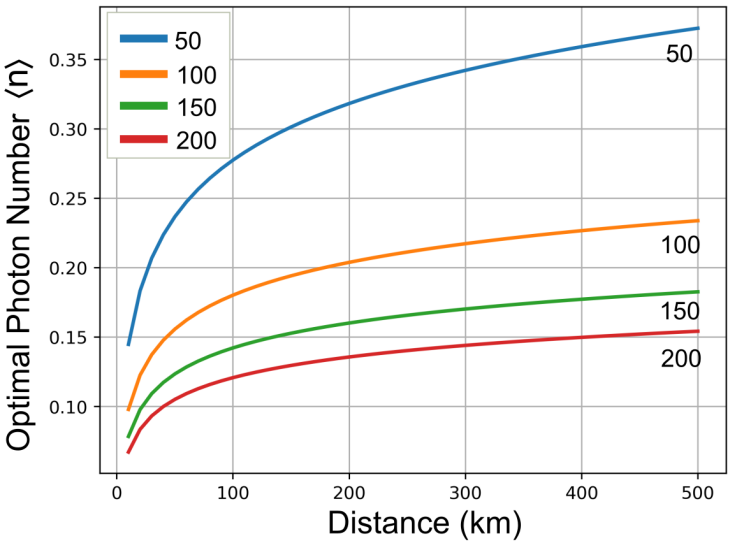

Figure 5.14: *The optimal value of $\langle n \rangle$ for different number of allowed attempts A (legend and plot label) against the distance between the end points of the repeater. The length of a repeater segment is set at 10 km.*

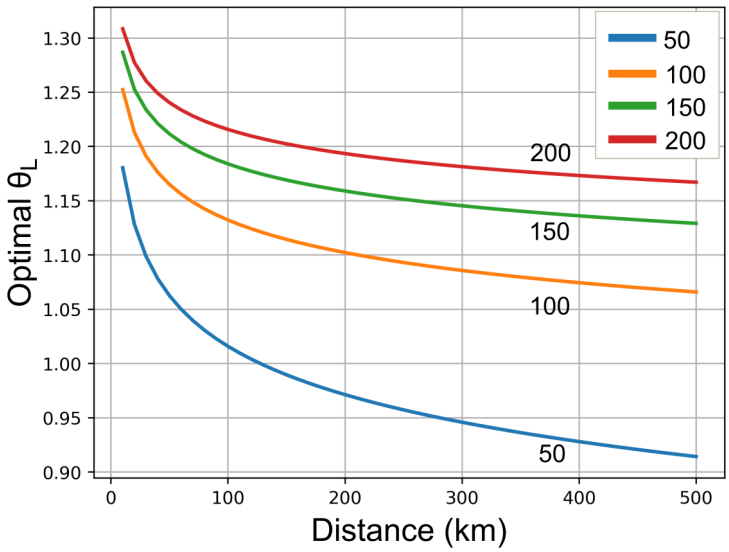

Figure 5.15: *The optimal value of θ_L for different number of allowed attempts A (legend and plot label) against the distance between the end points of the repeater. The length of a repeater segment is set at 10 km.*

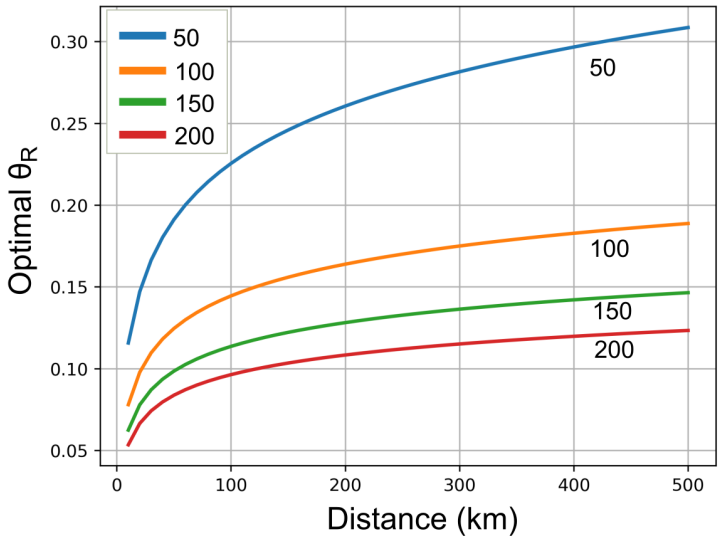

Figure 5.16: *The optimal value of θ_R for different number of allowed attempts A (legend and plot label) against the distance between the end points of the repeater. The length of a repeater segment is set at 10 km.*

registers from Eq. 5.62,

$$\rho = \frac{1}{2}\begin{pmatrix} 1 & 0 & 0 & -e^{i(\phi+\gamma)} \\ 0 & 0 & 0 & 0 \\ 0 & 0 & 0 & 0 \\ -e^{-i(\phi+\gamma)} & 0 & 0 & 1 \end{pmatrix} = |\gamma\rangle\langle\gamma|\,, \tag{5.85}$$

we have assumed no loss ($\eta = 1$) and,

$$|\gamma\rangle = \frac{1}{\sqrt{2}}(|00\rangle - e^{-i(\phi+\gamma)}|11\rangle). \tag{5.86}$$

Assuming that the phase error γ is normally distributed with variance δ^2, then the ensemble arising from this stochastic phase error is described by the density matrix,

$$\rho_\delta = \frac{1}{\sqrt{2\pi}\delta}\int_{-\infty}^{\infty} d\gamma e^{-\frac{\gamma^2}{2\delta^2}} |\gamma\rangle\langle\gamma| \tag{5.87}$$

Picking $\phi = \pi$, we compute the quantum bit error rate as,

$$\begin{aligned} Q &= \langle+|\langle-|\rho_\delta|+\rangle|-\rangle + \langle-|\langle+|\rho_\delta|-\rangle|+\rangle \\ &= \frac{1-e^{-\delta^2/2}}{2} \end{aligned} \tag{5.88}$$

For $Q = 0.01$ we find $\delta = 200$ mrad.
Given two copies of $|\gamma\rangle$ with different stochastic phase shifts γ_1 and γ_2,

$$\begin{aligned} |\gamma_1\rangle &= \frac{1}{\sqrt{2}}(|0\rangle_{11}|0\rangle_{12} - e^{-i(\phi+\gamma_1)}|1\rangle_{11}|1\rangle_{12}) \\ |\gamma_2\rangle &= \frac{1}{\sqrt{2}}(|0\rangle_{21}|0\rangle_{22} - e^{-i(\phi+\gamma_2)}|1\rangle_{21}|1\rangle_{22}) \end{aligned} \tag{5.89}$$

We perform a Bell measurement on qubits 12 and 21 to enact an entanglement swap,

$$\begin{aligned} &\frac{1}{\sqrt{2}}(\langle 0|_{12}\langle 0|_{21} + \langle 1|_{12}\langle 1|_{21})|\gamma_1\rangle|\gamma_2\rangle \\ &\propto |0\rangle_{11}|0\rangle_{22} + e^{-i(2\phi+\gamma_1+\gamma_2)}|1\rangle_{11}|1\rangle_{22}\,, \end{aligned} \tag{5.90}$$

where we assumed a particular Bell measurement outcome. However, independently of what Bell measurement outcome occurred, we find that the stochastic phase angle is a sum or difference of γ_1 and γ_2. We may then deduce that after s swaps, the accumulated phase error will be a sum of $s+1$ independent random phases. If each independent random phase γ_k is normally distributed with variance δ^2, then the accumulated random phase obtained from a repeater with M segments will be normally distributed with variance $M\delta^2$.

Allowing for the possibility of thermal noise in the repeater, we consider the presence of thermal photons in the generated TMSV states. The thermal TMSV states are obtained by two-mode squeezing two thermal states, each with average photon-number n_T. In Fig. 5.17 we show how the secret key rate changes as we vary the expected number of thermal photons n_T.

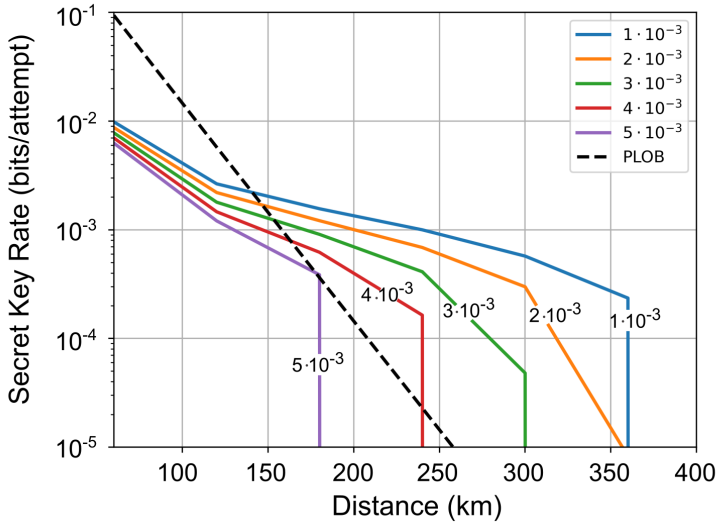

Figure 5.17: *We vary the expected number of thermal photons n_T in both arms of the TMSV state. The value of n_T is annotated to each curve. A is close to 500 for all plots. The length of a repeater segment is 60 km. We observe that at $n_T = 5 \cdot 10^{-3}$, the repeater can no longer beat the PLOB bound.*

Chapter 6

Modular interactions and Gottesman-Kitaev-Preskill states

In this section we present three protocols for realizing an interaction between an oscillator and a set of qubits, with the interaction being modular, or periodic, in the q and p quadratures of the oscillator. This interaction is then used to generate approximate Gottesman-Kitaev-Preskill (GKP) states [98], both with and without utilizing a projective measurement. The proposed modular interaction can also be used for error-correcting the GKP states through a modular measurement. The structure of the section is as follows, we begin by introducing the modular observables and the GKP states. We then present a simple modular interaction between a qubit and an oscillator, already employed in experiments, and show how repeated application of the interaction can be used to probabilistically generate a GKP state of the oscillator [99]. Subsequently we describe how a collection of qubits can realize a modular interaction with an oscillator, effectively by encoding quadratures into the joint qubit state. This interaction is then used for deterministically preparing a GKP state after a single interaction between the qubits and oscillator.

The non-commutativity between the q and p quadrature operators, assumed by the canonical commutation relation of quantum optics $[q, p] = 2i$, is a central aspect of quantum optics and enforces that the spread in q and p associated with a quantum state, must always satisfy $\Delta q \Delta p \geq 1$. However, it has been noted that the corresponding modular observables $q_m = q \pmod{L}$ and $p_m = p \pmod{2\pi/L'}$ obey the relation,

$$\mathrm{e}^{imp_m L'} \mathrm{e}^{in2\pi q_m/L} = \mathrm{e}^{in2\pi q_m/L} \mathrm{e}^{imp_m L'} \tag{6.1}$$

for L and L' satisfying $L'/L = k/2$ where k is an integer. We follow the proof given in [30]. We consider the exponentiated operators and note the relations,

$$\begin{aligned} \mathrm{e}^{in2\pi q_m/L} f &= \mathrm{e}^{in2\pi q/L} f \\ \mathrm{e}^{imp_m L'} f &= \mathrm{e}^{impL'} f, \end{aligned} \tag{6.2}$$

for an arbitrary test function f and for whole numbers $n, m \in \mathcal{Z}$. Then it follows,

$$\begin{aligned} \mathrm{e}^{imp_m L'} \mathrm{e}^{in2\pi q_m/L} f &= \mathrm{e}^{imp_m L'} \mathrm{e}^{in2\pi q_m/L} e^{-imp_m L'} \mathrm{e}^{imp_m L'} f \\ &= \mathrm{e}^{impL'} e^{in2\pi q/L} \mathrm{e}^{-impL'} \mathrm{e}^{impL'} f = \mathrm{e}^{in2\pi(q+2mL')/L} \mathrm{e}^{impL'} f \\ &= \mathrm{e}^{inm4\pi L'/L} e^{in2\pi q/L} \mathrm{e}^{impL'} f = \mathrm{e}^{in2\pi q_m/L} \mathrm{e}^{imp_m L'} f, \end{aligned} \tag{6.3}$$

and we arrive at the sought result. Looking for a common eigenstate of q_m and p_m one finds the family of unnormalizable eigenstates,

$$|L\rangle = \sum_{s=-\infty}^{\infty} e^{i\frac{1}{2}k(x-sL)} |x - sL\rangle, \tag{6.4}$$

for arbitrary x and k, and where $|x - sL\rangle$ is a q-quadrature eigenstate centred on $x - sL$. These states have eigenvalues $x \pmod L$ for $q_m = q \pmod L$ and eigenvalues $k \pmod{\frac{4\pi}{L}}$ for $p_m = p \pmod{4\pi/L}$. We note that $|L\rangle$ is not normalizable, and does not constitute a proper quantum state. However, the state can be approximated, and its approximation has been utilized in the construction of bosonic codes, namely GKP codes for encoding an error-correctable qubit in an oscillator. We may generalize $|L\rangle$, defining a periodic state as one which can be written,

$$|L\rangle = \mathcal{N} \sum_{s=-T}^{T} \lambda_s D_q(sL) |\psi\rangle, \tag{6.5}$$

where $D_q(d) = e^{-i\frac{d}{2}p}$ is the displacement operator in q and $|\psi\rangle$ is an arbitrary state. λ_s are weights and $\mathcal{N}$ is the normalization. If $|\psi\rangle$ is localized in the q quadrature, then we will refer to $|L\rangle$ as a peaked periodic state.
The approximate GKP states are an instance of a periodic peaked state and can be written as,

$$|G(\phi)\rangle = \mathcal{N}_0 \sum_{s=-\infty}^{\infty} e^{-(\kappa(2s+\phi)\sqrt{\pi})^2/2} \int_{-\infty}^{\infty} dq \pi^{-1/4} \Delta^{-1/2} e^{-q^2/(2\Delta^2)} |q + (2s+\phi)\sqrt{\pi}\rangle, \tag{6.6}$$

where $\mathcal{N}_0$ is the normalization. ϕ shifts the GKP state and $\phi = 0$ corresponds to logical 0 and $\phi = 1$ corresponds to logical 1. We will be considering states for which $\phi \in]0, 1[$ as shifted GKP states.

6.1 Peaked periodic states as fixed points

In this section we relate the approximate GKP states to the fixed points of a sequence of projective measurements. We show how repeatedly interacting a qubit and

an oscillator and measuring the qubit, quite generally produces localized periodic states. This section serves as an introduction to the idea of modular measurements, and protocols similar to the one described in this section have already been realized experimentally [99]. The main protocol, which can perform a modular measurement of an oscillator via a single interaction with the oscillator, will be given in the next section.

We initialize an oscillator ω in a state $|\psi_0\rangle_\omega$ and a qubit in a state in the yz-plane having the angle v_0 with the z-axis. We label this state as $|v_0\rangle_q$, given by

$$|v_0\rangle_q = \cos(v_0/2)\,|0\rangle_q + i\sin(v_0/2)\,|1\rangle_q\,. \tag{6.7}$$

We then interact the qubit and oscillator using the unitary $U = e^{itgq\sigma_x}$ where q is a quadrature operator of the oscillator, σ_x is the Pauli x operator for the qubit, g is the interaction frequency and t is the interaction time. Expanding $|\psi_0\rangle_\omega$ in the q eigenstates $|x\rangle_\omega$ we obtain,

$$\begin{aligned}|\Psi\rangle &= e^{itgq\sigma_x}\,|\psi_0\rangle_\omega\,|v_0\rangle_q \\ &= \int_{-\infty}^{\infty} dx\psi_0(x)\,|x\rangle_\omega\left(\cos(gtx+v_0/2)\,|0\rangle_q + i\sin(gtx+v_0/2)\,|1\rangle_q\right)\end{aligned} \tag{6.8}$$

where $|0\rangle_q$ and $|1\rangle_q$ are spin up and down along the z axis. We introduce the rescaled quadrature coordinate $\theta = 2gtx$ and obtain,

$$\begin{aligned}|\Psi\rangle &= \int_{-\infty}^{\infty}\frac{d\theta}{2gt}\psi_0\left(\theta\right)|\theta\rangle_\omega\left(\cos\left(\frac{\theta+v_0}{2}\right)|0\rangle_q + i\sin\left(\frac{\theta+v_0}{2}\right)|1\rangle_q\right) \\ &= \int_{-\infty}^{\infty}\frac{d\theta}{2gt}\psi_0\left(\theta\right)|\theta\rangle_\omega\,|v_0+\theta\rangle_q\end{aligned} \tag{6.9}$$

where $\psi_0\left(\theta\right)$ and $|\theta\rangle_\omega$ are shorthand for $\psi_0\left(\frac{\theta}{2gt}\right)$ and $|\frac{\theta}{2gt}\rangle_\omega$ respectively. We notice that if the wavefunction $\psi_0(\theta)$ matches a peaked periodic state of period 2π in θ, then there is no entanglement between the qubit and oscillator. I.e. tracing out the oscillator we find the state of the qubit,

$$\begin{aligned}\rho_q = \int_{-\infty}^{\infty}\frac{d\theta}{2gt}|\psi_0(\theta)|^2&\left(\cos\left(\frac{\theta+v_0}{2}\right)|0\rangle_q + i\sin\left(\frac{\theta+v_0}{2}\right)|1\rangle_q\right) \\ &\otimes\left(\cos\left(\frac{\theta+v_0}{2}\right)\langle 0|_q - i\sin\left(\frac{\theta+v_0}{2}\right)\langle 1|_q\right)\end{aligned} \tag{6.10}$$

if $|\psi_0(\theta)|^2 = \sum_{s=-\infty}^{\infty}|\lambda_s|^2\delta\left(\theta-\theta_0+s2\pi\right)$ then,

$$\begin{aligned}\rho_q = &\left(\cos\left(\frac{\theta_0+v_0}{2}\right)|0\rangle_q + i\sin\left(\frac{\theta_0+v_0}{2}\right)|1\rangle_q\right) \\ &\otimes\left(\cos\left(\frac{\theta_0+v_0}{2}\right)\langle 0|_q - i\sin\left(\frac{\theta_0+v_0}{2}\right)\langle 1|_q\right).\end{aligned} \tag{6.11}$$

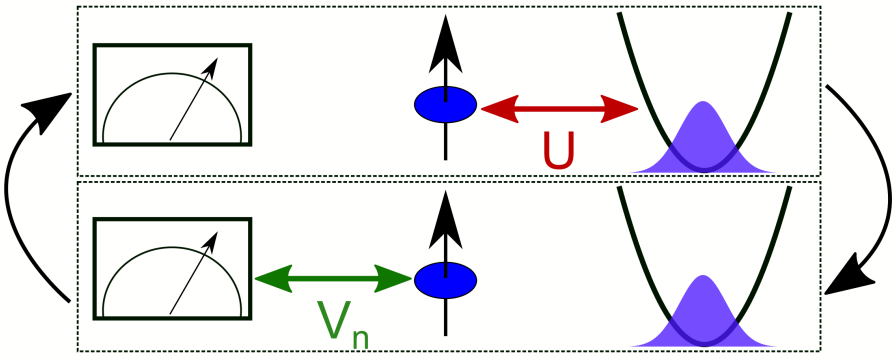

Figure 6.1: *An oscillator (right) interacts with a qubit (middle) via the unitary U (see text). The qubit is then measured along the direction making the angle V_n with the z-axis in the yz-plane (left). Then the qubit again interacts with the oscillator via U, and again we measure the qubit. The sequence is repeated N times in total.*

The qubit is observed to be in a pure state and there is no entanglement between the oscillator and qubit. One might then suspect, that repeatedly interacting an oscillator with a qubit via U, followed by a projective measurement of the qubit, might evolve the oscillator until it eventually reaches a peaked periodic state, at which point a measurement of the qubit wont affect the oscillator state. The question is then what sequences of projective measurements will lead the oscillator toward such a fixed point. To answer this question, we determine the state resulting from repeatedly interacting the oscillator and the qubit via U and measuring the qubit state. The projective measurement in round n is assumed to occur along the direction making the angle V_n with the z-axis in the yz-plane, and the result of the measurement is to project the qubit into a state $|v_n\rangle_q$, with v_n being either V_n or $V_n + \pi$. See Fig. 6.1 for a sketch of the interaction. The joint state of the qubit and oscillator evolves as,

$$\begin{aligned} |v_0\rangle_q |\psi_0\rangle_\omega &\xrightarrow{U} \int_{-\infty}^{\infty} \frac{d\theta}{2gt} \psi_0(\theta) |\theta\rangle_\omega |v_0 + \theta\rangle_q \\ &\xrightarrow{M_1} \int_{-\infty}^{\infty} \frac{d\theta}{2gt} \psi_0(\theta) |\theta\rangle_\omega |v_1\rangle \langle v_1|v_0 + \theta\rangle \end{aligned} \tag{6.12}$$

where M_1 implies that we perform measurement 1, projecting onto $\langle v_1|$. Continuing,

$$\begin{aligned} &\xrightarrow{U} \int_{-\infty}^{\infty} \frac{d\theta}{2gt} \psi_0(\theta) |\theta\rangle_\omega |v_1 + \theta\rangle_q \langle v_1|v_0 + \theta\rangle \\ \xrightarrow{M_2} &\int_{-\infty}^{\infty} \frac{d\theta}{2gt} \psi_0(\theta) |\theta\rangle_\omega |v_2\rangle_q \langle v_2|v_1 + \theta\rangle \langle v_1|v_0 + \theta\rangle \end{aligned} \tag{6.13}$$

and so forth. The oscillator state resulting from N rounds of this sequence is then,

$$\begin{aligned}|\psi\rangle &= \int_{-\infty}^{\infty} \frac{d\theta}{2gt}\psi_0(\theta)\,|\theta\rangle_\omega \prod_{n=1}^{N} \langle v_n|v_{n-1}+\theta\rangle_q \\ &= \int_{-\infty}^{\infty} \frac{d\theta}{2gt}\psi_0(\theta)\,|\theta\rangle_\omega \prod_{n=1}^{N} \langle v_n - v_{n-1}|\theta\rangle_q \end{aligned} \tag{6.14}$$

We rearrange the expression, pulling the projections out front,

$$|\psi\rangle = \bigotimes_{n=1}^{N} \langle v_n - v_{n-1}|_n \int_{-\infty}^{\infty} \frac{d\theta}{2gt}\psi_0(\theta)\,|\theta\rangle_\omega \bigotimes_{n=1}^{N} |\theta\rangle_n \tag{6.15}$$

We notice that the integrand is an entangled superposition of a particular quadrature and N qubits (labelled as n) occupying the same position θ on the Bloch's sphere, located in the yz-plane. Of course there is only a single qubit being cycled, but we can describe the scheme as an oscillator interacting with N qubits. We define the qubit states,

$$\begin{aligned}|\alpha\rangle &= \bigotimes_{n=1}^{N} |v_n - v_{n-1}\rangle_n \\ |\beta(\theta)\rangle &= \bigotimes_{n=1}^{N} |\theta\rangle_n \,. \end{aligned} \tag{6.16}$$

We note that $\langle\alpha|\beta(\theta)\rangle$ is periodic in θ since $|\beta(\theta+2\pi)\rangle = (-1)^N\,|\beta(\theta)\rangle$. Note that the state $|\theta\rangle_n$ is given in Eq. 6.7 by the replacement $v_0 \to \theta$.
We find that $\langle\beta(\theta')|\beta(\theta)\rangle = \cos\left(\frac{\theta'-\theta}{2}\right)^N$ is peaked around $\theta'-\theta = 0 \pmod{2\pi}$, with the width of the peaks in θ decreasing for larger N. We Taylor expand to second order around $d\theta = \theta' - \theta = 0$, obtaining,

$$\langle\beta(\theta+d\theta)|\beta(\theta)\rangle \approx \left(1 - \frac{1}{2}(d\theta/2)^2\right)^N \approx (e^{-d\theta^2/8})^N = e^{-\frac{1}{2}\frac{d\theta^2}{4/N}}. \tag{6.17}$$

So in the limit of large N the peaks will be gaussians of width $2/\sqrt{N}$. Hence states $|\beta(\theta)\rangle$ differing by $d\theta > 2/\sqrt{N}$ will be approximately orthogonal and can be distinguished by a single measurement of the N qubits. Such a measurement will in turn determine $\theta \pmod{2\pi}$ to within an accuracy of $2/\sqrt{N}$. Since we have $\theta = 2gtx$ we have performed a modular measurement of the q-quadrature of the oscillator. Such a measurement will indeed projectively prepare a peaked periodic state, as indicated in Fig. 6.2 a.

Distinguishing the states $|\beta(\theta)\rangle$ corresponds to determining the direction of the combined spin of the N qubits. In round n we project onto the state $|v_n - v_{n-1}\rangle$

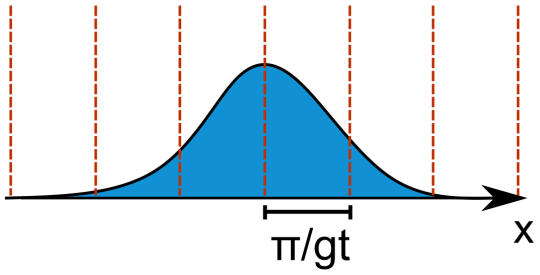

Figure 6.2: *Determining* $\theta \pmod{2\pi}$ *projects an oscillator state into a peaked periodic state of period* π/gt *in the* x *quadrature, with the envelope over the peaks being determined by the initial oscillator state. The initial oscillator state is the blue gaussian and the projection is the red dashed lines.*

which is either $|V_n - V_{n-1}\rangle$ or $|V_n - V_{n-1} + \pi\rangle$ corresponding to the two eigenstates of the spin operator $\sigma^{(n)} = \cos(V_n - V_{n-1})\sigma_z^{(n)} + \sin(V_n - V_{n-1})\sigma_y^{(n)}$. For brevity, we will denote $\Delta_n = V_n - V_{n-1}$. Hence the probability $|\langle\alpha|\beta(\theta)\rangle|^2$ corresponds to a particular sequence of outcomes $|\alpha\rangle$, obtained by measuring the N observables $\sigma^{(n)}$ of the state $|\beta(\theta)\rangle$. We will now show that a measurement of the N observables $\sigma^{(n)}$ resolves θ to within an error scaling as $1/\sqrt{N}$. It therefore follows that a particular outcome $|\alpha\rangle$ can typically only be consistent with a range of θ dropping as $1/\sqrt{N}$. Hence the amplitudes $\langle\alpha|\beta(\theta)\rangle$ must typically be localized in θ to within an uncertainty scaling as $1/\sqrt{N}$.

The average spin direction of the N qubits in the yz-plane is given by the operator,

$$\bar{\sigma} = \frac{1}{N}\sum_{n=1}^{N} \sigma^{(n)} \begin{pmatrix} \cos(\Delta_n) \\ \sin(\Delta_n) \end{pmatrix}, \tag{6.18}$$

where the first element is the z component, and the second is the y component. If we assume that the angles Δ_n cover the circle uniformly then we obtain the following expectation value,

$$\begin{aligned} \mathrm{E}[\bar{\sigma}] = \langle\beta(\theta)|\bar{\sigma}|\beta(\theta)\rangle &= \frac{1}{N}\sum_{n=1}^{N} \langle\theta|\sigma^{(n)}|\theta\rangle_n \begin{pmatrix} \cos(\Delta_n) \\ \sin(\Delta_n) \end{pmatrix} \approx \frac{1}{2}\begin{pmatrix} \langle\theta|\sigma_z|\theta\rangle_q \\ \langle\theta|\sigma_y|\theta\rangle_q \end{pmatrix} \\ &= \frac{1}{2}\begin{pmatrix} \cos(\theta/2)^2 - \sin(\theta/2)^2 \\ 2\cos(\theta/2)\sin(\theta/2) \end{pmatrix} = \frac{1}{2}\begin{pmatrix} \cos(\theta) \\ \sin(\theta) \end{pmatrix}, \end{aligned} \tag{6.19}$$

with the approximations being valid for large N. This expectation value, valid for

large N, is seen to be independent of N. We also obtain the variance,

$$\begin{aligned}\mathrm{Var}[\bar{\sigma}] &= \frac{1}{N^2}\sum_{n=1}^{N}\mathrm{Var}\left[\sigma^{(n)}\right]\begin{pmatrix}\cos(\Delta_n)^2\\ \sin(\Delta_n)^2\end{pmatrix}\\ &= \frac{1}{N^2}\sum_{n=1}^{N}\left(\langle\theta|\left(\sigma^{(n)}\right)^2|\theta\rangle_n - \langle\theta|\sigma^{(n)}|\theta\rangle_n^2\right)\begin{pmatrix}\cos(\Delta_n)^2\\ \sin(\Delta_n)^2\end{pmatrix}\\ &\approx \frac{1}{N}\begin{pmatrix}\frac{1}{2}-\frac{3}{8}\langle\theta|\sigma_z|\theta\rangle_q^2-\frac{1}{8}\langle\theta|\sigma_y|\theta\rangle_q^2\\ \frac{1}{2}-\frac{1}{8}\langle\theta|\sigma_z|\theta\rangle_q^2-\frac{3}{8}\langle\theta|\sigma_y|\theta\rangle_q^2\end{pmatrix},\end{aligned} \tag{6.20}$$

with the approximations being increasingly valid for larger N. So as we increase N the expectation value of $\bar{\sigma}$ converges to a θ dependent vector, whereas the variance converges to zero. From $\mathrm{E}[\bar{\sigma}]$ we may determine θ as $\theta = \arcsin(2\mathrm{E}[\bar{\sigma}_y])$ and by linear error propagation we have that the uncertainty in θ scales as,

$$\Delta\theta \sim \frac{1}{\sqrt{N}}. \tag{6.21}$$

So for large N a measurement of the N qubits will resolve θ to within an accuracy that scales as $1/\sqrt{N}$. It follows that the range of θ consistent with an outcome $|\alpha\rangle$ will typically scale as $1/\sqrt{N}$. This implies that the amplitude of the oscillator $\psi(\theta) = \psi_0(\theta)\langle\alpha|\beta(\theta)\rangle$ will be increasingly localized around a particular value of θ (mod 2π) as we increase N. It follows that a large class of measurement sequences, characterized by the angles V_n, will lead the system into a peaked periodic state. We now determine numerically the fidelity between such peaked periodic states and GKP states for a particular protocol.

We initialize the oscillator in an anti-squeezed state of standard deviation B,

$$|\psi\rangle = \frac{1}{\sqrt{\pi^{1/2}B}}\int_{-\infty}^{\infty}dx\exp\left(-\frac{q^2}{2B^2}\right)|x\rangle \tag{6.22}$$

We will be using $B = 6$. We interact the oscillator with a qubit using the unitary U. We measure qubit n along the angle $V_n = \frac{2\pi}{N}\sum_{k=0}^{n-1}k$ with the z-axis in zy-plane. We sample measurement outcomes according to their probability and find that typical states generated by the measurement sequence are periodic superpositions of gaussian peaks with period π/gt in the q quadrature. Picking $gt = \sqrt{\pi}/2$ we obtain GKP states. Two example states are shown in Fig. 6.3. In Fig. 6.4 a we show how the standard deviation of the peaks scale in N for even N, we find that they follow a $1/\sqrt{N}$ law as expected. In Fig. 6.4 b we show how the value of (even) N affects the average fidelity of the resulting state and the most similar approximate GKP state, i.e. we optimize over Δ, κ, and ϕ in Eq. 6.6. Note that for odd N the states prepared by the protocol closely resembles GKP states shifted by $\frac{\sqrt{\pi}}{2}$ in the

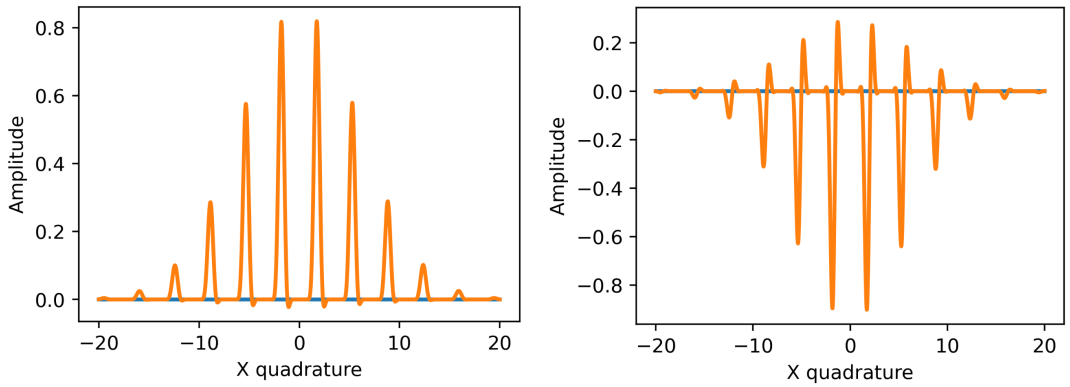

Figure 6.3: *Examples of two states produced by the probabilistic protocol with 12 interactions ($N = 12$). The leftmost state closely resembles a GKP state, and these tend to be the most common result.*

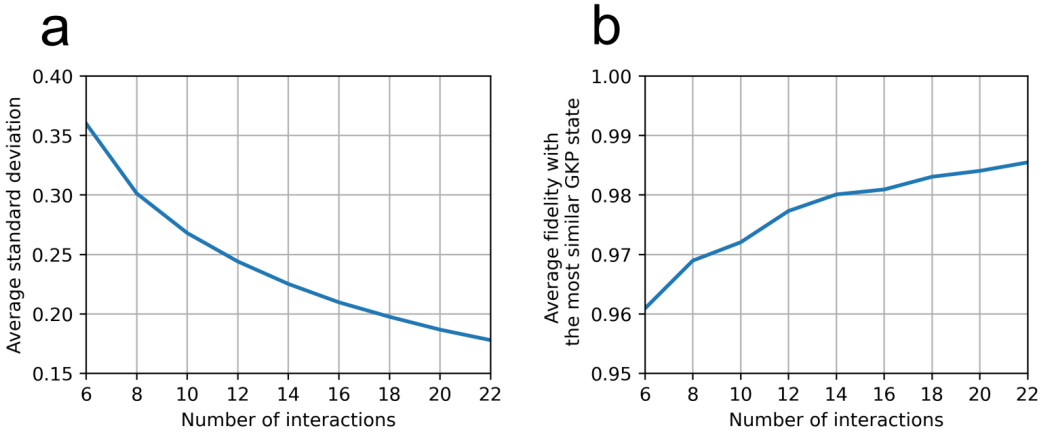

Figure 6.4: *We sample $4 \cdot 10^4$ trajectories corresponding to different measurement outcomes.* ***a.*** *We show the average of the squeezing parameter Δ of the most similar GKP state.* ***b.*** *We show the average fidelity between a state generated by the protocol and the closest GKP state.*

p-quadrature. We see that the protocol prepares approximate GKP states, with the average fidelity and squeezing increasing as N is increased.
Note that the average fidelity is reduced by instances where the generated state is not a periodic superposition of gaussians, but rather a periodic superposition of some other localized state, as shown in Fig. 6.3 to the right. We label such states as outliers when the fidelity with the closest GKP state is less than 0.9. We find that the probability of obtaining an outlier is around 4-5% for reasonable values of N, but with a tendency to drop for larger N, with the probability being 1-2% for $N = 100$.

6.2 Encoding quadratures into qubits

We now present two protocols for preparing GKP states, based on certain discrete quadrature operators we can define for a set of qubits. These simulated quadratures differs from continuous variable quadratures by the fact that they are modular, i.e. the associated displacement operators have periodic boundary conditions, and displacing the qubits far enough through the eigenstates of the quadratures will bring the qubits back to the initial state. We will start by introducing some basic notions of discrete quantum mechanics [5], [100].
Given a collection of d_Q qubits we form a qudit of dimension $N = 2^{d_Q}$. We denote the associated logical basis states as $|x_k\rangle$ for $k \in \{-N/2, -N/2-1\}$. Given the binary state $|x_k\rangle = |j_{d_Q}, j_{d_Q-1}, \ldots, j_2, j_1\rangle$ we will associate the value of k,

$$k = \sum_{k=1}^{d_Q} j_k 2^{k-1} - N/2 \tag{6.23}$$

E.g. with 3 qubits we have the equalities,

$$\begin{aligned} |x_{-4}\rangle &= |000\rangle \ , \ |x_{-3}\rangle = |001\rangle \\ |x_{-2}\rangle &= |010\rangle \ , \ |x_{-1}\rangle = |011\rangle \\ |x_0\rangle \ &= |100\rangle \ , \ |x_1\rangle \ = |101\rangle \\ |x_2\rangle \ &= |110\rangle \ , \ |x_3\rangle \ = |111\rangle \end{aligned} \tag{6.24}$$

We introduce a discrete x-quadrature operator,

$$X_N = \sum_{k=-N/2}^{N/2-1} k \, |x_k\rangle \langle x_k| \, . \tag{6.25}$$

We label it as a quadrature operator by the fact that it has a linear spectrum with both positive and negative values. Applying the discrete Fourier transform, i.e. the

quantum Fourier transform F_N (QFT), we may transform the x-quadrature into a conjugate discrete y-quadrature operator,

$$Y_N = F_N X_N F_N^\dagger \tag{6.26}$$

where

$$F_N = \frac{1}{\sqrt{N}} \sum_{n,m=-N/2}^{N/2-1} e^{i2\pi nm/N} \left|x_m\right\rangle \left\langle x_n\right|, \tag{6.27}$$

and the circuit generating F_N is sketched in Fig. 6.5 a [5], where we use the gate R_k which can be written in the σ_z-basis as,

$$R_k = \begin{pmatrix} 1 & 0 \\ 0 & \mathrm{e}^{2\pi i/2^k} \end{pmatrix}, \tag{6.28}$$

i.e. $|0\rangle = \begin{pmatrix} 1 & 0 \end{pmatrix}^T$ is left unchanged by R_k. Y_N has eigenvectors,

$$\left|y_n\right\rangle = \frac{1}{\sqrt{N}} \sum_{k=-N/2}^{N/2-1} e^{i2\pi nk/N} \left|x_k\right\rangle, \tag{6.29}$$

with eigenvalues $y_n = n \in [-N/2; N/2-1]$. Y_N is the generator of discrete translations in the logical basis, i.e. the operator, $D_x(d) = e^{-i\frac{2\pi}{N} Y_N d}$, shifts a logical state by $d \in \mathbb{Z}$ positions in a modular fashion. This property can be understood by examining the overlap $\left\langle x_l\right| D_x(d) \left|x_k\right\rangle$. Expanding Y_N into eigenvectors $\left|y_n\right\rangle$ we obtain,

$$\begin{aligned} \left\langle x_l\right| D_x(d) \left|x_k\right\rangle &= \sum_{n=-N/2}^{N/2-1} e^{-i\frac{2\pi}{N} y_n d} \left\langle x_l|y_n\right\rangle \left\langle y_n|x_k\right\rangle = \frac{1}{N} \sum_{n=-N/2}^{N/2-1} e^{i2\pi n(l-k-d)/N} \\ &= \begin{cases} e^{-i\pi sN} & \text{if } l-k-d = sN \text{ for } s \in \mathbb{Z} \\ 0 & \text{otherwise} \end{cases} \end{aligned} \tag{6.30}$$

since $\left\langle y_n|x_k\right\rangle = \left\langle x_n|F_N^\dagger|x_k\right\rangle = e^{-i2\pi nk/N}/\sqrt{N}$ and $y_n = n$. The above sum is related to the Dirichlet kernel, and for integral values of l, k, d we find that $\left\langle x_l\right| D_x(d) \left|x_k\right\rangle$ is only non-zero for $l-k-d = sN$ where s is an arbitrary integer. By assumption l is restricted to the interval $[-N/2, N/2-1]$, so we should pick s such that $l = sN+k+d$ lies in this interval. Hence we have shifted the logical state by d positions in a modular fashion. E.g. if $N = 8$, $k = -1$ and $d = 6$, then we find $l = -3$, and we see that we have shifted the logical basis state by 6 positions. Furthermore, since N is even by construction, we can set the phase factor $e^{-i\pi sN}$ to 1.
We note that under certain circumstances $D_x(d)$ can also perform non-integral shifts

via interpolation, this property will turn out to be important for our protocol. To flesh out this property, we define the continuous function $v(y)$ with period N, which is well described by frequencies smaller than $1/2$, such that v has the Fourier series,

$$v(y) = \sum_{n=-N/2}^{N/2-1} \frac{1}{\sqrt{N}} e^{i2\pi ny/N} v_n \tag{6.31}$$

where v_n is the Fourier coefficients, and we cut the sum under the assumption that v_n vanishes for $|n| \geq N/2$, enforcing that $v(y)$ is described by frequencies smaller than $1/2$. We introduce the vector $|v\rangle$ with amplitudes,

$$\langle x_k|v\rangle = \sum_{n=-N/2}^{N/2-1} \langle x_k|y_n\rangle \langle y_n|v\rangle = \sum_{n=-N/2}^{N/2-1} \frac{1}{\sqrt{N}} e^{i2\pi nk/N} \langle y_n|v\rangle . \tag{6.32}$$

Comparing Eq. 6.31 and 6.32 we see that if we pick $v_n = \langle y_n|v\rangle$, then we have the relation,

$$|v\rangle = \sum_{k=-N/2}^{N/2-1} \langle x_k|v\rangle |x_k\rangle = \sum_{k=-N/2}^{N/2-1} v(k) |x_k\rangle \tag{6.33}$$

We then apply the displacement operator to $|v\rangle$,

$$\langle x_l| D_x(d) |v\rangle = \frac{1}{\sqrt{N}} \sum_{n=-N/2}^{N/2-1} e^{i2\pi n(l-d)/N} \langle y_n|v\rangle = v(l-d) . \tag{6.34}$$

We observe that the effect of the displacement operator is to transform the amplitudes $v(l)$ into $v(l-d)$. Since $v(y)$ is a continuous function, the translation will be meaningful for continuous values of d, and the displaced amplitudes $\langle x_l| D_x(d) |v\rangle$ are obtained by sampling from a translation of $v(y)$.

Since the discrete system under study is built from qubits, we can construct X_N using the Hamiltonian,

$$X_N = -\sum_{n=1}^{d_Q} 2^{n-2} \sigma_z^{(n)} - 1/2 \tag{6.35}$$

where $\sigma_z^{(n)}$ is the Pauli Z operator for the n'th qubit (with the first qubit being rightmost when we write up the ket), i.e. we have, $\sigma_z^{(n)} |0\rangle_n = |0\rangle_n$ and $\sigma_z^{(n)} |1\rangle_n = -|1\rangle_n$. We assume that we have access to Rabi interactions between each of the qubits and an oscillator, i.e. we will assume we have access to the interaction Hamiltonian,

$$H_I = qX_N = -\sum_{n=1}^{d_Q} 2^{n-2} q \sigma_z^{(n)} - (1/2)q, \tag{6.36}$$

where q is the q quadrature of the oscillator. A similar interaction with a single qubit was used in [101]. The last term in H_I then amounts to a p displacement of the oscillator. Then we observe the following result,

$$F_N e^{-i\tau_I H_I/2} F_N^\dagger = e^{-i\tau_I q Y_N/2} = D_x\left(\frac{N\tau_I q}{4\pi}\right), \tag{6.37}$$

hence we can displace the qudit through the logical basis states, conditioned on the quadrature of the oscillator q. Since q has a continuous spectrum, it is advantageous to study qudit states for which the x-quadrature distribution is well interpolated by a low frequency function $v(y)$, as described above. We choose the qudit state $|v\rangle$ prepared by the circuit shown in Fig 6.5 b acting on the input state $|0,0,\ldots,0\rangle$. We denote the circuit shown in Fig. 6.5 b by the unitary U_v. The angles θ_k listed in the circuit in Fig. 6.5 b, are chosen to generate an exponential decay across the logical basis, with $\mathrm{RY}(\theta_k) = e^{-i(\theta_k/2)\sigma_y^{(k)}}$ and $\mathrm{RZ}(\omega_v) = e^{-i(\omega_v/2)\sigma_z}$. The application of the CNOT gates and the $\mathrm{RY}(\pi/2)$ gate mirror the amplitude distribution, thereby creating a symmetric double exponential. The angles ϕ_v and ω_v are used to create an arbitrary superposition of two central positions, as shown in Fig. 6.5 c, with ϕ_v controlling the relative amplitude and ω_v controlling the relative phase. We will set $\theta_k = \pi$ for $k > 1$, and tune θ_1 to mimic a narrow bell curve, we find that $\theta_1 = 2.6$ works well. A sketch of the resulting state with 4 qubits is shown in Fig. 6.5 c. In general we may generate a double exponential distribution by picking $\theta_k = 2\mathrm{acot}\left(e^{-2^{k-1}x}\right)$ for arbitrary x. The rationale for these angles come from considering the product,

$$\begin{aligned}&(c_1|0\rangle + |1\rangle)(c_2|0\rangle + |1\rangle)(c_3|0\rangle + |1\rangle)\\ &= c_1c_2c_3|000\rangle + c_2c_3|100\rangle + c_1c_3|010\rangle + c_3|110\rangle + c_1c_2|001\rangle\\ &\qquad + c_2|101\rangle + c_1|011\rangle + |111\rangle\end{aligned} \tag{6.38}$$

which is clearly an exponential decay over the logical basis if $c_k = e^{-2^{k-1}x}$. Comparing this with the action of the RY gate, $e^{-i(\theta_k/2)\sigma_y^{(k)}}|0\rangle = \cos(\theta_k/2)|0\rangle + \sin(\theta_k/2)|1\rangle = \sin(\theta_k/2)\left(\cot(\theta_k/2)|0\rangle + |1\rangle\right)$ we conclude $\cot(\theta_k/2) = e^{-2^{k-1}x}$.

6.2.1 Measurement-based protocol

We can now describe the measurement based protocol. The protocol is sketched in Fig. 6.6 a with $U_I = e^{-i\tau_I H_I/2}$. Briefly stated, the measurement based protocol proceeds as follows,

1. The qubit state is initialized using U_v
2. The inverse QFT is applied to the qubits

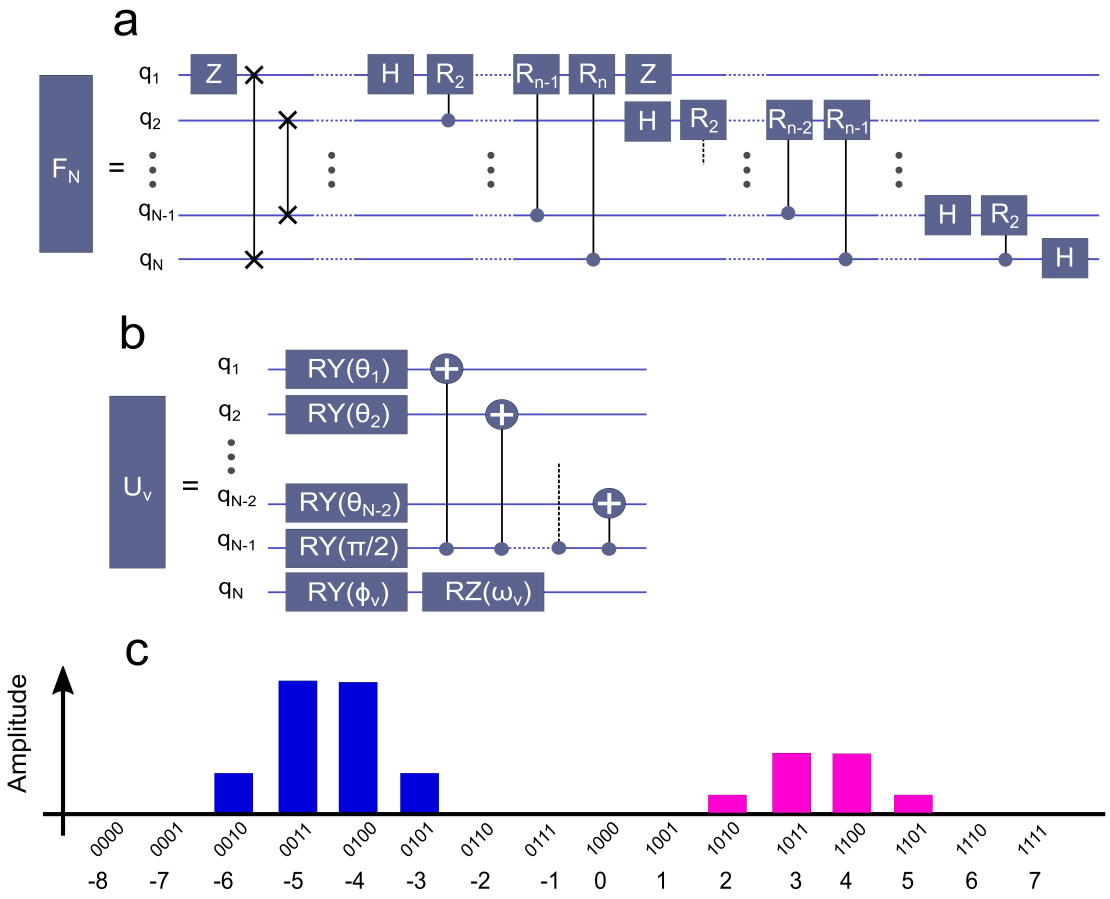

Figure 6.5: ***a*** *Quantum circuit for the version of the quantum Fourier transform used in this work.* ***b*** *Circuit for preparing the family of qubit states* $|v\rangle$*. The circuit corresponds to the unitary* U_v*. The controlled gates are controlled not gates. We pick* $\theta_k = \pi$ *for* $k > 1$*, and* θ_1 *is chosen so that the resulting state resembles a gaussian distribution, we find that* $\theta_1 = 2.6$ *works well. This distribution can be brought into an arbitrary superposition of two central positions by tuning the relative amplitude via* ϕ_v *and the relative phase via* ω_v*.* ***c*** *Sketch of a quantum state generated by the unitary* U_v *given in b, with 4 qubits initially in the state* $|0,0,0,0\rangle$*. On the x-axis we give the logical state of the qubits, and the associated eigenvalue of the* X_N *operator. The center of the left peak is* $k_0 = -4.5$*.*

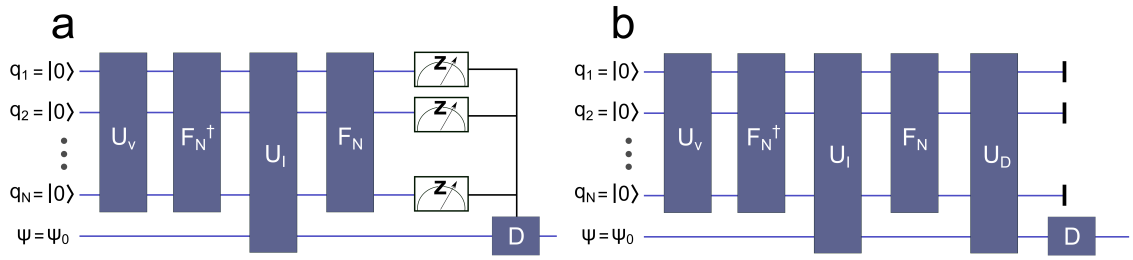

Figure 6.6: ***a*** *Measurement based protocol.* Ψ *represents the oscillator and* q_n *are qubits. A displacement (D) is applied based on the measurement outcomes in the Z basis.* ***b*** *Measurement-free protocol. A disentangling operation* U_D *is applied on the oscillator and qubits. The final displacement* D *is to correct for the fact that the qubit state (Fig. 6.5 c) is not centred on 0 in the* X_N *eigenvalues.*

3. The qubits interact with the oscillator through U_I
4. The QFT is applied to the qubits
5. A Pauli-Z measurement is applied to each of the qubits. Based on the measurement outcomes a displacement D is applied to the oscillator.

The final state of the oscillator is given by,

$$|\psi\rangle = D_q\left(-\frac{4\pi}{N\tau_I}(l-k_0)\right)\langle x_l|\, F_N U_I F_N^\dagger\, |v\rangle\, |\psi_0\rangle \tag{6.39}$$

where $D_q(d) = e^{-i\frac{d}{2}p}$ is a q displacement of the oscillator by d and $k_0 = -N/4 - 1/2$. $|\psi_0\rangle$ is the initial oscillator state and $|x_l\rangle$ is the logical state of the qubits corresponding to the measurement outcomes with eigenvalue l. We can understand the rationale behind the protocol by breaking $|v\rangle$ into two parts, corresponding to the two peaks in Fig. 6.5 c $|v\rangle = c_1\,|v_1\rangle + c_2\,|v_2\rangle$, with $|v_1\rangle$ being the left-most peak, given by the superposition,

$$|v_1\rangle = \sum_{k=-N/2}^{N/2-1} \langle x_k|v_1\rangle\, |x_k\rangle\,. \tag{6.40}$$

We introduce the continuous amplitude distribution $v_1(y)$, described by the Fourier series,

$$v_1(y) = \sum_{n=-N/2}^{N/2-1} \frac{1}{\sqrt{N}} e^{i2\pi ny/N}\, \langle y_n|v_1\rangle\,. \tag{6.41}$$

We will assume that the amplitudes $\langle x_k|v_1\rangle$ are approximately described by a gaussian of standard deviation B, i.e. $\langle x_k|v_1\rangle \approx \mathcal{N} e^{-(k-k_0)^2/2B^2}$, which we assume vanish

for $|k| \geq N/2$. Note that $k_0 = -N/4 - 1/2$ (see Fig. 6.5 c) and so this is true if $N/4 > B$. Then we can evaluate the Fourier coefficients,

$$\begin{aligned}\langle y_n|v_1\rangle &= \frac{1}{\sqrt{N}}\sum_{k=-N/2}^{N/2-1} e^{-i2\pi nk/N}\langle x_k|v_1\rangle \approx \mathcal{N}\frac{1}{\sqrt{N}}\sum_{k=-\infty}^{\infty} e^{-i2\pi nk/N}e^{-(k-k_0)^2/2B^2} \\ &= \mathcal{N}\sqrt{\frac{2\pi B^2}{N}}e^{-i2\pi nk_0/N}\sum_{s=-\infty}^{\infty} e^{-2\pi isk_0}e^{-\frac{1}{2}\left(\frac{s+n/N}{1/(2\pi B)}\right)^2}, \end{aligned} \tag{6.42}$$

where we used the Poisson sum formula. Since n/N is bounded by $\pm 1/2$ we can replace the sum by its argument evaluated in $s = 0$ provided $B > 1/\pi$,

$$\approx \mathcal{N}\sqrt{\frac{2\pi B^2}{N}}e^{-i2\pi nk_0/N}e^{-\frac{1}{2}\left(\frac{n/N}{1/(2\pi B)}\right)^2}, \tag{6.43}$$

Then we have,

$$v_1(y) \approx \sum_{n=-N/2}^{N/2-1}\frac{1}{\sqrt{N}}e^{i2\pi n(y-k_0)/N}\left[\mathcal{N}\sqrt{\frac{2\pi B^2}{N}}e^{-\frac{1}{2}\left(\frac{n}{N/(2\pi B)}\right)^2}\right], \tag{6.44}$$

which is approximately the Fourier series of the gaussian $G(y-k_0) = \mathcal{N}e^{-\frac{(y-k_0)^2}{2B^2}}$. It follows that the continuous function $v_1(y)$ is approximately a periodic superposition of gaussian peaks with period N, a central peak at position $k_0 = -N/4 - 1/2$, and a width of B, provided $N/4 > B > 1/\pi$. We then examine the following term, appearing in Eq. 6.39,

$$\begin{aligned}\langle x_l|\, F_N U_I F_N^\dagger\, |v_1\rangle\, |\psi_0\rangle &= \int_{-\infty}^{\infty} dq\, \langle x_l|\, D_x\left(\frac{N\tau_I q}{4\pi}\right)|v_1\rangle\, \psi_0(q)\, |q\rangle \\ &= \int_{-\infty}^{\infty} dq v_1\left(l - \frac{N\tau_I}{4\pi}q\right)\psi_0(q)\, |q\rangle\,, \end{aligned} \tag{6.45}$$

and we see that the interaction has the effect of modulating the initial oscillator wavefunction $\psi_0(q)$ by a periodic superposition of gaussian peaks $v_1\left(l - \frac{N\tau_I}{4\pi}q\right)$. The function $v_1\left(l - \frac{N\tau_I}{4\pi}q\right)$ has period $T_q = 4\pi/\tau_I$ in q and has a central peak centred on $q = q_0^{(1)} = \frac{T_q}{N}(l - k_0)$. Furthermore, the gaussian peaks have width $\Delta q = T_q B/N$ in q, and since N grows exponentially in the number of qubits, we see that the width of the peaks decrease exponentially in the number of qubits. We note that the effect of the interaction on the oscillator wavefunction is equivalent to having performed a modular measurement of $q \pmod{T_q}$ obtaining the outcome $q \pmod{T_q} = q_0^{(1)} \pmod{T_q}$. The underlying reason being, that having observed the logical state $|x_l\rangle$ of the qubits, then this observation corresponds to some shift of the initial logical state (centred on k_0), with the shift being generated by some quadrature value

$q = q_s$. However this shift is not just consistent with $q = q_s$, but it is also consistent with $q = q_s + kT_q$ where k is an arbitrary integer, since the displacement through the logical basis is modular/periodic.
Including the second part of the qubit state, i.e. $|v_2\rangle$, we see that we create the superposition,

$$\langle x_l| F_N U_I F_N^\dagger |v\rangle |\psi_0\rangle = \int_{-\infty}^{\infty} dq \left[c_1 v_1 \left(l - \frac{N}{T_q} q \right) + c_2 v_2 \left(l - \frac{N}{T_q} q \right) \right] \psi_0(q) |q\rangle , \tag{6.46}$$

where $v_2\left(l - \frac{N}{T_q}q\right)$ is also a periodic superposition of gaussians with period T_q in q, but the central gaussian is centred on $q_0^{(2)} = \frac{T_q}{N}(l + k_0 + 1)$ in q, corresponding to a shift by $-T_q/2$ in q relative to $q_0^{(1)}$.
We then displace the oscillator by $-q_0^{(1)}$ such that the peaks of $v_1\left(l - \frac{N}{T_q}q\right)$ are centred on $q = 0$. We let the initial oscillator state be a gaussian $\psi_0(z) = \psi_G(z - z_0) = C \exp\left(-\frac{(z-z_0)^2}{2W^2}\right)$ with $C = \pi^{-1/4} W^{-1/2}$. We then obtain,

$$\begin{aligned}
(6.39) &= \int_{-\infty}^{\infty} dq v \left(l - \frac{N}{T_q} q \right) \psi_0(q) |q - q_0^{(1)}\rangle \\
&= \int_{-\infty}^{\infty} dz v \left(k_0 - \frac{N}{T_q} z \right) \psi_0 \left(z + q_0^{(1)} \right) |z\rangle \\
&= \int_{-\infty}^{\infty} dz v \left(k_0 - \frac{N}{T_q} z \right) \psi_G \left(z - z_0 + q_0^{(1)} \right) |z\rangle
\end{aligned} \tag{6.47}$$

We pick $z_0 = -\frac{T_q}{N} k_0$ so that $\psi_G\left(z - z_0 + q_0^{(1)}\right)$ is centred on $z = 0$ when $l = 0$, thereby obtaining,

$$= \int_{-\infty}^{\infty} dz v \left(k_0 - \frac{N}{T_q} z \right) \psi_G \left(z + l \frac{T_q}{N} \right) |z\rangle . \tag{6.48}$$

which will approximately be a superposition of a logical 0 and logical 1 GKP state if we pick $\tau_I = 2\sqrt{\pi}$. Note that l shifts the envelope ψ_G, making the state somewhat lopsided for large $|l|$. In Fig. 6.7 we show the wavefunctions of a few example states generated by the protocol for various N with $W = 6$, using $\theta_1 = 2.6$ and $\theta_k = \pi$ for $k > 1$. We note that if the initial oscillator state has a characteristic width W, and if the period of the peaks of $v\left(k_0 - \frac{N}{T_q} z\right)$ is larger than this width, i.e. $T_q \gg W$, then the state resulting from the above interaction is approximately a squeezed state of standard deviation Δq.

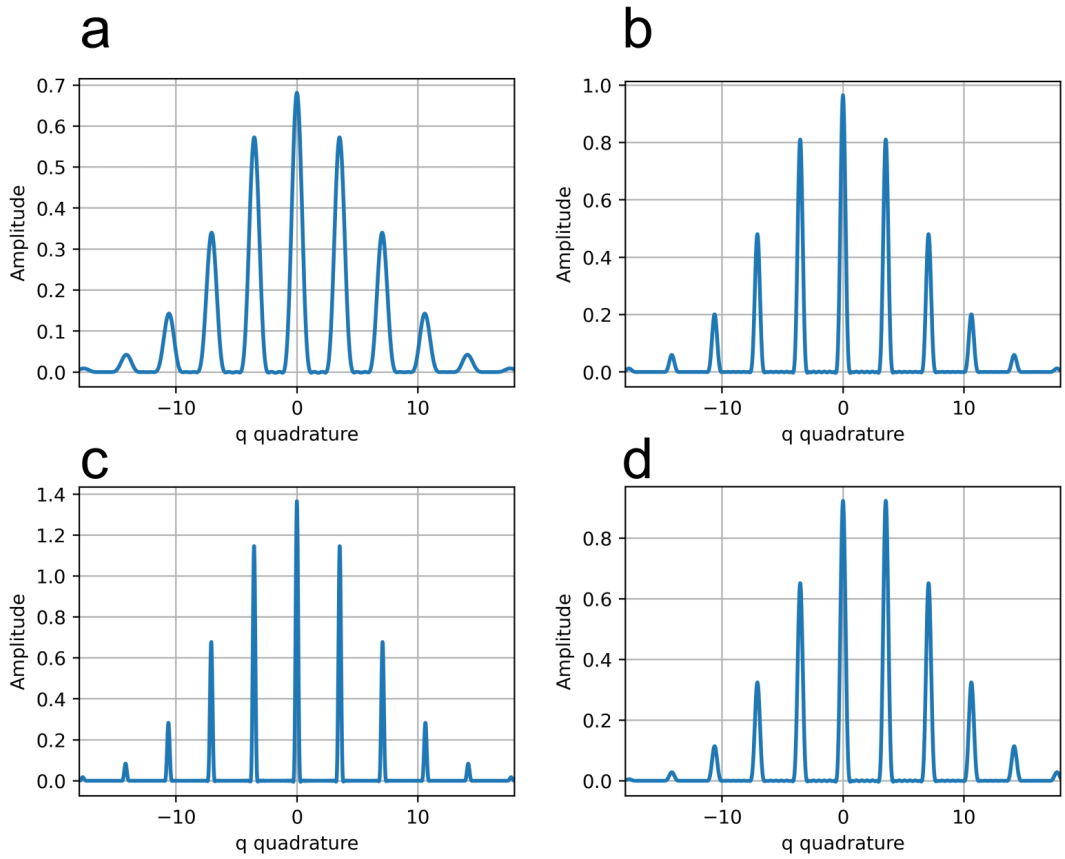

Figure 6.7: *Wavefunctions for states created by the measurement based protocol. All figures assume that the initial gaussian has a width of* $W = 6$*, corresponding approximately to 15.5 dB of squeezing, and that* $\phi_v = 0$ *(defined in Fig. 6.5 b). The small oscillations are due to* $|v\rangle$ *not being a perfect gaussian, i.e. the amplitudes* $\langle x_k|v\rangle$ *are not exactly giving by* $e^{-(k-k_0)^2/2B^2}$*.* ***a*** *Wavefunction resulting from outcome* $l = 0$*, with 3 qubits corresponding to* $N = 8$*.* ***b*** *Wavefunction resulting from outcome* $l = 0$*, with 4 qubits corresponding to* $N = 16$*.* ***c*** *Wavefunction resulting from outcome* $l = 0$*, with 5 qubits corresponding to* $N = 32$*.* ***d*** *Wavefunction resulting from outcome* $l = -8$*, with* $N = 16$ *corresponding to 4 qubits. We observe that the wavefunction is lopsided, this is a general feature for outcomes* l *close to* $\pm N/2$*.*

6.2.2 Measurement-free protocol

We may convert the above protocol into a measurement-free protocol by introducing a second interaction between the qubits and the oscillator, as sketched in Fig. 6.6 b,

$$U_D = e^{-i(\tau_D/2)pX_N}. \tag{6.49}$$

Provided that we can pick τ_D so that $\tau_D = -\frac{T_q}{N}$, then U_D approximately disentangles the qubits and oscillator, leaving the oscillator in a periodic superposition of gaussian peaks. Just prior to the application of U_D we have the state of the oscillator and qubits,

$$\begin{aligned}
|\Psi\rangle &= F_N U_I F_N^\dagger |v\rangle |\psi_0\rangle \\
&= \sum_{l=-N/2}^{N/2-1} |x_l\rangle \langle x_l| F_N U_I F_N^\dagger |v\rangle \int_{-\infty}^{\infty} dq \psi_0(q) |q\rangle \\
&= \int_{-\infty}^{\infty} dq \psi_0(q) \sum_{l=-N/2}^{N/2-1} \langle x_l | D_x \left(\frac{N}{T_q} q\right) |v\rangle |x_l\rangle |q\rangle \\
&= \int_{-\infty}^{\infty} dq \psi_0(q) \sum_{l=-N/2}^{N/2-1} v\left(l - \frac{N}{T_q} q\right) |x_l\rangle |q\rangle .
\end{aligned} \tag{6.50}$$

We then apply U_D,

$$\begin{aligned}
U_D |\Psi\rangle &= \int_{-\infty}^{\infty} dq \psi_0(q) \sum_{l=-N/2}^{N/2-1} v\left(l - \frac{N}{T_q} q\right) e^{i\frac{T_q}{2N} X_N p} |x_l\rangle |q\rangle \\
&= \int_{-\infty}^{\infty} dq \psi_0(q) \sum_{l=-N/2}^{N/2-1} v\left(l - \frac{N}{T_q} q\right) |x_l\rangle |q - l\frac{T_q}{N}\rangle \\
&= \int_{-\infty}^{\infty} dz \sum_{l=-N/2}^{N/2-1} \psi_0\left(z + \frac{T_q}{N} l\right) v\left(-\frac{N}{T_q} z\right) |x_l\rangle |z\rangle
\end{aligned} \tag{6.51}$$

We center $v_1(-\frac{N}{T_q}z)$, such that v has a peak in $z = 0$, by displacing in q by $\frac{T_q}{N}k_0$,

$$\begin{aligned}
&D_q\left(\frac{T_q}{N}k_0\right) U_D |\Psi\rangle \\
&= \int_{-\infty}^{\infty} dz \sum_{l=-N/2}^{N/2-1} \psi_0\left(z + \frac{T_q}{N}(l - k_0)\right) v\left(k_0 - \frac{N}{T_q} z\right) |x_l\rangle |z\rangle .
\end{aligned} \tag{6.52}$$

We will assume $\psi_0(z) = \psi_G(z - z_0) = C \exp\left(-\frac{(z-z_0)^2}{2W^2}\right)$ with $z_0 = -\frac{T_q}{N} k_0$, then we obtain,

$$= \int_{-\infty}^{\infty} dz \sum_{l=-N/2}^{N/2-1} \psi_G \left(z + \frac{T_q}{N} l\right) v \left(k_0 - \frac{N}{T_q} z\right) |x_l\rangle |z\rangle \tag{6.53}$$

Provided that $\psi_G(q)$ varies slowly in q, so that it doesn't change much over the period T_q, then we observe that there is only a small amount of entanglement between the oscillator and the qubits in the above expression, since l is bounded by $\pm N/2$. This will be approximately true if $W \gg T_q$. Under this assumption we can rewrite Eq. 6.53 as,

$$\approx \int_{-\infty}^{\infty} dz \psi_G(z)\, v \left(k_0 - \frac{N}{T_q} z\right) |z\rangle \sum_{l=-N/2}^{N/2-1} |x_l\rangle . \tag{6.54}$$

The state of the oscillator is then,

$$|\psi\rangle = \int_{-\infty}^{\infty} dz \psi_G(z)\, v \left(k_0 - \frac{N}{T_q} z\right) |z\rangle , \tag{6.55}$$

which is a superposition of a logical zero and logical one GKP state provided that $\tau_I = 2\sqrt{\pi}$.
Without invoking the above approximation we can describe the state of the oscillator using the density matrix,

$$\rho_\psi = \int_{-\infty}^{\infty} dz \int_{-\infty}^{\infty} dy \sum_{l=-N/2}^{N/2-1} \psi_G \left(z + \frac{T_q}{N} l\right) \psi_G \left(y + \frac{T_q}{N} l\right)^* v \left(k_0 - \frac{N}{T_q} z\right) v \left(k_0 - \frac{N}{T_q} y\right)^* |z\rangle \langle y| . \tag{6.56}$$

We plot the Wigner function of the state in Eq. 6.56 for various values of N and W, using $\theta_1 = 2.6$ and $\theta_k = \pi$ for $k > 1$. The results are shown in Fig. 6.8

6.3 Summary

We've introduced three protocols for preparing approximate GKP states, as defined in Eq. 6.6.
The first protocol proceeded by repeatedly interacting an oscillator and a qubit via the unitary $U = e^{itgq\sigma_x}$, and then measuring the spin of the qubit along a particular direction V_n in round n. We assumed that the directions V_n were different in each round of interaction, and that the directions V_n were uniformly distributed over the

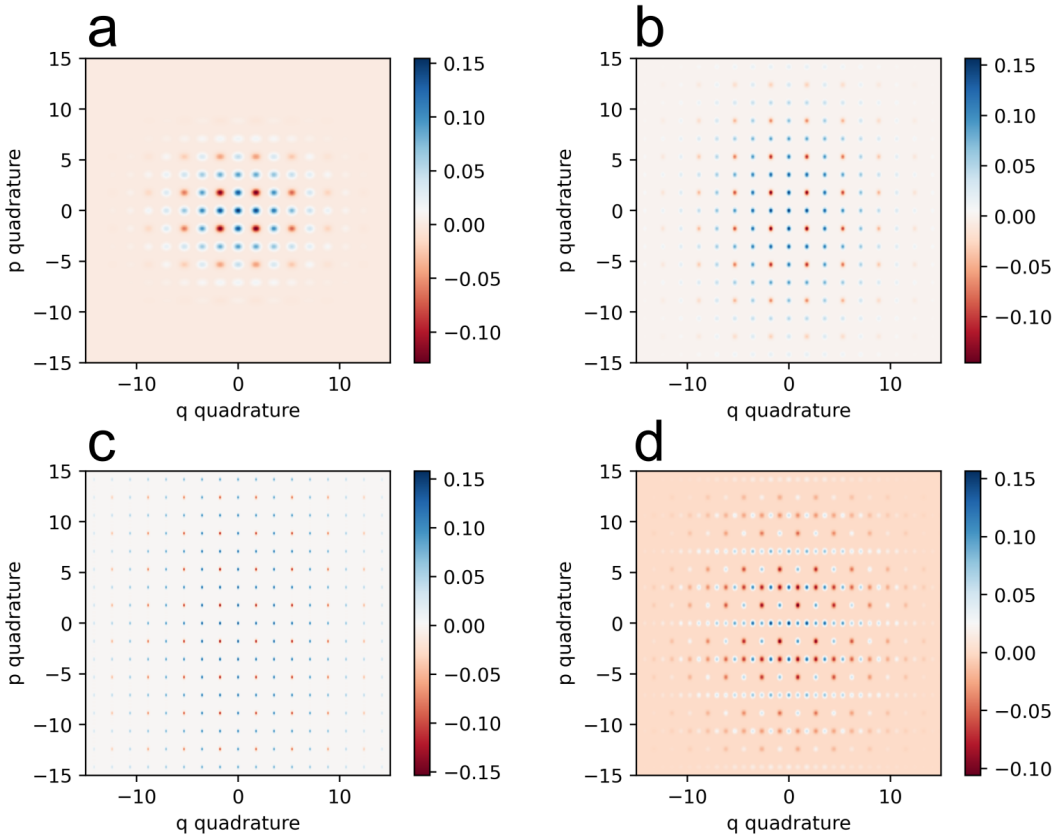

Figure 6.8: *Wigner functions for states created by the measurement free protocol. We set $\phi_v = 0$ for all plots except d* ***a*** *Wigner function for 3 qubits with $W = 6$.* ***b*** *Wigner function for 4 qubits with $W = 8$.* ***c*** *Wigner function for 5 qubits with $W = 10$.* ***d*** *Wigner function for 4 qubits with $W = 8$ and $\phi_v = \pi/2$ and $\omega_v = \pi/2$.*

circle. We showed that the oscillator would then tend toward a peaked periodic state as we increase the number of rounds of interaction N, regardless of the measurement outcomes. The resulting peaked periodic state often resembled an approximate GKP state with the fidelity with the most similar GKP state often being in excess of 0.97 .

The second protocol was based on interacting a collection of qubits with an oscillator. We defined quadrature operators for the set of qubits and showed that the sequence of interactions,

$$\langle x_l | \, F_N U_I F_N^\dagger \, |v\rangle \, |\psi_0\rangle \tag{6.57}$$

performs a modular measurement of the oscillator, i.e. we measure $q \pmod{T_q}$, if the qubit state $|v\rangle$ is localized in the eigenvalues of the X_N quadrature. This modular measurement will in turn prepare a GKP state, if the oscillator wavefunction is initially a broad gaussian in the q quadrature, preferably centred on $-\frac{T_q}{N}k_0$ in q, and given that $\tau_I = 2\sqrt{\pi}$.

Finally, we showed that we don't need the projective measurement of the qubits, if we instead perform the interaction sequence,

$$D_q\left(\frac{T_q}{N}k_0\right) U_D F_N U_I F_N^\dagger \, |v\rangle \, |\psi_0\rangle \, . \tag{6.58}$$

In this case we obtain a GKP state if the initial oscillator state $|\psi_0\rangle$ is gaussian and centred on $-\frac{T_q}{N}k_0$ in q, and has standard deviation W satisfying $W \gg T_q$.

Chapter 7

Conclusion

We have in this thesis proposed a number of experiments. We will now summarize some of our findings, and discuss possible directions for future research.

In chapter 4 we put forward the paper *Proposal for a long-distance nonlocality test with entanglement swapping and displacement-based measurements* [9], which gives an analysis of an experiment for demonstrating nonlocality with multiple parties separated by channels of non-unit transmission. The components used in the setup were restricted to standard quantum optical elements. This was done to increase the experimental feasibility of the proposal. The analysed setup is resilient toward transmission losses from propagation in the channels connecting the parties. We found that the transmission of these channels could be down to 10%, and the W^3ZB inequality could still be broken. The experiment is however, sensitive toward losses in the channels connecting the detector and two-mode squeezer associated to each party. However, the setup can be made more resilient toward this loss by increasing the number of parties. With 4 parties the transmission of these channels can be as low as 82 %. Dark counts at the heralding detectors was found to be very detrimental toward the non-locality of the state shared by the parties. We found that the probability of a dark-count at a heralding detector cannot be much larger than 1 in 10^4, or the experiment fails. The experiment is however very robust toward phase noise. This is in line with the findings of the related study [56]. The experiment is also robust toward amplitude noise, with an acceptable relative amplitude noise of up to around 25 %. The analysed experimental scenario appears well suited for conference style DI-QKD [102], perhaps with some slight changes that would make a particular party the preferred reconciliator. This could be a direction for future research. We thank Masahiro Takeoka of Keio university and his students for suggestions in this direction.

We then presented a scheme for entanglement generation by distributing two-mode squeezed states between a pair of qubit registers. This scheme was published in the paper *Quantum repeater using two-mode squeezed states and atomic noiseless*

amplifiers [10]. The qubits could occupy a bright and a dark state, which facilitated the generation of a light-matter entangled state. Purification and amplification was performed using quantum scissor operations. For the case of a single qubit in each register, we attempted to stack such registers into a repeater, and gauged the sensitivity of the scheme against various sources of error. We found bounds on experimental errors that must be met, in order that this repeater can beat the PLOB bound. Perhaps most critically, loss of emitted photons from the optically active qubits shouldn't be larger than 1 percent. We expect that this is beyond the reach of current experimental capabilities. The scheme as presented, is therefore currently not a viable route to breaking the PLOB bound, unless the scheme is modified to relax the stated tolerances.

Finally, we've presented three protocols for preparing approximate GKP states. The first protocol proceeded by repeatedly interacting an oscillator and a qubit, and measuring the spin of the qubit along a particular direction V_n. We assumed that the directions V_n were different in each round of interaction, and that the directions V_n were uniformly distributed over the circle. We showed that the oscillator would then tend toward a peaked periodic state as we increase the number of rounds of interaction, regardless of the measurement outcomes. The second two protocols were based on interacting a collection of qubits with an oscillator. We defined quadrature operators for the set of qubits and showed that a particular sequence of interactions perform a modular measurement of the oscillator. This modular measurement will in turn prepare a GKP state, if the oscillator is initially in a squeezed state. We presented both a measurement based and a measurement free protocol. It remains to be worked out what physical systems could implement the proposed protocols. In this connection one must include relevant experimental errors to correctly gauge the feasibility of the protocols. Finally, the protocols must be benchmarked against existing protocols to establish their relevance. Steps in this direction are being taken in collaboration with Peter Rabl from the Technical University of Munich.

Bibliography

[1] A. Ferraro, S. Olivares, and M. G. A. Paris, *Gaussian states in continuous variable quantum information*. Bibliopolis, 2005, ISBN: 88-7088-483-X. DOI: 10.48550/ARXIV.QUANT-PH/0503237. [Online]. Available: https://arxiv.org/abs/quant-ph/0503237.

[2] G. S. Agarwal, *Quantum Optics*. Cambridge University Press, 2013, ISBN: 978-1-107-00640-9.

[3] L. E. Ballentine, *Quantum Mechanics A Modern Development 2nd Edition*. World Scientific, 2015, ISBN: 978-981-4578-58-5.

[4] S. M. Barnett, *Quantum Information*. Oxford University Press, 2009, p. 11, ISBN: 978-0-19-852763-3.

[5] M. Nielsen and I. Chuang, *Quantum Computation and Quantum Information*. Cambridge University Press, 2010, ISBN: 978-1-107-00217-3.

[6] N. Bohr, "Can quantum-mechanical description of physical reality be considered complete," *Phys. Rev.*, vol. 48, pp. 696–702, 8 1935.

[7] N. Brunner, D. Cavalcanti, S. Pironio, *et al.*, "Bell nonlocality," *Rev. Mod. Phys.*, vol. 86, no. 2, p. 419, 2014.

[8] S. Pironio, A. Acín, N. Brunner, *et al.*, "Device-independent quantum key distribution secure against collective attacks," *New Journal of Physics*, vol. 11, p. 045 021, 2009.

[9] A. J. E. Bjerrum, J. B. Brask, J. S. Neergaard-Nielsen, and U. L. Andersen, "Proposal for a long-distance nonlocality test with entanglement swapping and displacement-based measurements," *Phys. Rev. A*, vol. 107, p. 052 611, 5 2023.

[10] A. J. E. Bjerrum, J. B. Brask, J. S. Neergaard-Nielsen, and U. L. Andersen, "Quantum repeater using two-mode squeezed states and atomic noiseless amplifiers," *Phys. Rev. A*, vol. 107, no. 4, p. 042 606, 2023. DOI: 10.1103/PhysRevA.107.042606.

[11] K. Fukui, R. N. Alexander, and P. van Loock, "All-optical long-distance quantum communication with gottesman-kitaev-preskill qubits," *Phys. Rev. Res.*, vol. 3, p. 033 118, 3 2021.

[12] C. Cohen-Tannoudji, J. Dupont-Roc, and G. Grynberg, *Photons and Atoms Introduction to Quantum Electrodynamics*. Wiley-VCH, 2004, ISBN: 978-0-471-18433-1.

[13] D. J. Griffiths, *Introduction to Quantum Mechanics*. Pearson, 2005, ISBN: 0-13-111892-7.

[14] N. D. Mermin, "Hidden variables and the two theorems of john bell," *Rev. Mod. Phys.*, vol. 65, pp. 803–815, 3 1993.

[15] C. Gerry and P. Knight, *Introductory Quantum Optics*. Cambridge University Press, 2008, ISBN: 978-0-521-52735-4.

[16] C. Weedbrook, S. Pirandola, R. García-Patrón, *et al.*, "Gaussian quantum information," *Rev. Mod. Phys*, vol. 84, pp. 621–669, 2012.

[17] W. B. Case, "Wigner functions and weyl transforms for pedestrians," *American Journal of Physics*, vol. 76, pp. 937–946, 10 2008.

[18] C. Cui, C. N. Gagatsos, S. Guha, and L. Fan, "High-purity pulsed squeezing generation with integrated photonics," *Phys. Rev. Res.*, vol. 3, p. 013 199, 1 2021.

[19] M. G. Raymer and C. J. McKinstrie, "Quantum input-output theory for optical cavities with arbitrary coupling strength: Application to two-photon wave-packet shaping," *Phys. Rev. A*, vol. 88, p. 043 819, 4 2013.

[20] I. Pitowsky, "George boole's 'conditions of possible experience' and the quantum puzzle," *The British Journal for the Philosophy of Science*, vol. 45, no. 1, pp. 95–125, 1994.

[21] J. S. Bell, *Speakable and Unspeakable in Quantum Mechanics*. Cambridge University Press, 2013, ISBN: 978-0-521-52338-7.

[22] L. E. Ballentine, "The statistical interpretation of quantum mechanics," *Rev. Mod. Phys.*, vol. 42, pp. 358–381, 4 1970.

[23] A. Einstein, B. Podolsky, and N. Rosen, "Can quantum-mechanical description of physical reality be considered complete," *Phys. Rev.*, vol. 47, pp. 777–780, 10 1935.

[24] G. M. Ziegler, *Lectures on Polytopes*. Springer, 2007, ISBN: 978-1-4613-8431-1.

[25] T. Christof and A. Löbel, *A polyhedron representation transformation algorithm*, `https://porta.zib.de/`, visited 18-09-2023.

[26] J. Clauser, M. Horne, A. Shimony, and R. Holt, "Proposed experiment to test local hidden-variable theories," *Phys. Rev. Lett*, vol. 23, p. 880, 1969.

[27] D. J. Griffiths, *Introduction to Electrodynamics Fourth Edition*. Pearson, 2015, ISBN: 978-0-321-84781-2.

[28] J. Bell, "Atomic-cascade photons and quantum-mechanical nonlocality," *Comments on Atomic and Molecular Physics*, vol. 9, pp. 121–126, 1980.

[29] H. price, *Time's Arrow and Archimedes' Point*. Oxford University Press, 1996, ISBN: 0-19-510095-6.

[30] Y. Aharonov and D. Rohrlich, *Quantum Paradoxes*. Wiley, 2005, ISBN: 978-3-527-40391-2.

[31] B. Russell, "On the notion of cause," *Proceedings of the Aristotelian Society*, vol. 13, pp. 1–26, 1912.

[32] A. Aspect, J. Dalibard, and G. Roger, "Experimental test of bell's inequalities using time-varying analyzers," *Phys. Rev. Lett*, vol. 49, no. 25, pp. 1804–1807, 1982.

[33] A. Aspect, P. Grangier, and G. Roger, "Experimental realization of einstein-podolsky-rosen-bohm gedankenexperiment: A new violation of bell's inequalities," *Phys. Rev. Lett*, vol. 49, no. 2, pp. 91–94, 1982.

[34] B. Hensen, H. Bernien, A. E. Dréau, *et al.*, "Loophole-free bell inequality violation using electron spins separated by 1.3 kilometres," *Nature*, vol. 526, pp. 682–686, 2015.

[35] S. Popescu and D. Rohrlich, "Quantum nonlocality as an axiom," *Foundations of Physics*, vol. 24, no. 3, pp. 379–385, 1994.

[36] R. F. Werner and M. M. Wolf, "All-multipartite bell-correlation inequalities for two dichotomic observables per site," *Phys. Rev. A*, vol. 64, p. 032 112, 2001.

[37] J.-D. Bancal, N. Gisin, and S. Pironio, "Looking for symmetric bell inequalities," *J. Phys. A: Math. Theor.*, vol. 43, p. 385 303, 2010.

[38] J. Bell, "On the einstein podolsky rosen paradox," *Physics*, vol. 1, pp. 195–200, 1964.

[39] S. J. Freedman and J. F. Clauser, "Experimental test of local hidden-variable theories," *Phys. Rev. Lett*, vol. 28, no. 14, pp. 938–941, 1972.

[40] L. K. Shalm, E. Meyer-Scott, B. G. Christensen, *et al.*, "Strong loophole-free test of local realism," *Phys. Rev. Lett*, vol. 115, p. 250 402, 2015.

[41] M. Giustina, M. A. M. Versteegh, S. Wengerowsky, *et al.*, "Significant-loophole-free test of bell's theorem with entangled photons," *Phys. Rev. Lett*, vol. 115, p. 250 401, 2015.

[42] W. Rosenfeld, D. Burchardt, R. Garthoff, *et al.*, "Event-ready bell test using entangled atoms simultaneously closing detection and locality loopholes," *Phys. Rev. Lett*, vol. 119, p. 010 402, 2017.

[43] J. Wilms, Y. Disser, G. Alber, and I. C. Percival, "Local realism, detection efficiencies, and probability polytopes," *Phys. Rev. A*, vol. 78, p. 032 116, 2008.

[44] I. Gerhardt, Q. Liu, A. Lamas-Linares, *et al.*, "Experimentally faking the violation of bell's inequalities," *Phys. Rev. Lett*, vol. 107, p. 170 404, 2011.

[45] W. Zhang, T. van Leent, K. Redeker, *et al.*, "A device-independent quantum key distribution system for distant users," *Nature*, vol. 607, pp. 687–691, 2022.

[46] A. Acín, N. Gisin, and L. Masanes, "From bell's theorem to secure quantum key distribution," *Phys. Rev. Lett*, vol. 97, p. 120 405, 2006.

[47] R. Arnon-Friedman, F. Dupuis, O. Fawzi, *et al.*, "Practical device-independent quantum cryptography via entropy accumulation," *Nature Communications*, vol. 9, p. 459, 2018.

[48] A. K. Ekert, "Quantum cryptography based on bell's theorem," *Phys. Rev. Lett*, vol. 67, no. 6, pp. 661–663, 1991.

[49] U. Vazirani and T. Vidick, "Fully device-independent quantum key distribution," *Phys. Rev. Lett*, vol. 113, p. 140 501, 2014.

[50] J. B. Brask and R. Chaves, "Robust nonlocality tests with displacement-based measurements," *Phys. Rev. A*, vol. 86, no. 1, 010103(R), 2012.

[51] M. Żukowski, A. Zeilinger, M. A. Horne, and A. K. Ekert, "Event-ready-detectors" bell experiment via entanglement swapping," *Phys. Rev. Lett.*, vol. 71, p. 4287, 1993.

[52] L.-M. Duan, M. D. Lukin, J. I. Cirac, and P. Zoller, "Long-distance quantum communication with atomic ensembles and linear optics," *Nature*, vol. 414, pp. 413–418, 2001.

[53] U. L. Andersen and T. C. Ralph, "High-fidelity teleportation of continuous-variable quantum states using delocalized single photons," *Phys. Rev. Lett.*, vol. 111, p. 050 504, 2013.

[54] C. H. Bennett, G. Brassard, and C. Crépeau, "Teleporting an unknown quantum state via dual classical and einstein-podolsky-rosen channels," *Phys. Rev. Lett.*, vol. 70, no. 13, pp. 1895–1899, 1993.

[55] S. L. Braunstein and A. Mann, "Measurement of the bell operator and quantum teleportation," *Phys. Rev. A*, vol. 51, no. 3, R1727–R1730, 1995.

[56] J. B. Brask, R. Chaves, and N. Brunner, "Testing nonlocality of a single photon without a shared reference frame," *Physical Review A*, vol. 88, no. 1, p. 012 111, 2013.

[57] A. Laghaout, G. Björk, and U. L. Andersen, "Realistic limits on the nonlocality of an n-partite single-photon superposition," *Phys. Rev. A*, vol. 84, p. 062 127, 2011.

[58] R. Chaves and J. B. Brask, "Feasibility of loophole-free nonlocality tests with a single photon," *Phys. Rev. A*, vol. 84, p. 062 110, 2011.

[59] T. Ralph and A. Lund, "Nondeterministic noiseless linear amplification of quantum systems," *AIP Conference Proceedings*, vol. 1110, pp. 155–160, 2009. DOI: 10.1063/1.3131295.

[60] H. Weinfurter and M. Żukowski, "Four-photon entanglement from down-conversion," *Phys. Rev. A*, vol. 64, 010102(R), 2001.

[61] M. Żukowski and Č. Brukner, "Bell's theorem for general n-qubit states," *Phys. Rev. Lett.*, vol. 88, p. 210 401, 2002.

[62] R. F. Werner and M. M. Wolf, "Bell inequalities and entanglement," *Quantum Information and Computation*, vol. 1, pp. 1–25, 2001.

[63] G. Bacciagaluppi and R. Hermens, "Bell-inequality violation and relativity of pre- and postselection," *Phys. Rev. A*, vol. 104, p. 012 201, 2021.

[64] N. Gisin and R. Thew, "Quantum communication," *Nature Photonics*, vol. 1, p. 165, 2007.

[65] S. Pirandola, U. L. Andersen, L. Banchi, *et al.*, "Advances in quantum cryptography," *Advances in Optics and Photonics*, vol. 12, pp. 1012–1097, 2020.

[66] H. J. Kimble, "The quantum internet," *Nature*, vol. 453, pp. 1023–1030, 2008. DOI: 10.1038/nature07127.

[67] S. Wehner, D. Elkouss, and R. Hanson, "Quantum internet: A vision for the road ahead," *Science*, vol. 362, p. 303, 2018.

[68] H. J. Briegel, W. Dür, J. I. Cirac, and P. Zoller, "Quantum repeaters: The role of imperfect local operations in quantum communication," *Phys. Rev. Lett.*, vol. 81, p. 5932, 1998.

[69] S. Muralidharan, L. Li, J. Kim, *et al.*, "Optimal architectures for long distance quantum communication," *Sci. Rep.*, vol. 6, p. 20 463, 2016.

[70] N. Sangouard, C. Simon, H. de Riedmatten, and N. Gisin, "Quantum repeaters based on atomic ensembles and linear optics," *Rev. Mod. Phys.*, vol. 83, p. 33, 2011.

[71] N. Sangouard, R. Dubessy, and C. Simon, "Quantum repeaters based on single trapped ions," *Phys. Rev. A*, vol. 79, p. 042 340, 2009.

[72] I. Usmani, M. Afzelius, H. de Riedmatten, and N. Gisin, "Mapping multiple photonic qubits into and out of one solid-state atomic ensemble," *Nat. Commun.*, vol. 1, p. 12, 2010.

[73] A. Wallucks, I. Marinković, B. Hensen, *et al.*, "A quantum memory at telecom wavelengths," *Nat. Phys.*, vol. 16, pp. 772–777, 2020.

[74] T. C. Ralph, "Quantum error correction of continuous-variable states against gaussian noise," *Phys. Rev. A*, vol. 84, p. 022 339, 2011.

[75] J. Dias and T. C. Ralph, "Quantum repeaters using continuous-variable teleportation," *Phys. Rev. A*, vol. 95, p. 022 312, 2017.

[76] J. Dias and T. C. Ralph, "Quantum error correction of continuous-variable states with realistic resources," *Phys. Rev. A*, vol. 97, p. 032 335, 2018.

[77] K. P. Seshadreesan, H. Krovi, and S. Guha, "Continuous-variable entanglement distillation over a pure loss channel with multiple quantum scissors," *Phys. Rev. A*, vol. 100, p. 022 315, 2019.

[78] K. P. Seshadreesan, H. Krovi, and S. Guha, "Continuous-variable quantum repeater based on quantum scissors and mode multiplexing," *Phys. Rev. Research*, vol. 2, p. 013 310, 2020.

[79] M. Ghalaii and S. Pirandola, "Capacity-approaching quantum repeaters for quantum communications," *Phys. Rev. A*, vol. 102, p. 062 412, 2020.

[80] J. Dias, M. S. Winnel, N. Hosseinidehaj, and T. C. Ralph, "Quantum repeater for continuous variable entanglement distribution," *Phys. Rev. A*, vol. 102, p. 052 425, 2020.

[81] F. Furrer and W. J. Munro, "Repeaters for continuous variable quantum communication," *Phys. Rev. A*, vol. 98, p. 032 335, 2018.

[82] D. T. Pegg, L. S. Phillips, and S. M. Barnett, "Optical state truncation by projection synthesis," *Physical Review Letters*, vol. 81, pp. 1604–1606, 1998.

[83] F. Rozpędek, R. Yehia, K. Goodenough, *et al.*, "Near-term quantum-repeater experiments with nitrogen-vacancy centers: Overcoming the limitations of direct transmission," *Phys. Rev. A*, vol. 99, p. 052 330, 2019.

[84] P. C. Maurer, G. Kucsko, C. Latta, *et al.*, "Room-temperature quantum bit memory exceeding one second," *Science*, vol. 336, p. 1283, 2012.

[85] M. W. Doherty, N. B. Manson, P. Delaney, *et al.*, "The nitrogen-vacancy colour centre in diamond," *Physics Reports*, vol. 528, pp. 1–45, 2013.

[86] H. Bernien, B. Hensen, W. Pfaff, *et al.*, "Heralded entanglement between solid-state qubits separated by three metres," *Nat. Lett.*, vol. 497, pp. 86–90, 2013.

[87] G. Vidal and R. F. Werner, "Computable measure of entanglement," *Phys. Rev. A*, vol. 65, p. 032 314, 2002.

[88] M. V. G. Dutt, L. Childress, L. Jiang, *et al.*, "Quantum register based on individual electronic and nuclear spin qubits in diamond," *Science*, vol. 316, no. 5829, pp. 1312–1316, 2007.

[89] L. Robledo, L. Childress, H. Bernien, *et al.*, "High-fidelity projective read-out of a solid-state spin quantum register," *Nature*, vol. 477, no. 5829, 2011.

[90] F. Dolde, V. Bergholm, Y. Wang, *et al.*, "High-fidelity spin entanglement using optimal control," *Nature Comm.*, vol. 5, no. 8451, 2014.

[91] W. Pfaff, B. J. Hensen, H. Bernien, *et al.*, "Unconditional quantum teleportation between distant solid-state quantum bits," *Science*, vol. 345, no. 6196, pp. 532–535, 2014.

[92] S. Pirandola, R. Laurenza, C. Ottaviani, and L. Banchi, "Fundamental limits of repeaterless quantum communications," *Nature Communications*, vol. 8, p. 15 043, 2017.

[93] J. Barrett, L. Hardy, and A. Kent, "No signalling and quantum key distribution," *Phys. Rev. Lett.*, vol. 95, p. 010 503, 2005.

[94] A. J. E. Bjerrum, *Package for quantum optics in the fock basis*, `https://github.com/qpit/Numerical-Fock-Basis-Optics`, 2022.

[95] R. García-Patron, "Quantum information with optical continuous variables : From bell tests to key distribution," *Thesis, Université Libre de Bruxelles*, pp. 185–203, 2007.

[96] I. Devetak and A. Winter, "Distillation of secret key and entanglement from quantum states," *Proc. R. Soc. A*, vol. 461, p. 207, 2005.

[97] N. K. Bernardes, L. Praxmeyer, and P. van Loock, "Rate analysis for a hybrid quantum repeater," *Physical Review A*, vol. 83, p. 012 323, 2011.

[98] D. Gottesman, A. Kitaev, and J. Preskill, "Encoding a qubit in an oscillator," *Phys. Rev. A*, vol. 64, p. 012 310, 1 2001.

[99] P. Campagne-Ibarcq, A. Eickbusch, S. Touzard, *et al.*, "Quantum error correction of a qubit encoded in grid states of an oscillator," *Nature*, vol. 584, pp. 368–372, 2020.

[100] T. S. Santhanam and A. R. Tekumalla, "Quantum mechanics in finite dimensions," *Foundations of Physics*, vol. 6, pp. 583–587, 5 1976.

[101] J. Hastrup, K. Park, J. Brask, *et al.*, "Measurement-free preparation of grid states," *npj Quantum Inf*, vol. 7, 17 2021.

[102] T. Holz, H. Kampermann, and D. Bruß, "Genuine multipartite bell inequality for device-independent conference key agreement," *Phys. Rev. Res.*, vol. 2, p. 023 251, 2 2020.